Programa de Doctorado en Biomedicina (B11.56.1)

Departamento de Química Farmacéutica y Orgánica

European Doctoral Thesis

Chem-NAT: A unique chemical approach for Nucleic Acids Testing

Doctoral candidate: Mª Angélica Luque González

Thesis supervisors: Dr. Juan José Díaz Mochón and Dra. Rosario Mª Sánchez Martín

Granada, XX de Marzo de 2018

A mi familia, por quererme y cuidarme, por enseñarme, por animarme y por acompañarme en cada etapa.

Agradecimientos

Tengo tanta gente a la que agradecer, tantas cosas en mi mente que no sé ni por dónde empezar y de antemano intuyo que algo se quedará en el tintero, jajaja. En primer lugar quiero dar las gracias a mi "familia laboral", a Juanjo y Rosario por su capacidad de trabajo, por su emoción y entusiasmo, por su calidad profesional y humana, por confiar en mí y darme la oportunidad de formar parte de este proyecto; por estar siempre buscando lo mejor para mí, para mi futuro y para mi desarrollo; por hacerme evolucionar. Y como no a mis compañeros y amigos que han ido formando parte del grupo Nanochembio: Juandi, Bea, Tere, Juan Antonio, Patri, Victoria, Javi, Rafa, Antonio, Mari Paz, Agustín, Jose, Mari Fe…por compartir sus conocimientos, por ayudarme y apoyarme, por compartir buenos ratos, risas. Y, tengo que hacer especial mención a Antonio porque más que un compañero de grupo, ha sido un verdadero amigo, por tantas horas compartidas, por consejos, por las cosas en las que me has ayudado, por las confidencias y los cotilleos, jajaja. Y, a falta de una, tengo la suerte de tener una segunda familia laboral, gracias a mis compañeros DestiNA Genomica (Mavys, Bárbara, Antonio Marín, Antonio Fara, Javi, Pepo, Quique, Salvo, Hugh, Margaret, David) por acogerme en el mundo empresarial, por enseñarme y guiarme, por preocuparse por mí y buscar lo mejor para mí y por las risas y ratos de laboratorio compartidos.

A la gente del departamento de química farmacéutica y orgánica, Vero, Mª Eugenia, Belén, Olga, Lucía, Joaquín por acompañarme en mis comienzos, dedicar tiempo a enseñarme, compartir buenos ratos y por el cariño que me habéis transmitido siempre. A Lola y Guille por esos comidas en el zulo interrumpidas por las tutorías y la fotocopiadora, jajajaj. Y en especial a Ana, por enseñarme, por su pasión, por su capacidad de trabajo, por estar pendiente de mí y ayudarme y por darme mi primera oportunidad.

A mis compis del Lab13a&b, perdón que ahora es Lab13&19 (Lidia, Tere, Sonia, Álvaro, Carmen, Antonio, Rafa, Jose, Alejandra, Pablo, Mari) porque hemos compartido muchas cosas juntos, desde horas de laboratorio, desayunos y comidas, salidas, fiestas, viajes. Por esas conversaciones frikis, por esas risas cuando yo pillaba las bromas media hora después…jajaja. Ah! Y que no se me olvide que voy a patentar la frase "Pon una Tere en tu vida" porque no sé cómo lo hace pero pese a sus cosas, a su carga de trabajo siempre está de buen humor, dispuesta a ayudarte y a animarte; gracias por el apoyo informático, por los consejos, por los ánimos…eres una chica "multitask".

A mis researchers, mis genyos (Patri, Antonio, Javi, Silvia, Carlos Peris, Orlando, Diego, Inma, Alba, Joan, Julia, Joel, Paola, Carlos Baliñas, Manu, Mati, Paola, Marina, Carmen Belén, Luz, Agustín, Helena) porque sin ellos, estos años tampoco hubiesen sido lo mismo. Porque una persona es un conjunto de cosas y los pequeños momentos, la sonrisa de buenos días, las risas a mi costa,

bueno venga las risas "conmigo"…pueden cambiarlo todo. Y como no, por esos viajes inolvidables, esas rutillas y esas fiestas, las salidas que sabíamos a la hora a la que quedábamos pero no cuándo íbamos a acabar. Gracias por traer esos momentos de felicidad, alegría y buen humor.

A mis niñas madrileñas, porque pese a que estuvimos un tiempo desconectadas, la amistad si es buena y sincera siempre está ahí. Gracias por ese reencuentro, por esa amistad, por los ánimos y por los ratitos que pasamos juntas.

A mi familia, porque siempre habéis estado ahí incondicionalmente, apoyándome y luchando por mí, haciéndome creer en mí y seguir adelante por muy oscuro que viese el camino. Por cada palabra de aliento, por cada abrazo, por cada beso e, incluso aunque parezca tonto, por cada regañina; porque si hoy esto es posible es en gran parte por vosotros. Por darme oportunidades y opciones, por comprenderme y escucharme, por acompañarme en el camino. Por esas miradas de amor, de esperanza, de confianza. Por buscar lo mejor para mí, por esforzaros cada día para que no me faltase de nada. Porque habéis estado conmigo en cada momento, esto es por vosotros y para vosotros. A mis padres, porque la tesis es el mejor reflejo de vuestra influencia, habéis sido un ejemplo para mí, de trabajo duro, de sacrificio y esfuerzo, de luchar contra las adversidades, de dedicación, de amor y cariño incondicional…gracias. A mi hermano, porque pese a ser menor que yo me ha demostrado su madurez, su sensatez, su dedicación, sus ganas de hacer algo diferente, porque una hermana no podría estar más orgullosa de tener a un hermano así. Y, cómo no, por esas conversaciones y consejos de los que tanto he aprendido, por abrirme los ojos y hacerme ver las cosas con otra perspectiva. A mis abuelos y mis tíos, por esas conversaciones, por preocuparos por mí, por estar pendientes de mí desde pequeña…La familia se hace con roce y cariño, con cuidado y respeto, con esfuerzo e interés y, he tenido la suerte de que en mi caso todo eso y mucho más sea una realidad. Os quiero mucho.

La doctoranda Mª Angélica Luque González y los directores de la tesis Dr. Juan José Díaz Mochón y la Dra. Rosario Mª Sánchez Martín garantizamos, al firmar esta tesis doctoral, que el trabajo realizado por la doctoranda bajo la dirección de los directores de tesis y hasta donde nuestro conocimiento alcanza, en la realización del trabajo, se han respetado los derechos de otros autores a ser citados, cuando se han utilizado resultados o publicaciones.

The doctoral candidate Mª Angélica Luque González and the thesis supervisors Dr. Juan José Díaz Mochón and Dra. Rosario Mª Sánchez Martín guarantee, by signing this doctoral thesis, that the work has been done by the doctoral candidate under the direction of the thesis supervisors and, as far as our knowledge reaches, in the performance of the work, the rights of other authors to be cited (when their results or publications have been used) have been respected.

Lugar y fecha/ Place and date:

Granada, XX de Marzo de 2018

Directores de la Tesis/Thesis supervisors

Juan José Díaz Mochón   Rosario Mª Sánchez Martín

Doctoranda/Doctoral candidate

Mª Angélica Luque González

Firma/signed

Firma/signed

Quality criteria to apply for the degree of "International Ph.D." by the University of Granada

To apply for the mention of "International Doctorate", the doctoral candidate leans on:

1. Two accepted and published scientific articles in relevant journals on the field of knowledge of the doctoral thesis, here signed by the doctoral candidate, including part of the thesis results.

> **1.1. <u>María Angélica Luque-González</u>**, Mavys Tabraue-Chávez, Bárbara López-Longarela, Rosario María Sánchez-Martín, Matilde Ortiz-González, Miguel Soriano-Rodríguez, José Antonio García-Salcedo, Salvatore Pernagallo, Juan José Díaz-Mochón. "Identification of Trypanosomatids by detecting Single Nucleotide Fingerprints using DNA analysis by Dynamic Chemistry with MALDI-ToF". Talanta, Volume 176, 1 January 2018, Pages 299-307. Impact Factor (2016): 4.162; SJR (2016): 1.162, Chemistry-Analytica 9/76.

> **1.2.** Seshasailam Venkateswaran, **<u>María Angélica Luque-González</u>**, Mavys Tabraue-Chávez, Mario Antonio Fara, Barbara López-Longarela, Victoria Cano-Cortes, Francisco Javier López-Delgado, Rosario María Sánchez-Martín, Hugh Ilyine, Mark Bradley, Salvatore Pernagallo, and Juan José Díaz-Mochón. Novel bead-based platform for direct detection of unlabeled nucleic acids through Single Nucleobase Labeling. Talanta, Volume 161, December 2016, Pages 489-496. Impact Factor (2016): 4.162; SJR (2016): 1.162, Chemistry-Analytica 9/76.

2. Two international internships in a foreign research centre:

> 2.1. May-August 2017: Internship in Edinburgh Molecular Imaging Ltd. Edinburgh, UK. Project: "Development of a multimodal agent for cancer imaging", under the supervision of Dr. Christophe Portal, Head of Chemistry at EMI and Dr. Ian A. Wilson, CEO at EMI. Funding: Ayudas a la movilidad predoctoral para la realización de estancias breves en centros de I+D 2016, Ministerio de Economía, Industria y Competitividad.

> 2.2. October-December 2014: Internship in the laboratory of Professor Mark Bradley in the school of Chemistry of the University of Edinburgh and in DestiNA Genomics Ltd., Edinburgh, UK. Project: "Synthesis of DGL probes and BOT-Nucleobases for DNA sequence analysis", under the supervision of Prof. Mark Bradley and Dra. Annamaria Lilienkampf. Funding: II Convocatoria de Ayudas a la enseñanza práctica dirigidas a estudiantes de másteres oficiales y programas de doctorado de la Universidad de Granada, CEI-BioTic, curso Académico 2013/2014.

3. According to the University of Granada criteria to obtain an "international doctorate" degree, this doctoral thesis has been written and it will be later defended in English. This language have been chosen because it is the main language used for scientific communication, the vast majority of scientific texts are written in English and it might avoid misunderstanding by following the English scientific terminology, abbreviation and acronyms. An abbreviation and acronym table has been also included to facilitate the reading. Additionally and following the requirement of the University of Granada, some parts of the document (abstract and conclusions) have been also written in Spanish and the conclusions will be presented in Spanish.

Grants and funding

Index

Abstract/Resumen

Abstract

Nucleic acid tests, "NAT", refers to molecular techniques to detect nucleic acid used to identify pathogenic species such as bacteria and viruses and also genetic biomarkers related to diseases, such as cancer, drug performances and drug toxicities. This kind of assays is increasingly being used as routine tests in the cost challenged medical health systems, animal health, food safety and drug development by pharmaceutical companies. NAT has created an expanding global market which will grow at a compound annual growth rate (CAGR) of nearly 10% by 2020.

Within the PCR-based dominated NAT market, a new type of NAT, which does not fully rely on PCR, has been recently proposed. The chemistry-based approach is based on dynamic chemistry and uses abasic PNA probes (DGL probes) and aldehyde-reactive modified nucleobases (SMART-Nucleobases, SMART-NBs), allowing nucleic acid reading with single-base resolution. The specificity of the method relies on two steps which need both to occur in order to create a readable signal: 1) perfect hybridization between a DGL probe and its target nucleic acid and 2) a specific thermodynamic-controlled incorporation to the DGL probe of a SMART-NB which is complementary to the nucleotide under interrogation following Watson-Crick base pair ruling. As a result, the system removes the chances of a false-positive result.

The aim of this project was to develop new molecular assays, based on this chemistry-based approach, which offered diagnostic capabilities for rapid identification of both pathogens and circulating biomarkers. These new molecular assays aimed to offer advantages in terms of result consistency, time, cost and ease of use.

Two different target nucleic acids were studied:

a) miR-122, a hepato-specific microRNA which is an early and more sensitive indicator of drug-induced liver injury than other currently used biomarkers such as ALT or AST. It can be also used in drug-development processes to assess *in vitro* cellular toxicity. To do so, the 'Single Nucleobase Labeling' (SNL) approach was first developed during this thesis.

b) Trypanosomatids 28S ribosomal RNA coding gene: *L. major*, *T. brucei* and *T. cruzi*. Three closely related species with high homology gene sequences which cause devastating diseases. They can give cross-reaction and so misdiagnosis which would result in an ineffective drug-based treatment, suffering the side effects and the disease symptoms. To

tackle this issue, the 'Single Nucleotide Fingerprints' concept was developed for the first time during this thesis.

The chemistry-based technology for nucleic acid testing was integrated within different platforms, which were already used in diagnostic laboratories, to expand their utility and thus develop novel diagnostic tests. The tested platforms were:

a) In-Check™ LoC from STmicroelectronics® for an array-based fluorescence-based detection of miR-122

b) Magplex® microspheres from Luminex® for a bead-based fluorescent assay for the detection of miR-122.

c) Reaction in solution using MALDI-TOF mass spectrometry as readout tool for the identification and differentiation of three trypanosomatid species *L. major*, *T. brucei* and *T. cruzi*.

d) HibridSpot™12 (DNA flow) system from Vitro® group for an array-based colorimetric assay for the differentiation of trypanosomatids *L. major* and *T. cruzi*.

The results obtained from this project were undertaken by DestiNA Genomica S.L. Regarding the bead-based assay, a new platform, SiMoA™, has been successfully used to detect miR-122 from patients serum. On the other hand, the colorimetric-based assay for trypanosomatid differentiation has been adapted to a more reproducible, specific, accurate and easier to perform platform, DestiNA spin-tube. This final product might be the first product commercialized by DestiNA Genomica S.L.

Resumen

Los test de ácidos nucleicos, "NAT", hacen referencia a las técnicas moleculares que se utilizan para la identificación de especies patógenas como bacterias y virus así como para la identificación de biomarcadores relacionados con el desarrollo de enfermedades, por ejemplo cáncer; con la respuesta del organismo a un tratamiento farmacológico y la toxicidad del mismo. El uso de este tipo de ensayos está en aumento, especialmente en sistemas sanitarios con pocos recursos económicos, salud animal, seguridad alimentaria, desarrollo de fármacos por la industria farmacéutica…De hecho, los NAT suponen un mercado global en expansión que tendrá una tasa de crecimiento compuesta del 10% para 2020.

Dentro del mercado de los NAT, fundamentalmente basado en ensayos de PCR, se propone un nuevo tipo de NAT que no depende por completo de amplificación de la diana por PCR. Se trata de un nuevo enfoque de NAT basado en un proceso de química dinámica y en el que se utilizan sondas

de PNA abásicas (sondas DGL) y bases nitrogenadas modificadas con un grupo aldehído (SMART-Nucleobases, SMART-NBs), permite la "lectura" de ácidos nucleicos con resolución de una sola base. La especificidad de la metodología propuesta se debe al hecho de que deben cumplirse 2 requisitos para obtener una señal: 1) una hibridación perfecta entre una sonda DGL y su ácido nucleico diana y 2) una incorporación específica y controlada termodinámicamente de una SMART-NB en la posición abásica de una sonda DGL que debe ser complementaria, según las reglas de apareamiento de bases propuestas por Watson y Crick, a la del nucleótido estudiado en el ácido nucleico diana. Como consecuencia de estos requisitos, se minimizan las posibilidades de obtener falsos-positivos.

El objetivo de este proyecto era desarrollar nuevos ensayos moleculares que basados en este enfoque químico ofreciesen alternativas de diagnóstico capaces de identificar rápidamente tanto patógenos como biomarcadores circulantes. Los nuevos ensayos moleculares propuestos tienen como objetivos aportar beneficios a nivel económico, reducir el tiempo necesario para la obtención de los resultados así como proporcionar una mayor consistencia de los mismos y simplificar los ensayos de modo que no sea necesario la utilización de equipos o la intervención de personal altamente especializados.

Se han estudiado dos ácidos nucleicos diferentes:

a) miR-122, un microRNA hepato-específico propuesto como biomarcador de daño hepático inducido por fármacos ya que es mucho más sensible y específico que otros biomarcadores actualmente utilizados en clínica como ALT o AST. Además, podría utilizarse en los procesos de desarrollo de fármacos para determinar la toxicidad celular *in vitro*. Para conseguir este objetivo, se seguirá la primera estrategia desarrollada durante esta tesis 'Single Nucleobase Labeling' –"marcaje de una sola nucleobase"-.

b) El gen que codifica para el RNA ribosomial 28S: *L. major*, *T. brucei* and *T. cruzi*. Se trata de tres especies de parásitos relacionadas filogenéticamente, con una alta homología de secuencia y que causan enfermedades devastadoras. Debido a su alta homología pueden dar lugar a reacciones cruzadas y un diagnóstico erróneo lo que supondría instaurar un tratamiento farmacológico inadecuado y sufrir no sólo los efectos de la enfermedad sino también los efectos secundarios del tratamiento. Para abordar este problema, durante la tesis se desarrolló el concepto de 'Single Nucleotide Fingerprint' –huella nucleotídica única-.

La tecnología propuesta para la "lectura" química de ácidos nucleicos se integró en diferentes plataformas, algunas de las cuales ya estaban siendo utilizadas en laboratorios de diagnóstico, para conseguir así expandir su utilidad y poder desarrollar nuevos test de diagnóstico.

a) In-Check™ LoC de STmicroelectronics® para una detección fluorescente de miR-122.

b) Microesferas Magplex® de Luminex® para una detección fluorescente de miR-122 usando microesferas como plataforma.

c) Reacción en solución con detección mediante espectrometria de masas MALDI-TOF para la identificación y diferenciación de tres especies de tripanosomatidos: *L. major*, *T. brucei* and *T. cruzi*.

d) Sistema HibridSpot™12 (tecnología "DNA flow") del grupo Vitro® para el desarrollo de un test colorimétrico para la diferenciación de *L. major* and *T. cruzi*.

Los resultados obtenidos de este proyecto fueron utilizados como punto de partida por DestiNA Genomica S.L. En relación al ensayo utilizado microesferas como plataforma, se ha llevado a caba la detección de miR-122 en suero de pacientes utilizado una nueva plataforma, SiMoA™. Por otro lado, el test colorimétrico desarrollado para la diferenciación de parásitos tripanosomátidos se ha adapatado a una nueva plataforma más sencilla y que proporciona resultados más reproducibles, específicos y precisos, "DesitNA-spin-tube". El producto final podría convertirse en el primer producto comercializado por DestiNA Genomica S.L.

Abbreviations

A	Adenine (neutral PNA monomer or DNA monomer)
Aglu	Adenine (chiral and negatively charged PNA monomer)
ALT	Alanine transaminase
aPCR	Asymmetric PCR
AST	Aspartate transaminase
C	Cytosine (neutral PNA monomer or DNA monomer)
Chem-NAT	Dynamic chemical approach for nucleic acid testing
Cglu	Cytosine (chiral and negatively charged PNA monomer)
CSF	Cerebro Spinal Fluid
DGL probe	Probes with a PNA backbone and an abasic site
DILI	Drug-induced-liver-injury
DNA	Desoxirribonucleic acid
dsDNA	Double-stranded DNA
G	Guanine (neutral PNA monomer or DNA monomer)
Genomic DNA	gDNA
Gglu	Guanine (chiral and negatively charged PNA monomer)
GL	Chiral negatively charged abasic monomer
Lm	*Leishmania major*
LoC	Lab-on-Chip
MALDI-TOF	Matrix-assisted Laser-desorption/ionization Time of Flight
MFI	Median Fluorescence Intensity
miRNA	microRNA
mRNA	Messenger RNA
$NaBH_3CN$	Sodium Cianoborohydride (reducing agent)
PNA	Peptide Nucleic Acid
Rluc	Renilla luciferase
RNA	Ribonucleic acid
rRNA	Ribosomal RNA
SAPE	Streptavidin-R-phycoerithrin conjugate

SMART-A	N9-Aldehyde-modified Adenine
SMART-C	N3-Aldehyde-modified Cytosine
SMART-C-PEG$_2$-Biotin	N3-Aldehyde-modified Cytosine bearing a PEG spacer and a biotin tag
SMART-C-sulfoCy5	N3-Aldehyde-modified Cytosine bearing a sulfoCy5 tag
SMART-G	N9-Aldehyde-modified Guanine
SMART-NB	SMART-Nucleobases: aldehyde-modified nitrogenous bases
SMART-T	N3-Aldehyde-modified Tymine
S/N	Signal to Noise or Signal to background ratio
SNF	Single Nucleotide Fingerprint
SNL	Single Nucleobase Labeling
sPCR	Symmetric PCR
ssDNA	Single-stranded DNA
T	Thymine (neutral PNA monomer or DNA monomer)
Tb	*Trypanosoma brucei*
Tc	*Trypanosoma cruzi*
Tglu	Thymine (chiral and negatively charged PNA monomer)
Xx	Amino-miniPEG-linker
"_"	Neutral abasic monomer

Rationale and objectives

Justification

This Project aimed to develop set of reagents, protocols and assay platforms which were able to perform novel molecular assays based on the novel chemistry-based technology for nucleic acid reading with single base resolution. Target nucleic acids under study are related to pathogens diseases, thus driving treatment choices, and drug induced liver injury.

This Project has led to the development of novel molecular assays based on platforms with multiplexing capability. The project benefits from 1) the high specificity of the technology used, already validated for the genotyping of cystic fibrosis patients, and based on a dynamic chemistry process for the detection of nucleic acid and 2) the integration of the chemistry-based technology within commercial diagnostic platforms (microspheres, membranes, LoC) in comparison with the instrumentation required for the MALDI-TOF detection.

Objectives

Objective 1: Development of a test for the detection of microRNAs using a hepato-specific microRNA –miR-122- as a model.

The following specific aims were developed:

1.1. Fluorescent detection using the In-check™ LoC platform (STMicroelectronics®)

1.1.1. Design, synthesis and characterization of a DGL probe for the miR-122 detection.

1.1.2. Immobilization of the DGL probes on the chip surface.

1.1.3. Validation of the functionality of the DGL probes linked to the platform.

1.1.4. Validation of the dynamic incorporation of a fluorescently-labeled SMART-NB on the DGL probe immobilized on the LoC.

1.2. Fluorescent detection using fluorescent magnetic microspheres (Luminex®) as platform

1.2.1. Coupling of the DGL probes to the magnetic.

1.2.2. Validation of the functionality of the DGL probes coupled to the magnetic microspheres.

1.2.3. Validation and optimization of the dynamic incorporation process of a biotinylated SMART-NB on DGL probe-functionalized microspheres and next development of a fluorescent signal.

Objective 2: Development of a test for the detection, identification and differentiation of three trypanosomatids species (Leishmania major, Trypanosoma cruzi y Trypanosoma brucei).

The following specific aims were carried out:

2.1. Mass-based detection, MALDI-ToF mass spectrometry.

2.1.1. Design, synthesis and characterization of the DGL probes for the differentiation of the three trypanosomatid species.

2.1.2. Validation of the new DGL probes and the dynamic incorporation of the SMART-NBs by MALDI-TOF MS for the differentiation of the three trypanosomatids species in a single test.

2.1.3. Development of a protocol for the identification of the trypanosomatid parasite using genomic DNA as template and MALDI-TOF as readout tool.

2.1.3.1. Design of primers and PCR optimization to amplify the target sequence within the genomic DNA.

2.1.3.2. Validation and optimization of the methodology for the detection and identification of a trypanosomatid from the amplicon product and using MALDI-TOF as readout tool.

2.2. Colorimetric detection

2.2.1. Adaptation of the assay developed for the identification of trypanosomatids by MALDI-TOF to a new diagnostic platform –membranes- for a colorimetric detection.

2.2.1.1. Modification and optimization of the DGL probes to adapt them to the new platform.

2.2.1.2. Immobilization of the DGL probes on the membranes.

2.2.1.3. Validation and optimization of the colorimetric process for the detection of the biotinylated SMART- Nucleobase incorporated on the immobilized DGL probe.

2.2.1.4. Development of a protocol for the identification and differentiation of the amplified sequence from the trypanosomatid parasites using a colorimetric detection.

Chapter 1: General introduction: nucleic acids, nucleic acids testing and nucleic acid-templated base-filling reactions

Chapter 1: General introduction: nucleic acids, nucleic acids testing and nucleic acid-templated base-filling reactions

Molecular pathology is a new area in laboratory medicine focuses on the detection, characterization and/or quantification of nucleic acids to help with the diagnosis of human diseases. According to its specialization, it can be divided in 5 subareas: hematology/oncology, solid tumors, genetics, pharmacogenetics and infectious diseases. It is particularly interesting for the later application since it can be used to identify pathogens that are difficult to culture [1]. Molecular diagnostics in a medical context refers to assays that use biomarkers either nucleic acids or proteins to a wide variety of applications such as identification and characterization of pathogens –agent causing diseases, antibiotic resistance, virulence of a strain-, monitoring a host response indicative of disease, of the response to a drug –changes in proteins and/or gene expression-, study genetic markers related to predisposition to a disease, etc. Tests can be immunoassays if they look for a protein-based marker or nucleic acid-based assays (Nucleic Acid Testing-NAT) if they interrogate the presence of a genetic marker either pathogen or human. A great effort and progress has been made to develop both types of molecular diagnostics assays [2, 3]. These NAT assays comprise several steps: lysis when the target are intracellular nucleic acids, nucleic acid isolation, reverse transcription if the target is RNA, nucleic acid enzymatic amplification, and real-time or end-point detection of the amplification products [4].

Nowadays, the quickest test looking for biomarkers are immunoassays. However, nucleic acid-based assays offer some advantages over immunoassays [4]:

- They have a greater sensitivity thanks to the target sequence amplification what implies that less amount of sample is required and that they can be used for an early detection.

- They have a higher specificity.

- When the target sequence is already sequenced, these assays can be adapted to detect almost any target and they usually require less time to optimize primers for amplification and probes for hybridization; in comparison with immunoassays which usually use monoclonal antibodies needing thus longer development time.

- They can easily be automated.

- They can be configured in a multiplex format so that multiple targets can be analyzed simultaneously

- They can be done on inactivated or sterilized samples which is an important safety advantage.

The drawbacks of nucleic acid-based assays compared with immunoassays might be [4]:

- They require more sample preparation such as cells lysis; nucleic acids extraction; removing of substances present in the sample –i.e. heme in blood- that inhibit PCR, reverse-transcription…; concentration of nucleic acids to do amplification reactions and later detection in small volumes. On the other hand, immunoassays can be done on unprocessed samples.

- They need more instrumentation that needs to have a precise temperature control system such as thermocyclers for amplification of nucleic acids, more labor and sometimes expertise personnel.

There has been an increasing effort in developing on-site Nucleic Acid-based Tests (NATs). New devices able to implement these in vitro diagnostic tests are being developed aiming to create assays with improved diagnostic performances (sensitivity and reliability), cost-effective, easy-to-perform, that can be carried out with portable instruments and that require little sample processing [4, 5].

There are two kinds of nucleic acid-based assays based on how detection is achieved either by target amplification or signal amplification. Whereas target amplification techniques use enzymes to increase the number of target molecules; signal amplification approaches use highly sensitive reporter molecules or probes to detect the starting target concentration [1, 2].

NATs are applied to a wide range of human conditions such as infectious diseases, inherited diseases and disorders (by identifying mutations that can cause inherited disorders such as cystic fibrosis, sickle cell disease, thalassemia, Tay-Sachsdisease, etc), prenatal diagnosis (to determine the health of the unborn fetus), tissue typing, oncology (such as cervical cancer screening using real-time PCR for HPV which has replaced the Pap smear), cardiology, etc The information obtained from an assay can be increased by multiplexing which is attracting in detection (such as in coinfection conditions), identification (for example distinguishing closely related pathogenic strains), drug susceptibility testing of microbial pathogens, etc. Multiplexing of nucleic acids can be achieved at the chemistry of the assay, when detecting the signal or when processing the data [2, 3, 6].

Regarding the assay chemistry, if a target amplification approach is followed the marker is amplified to increase the amount of template and then it is detected using a labeled probe; whereas

if a signal amplification strategy is used, the target remains at the original concentration and it is the signal obtained from the probe what is amplified [2]. The most common target amplification technique is multiplex PCR followed by an "end point" detection by gel or capillary electrophoresis. Because electrophoresis is not a high-throughput technique, other platforms have been coupled to PCR like flow cytometry, microarrays, reverse line blot hybridization…This is useful for determining the presence or absence of a target, but sometimes quantification is required for example in mixed infections or in cell-free nucleic acids used as biomarkers for pathogen detection, monitoring tumor progression, early diagnosis, etc. In this case, multiplex RT-PCR is increasingly being used although it has a limited plex level [2].

The detection component of most diagnostic tests is based on optical methods, mainly fluorescence, chemiluminiscence and colorimetry. They can inform about the presence or absence of a target, but some can be used to quantify the signal. Detection multiplexing can be achieved by simultaneously detecting multiple signals or by detecting multiple samples.

Presymptomatic detection of infectious diseases and genetic screening are needed to allow an early intervention. The increasing information on human and pathogen genetics supports the development of nucleic acid-based assays, which not only facilitate timely detection but they also offer higher confidence in results and more information per assay. [2].

Prior to amplification, NAT usually requires a sample preparation procedure to disrupt the cells (pathogens, infected cells…), extract and purify nucleic acids. To do so, disruption techniques such as chemical (chaotropic salts), mechanical (grinding, heat, sonication, microwave…) can be used followed by mechanical or magnetic separation to isolate the purified nucleic acids. NATs have been miniaturized using different LoC techniques like conventional closed channel microfluidic methods, droplet microfluidic techniques…but almost all of them require off-chip sample preparation [7].

1.1. Nucleic acids

In 1953 James Watson, Francis Crick, Maurice Wilkins and Rosalind Franklin discovered the structure of DNA [8] emphasizing two features: 1) the complementarity of the nitrogenous bases on the two strands (adenine complementary to thymine and guanine complementary to cytosine) and 2) the double-helical nature of the DNA polymer (right-handed double helix).
DNA and RNA are polynucleotides strands. DNA molecules are formed by two strands whereas RNA is single stranded. Nucleotides are composed of five-carbon sugars to which are attached phosphate groups and a nitrogenous base. In the case of DNA, the sugar is deoxyribose with a

single phosphate group (esterified at the 5' hydroxyl) and the bases can be adenine, guanine, cytosine and thymine. The bases are linked to the C1' of the sugar by the N9 of purines or the N1 of pyrimidines. In RNA molecules, the sugar is ribose and one of the bases, thymine, is replaced by uracil. The order of these bases determines the DNA's instructions (genetic code). Therefore, the backbone of each strand is a repeating phosphate- sugar polymer covalently linked by phosphodiester bonds between the hydroxyl group at position 3' of one nucleotide and the phosphate of another nucleotide. DNA molecules adopts a three dimensional structure, a right-handed double helix. The two strands of a DNA molecule are hold together by the hydrogen bonds between the nitrogenous bases portions of the nucleotides (adenine pairs with thymine by two hydrogen bonds whereas cytosine pairs with guanine though three hydrogen bonds). As a result, all the bases are on the inside of the helix and the sugar-phosphate backbones are on the outside. The members of each base pair can fit within the double helix if the two strands are antiparallel, this is that the polarity of one strand is oriented opposite to that of the other strand (the 5' end with the terminal phosphate group of one strand aligns with the 3'end with the terminal hydroxyl of the other strand). Hydrophobic and van der Waals interactions between the stacked adjacent base pairs also contribute to the stability of the DNA structure. The helix turns every 3.4 nm, having 10 pairs per turn, this is known as the B form of the DNA. On the outside, the spaces between the two strands form a major and a minor groove. Other alternative structures are possible, the A form is found in very low humidity conditions, it is more compact with 11 bases per turn; and the Z form which is a left-handed helix [9, 10].

1.1. Factors involved in strands stability and helix formation

There are different factors to take into account when a duplex is going to be formed:

a) **Hydrogen bonding:** it is mainly an electrostatic interaction between an acidic proton and a good electron donor [11].

b) **Base stacking:** aromatic π-π stacking occurs mostly between bases of the same strand of the helix, although it also happens between bases in opposite strands of a duplex due to the helical twix. Strengthening intrastrand base stacking would contribute to preorganization of the single strand and so to its binding to a target. Factors such as dispersion forces, dipole-induced dipole attractions, solvophobic effect and electrostatics might influence base stacking [11].

c) **Electrostatic effects:** the negative charges of the phosphate groups in nucleic acids have to be neutralized by counterions such as metal ions, organic amines, positively charged

proteins, etc. This fact reflects the strong influence of ionic strength on DNA/DNA duplex formation (strongly stabilized when increasing salt concentration) [12]. The repulsion between negative charges of nucleic acids phosphodiester backbone of two strands can affect double helix formation. It is an enthalpic factor that can destabilizes, depending on the ionic strength, the final duplex. So, modifications such as neutral or positively charged backbones have been carried out [11].

d) Entropy and enthalpy: The formation of nucleic acid duplexes is entropically unfavorable because of the fixation of bond rotations. However, it is entalpically very favorable because of the formation of many hydrogen bonds and the π-π stacked contacts. So nucleic acid complexation is an enthalpically-driven process [11].

e) Solvation: in the single stranded form, nucleic acids are well-solvated due to the formation of hydrogen bonds with many water molecules; some of these bonds are lost when forming the duplex and bonds between the two strands [11].

f) Affinity and selectivity: many oligonucleotides applications benefit from increased affinity and selectivity (ability to discriminate closely related sequences). A high affinity means a slow dissociation from a target and so longer time for detection or for inhibition of a biological process, ability to bind even at low concentrations. However, increasing affinity can be tricky since if the compound does not have enough selectivity, it can bind to undesired targets. Rigidifying the oligonucleotides prior binding to their targets makes them have a structure more similar to that of the bound conformation which compensates the entropic effect mentioned since less bond rotations are fixed during complexation and this would contribute to enhance affinity. Different approaches have been tried in order to preorganize nucleic acid strands and so improve their affinity and/or specificity[11]:

- **Base stacking** interaction in nucleic acids is mainly intrastrand; as a result, by strengthening it, oligonucleotides will preorganize into a more helical conformation and so lowering the entropic cost of duplex formation. Different strategies can be followed to enhance base stacking [11]:

1) Adding substituents to nucleobases: introducing methyl or alkyne groups at C-5 of pyrimidines are stabilizing because of the higher polarizability which increases van der Waals interactions with neighbouring bases. Regarding purines, changing the nitrogen at N-7 by a carbon and functionalizing it with different methyl, bromine or chlorine groups can additionally stabilize the helix.

2) Increasing the surface area of the bases, for example by adding aromatic heterocyclic groups at C-5 of pyrimidines stabilizes the helix by enhancing stacking.

3) Using non-polar base analogues: the addition of strongly stacking bases, such as aromatic hydrocarbons, at the end of the helix can stabilize the helix even if these bases are not involved in base pairing.

- **Limiting bond rotation prior to complexation**. There are different options [11]:

1) Backbones with restricted rotation freedom which replace the phosphodiester backbone: it is common to use amide bonds due to the restricted rotation in the carbonyl-nitrogen bond, this is present in peptide nucleic acids (PNAs) and amide linkages.

2) Bicyclos: rigidifying the flexible furanose ring, for example, Leumann et al. added an ethylene bridge from C3' to C5' which adds a second five-membered ring to the natural structure.

3) Hexoses: five-membered rings (pyranose) are more flexible than six-membered ones (furanose).

4) Circular structures: cyclizing a chain limits its conformational freedom. One example was the addition of loops which close the ends of the strand and create dumbbell-like structures.

1.2. Nucleic acid mimics

Native oligonucleotides and their analogues are widely used: 1) in research as tools for biochemistry and molecular biology; 2) in molecular diagnostics for identifying genes-causing diseases and pathogens; 3) in therapy (antisense or antigene strategies). These applications rely on the ability of these compounds to form specific and stable helical complexes. When two nucleic acid strands hybridize by base pairing they usually adopt a right-handed double helix form. Because of base pairing, the sugar-phosphate backbone of both strands brings closer increasing the electrostatic repulsion between the phosphate groups and so counterions must bind to nucleic acids strands through Coulomb interaction [11, 13, 14].

To circumvent limitations of standard nucleic acids, different nucleic acid analogs have been explored. When designing them, efforts are focused on overcoming limitations of natural nucleic acids, easing the synthetic process, enhancing affinity and selectivity, increasing the resistance to

degrading factors such as nucleases, improving the thermodynamic properties, improving their pharmacokinetic behaviour and furnishing the ability to cross biological membranes. They can have a modified or replaced the nitrogenous base (C5-modified uridine nucleosides, *N*3-modified cytidine nucleosides, nonpolar nucleosides replaced with an aromatic hydrocarbon group, etc.) or they can have a modification on the sugar-phosphate backbone (2-*O*-modified RNA, phosphorothioate DNA, morpholino oligonucleotide, peptide nucleic acid, locked nucleic acid, etc.) [13, 14].

Regarding the effects of these chemical modifications on the binding affinity it has to be considered the factors that affect the thermodynamic stability of the duplexes. First, the hydrogen bonding and base stacking (π-π stacking); when base modifications that increase the number of hydrogen bonds or the π-surface area (adding an extra aromatic ring) of the bases are introduced, the affinity usually increases. Non-hydrogen bonding analogs have also been developed having an aromatic hydrocarbon group instead of the nitrogenous base, because the lack of hydrogen bonding groups they can pair with any nitrogenous bases with no discrimination. Less-polar compounds stack more strongly and the pyrene stacking is one of the strongest; however, the interaction with a strong stacking group can disrupt the helical structure of DNA. Second, the electrostatic repulsion between backbones is a destabilizing factor; this can be circumvented by replacing the backbone with a neutral or cationic backbone. Third, the hydration of the duplex since any modification should be hydrated in the duplex form. These factors contribute to a negative enthalpy change on hybridization, which is the driving force for duplex formation. However, hybridization is also accompanied by an unfavorable loss of entropy. This drawback might be surpassed by rigidifying the backbone so when it is in a single stranded form it is already preorganized in a helical base stacked conformation [13-15].

Because of these properties nucleic acid analogs are tools for molecular biology, DNA based diagnostics, genomics, and therapeutics. These modified oligonucleotides can be used to control gene expression. Their mechanism of action is mainly via Watson-Crick base pairing with a specific mRNA and the subsequent inhibition of translation (antisense) or with a duplex DNA by Hoogsten base pairing forming a triple helix and inhibiting transcription (antigene) [13-15].

However, the nucleic acid mimics that have had a wider application in the molecular biology field have been the ones with modifications on the sugar-phospate backbone, in particular, morpholino oligonucleotide, locked nucleic acid and peptide nucleic acid.

1.2.1. Morpholino

Morpholino was devised by James Summerton in 1985. It was designed to circumvent cost problems associated with DNA analogs since their synthesis use cheaper ribonucleosides to which an amine is introduced by a ribose-to-morpholine transformation and monomers are coupled by the nitrogen without needing catalyst or post-coupling oxidation (Figure 1). Thymine is usually used instead of uracil to favor RNA invasion and increase Tm. The nonionic phosphorodiamidate-linked morpholino oligoes are soluble in water because of their good base stacking, better than that in DNA.
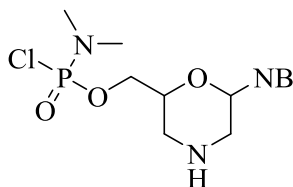
Figure 1: Morpholino subunit. NB: nitrogenous base.

Morpholino oligoes are resistant to nucleases. Their binding affinity is relatively insensitive to the ionic strength of the medium. The morpholino-RNA duplexes are more stable than the duplexes DNA-RNA.

They act by a steric blocking mechanism and do not activate RNase H. This is advantageous because it prevents many sequences which are only partially complementary to be cleaved. Morpholinos are used for ansisense applications, correcting splicing errors in pre mRNA in cultured cells and extracorporal treatment of thalasssemic patients' cells. They have also been used to target zygotic RNAs without inhibiting the maternal RNAs coded by the same gene by targeting the intron-exon splice junctions which are absent in maternal mRNA. Thus morpholinos revolutionized the developmental biology field providing a tool to block the expression of a gene during embryogenesis in model organisms such as zebra fish, frog, sea urchin, chick, etc. [14, 15].

1.2.2. Locked nucleic acid (LNA)

LNA was described in 1998 by Singh et al. They are conformational restricted oligonucleotide analogs: they consist of bicyclic units which have a bond between the 2'-oxygen and the 4'-carbon atoms (Figure 2) [14].
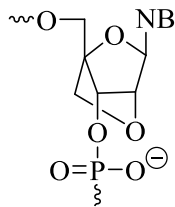
Figure 2: Chemical structure of Locked nucleic acid monomer. NB: nitrogenous base.

They can be synthesized either as fully modified LNA or as LNA-DNA and LNA-RNA chimera, since fully modified LNA longer than eight oligonucleotides tend to aggreagate. The LNA–RNA and LNA–DNA hybrids retain features of natural nucleic acid duplexes, such as Watson–Crick base pairing, base stacking, and a right-handed helical conformation. LNA are a kind of RNA mimic which fits into an A-type duplex geometry. LNAs stabilize duplexes by preorganization or improved stacking. RNA strands are barely perturbed by varying the number of LNA monomers in the complementary strand which corroborates the fact that the RNA strands in duplexes are rigid and A-like. On the other hand, when LNA monomers are incorporated into dsDNA duplexes, the B-like character decreases as LNA monomers are incorporated [14].

There are some guidelines when designing LNA oligoes: the LNA part should hybridize with the position where specificity and discrimination are needed; because of their strong hybridization, they should not have more than four continuous LNA; LNA self-complementarities should be avoided.

Oligonucleotides containing LNA have high affinity and thermal stability towards complementary DNA and RNA strands and good mismatch discrimination. As a result, they can be used in any hybridization assay which requires high specificity and/or reproducibility as dual-labeled probes (for example incorporation LNA into Taqman® probes), in situ hybridization probes, molecular beacons and PCR primers. They have also been used in antisense drug development and therapeutics. In addition, LNA oligonucleotides are stable in serum, have low toxicity in vivo and can be taken up by mammalian cells. They can be used for regulating gene expression by silencing mRNA which can be achieved by inhibition (probably by steric blocking of the template RNA), splicing alteration, translational arrest, redirection of polyadenylation and degradation of mRNA by ribonuclease H (LNA activate the ribonuclease H and DNA-RNA hybrids are recognized and RNA strand suffer a endonucleolytic cleavage yielding a 3'-hydroxyl and a 5'-phosphate at the hydrolysis site) [14].

1.2.3. Peptide Nucleic Acids (PNAs)

Peptide nucleic acids (PNAs) were developed by Peter Nielsen during the 1980s. PNA are structural mimics of nucleic acids where the sugar-phosphate backbone has been replaced by a polyamide

backbone consisting of N-(2-aminoethyl)glycine units to which nitrogenous bases are attach *via* a methylene carbonyl linker (Figure 3A).

There are two kinds of PNAs depending on how the nucleobase is attached to the backbone: 1) PNAs whose backbone consists of amino-acid residues which carry the nucleobase in the side chain. 2) PNAs which consist of N-(aminoalkyl) amino acid units to which secondary nitrogen nucleobases are attached with the carboxyalkyl linker (Figure 3B).

A)

DNA: sugar phosphate backbone   PNA: N-(2-aminoethyl)glycine

B)   **PNA**
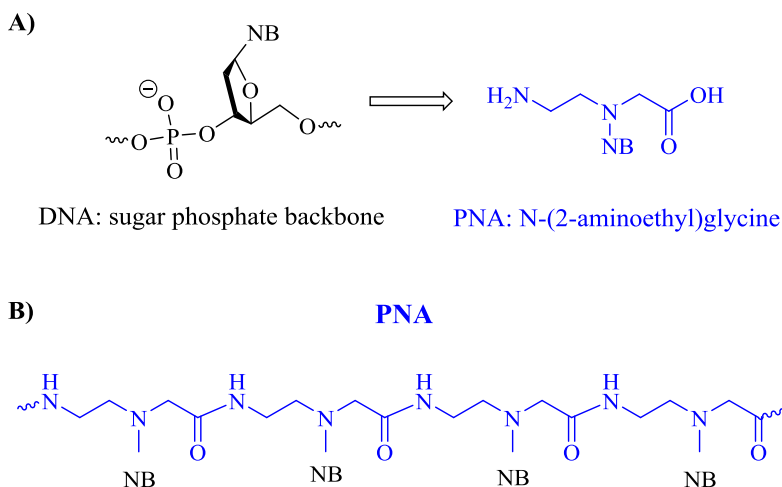
Figure 3: A) Chemical structure modifications from DNA to PNAs: the sugar phosphate backbone is replace by N-(2-aminoethyl)glycine units. B) General structure of a PNA backbone, the nitrogenous bases are covalently linked to the Nitrogen atom of the glycine, monomers can be coupled so that whatever desired nucleobases sequence can be synthesized.

PNAs bind to complementary nucleic acid strands (PNA, DNA, RNA) usually in an antiparallel orientation by aligning the amino end of the PNA with the 3' end of the nucleic acid following Watson-Crick base pairing rules (Figure 4). They have a higher affinity for RNA than for DNA. They are quite acid-stable. They are resistant to degradation by protesases and nucleases. Because of their uncharged nature, PNA are poor water-soluble and have a tendency to aggregate. Water solubility can be improved by introducing negative or positive charges, for example adding lysine residues either at the carboxy end or as a backbone modification instead of glycine. However, these uncharged nature and so lack of electrostatic repulsion makes PNA have a stronger binding towards DNA and RNA strands, making more stable duplexes compared with DNA-DNA or DNA-RNA duplexes A mismatch cause a high destabilizing effect in PNA containing- duplexes which remark the advantageous use of these nucleic acid analogues in diagnosis protocols to identify point mutations. The PNA-DNA and PNA-RNA duplexes are thermally more stable. They can adapt to

its partner strand, regarding sugar puckering PNA oligonucleotides adopts an A- or B- conformation in terms of sugar puckering in the PNA-RNA and PNA-DNA duplexes respectively [14, 16].
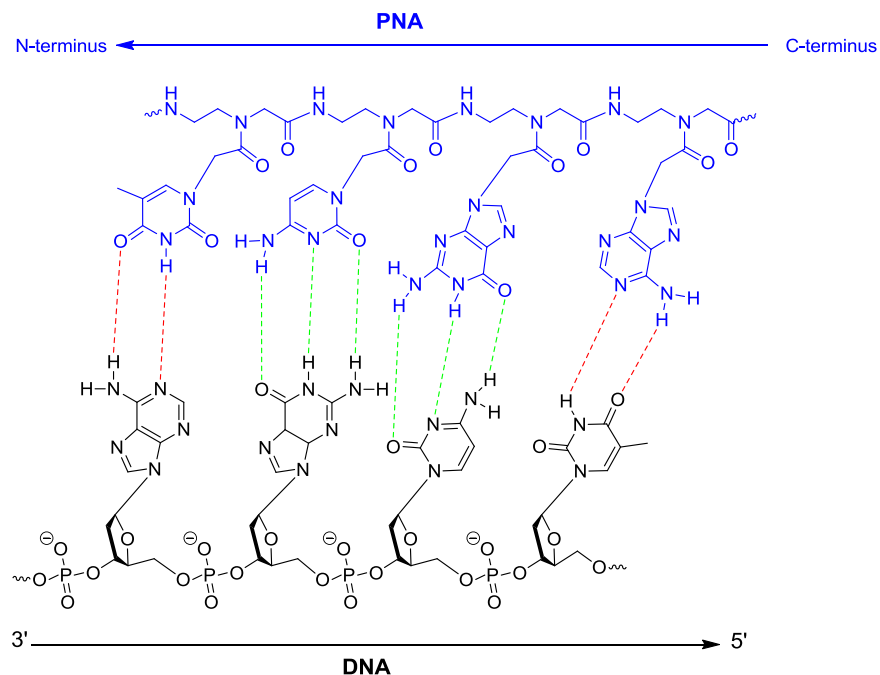
Figure 4: Example of hybridization between a PNA and a DNA strand: the 3'-end of the DNA (black structure) aligns with the N-terminus of the PNA strand (blue structure); hydrogen bonds are formed between the nitrogenous bases of both strand following Watson-Crick base pairing rules: 2 between Adenine and Thymine (red dashed line) and three between Cytosine and Guanine (green dashed line).

Regarding PNA:DNA interactions, the melting temperatures increases with the PNA length because there are more base pairings. The longer the length of the PNA, the higher the number of hydrogen bonds which is reflected by the formation of more stable duplexes and the higher enthalpy gain, while at the same time there are higher losses of degrees of freedom and so entropy loss. A balance has to be achieved since it has been observed that the longer the PNA strand the higher specificity whereas the shorter the PNA the better discrimination power for a mismatch (higher variation in the melting temperature between the fully match PNA/DNA duplex and a duplex with a single mismatch) [12].

PNAs are biologically stable and resistant to enzymatic degradation; their half-life inside the cells is of at least 48h compared to the 15 min of DNA and RNA oligonucleotides. As a result of these properties they can be used for antisense and antigene strategies. PNAs can bind specifically to their complementary mRNA and inhibit its translation. PNAs *in vivo* delivery can be improved by

coupling them to DNA oligomers, receptor ligands or peptides such as cell penetrating peptides or by incorporated them into liposomes [14].

They can work as antigene agents arresting transcription. They form structures like a triple helix structure, a strand invaded or a strand-displacement complex with DNA which creates a structural hindrance which blocks the RNA polymerase. One obstacle is that the formation of these complexes is slow at physiological salt conditions; however, PNA binding to supercoiled DNA is faster compared to linear DNA, which is advantageous since the transcriptionally active chrormosomal DNA is negatively supercoiled. PNAs were also used in therapeutics. An antibody/PNA adduct is used to assist its binding to cancer-specific antigens on the surface of cancerous cells, then a second PNA labeled with a radioisotope hybridizes with the first one which allows concentrating the isotope in the proximity to the cancer cells. PNAs have also been used for detecting single base mutation by PCR, a technique called PNA-directed PCR clamping which inhibit the amplification of a specific target by competition of the PNA with one of the PCR primer sites. They have also been used as probes for gene cloning and mutation detection. Although PNAs are not recognized by enzymes such as DNA and RNA poymerases, they can be used as primers if a normal nucleotide is added at the end of the molecule. They can be used as nucleic acid probes with great stability and good single-base mismatch selectivity. For example, they can be immobilized onto optical or mass-sensitive transducers to detect complementary strands or a mismatch in a sample or they can be used in fluorescence in situ hybridization (FISH) assays [14].

The attractive features of PNAs have made many biotech companies to include them. The major PNA products are: probes for diagnostic, libraries, arrays and molecules for messenger RNA (mRNA) and/or microRNA (miRNA) inhibition [16].

1.2.4.1. PNA characterization by MALDI-TOF

Mass-spectrometry is used to characterize materials. Thanks to the development of "techniques such as electrospray ionization (ESI) and matrix-assisted laser desorption/ionization (MALDI), a "soft ionization" is achieved with little to no fragmentation. MALDI-TOF has advantages over other mass-spectrometry methods like the ability to differentiate components in a mixture, the capability to achieve low detection limits and the compatibility with components used in biological sample such as salts and buffers. A matrix is needed to assist ionization which absorbs the energy of the laser and transfers it to the molecule to be analyzed.

PNAs have characteristics of nucleic acids and peptides so matrices for both biomolecules might be used. However, protein matrices (SA, CHCA, DHB) produced higher ion signals than DNA

matrices (3-HPA, ATT, THA) being Sinapinic acid the one which provides the best signal-to-noise ratio. PNA ionization occurs both in the positive and negative mode; it is not common to form adduct or to observe multiply-charged species. MALDI-TOF can also be used to assess sample purity: several peaks below the one of the molecular ion are found in a freshly synthesized PNA sample. These impurity peaks correspond to the byproducts (truncated PNA) obtained during PNA synthesis [17].

1.2.4.2. PNA features and chemical modifications

PNAs can invade dsDNA either by Watson-Crick base pairing to form 1:1 PNA/DNA complex or in combination with Hoogsteen base pairing to form a 2:1 complex [18]. PNA:RNA duplexes adopt an A-form whereas PNA:DNA duplexes have an form intermediate between A- and B-form [19]. Among the most interesting PNA modifications regarding ease of synthetic process, diversity of functional group and conformational preorganization is the introduction of a chiral center at the γ position of the PNA backbone (Figure 5). Indeed, PNAs, which as individual strands do not have a well-defined conformation, can be preorganized into a right (RH) or left (LH) helical motif by introducing a stereogenic center at the γ-backbone. These RH- (Figure 5B) and LH- (Figure 5C) γ-PNA oligonucleotides hybridize with another nucleic acid strand which contains a complementary base sequence and matches helical sense. Specifically, installing a γ-(S)-chiral center (prepared from L-aminoacids) contributes to enhance PNAs binding affinity and sequence selectivity because of their preorganization into a right-handed helical motif (Figure 5B). Despite the strong binding affinity of γPNAs, they can discriminate between closely related sequences which is reflected by the comparison of melting profiles between a perfect match and a single-base mismatch duplexes where destabilization (ΔTm) is at least -20ºC. The stereochemistry of the lysine residues introduced at the C-terminus of the PNA strand to increase water solubiity and reduce self-aggregation does not affect the helical conformation of the PNA [20].
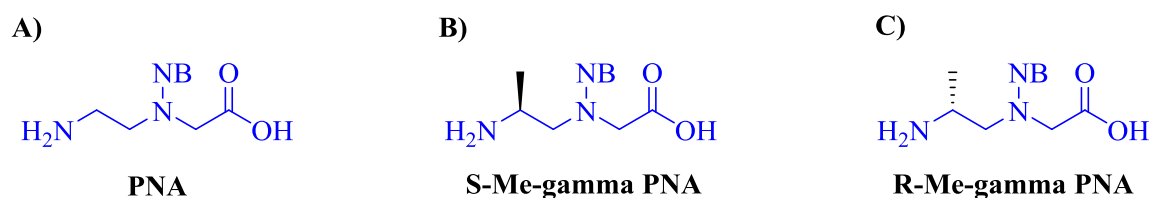
Figure 5: Standard PNA monomer and γ-position stereochemical modification of standard PNA monomer. Unmodified PNA monomer (a). The introduction of a substituent at the γ-position of the monomer backbone can help to preorganize the PNA strand into a right (γ-(S)-chiral center) (b) or a left (γ-(R)-stereocenter) helical motif (c). In addition, substituents can be either neutral or positively or negatively charged.

The introduction of a positively or negatively charged substituent at the γ position of a PNA monomer also contributes to preorganize the PNA backbone and so enhance PNA:DNA duplex stability. Although the neutral backbone of PNA was supposed to be key for its high binding affinity to complementary nucleic acids due to the lack of electrostatic repulsion; it was found that backbones with negatively charged side chains do not decrease its binding affinity. Generally negatively charged PNAs bind slightly weaker to DNA than positively charged PNAs do; whereas they bind stronger to RNA. However, positively charged PNAs have a negative dependence on salt concentration whereas negatively charged PNAs have a positive dependence; as a result, at medium to high salt concentration, negatively charged PNAs binds stronger than positively charged PNAs to both DNA and RNA [19].

1.2.4.3. PNAs in base-filling reactions

PNAs could be used for replication by base filling of an abasic site. The base-filling approach has two advantages: 1) the nucleobase monomer do not contain complementary functional groups so there is no self-reactivity and less, if any, non-templated reactions happen compared with backbone ligation approach. 2) The reaction site is close to the site of base pairing which increase sequence specifity. Two approaches are mainly used to react with the versatile free secondary amine of the abasic site: 1) Base filling with acetic acid-modified nucleobases which by an amine acylation would lead to native PNAs and 2) base filling with acetaldehydes-modified nucleobases which by a reductive amination would provide deoxyPNAs. Using any of these two strategies, a single base is sequence-specifically added to the abasic position of a PNA, although reductive amination has higher yield and selectivity probably due to the reversible formation of an iminium intermediate. Base-filling reactions are more efficient if the abasic site is in the middle of the strand and when the nucleobase to be incorporated in a purine which indicates the role of base-stacking interaction in promoting the reaction. In addition, guanine incorporates more efficiently than adenine and cytosine more than thymine which induces that base-pairing interaction might also influence base-filling reactions [21].

1.3. Hybridization technologies

For detection and diagnostic purposes, specific nucleic acid sequences can be detected by a short sequence of nucleotides, probes, which hybridize with the target nucleic acids. DNA and RNA can be detected by hybridization approaches, Southern and Northern, respectively, where gel-separated nucleic acid fragments are transferred to a nitrocellulose filters and then hybridized with radio- or fluorescent- labeled probes. Two configurations can be followed for the hybridization assay: a) the

target might be immobilized and the probes labeled (dot-blot assays) or b) the probes immobilized and the target labeled (reverse-dot-blot assays). A wide range of labels can be used such as radiolabel isotopes, fluorescent tags, biomolecules like biotin to be later recognized by streptavidin conjugates, etc. On the other hand, different hybridization formats can be employed either solid- or liquid-phase [22, 23].

Solution hybridizations are faster (5 to 10 times) than hybridization on solid supports, but a separation step is usually required before the final detection. Filter or solid-phase hybridizations are in the form of dot blots; however, they might be subject to more non-specific background than other formats. Approaches to reduce this non-specific background by removing non-specifically bound probe are being developed. A common solution is the use of a sandwich format which uses three components: a solid-phase bound capture probe, a target probe and a signal-generating probe. The target probe links the solid-phase and signal-generating probes, so if not present, no signal is generated and thus background is minimized [24].

1.3.1. Probes

Probes are generally short sequences of nucleic acids (LNA, PNA, DNA, RNA…) which bind to a specific and complementary region in the target nucleic acid under study. Thanks to the high homology of the target/probe duplex, stable hybridizations are achieved. Ideally, a probe should be a single-stranded nucleic acid complementary and able to hybridize specifically and solely with the target. Their size can vary from 10 to 10.000 bases or even more, although the most common length range is 14-40 bases. Longer probes provide a more stable hybridization but they need more time to be completed. On the other hand, short probes require shorter time to hybridize although they can lead to non-specific hybridizations and are more difficult to be labeled. However, the quicker hybridization, the higher stability, the ease of preparation and the ability to identify small changes in the target make short probes to be the mainly used in commercial assays. It must be avoided probes that self-hybridize or that hybridize with non-target nucleic acids [24].

There is a wide variation for probes labeling: : isotopes such as ^{32}P, ^{35}S, ^{125}I; enzymes like alkaline phosphatase, horseradish peroxidase; biotin –either through a photoactivated compound called photobiotin or using biotinylated nucleotide analogs- which can be later recognized by enzyme-labeled avidin molecules. It is common the addition of a spacer to separate the enzyme from the probe and so avoid any potential steric hindrance for hybridization and allow full functionality of the enzyme. Labels can be either incorporated into the probe or attached to it, usually by covalent linkage of reporter molecules [24].

1.3.2. Detection strategies

A method to enhance the detection is required to detect small amounts of nucleic acids either by amplifying the target (increasing the amount of target available for detection) or by amplifying the signal (equipping the probes with an amplification system able to generate a signal upon few hybridization reactions). Table 1 shows some of the main strategies used for nucleic acid detection. Signal amplification techniques are generally less sensitive than target amplification techniques; however, they are also less intensive computationally [2].

Table 1: Main methods used for the detection of nuceic acids

Detection methods			
Target amplification		**Signal amplification**	
Non-isothermal amplification methods	**Isothermal amplification methods**	**Non-enzymatic signal amplification**	**Enzymatic-based signal amplification**
PCR	Nucleicacid sequence-based amplification (NASBA)	Hybrid capture	Cleavage reactions
Real-time PCR	Helicase dependent amplification (HDA)	Branched chain DNA (bDNA)	Ramification amplification (RAM) or hyperbranched rolling circle or cascade rolling amplification
Ligase Chain Reaction (LCR)	Rolling circle amplification (RCA)		
Linked linear amplification	Recombinase polymerase amplification (RPA)		
Strand displacement amplification	Loop-mediated amplification (LAMP)		

1.3.2.1. Target amplification

Target amplification is the most common used technique. It uses enzymes to replicate the target nucleic acid. The main techniques are: polymerase chain reaction (PCR), transcription-mediated amplification (TMA), nucleic acid sequence-based amplification (NASBA), rolling cycle amplification (RCA), ligase chain reaction (LCR), and strand displacement amplification (SDA). Initially, these reactions were based on an "end point" analysis; but it changed after the development of real-time detection formats which allow monitoring the accumulation of amplicon while the reaction is taking place. These techniques provide sensitive and quantitative detection of PCR products (the rate of increase of amplification product is proportional to the amount of target present in the sample) quickly and in closed tubes so reducing the risk of contamination. As a result, in clinical diagnostics, "conventional amplification techniques" have been replaced by their "real-

time" analogs. The main differences between them are the use of several temperatures or a single one and if the target or probes are linear or circular [1, 3].

1.3.2.1.1.. Non isothermal amplification methods

a) PCR

It was first reported in 1987 by Kary Mullis. PCR consists of successive cycles of heating and cooling of the reaction to allow DNA denaturation, primer hybridization and primer enzymatic extension, increasing thus the number of specific nucleic acid fragments present in a sample. Amplification products are then mainly detected by gel electrophoresis. It cannot be used to quantify although computer software can analyze the intensity of the band and convert it into a relative amount of amplicon [24-26]. In 1989, it was seen as the "major scientific development" of the year [24, 25]. It can be applied in clinical, veterinary, food and environmental areas [3, 22, 24]. The use of a thermostable enzyme, *Taq* DNA polymerase, permitted semiautomation and simplification of the process becoming so commonly used in laboratories. PCR has some drawbacks, being contamination issues the main one; it can happen with any extraneous DNA fragment that could be amplified with the sample. Nowadays, many PCR modifications have been developed such as PCR with nested primers, inverse PCR, anchored PCR, amplification refractory mutation system.

b) Real-time PCR

PCR was later combined with fluorescent labeling which led to real-time PCR (RT-PCR or qPCR), a system able to monitor target amplification. It was developed by Higuchi et al [27]. Although the mechanism to generate the fluorescent signal varies, the signal is proportional to the amount of amplicon generated. So, it can determine the presence and also the copy number of a specific target. Fluorescent technologies used are either non-specific based on dyes such as SYBR Green which intercalate into the minor groove of the DNA during the reaction or specific; or they can be based on the use of sequence-specific probes such as TaqMan®, HybProbes, molecular beacons and Scorpion probes. Generally, real-time PCR is preferred due to convenience and shorter protocols (for example, there is no post-amplification analysis), higher precision compared to standard PCR, it allows the relative quantification and it implies lower risk of contamination by amplification products. However, they also have a risk to provide false negative results [3, 4, 22, 24-26].

TaqMan® probes consist of an oligonucleotide dually labeled with a fluorophore at the 5' end and a quencher at the 3' end. They bind to the target during the PCR reaction and are later cleaved by DNA polymerase separating so the fluorophore and the quencher and emitting fluorescence (Figure

6A) [3, 22]. HybProbes were developed for use in LightCycler® instrument. Two independent probes hybridize next to each other on the target DNA. They are commonly used for melting curve analysis. Molecular beacons are probes with a quencher and a fluorophore that adopt a non-fluorescent stem-loop structure when they are in solution and fluoresce upon binding to the target (Figure 6B) [3, 22]. There are other alternatives to detect amplicons such as lateral flow strips where PCR products have been obtained using primers conjugated to antigens, real-time monitoring based on changes on pH, turbidity, electrical conductivity, phosphate or ATP concentration. The main drawback of real-time PCR is its low multiplexing capability [1, 4, 26].
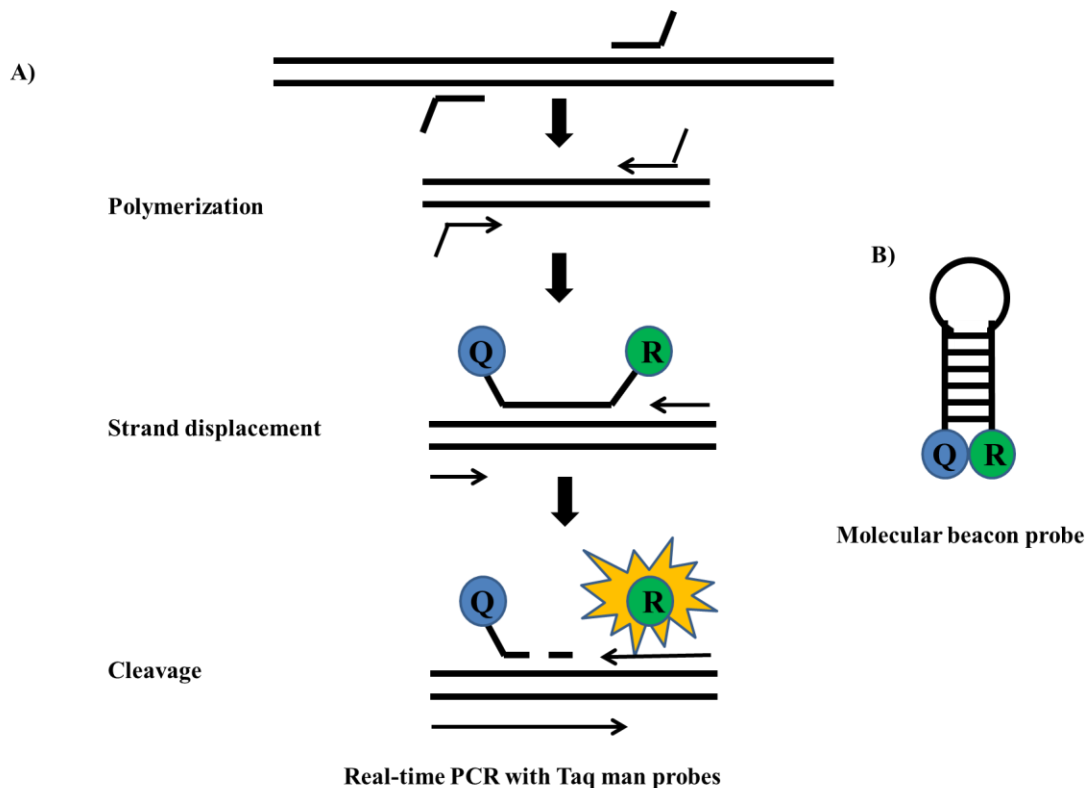
Figure 6: Sequence-specific probes to detect amplification reaction: A) Taqman probes and B) molecular beacon probes for amplification detection. Q: quencher moleculer, R: reporter molecule (fluorophore).

PCR and real-time PCR need to be done by expert technicians in laboratories equipped with hoods, centrifuges, temperature baths and thermal cyclers. Special care should be taken to avoid false results such as false-negative due to amplification inhibition by agents present in the sample; or either false-positive or false-negatives coming from contamination or mismatches between target and primers sequences. There are reagents – the sample and enzymes such as polymerase, reverse transcriptase, proteases- that need to be stored and used in cold conditions. Special measures have to be implanted to minimize cross-contamination. As a result of these factors, although PCR was

the first method used in molecular diagnostics, these factors have limited its use leading to the development of other molecular assays less demanding of for example computational capabilities and so creating tools for low-cost diagnostics in resource-limited areas [1, 4, 26].

c) Ligase Chain Reaction (LCR).

It uses a thermostable enzyme to join oligonucleotides which are close to each other. It is a cyclic reaction with a denaturalization, annealing and ligation step, being the ligation the key for the amplification reaction. Both ligated oligonucleotides and original sequences become templates for the next cycle (Figure 7A). It can detect as low as 10 nucleic acid targets. In this reaction, a single mismatch at the ligation point can prevent ligation, although this could be used to detect point mutations [24]. There is a modification called gapped-LCR (G-LCR) where several probes-primers complementary to different regions of the target bind to them in the annealing step. Then DNA polymerase elongates these probes and a ligase joins the different fragments [1].
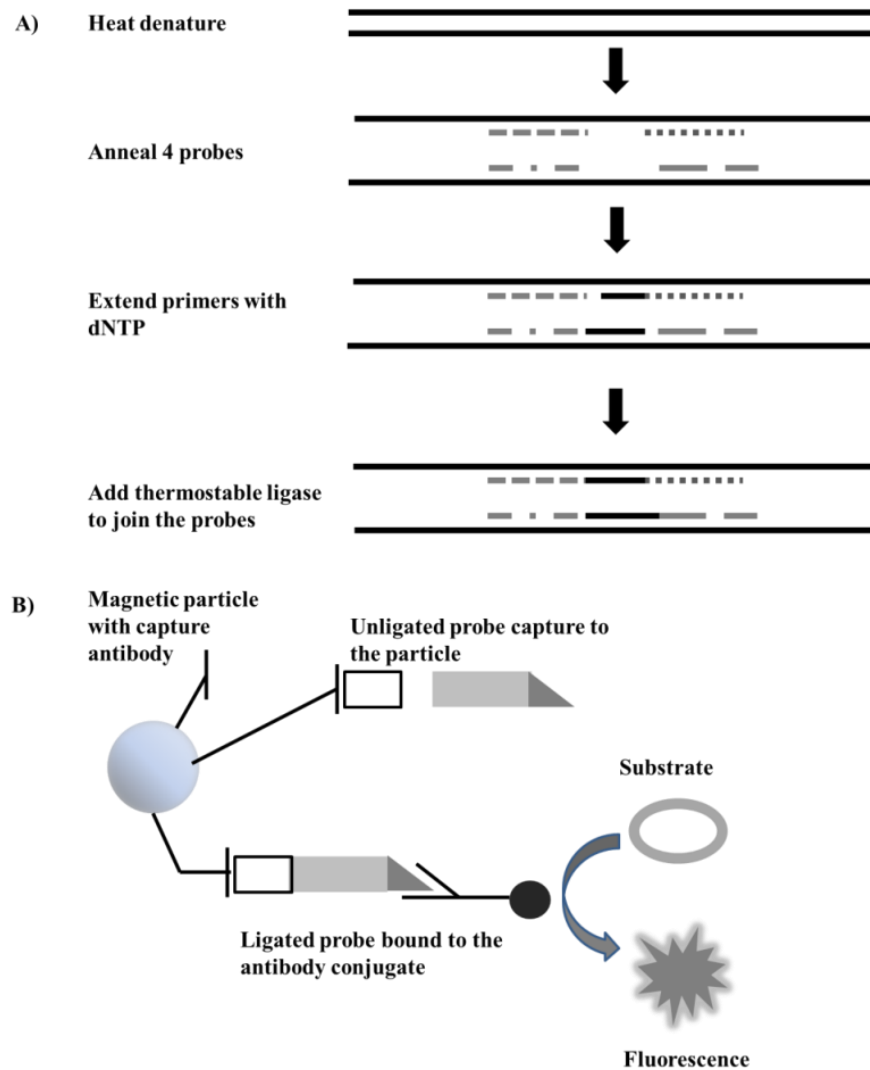
Figure 7: A) Ligase Chain Reaction, B) Ligase Chain Reaction Detection [1]

d) Linked Linear Amplification

It is a method similar to PCR but it uses multiple nested non-replicable primers. These primers contain a molecule (1,3-propanediol) that prevents replication during the elongation phase of the thermocycling reactions. The ends of the amplified strands cannot act as templates for amplification, so the products became smaller (Figure 8). This method benefits from the resistance to amplicon contamination and the ability to accommodate polymorphic targets and, thanks to the use of several primers, it avoids the false-negative results arising from these sequences [1].

1st cycle

2nd cycle
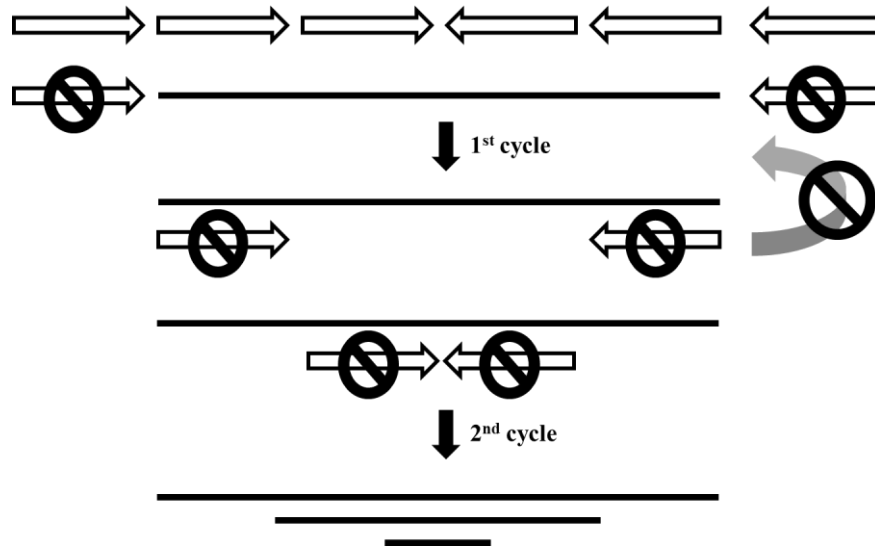
Figure 8: Linked-linear amplification [1].

e) Strand displacement amplification (SDA).

It requires enzymes and four primers to amplify the target sequence and displace the copied sequence; it also uses a chemically modified deoxynucleotide base (thiolated dCTP). There is a target generation phase where a primer with a restriction enzyme site binds to the complementary template and the strand is synthesized using a thermostable polymerase. A bumper primer displaces the strand generated from the primer that contains the restriction enzyme site. The incorporation of thiolated dCTP makes that the new strands cannot be digested by restriction enzymes. Then a thermostable restriction enzyme introduces a single-strand nick in the dsDNA. A thermostable polymerase extends the new strand displacing so the strand 3' to the nick. As a result, the strands that incorporate this restriction enzyme site lead to the generation of multiple copies of the target (Figure 9) [1].

Target generated containing engineered restriction enzyme site

Bumper primer binds and displaces the strand generated by restriction engineered primer

Restriction enzyme cleaves primer
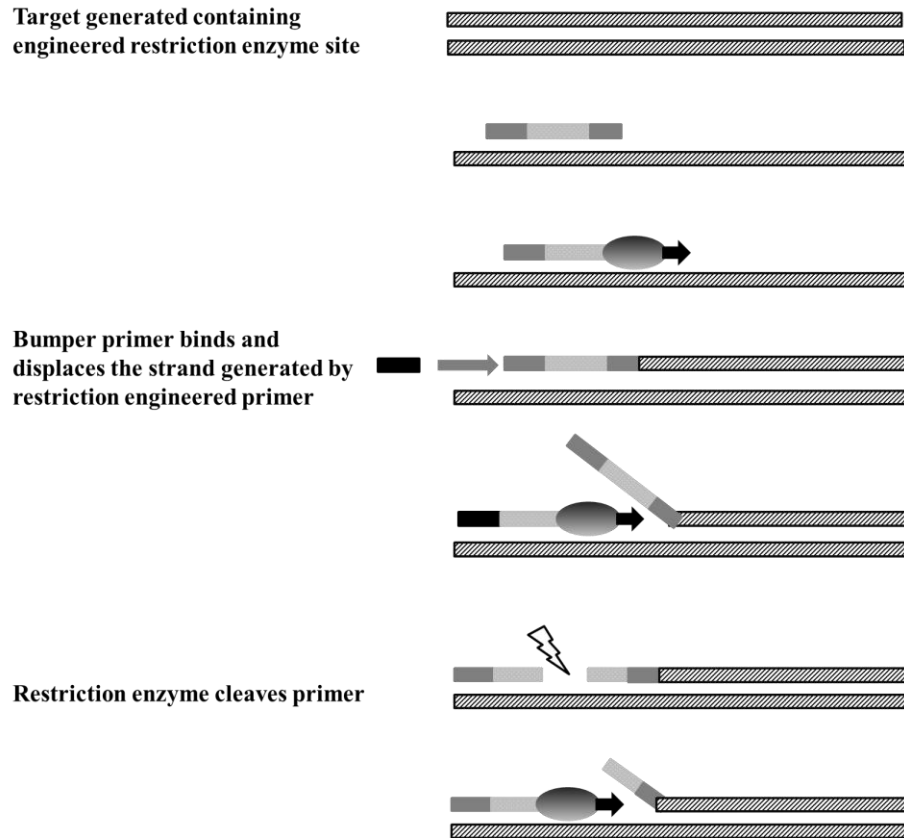
Figure 9: Strand displacement amplification (SDA) process [1].

1.3.2.1.2. Isothermal amplification

These technologies use a single reaction temperature for the amplification phase so simpler and cheaper instrumentation –water bath with resistive heaters or via exothermic chemical heating- can be used in comparison with thermal cycler used for PCR amplification. They have a high throughput since all steps can be done in the same tube [1, 26]. Some isothermal amplification methods are:

a) Transcription-based amplification systems

Transcription-based amplification methods include nucleic acid sequence-based amplification (NASBA) and transcription-mediated amplification (TMA). Both methods firstly reverse-transcribed RNA into DNA which is used as template for generating many RNA copies using a RNA polymerase and an isothermal RNA amplification. They differ in the reverse transcriptase they used, NASBA is from avian myeloblastosis virus and in TMA the enzyme is from Moloney murine leukemia virus. NASBA also requires the addition of RNase H (Figure 10) [26].
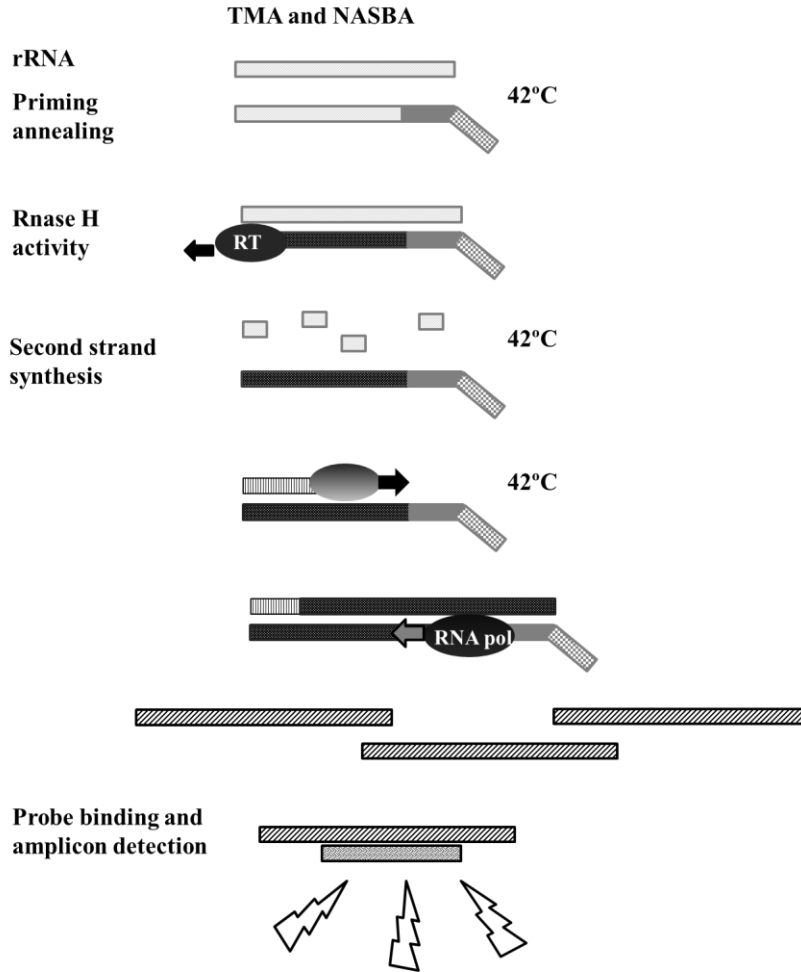
TMA and NASBA

Figure 10: Isothermal one-dimensional target or probe: TMA and NASBA [1].

a1) Nucleic acid sequence-based amplification (NASBA)

It was developed in 1991. It is an isothermal, enzymatic RNA-based nucleic acid amplification technique. It uses a reverse transcriptase, ribonuclease-H, RNA polymerase and two DNA oligonucleotide primers. The forward primer has an extension at 5'end which is the sequence of the promoter for the bacteriophage T7 DNA-dependent RNA polymerase. The reverse primer has another extension at the 5'end which is a sequence complementary to a DNA oligonucleotide probe labeled with a ruthenium-based electrochemiluminiscent (ECL) tag. Along with the amplification of the target sequence, the primer extensions are introduced in the amplicon allowing thus an efficient transcription of the template and detection by the ECL-tagged probe (Figure 11). 10^{12}-fold amplification can be achieved. Although is very sensitive, specific and quick technique; the ECL-NASBA applicability is limited by the cost of the equipment used for the ECL detection. An alternative is enzyme-linked oligonucleotide capture (EOC) detection where amplicons hybridize

with biotinylated capture probes bound which immobilize them onto streptavidin-coated surfaces. Then a digoxigenin-labeled probe and a conjugate anti-DIG antibody-alkaline phosphatase are added to produce a colorimetric end product which can be read using a spectrophotometer. Real-time NASBA uses DNA probes that have a stem-loop structure with a fluorophore and a quencher and upon hybridization, the probe unfolds, fluorescence quenching is interrupted and the probe fluoresces. Due to the simpler equipment required, EOC-NASBA is widely used compared to ECL-NASBA and RT-PCR. It is an amplification method able to be performed in developing countries and budget restricted laboratories which provides consistent results and with high sensitivity (higher than RT-PCR and comparable to methods such as virus culture which require days to complete). The main drawback of NASBA is that it is an RNA-based amplification procedure which limits its applicability to detect RNA targets such as RNA pathogens [25]. They use a primer with an RNA polymerase binding site and a region complementary to the target rRNA which acts as primer for the cDNA generation using a RNA polymerase. Then RNase H degrades the rRNA template. Using DNA polymerase and another primer, a dsDNA, which is a copy of the rRNA but with an RNA-polymerase binding region, is generated. This dsDNA finally acts as template for a RNA polymerase to generate RNA molecules. A probe complementary to the target is used to detect the amplified sequence [1, 24].
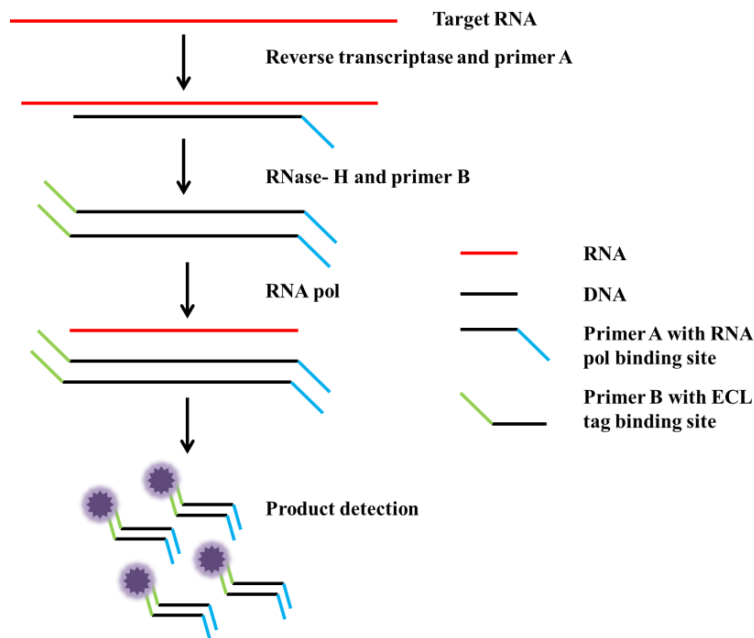
Figure 11: Nucleic acid sequence-based amplification (NASBA): the sequence of the target RNA is amplified by a reverse transcriptase and a primer and the RNA is hydrolyzed by RNase-H. Then, a reverse transcriptase and a second primer generate dsDNA which harbors the RNA polymerase as well as the ECL binding sites. A new RNA template is generated and the sequence of events is repeated [25].

b) Helicase dependent amplification (HDA)

Helicases were discovered in *Escherichia coli* in 1976 [28]. HDA takes advantage of the DNA helicase to separate complementary strands of double-stranded DNA (dsDNA) mimicking the denaturation mechanism in living organisms and avoiding the use of temperature cycling to produce single-stranded DNA (ssDNA). The helicase enzyme in the presence of ATP bind to DNA and moves through breaking the hydrogen bonds which link the two strands. The resulting ssDNA is coated by single-stranded binding proteins (SSBs). Two sequence-specific primers hybridize to the 3'-end of each ssDNA and they are subsequently extended by DNA polymerases producing dsDNA, which is a new substrate for DNA helicases (Figure 12) [28].
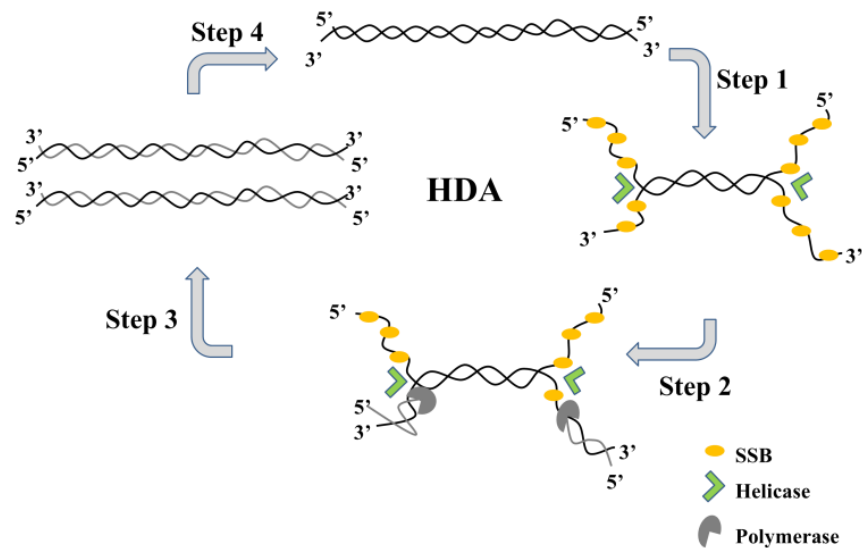
Figure 12: Scheme of the helicase-dependent amplification (HAD) process [28].

c) Rolling Circle Amplification (RCA)

A single-stranded nick initiates the replication by extending the strand upstream from the nick and occurs from the 5' to the 3'. The 3' nicked strand and the downstream from the nick are displaced as the new strand is being synthesized and rolled around the circular DNA molecule. A single-stranded tail that forms concatemeric units of the initial circle is formed which acts as template for the synthesis of a complementary strand (Figure 13) [1].
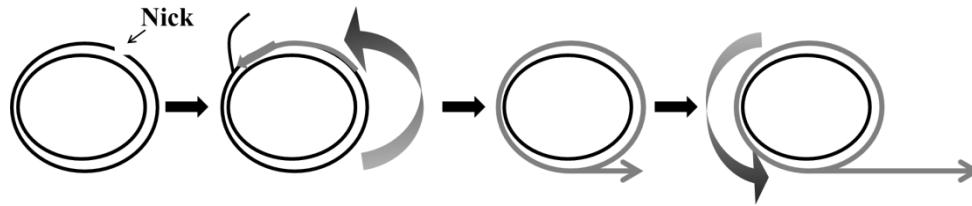
Figure 13: Scheme of the rolling cycling amplification (RCA) process [1].

d) Recombinase polymerase amplification (RPA)

It was introduced by Piepenburgh et al. in 2006 [29]. This method works at low temperature (37ºC) and combines the isothermal recombinase-driven primer targeting of the template with the strand-displacement DNA synthesis [28]. RPA uses nucleoprotein complexes formed by primers and recombinase proteins to facilitate the primer binding to the template DNA. These complexes scan the dsDNA by promoting the primer binding at the target sequence of dsDNA and the displacement of the non-template strand. This displaced strand is then stabilized by SSBs proteins and the recombinase disassembly leaves the 3'-end of the primer accessible to DNA polymerase. An exponential amplification is achieved with the cyclic replication of the process [28].

e) Loop-mediated amplification (LAMP).

An isothermal amplification method developed in 2000. It uses two sets of primers and a DNA polymerase with strand displacement activity. A pair of outer primers together with the DNA polymerase displace the amplified strand releasing ssDNA which adopts a hairpin form and so starts the loop for a cyclic amplification. The amplification occurs cyclically with each strand being displaced during elongation and adding new loops in each cycle. The product generated is stem-loop DNA with repeated inverted repeated sequences of the target. The LAMP product can be detected by different methods: 1) the by-products formed, pyrophosphate ions, can bind to magnesium ions and form white precipitate that can be visualized or via turbidity measurement which can quantify 2×10^3 to 2×10^9 copies of the initial DNA template; 2) by SYBR Green I incorporation; 3) by visual detection using low molecular weight polyethylenimine (PEI) which forms an insoluble complex with high molecular weight DNA (such as LAMP product) but not with a single-stranded anionic polymer of low molecular weight (such as DNA probes). In case of multiplexing, several probes labeled with different fluorophores are used, the fluorescence of the precipitate would vary depending on the probe hybridized to the LAMP target. It is a very specific assay since amplification does not happen unless the six regions on a target DNA are recognized by the primers; although designing workable primers can discourage LAMP use [25].

1.3.2.2. Signal amplification

These methods increase the detection of a target molecule rather than the molecule, improving so the sensitivity of the probes. A single hybridization event can be detected if the signal is amplified sufficiently [24]. They can be non-enzymatic signal amplification where the target is immobilized or localized using complementary probes. These probes can be either fluorescent or labeled with a molecule that is later recognized and developed by an alkaline phosphatase that generates a colorimetric or chemiluminiscence reaction. The other category is enzymatic methodologies that use enzymes to replicate or generate a reporter molecule but these are prone to false-positive when the reporter molecule contaminates the sample [1].

1.3.2.2.1. Non-enzymatic signal amplification

a) Hybrid capture

*T*he hybrid capture kits form Digene Inc (Gaithersburg, MD) can be used to detect HPV, CT/GC and HSV. Full-length RNA probes are used to detect HPVs and determine its oncogenic risk. These probes remove the possibility of false-negatives since hybridization is not inhibited by SNPs. An antibody specific to the duplex viral DNA-RNA probe and attached to the surface of a well plate captures this hybrid. Then another antibody conjugated to alkaline phosphatase recognizes the captured hybrid which is detected through a chemiluminescent substrate (Figure 14B).

b) Branched Chain DNA (bDNA)

It introduces multiple labels on the target nucleic acid and its limit of detection was similar to other amplification methods (for example, 50 molecules/mL of HIV). The sensitivity comes from the branched reporter probes: each probe can have 15 branches and each branch can later react with up to three probes labeled with enzymes such as alkaline phosphatase. As a result, each target is heavily labeled (Figure 14A) [30]. Another approach consists of using dendrimers which are built from DNA probes that hybridize and form layers in a geometric expansion creating a three-dimensional network onto which multiple labels can be attached [30]. Clinical assays from Bayer Diagnostics use bDNA technologies to detect HIV and HCV using several subtype-specific probes to capture the target molecule. These probes avoid genetic variations to result in false-negatives or inaccurate quantification. Oligomers complementary to the target and to an adaptamer hybridize to the captured target. Then, adaptamers hybridize to this intermediate molecule and are extended forming a branch by using extra alkaline phosphatase conjugated oligomers [1].

A) Branch chain DNA (bDNA)

Single stranded
RNA target

Hybridization

Capture probe

Adaptamer links to
alkaline phosphatase
and hybridizes

Addition of substrate produces a
colorimetric or chemiluminiscent reaction

B) Hybrid Capture

Hybridization

DNA   RNA probe

Antibody to DNA/RNA
duplex caputres the hybrid

Antibody conjugated to
alkaline phosphatase is
used to detect hybrid

Figure 14: No-enzymatic signal amplification methods [1].

1.5.2.2. Enzymatic-based signal amplification

They detect conformational changes in the target.

a) Cleavage reactions

They detect single-base changes in the Invader assay using linear probes. Flap enzymatic reactions use enzymes that detect changes in the secondary structure of the molecules that have hybridized. An invader oligomer overlaps a single base of interest in a target, and then a probe hybridizes with the target's base of interest. These three molecules form a structure that is recognized by a cleavase enzyme which cleaves the primary probe. These cleaved probes then match to the detection molecule which has a fluorochrome and a quencher flanking the single base of interest. Again, the structure of three strands of molecules gives a product cleavable by the cleavase enzyme which cleaves the secondary molecule releasing the fluorochrome and so detecting fluorescence. These reactions do not occur if the primary molecule does not bind to its complementary base (Figure 15) [1].
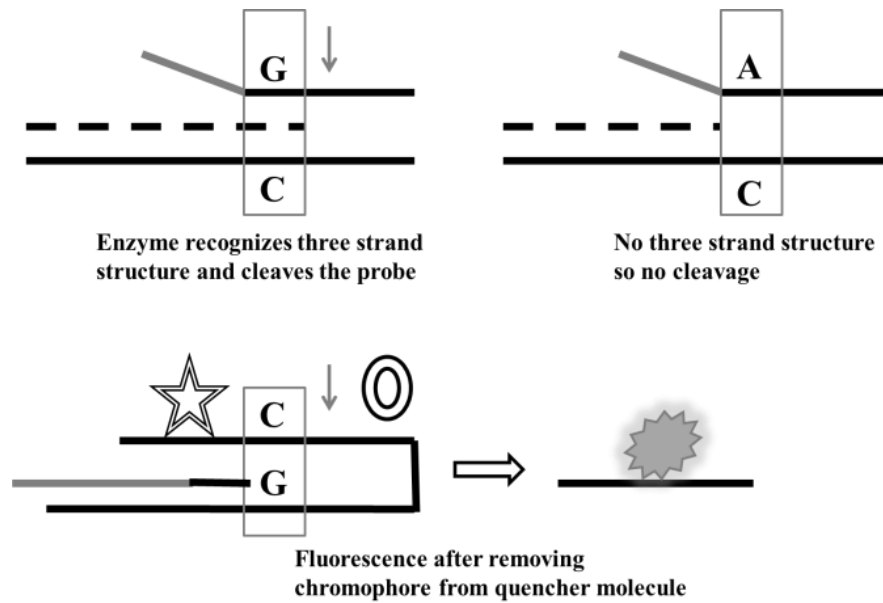
Figure 15: Enzymatic signal amplification-digestion-cleavase [1].

b) Ramification amplification (RAM) or hyperbranched rolling circle or cascade rolling amplification

It combines rolling circle amplification and strand displacement amplification to amplify a circular DNA probe that acts as reporter molecule. It uses a ligase that closes a circular probe which will then act as template for amplification with reverse and forward primers (Figure 16) [1].
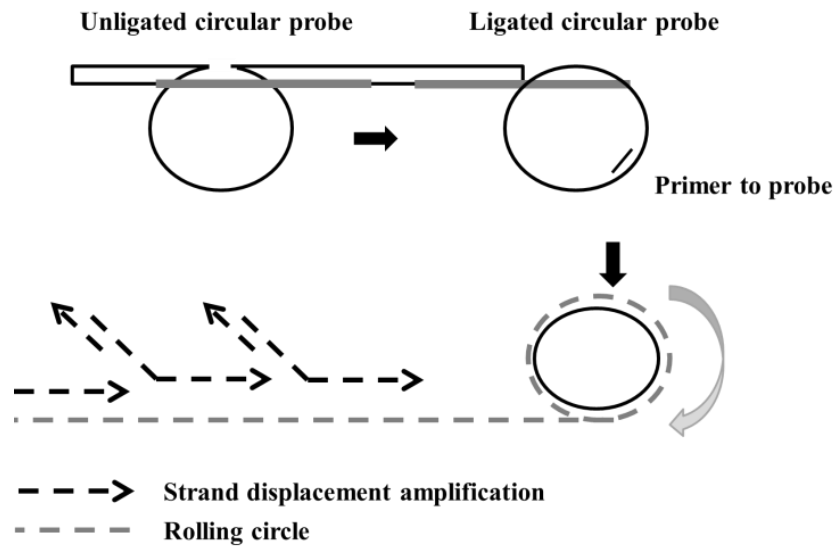
Figure 16: Enzymatic signal amplification ramification amplification [1].

1.3.4. Microarray

Microarrays are an evolution of M. E. Southern's work who first proposed the analysis of DNA fragments on nitrocellulose filters. This idea led to the dot-blot method in which several DNA targets are analyzed by forming an array of dots on a nitrocellulose filter. The reverse-dot-blot method was introduced for sequence typing of one target which hybridizes with an array of probes immobilized on a nylon membrane. As a result a single reverse-dot-blot assay can be used for example to do a genome analysis or to diagnose several pathogens. Nitrocellulose filters and nylon membranes are porous which can cause diffusion and merging of droplets limiting the number of probes immobilized, affecting the accuracy of the position of the dots and so the resolution of the array. Different alternatives have been used like glass and plastic slides. The immobilization of oligonucleotides on the surface of the arrays has been done using UV, molecular interactions like adsorption, biotin-streptavidin binding, thiol-gold interactions, covalent linkages, etc. The strategy used will depend on the application, the substrate, the sample and the environment. The dot size can be controlled by removing the diffusion effect and adjusting the hydrophobicity of the droplets and the surfaces. The "microarray" term started to be used thanks to the use of automatic spotting machines which allow the dot size and the array resolution to be in the micrometer scale [25]. Array-based detection formats benefit from the high number of probes that can be immobilized into a single assay which allow the simultaneous interrogation of several targets (microorganism, SNPs, etc) in a single experiment. The main drawbacks are the high cost of the equipment (hybridization stations, detectors, spotters) and that only one sample can be analyzed at a time. As microarray technology matures, different modifications are being developed such as microbeads (probes immobilized on internally died microspeheres), suspension arrays formats…[3].

Microarrays/chip technologies are not well suited for routine diagnosis where an early (depends on the sensitivity) and accurate (depends on the specificity) diagnostic is required. Although an amplification step can be added, this will mean an increase in time. The low sensitivity of microarrays is attributed to the hybridization and detection mechanisms. The hybridization process is slow since many collisions are needed before the target adopt the right orientation to hybridize with its complementary probe. The hybridization efficiency decreases when it is restricted to the surface of the array. Some approaches to improve hybridization have been employed such as increasing probe concentration; changing buffer composition, temperature; introducing a probe spacer, incorporating the photovoltaic effect [25].

1.3.5. Biosensors

There are different kinds of biosensors: metabolism-, antibody- and nucleic acid-based systems. Immunodiagnostics biosensors are faster and more robust than NA ones, however the latter are more specific and sensitive. Both features are increased if they are combined with an amplification step. There are two biosensors formats: 1) Direct assays in which the recognition element –probe- is linked to the transducer so the capture of the target is detected directly. This format is used in devices that detect changes in mass, refractive index, impedance… 2) Indirect assays, which represent the basis of the sandwich assay format in which a second recognition element –labeled probe- is added before detecting the target. These are especially useful in samples where non-specific absorption to the surface is a problem [3].

Different biosensors systems are used for nucleic acid detection:

- **Optical-based systems:** they are the most common. They can use labels, usually fluorescent; or they can be unlabeled –usually based upon surface plasmon resonance-. Target does not have to be labeled [3].

- **Piezoelectric biosensors:** the piezoelectric refers to a property of some materials –crystals- to generate an electric potential after a mechanical force. Adding mass to the surface of the sensor originates a change in the resonance frequency of the crystal proportional to the mass added. In other words, the sensor is weighing the addition of nucleic acids [3]. Piezoelectric sensors consist of probes immobilized on the surface of a crystal (usually quartz). Then the sensor is placed in a solution containing potential target nucleic acids which can bind to their complementary probes increasing the mass at the surface of the crystal an so decreasing the resonance frequency of the quarz oscillation. These systems provide real-time readout as well as simplicity of use. Although they can be difficult to regenerate after hybridization, economy of the scale can serve to make disposable detectors. Other drawbacks are the lack of sensitivity and specificity and the interferences with buffer composition [3].

- **Electrochemical biosensors:** they can measure current (amperometric), electrical potential (potentiometric), impedance (impedometric). These sensors are label-free, they are not affected by the turbidity or other optical properties of the sample and can amplify the signal. Nanopores are a class of electrochemical biosensors in which an electrically insulating material is permeated by one or more pores with diameters ranging from 10 to 150 nm [3].

The driving force leading to innovation in nucleic acid testing field is the need to develop simple, cost-effective and easy-to-use systems for daily use. The trend is for systems where multiple sample types can be analyzed simultaneously, which imply little sample preparation, fast turnaround time and large test menu. In addition, the instruments needed should be of low cost, have a small footprint and, if possible, miniaturized. In other words, the devices should be rapid, sensitive, adaptable (interchangeable probe cartridges), able to distinguish a specific target within a complex background, in a user-friendly and cheap format. The trend is to develop point-of-care (hospitals and clinicians) and point-of-patient (home, physician's offices) testing systems in which information can be transferred from one place to another allowing remote diagnosis by clinicians [3].

1.3.6. Limitations of nucleic acid amplification techniques for detection purposes

Amplification techniques have inherent problems that can affect the performance of the assay. For example, a polymorphic region can obstruct base-pairing with either primers or probes. A mis-incorporarion during the replication, especially when wrong base is introduced within the first three cycles, can interfere with end-point probe-based detection. Since the amplicon obtained does not reflect the target sequence, if this error is within the region complementary to the probe, there will be a mismatch which might avoid probe hybridization. Some approaches to overcome this might be lowering the annealing temperature -but this can lead to non-specific binding- or using a secondary probe detection step to increase specificity [1].

- False-positive results: These can be derived 1) from contamination issues (from other samples or from previous amplifications) due to the high sensitivity of the amplification reaction and so susceptible to contamination, 2) from the amplification of nucleic acids from dead organisms or 3) from the low specificity of the amplification. Some measures can be introduced to control these factors: using automated nucleic acid extraction techniques; processing negative samples all along the process to check contamination; running a second amplification with internal primers or hybridization with a specific probe to check the amplification specificity [31].

- False-negative results: they might be obtained because of a low sensitivity of the amplification reaction or because of the presence of polymerase inhibitors in the sample. Different approaches can be followed: extensive DNA purification to remove inhibitors and adding an artificial target to check the amplification [31].

1.4. DNA-Templated Base-Filling reaction on a DGL probe

Amongst commonly used molecular technologies for nucleic acid testing (NAT), DNA analysis by dynamic chemistry (Chem-NAT) is one of the most recent and promising technologies [32-34]. Nucleic acid analysis by dynamic chemistry harnesses Watson-Crick base pairing to template a dynamic reaction on a strand of abasic peptide nucleic acid (PNA)-based probes (DGL probes) (Figure 17).
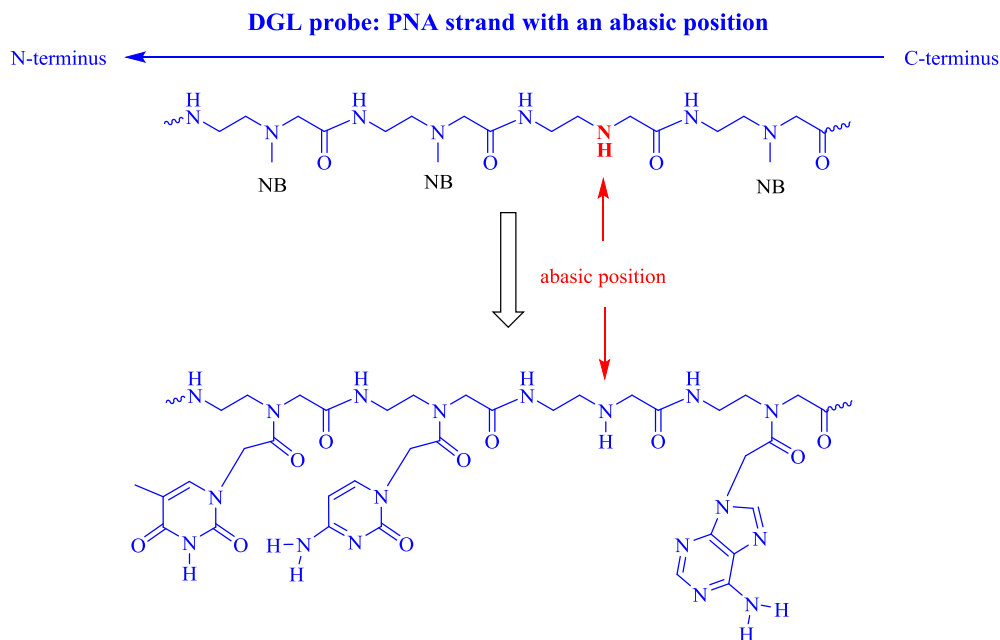
Figure 17: General structure of neutral DGL probe: it consists of a peptide nucleic acid backbone (N-(2-aminoehtyl) glycine units are coupled) with nitrogenous bases covalently linked to the Nitrogen atom of the glycine. A position lacking this nitrogenous base, abasic position, having instead a free secondary amine, is introduced. This abasic position would be placed so that it allows reading and identifying the nucleotide under interrogation. An example with three nitrogenous bases and an abasic position is shown.

DGL probes are designed to 'clamp' the region around the target DNA, selected to represent the sense sequence (the DGL probes were thus antisense, such that the DGL N-terminus lined up with the 3' end of the sense DNA). DGL probes are so capable of hybridizing with complementary target sequences such that the abasic position on the DGL probe lies opposite to a nucleotide on the nucleic acid strand under interrogation, creating the so-called "chemical pocket (Figure 18A, step 1). A reversible reaction, between reactive aldehyde-modified nucleobases (SMART-NBs) (Figure 18A, step 2 and Figure 18B) and the free secondary amine on the DGL probes, generates an iminium intermediate, which can be reduced (Figure 18A, step 3 and Figure 19) to a stable tertiary amine (chemical lock-up). Four iminium species (one for each base) will be thus generated, but the

one with the correct hydrogen bonding motif (obeying Watson–Crick base-pairing) will be the most thermodynamically stable product. Finally, DGL probes which are modified by a specific SMART-NB are read, allowing determining the nucleotide under interrogation [32, 33, 35].
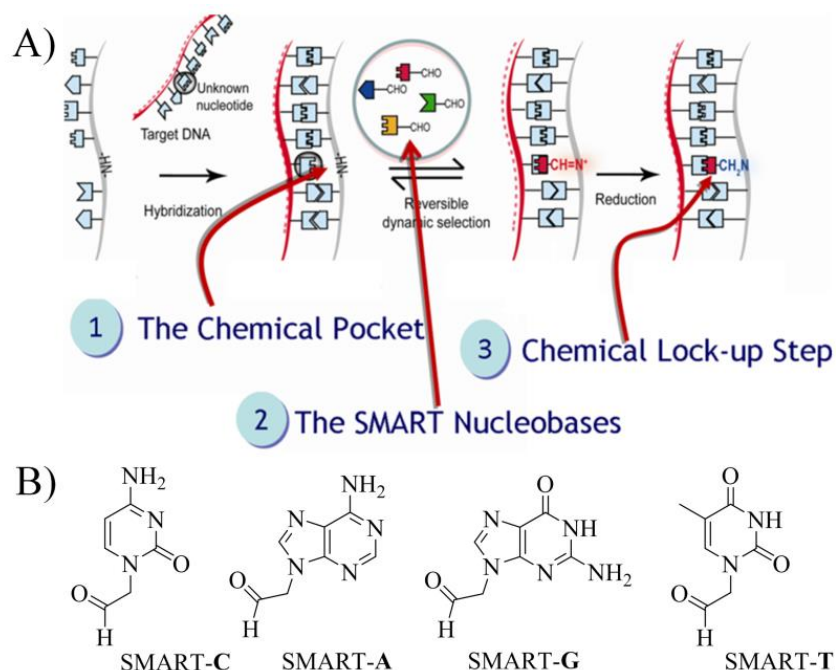
Figure 18: A) General scheme of the steps involved in DNA analysis by dynamic chemistry: 1) hybridization between a DGL probe and a complementary target nucleic acid that contains a nucleotide under interrogation; 2) dynamic incorporation of SMART-NB into the abasic position driven by the nucleotide under interrogation creating a reversible intermediate; 3) chemical lock-up of the reversible intermediate to give rise to a DGL probe modified by a SMART-NB. Reproduced with permission[32]. B) Chemical structure of the SMART-NBs [35].
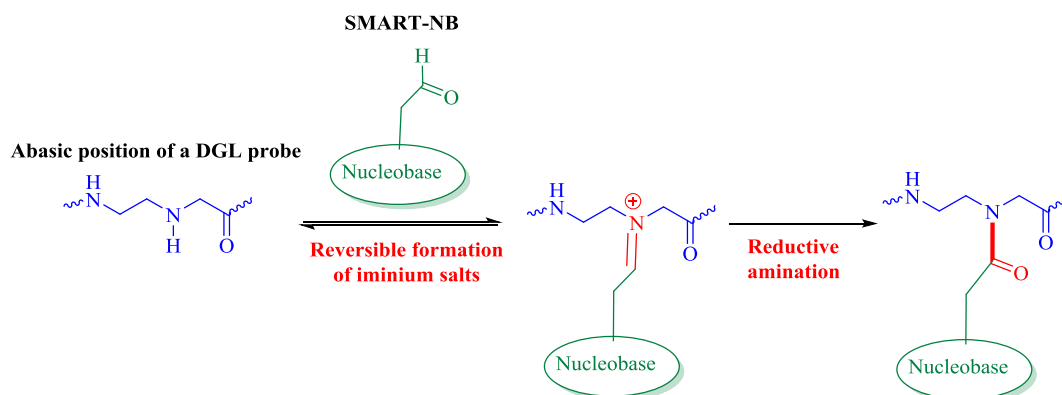
Figure 19: Chemical reaction that takes place in the chemical pocket: the aldehyde-modified nucleobases react with the secondary amine of the abasic position creating a reversible iminium intermediate. Only the right iminium intermediate, thermodynamically stabilized, is irreversible reduced.

The N-terminus of the DGL probe is modified depending on the readout tool and the kind of assay used (mass-, fluorescence-, colorimetric- based assays). If mass spectrometry is used for reading the results, a tryphenylphosphonium charge tag is used as N-terminal cap since it was observed that it enhanced MALDI-TOF detection limit [36]. Whereas if a platform-based assay is going to be carried out, a nucleophilic group, such as $-NH_2$ or $-SH$, is coupled at the N-terminal of the probe to allow its immobilization on the support.

Base-filling reactions performed at the middle of a DGL probe are more efficient than those carried out at the end which emphasizes the role of base-stacking interactions in the reaction. The dynamic iminium formation provides a route to reverse the generation of mis-templated products [32].

MALDI-TOF mass spectrometry was the first readout tool used for reading the results of the DNA-templated base-filling reactions [32]. The resulting mass spectra demonstrated selective incorporation of the SMART-NB complementary to the templating nitrogenous base on the DNA strand. The DGL probe signals suggested complete dehybridization from the DNA template, which may occur either upon addition of the acidic matrix or during desorption/ionization in the mass spectrometer. In some reactions, some unreacted DGL probe was observed. This peak may appear together with a peak of ~+14 Da which is hypothesized to be the result of a borane adduct due to the available free amine at the blank position of the probe (i. e. DGL#1 + BH_3) [32, 33].

Previous studies shown that guanine and cytosine are incorporated in greater yield and more selectively than either adenine or thymine (attributed to the greater number of templating hydrogen-bonds) [32]. Furthermore, purine bases were incorporated with greater yield and selectivity than pyrimidines (A > T; G > C), which may be due to greater π–stacking interactions associated with the bicyclic pyrimidine rings. It was also found that altering the starting concentrations of the SMART-NBs gave different product ratios. In accordance with Le Chatelier's principle for a system in dynamic equilibrium, increasing the concentrations of those bases with lower yield and selectivity under equimolar conditions resulted in improved yields and peak ratios for the "correct" templated product [32, 33].

Control reactions either in the absence of DNA or in the presence of a non-complementary nucleic acid have further demonstrated the role of DNA template in speeding up the reaction and promoting selective SMART-NB incorporation [32].

The effect of pH on the reaction outcome was also previously studied. As anticipated for iminium ion formation, conversions were better at mildly acidic pH; being pH 6 optimal. A mildly acidic pH strikes the balance between being high enough to provide sufficient free amine in the abasic position of the DGL probe to attack the carbonyl group of the aldehyde in the SMART-NBs, but

low enough for protonation of the carbonyl oxygen prior to nucleophilic attack, and also protonation of the resulting tetrahedral intermediate for elimination of water [32].

In previous works, Chem-NAT technology was successfully used to genotype 12 cystic fibrosis patients. This is a lethal recessive genetic disease that appears as a result of mutations in the gene coding for the cystic fibrosis transmembrane regulator. Despite the high number of mutations associated to it, around two-thirds are related to a 3 base-pair deletion, ΔF508. Patients were genotyped for two mutations associated to this disease: (i) the indel ΔF508, which is a 3 base-pair deletion which accounts for two-thirds of cases and (ii) the SNP, G551D, responsible for 1-2% of cases. The analysis of the SNP was straightforward (Figure 20A) whereas to analyze the indel, since the 3 bases deletion avoid the analysis with a single probe, two DGL probes were used: one to clamp the mutant and the second one to the wild-type sequence (Figure 20B) [33].
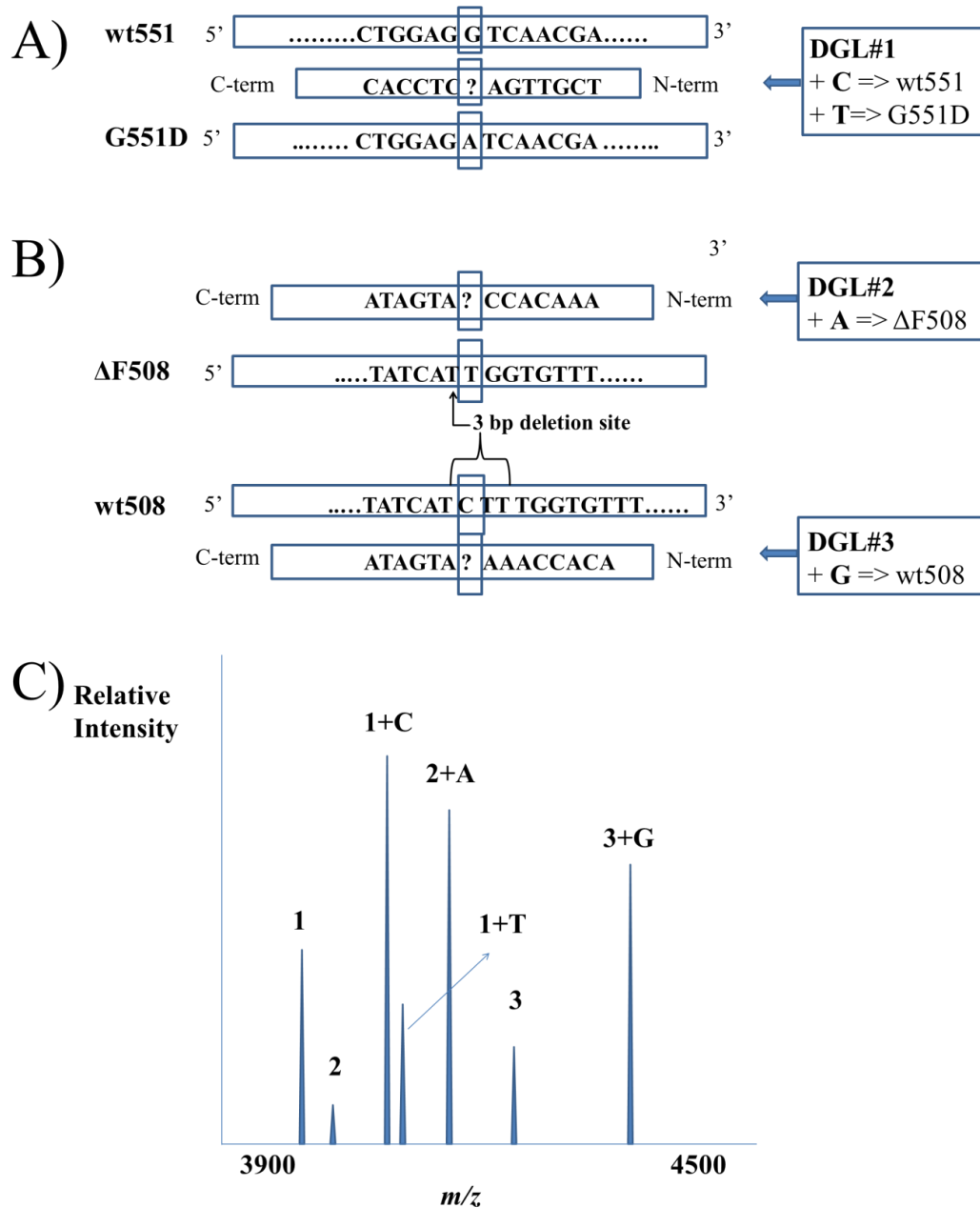
Figure 20: DGL probes sequences for cystic fibrosis indel ΔF508 and SNP G551D identification. A) One probe is used for SNP G551D genotyping: DGL#1. SMART-C incorporation means wild-type and SMART-T calls for the SNP G551D. B) Two probes are needed to identify the indel ΔF508 and differentiate the 3 base-pair deletion (DGL#2) from the wild-type sequence (DGL #3). If the spectrum shows SMART-A incorporation on DGL#2, it indicates the presence of the deletion; whereas if it is seen the incorporation of SMART-G on DGL#3, it means that it does not have the deletion and so it is a wild-type sequence. C) Representative MALDI-TOF spectrum for genotyping an individual heterozygous for both mutations where all possible SMART-NBs incorporation pattern are observed.

Another previous work reported the integration of Chem-NAT technology on STMicroelectronics In-check™ platform which contains a microarray area where nucleic acids are captured and identified by single nucleobase fluorescent labeling. This platform was evaluated and validated for detection of DNA sequences mimicking microRNA-122 (miR-122) and mengo virus RNA (MGV). Two DGL probes (DGL-miR122 and DGL-MGV) and a fluorescein-labeled SMART-Cytosine (SMART-C-FITC) were used. DGL probes specifically hybridized with their complementary target nucleic acids; then the templating nucleotide which lies opposite the abasic site templates the incorporation of its complementary SMART-NB, in this case, SMART-C-FITC, labeling the probe. This event is later scanned with the ST's optical reader. No mis-incorporation was observed due to non-specific SMART-C-FITC incorporation on DGL-MGV (Figure 21) [34].
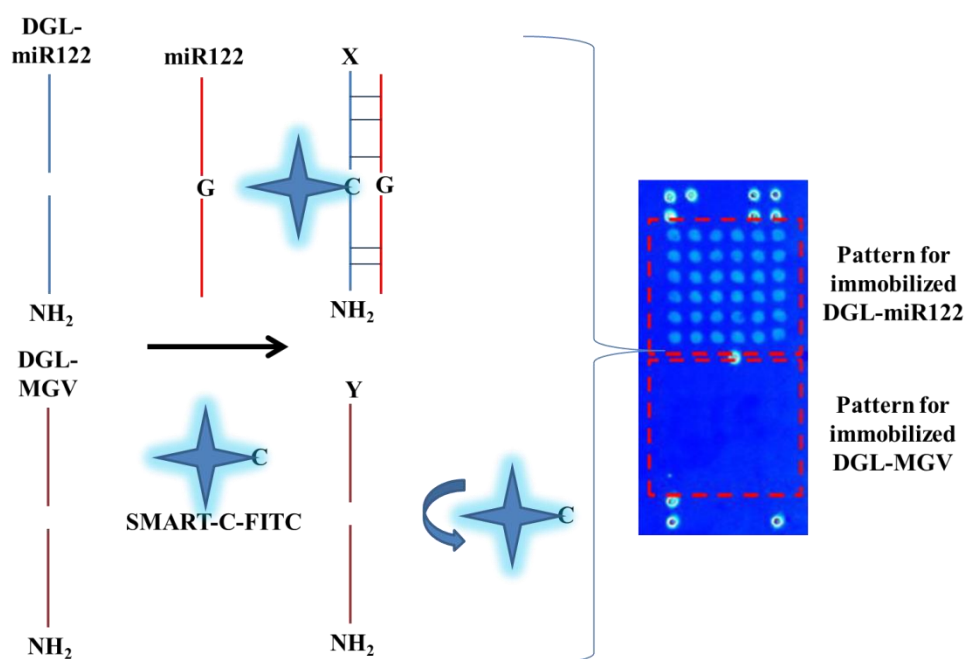
Figure 21: miR-122 detection by Chem-NAT technology on STMicroelectronics In-Check™ platform: Two DGL probes, DGL-miR122 and DGL-MGV, were immobilized on the LoC surface. DNA mimicking miR-122 sequence was used as target nucleic acid, hybridizing with its complementary probe and labeling it by SMART-C-FITC incorporation. No signal was observed on the other spotted DGL probes which highlighted the specificity of Chem-NAT technology.

Chapter 2: miR-122 detection by dynamic chemistry (Objective 1)

Chapter 2: miR-122 detection by dynamic chemistry (Objective 1)

2.1. Introduction

2.1.1. microRNAs

microRNAs (miRNA, miR) are a class of small (19-25 nucleotides) non-coding RNAs that regulates gene expression. They regulate aspects such as cell proliferation, phase change, cell differentiation, cellular function, organ development, metabolism, cell death, response to environmental stress [37-40].

miRNA genes are transcribed in the nucleus by RNA polymerase II leading to a long transcript called primary miRNA (pri-miRNA). This molecule is then processed by RNaseIII Drosha and the cofactor DGCR8 (DiGeorge syndrome critical region gene 8) which results in precursor miRNA (pre-miRNA). This precursor folded into a secondary stem-loop structure and is exported to the cytoplasm by Ran-GTP dependent transporter Exportin 5. Then, in the cytoplasm, the pre-miRNA is processed by the enzyme Dicer, another RNaseIII which cut the terminal loop releasing temporal RNA duplexes, miRNA/miRNA*. The two strands are separated by helicases and the mature strand, miRNA, is incorporated into RNA-induced silencing complex (RISC). Once incorporated in the RISC, miRNAs negatively regulate gene expression at the post-transcriptional level (Figure 22). miRNAs can base-pair to a target messenger RNA (mRNA), commonly the 3'-untranslated region (UTR), resulting in translational repression and exonucleolitic mRNA decay [37].
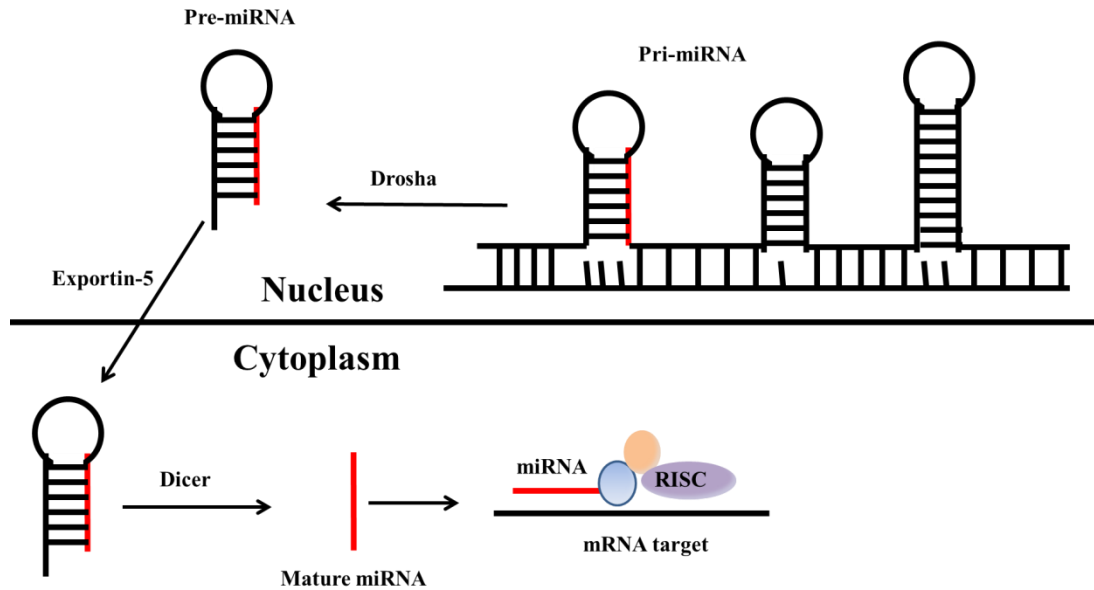
Figure 22: miRNA biogenesis: RNA transcribed pri-miRNA is processed by the endonuclease Drosha resulting in pre-miRNA which is exported to the cytoplasm and cleaved by Dicer to form the mature miRNA. This miRNA integrates in the RNA-induced silencing complex (RISC) and direct towards the target mRNA to regulates its expression [41].

As new miRNAs were being discovered, the research moved towards their functional characterization and their role in human diseases. It is especially useful the fact that some miRNAs can have characteristic tissue-specific, developmental stage-specific or disease-specific expression pattern. Due to variation of miRNAs' expression levels on different disease stages, they have been proposed as biomarkers for pathogenesis, diagnosis, screening, progression and therapy of diseases. Some of the proposed mechanisms by which miRNA expression patterns are altered are single point mutations in either miRNAs or their targets and epigenetic silencing of miRNA transcription units [38, 42-44].

On the other hand, due to miRNAs' role in these processes they can also be used therapeutically. There are two possible strategies [37]:

1) **miRNA reduction** is directed against a gain of miRNA function and consists of inhibiting miRNA by (i) small-molecules that regulates miRNA expression at the transcriptional level; (ii) antisense oligonucleotides that bind to miRNA and lead to duplex formation or miRNA degradation; (iii) miRNA masking by using molecules that bind to the 3'UTR of the target miRNA and inhibit its effects; (iv) miRNA sponges that are oligonucleotides structures whose sequence is complementary to miRNAs [37].

2) **miRNA replacement** is directed against a loss of miRNA function and imply reintroducing miRNA by introducing systemic miRNA (mimics) or inserting genes coding for miRNA into viral constructs [37].

The main problems about using miRNA therapeutically are: 1) the difficulty to get a tissue-specific delivery and an efficient cellular uptake and 2) the low efficiency of enhancing miRNA which has been in part overcome by the use of LNA constructs. Indeed, LNA-antimiR were successfully applied and used in the first miRNA-based clinical trial for the treatment of hepatitis C virus infection by targeting miR-122 [37, 45].

2.1.2. miRNA detection methods

Determining the expression levels of miRNAs is a challenge because of their small size, low abundance (0.01% of the total RNA mass), high homology sequences between different miRNAs, an expression level variation of up to four orders of magnitude between different miRNAS, the potential contribution of pre-miRNA and pri-miRNA to the signal and lack of common sequence features such as poly-A tail to facilitate their purification [38, 42, 46]. These features make PCR amplification technique inaccurate and inefficient because of the inability of primers to bind to these small templates; this is why more advanced methods than traditional PCR have emerged such as primer extension, isothermal exponential amplification and rolling cycle amplification [37]. An ideal miRNA detection method should be sensitive enough to quantify miRNA levels, it should be specific for detecting sequences with single nucleotides differences, it should be capable of processing multiple samples in parallel and it should be easy to perform without expensive equipment or reagents. The choice of the detection methods will depend on the experimental setting [42].

Most miRNA detection methods imply the knowledge of the sequence of the target miRNA. miRNA detection is mainly based on hybridization with a complementary nucleic acid probe. These hybridization methods can be divided into: solid-phase (a capture probe is absorbed or bound to a surface, they are more appropriate for high-throughput screening); solution-phase (hybridization occurs in solution; they are useful for in-vivo detection and require shorter analysis time) and in-situ hybridization [42]. Upon hybridization, a transducer converts it into a measurable signal. These signals can be detected in several ways: electrochemically, measuring fluorescence or bioluminescence intensities… [41, 42, 47].

2.1.2.1. Solid-phase methods:

a) Northern Blotting

A sample with miRNAs is run on an electrophoresis gel, transferred to a nitrocellulose membrane and fixed to it with a crosslinking procedure and soaked in a solution containing fluorescent or radiolabeled probe complementary to the target miRNA. It is a complex and time-consuming technique which may require radio-labeling; it needs large amounts of sample (10-30 μg); it is semiquantitative (although it reflects miRNA expression levels more accurately than other techniques such as cloning) and it has low detection efficiency (nanomole range). However, it is considered the gold-standard technique for miRNA detection and validation. The sensitivity problem has been minimized by adding locked-nucleic acids (LNAs) to the probe sequence which has increased the detection limit up to 10-fold compared with RNA or DNA probes [41, 47, 48].

b) Microarrays

Microarrays are being used in an attempt to reduce sample volume, analyze several samples simultaneously and decrease assay time [48]. miRNA microarrays are challenging since miRNA short length leaves very little sequence to work with for probes design. In addition, duplex melting temperature of each miRNA and its complementary DNA sequence varies so normalization of hybridization efficiency for each element cannot be achieved by reducing the length of the probe [46]. 5'-Amine-modified probes are immobilized onto glass slides through covalent crosslinking between the amino groups and the SAM (self-assembly monolayer) creating a ready-to-use microarray. These probes can have the same sequence than the target miRNA to detect complementary DNA (cDNA) which is produced via reverse-transcription using labeled primers with a fluorophore or biotinylated (these product are then detected by a conjugate streptavidin-fluorophore). Sometimes, the probes can be complementary to the target miRNA and the hybridization detected, for example, by fluorescent labeling of the miRNA previous hybridization. The main factors to be considered when designing a microarray platform are the design of the probes, the preparation of the samples (miRNA in this case) and the labeling of the nucleic acid (miRNA). The probes for miRNA arrays have two parts a linker –a poly(dT) or poly(dA) sequence with amine-modified terminus- to immobilize the probe on the glass slide and avoid the steric hindrance during hybridization; and the capture sequence which is usually complementary to the miRNA sequence. A good sample quality is required, this is usually achieved with commercial RNA extraction kit; however, due to the low abundance of miRNAs, an enrichment and isolation step of miRNAs from total RNA is recommended. Finally, miRNAs have to be labeled, it can be done directly by conjugating miRNA molecules with fluorophores or indirectly where miRNA

reverse transcripts, RT-PCR products or the in-vitro transcripts are labeled rather than the miRNAs themselves [48].

i) Direct labeling methods

They are easy to perform and avoid errors from reverse transcription and PCR. Different strategies can be followed:

- **Labeling of guanine:** using a guanine-labeling reagent such as Ulysis Alexa Fluor 546/647. It assumes that all miRNAs have guanosines; however, the signal intensity is going to be related to the guanosine content and so they cannot be used to compare different miRNA expression levels [46, 48-50].

- **Labeling by alkylating any reactive N heteroatom in the miRNA** mainly N7 of guanine and N3 of adenine and cytosine. The excess of reagent must be removed to avoid labeling of the probes on the microarray surfaces and they lack specificity for miRNA species [46].

- **Labeling through T4 RNA ligase:** this enzyme covalently couples the 5'end of a nucleotide sequence to the 3'-OH group of miRNAs. For example, this approach was used by Thomson et al. to add a fluorescence-modified dinucleotide such as pCU-Cy3 onto the 3'end of the miRNA [46, 48, 51].

- **Labeling through poly(A) polymerase enzyme (PAP):** this enzyme can add a 20-50 nucleotide sequence to each miRNA creating a 3' tail which is a mixture of standard and amine-modified bases. For example, this enzyme was used to add a poly(U) tail with amine-modified 3' UTP to the 3' end of the miRNA. This tail was then labeled with amine-reactive fluorophores. The degree of labeling of each miRNA is the same so signal can be used to compare their abundance. Sensitivity can be increased by increasing the number of amino-modified nucleotide introduced [46, 48, 52].

- **Labeling through chemical structure modification:** the 2', 3'-OH groups on ribose ring of the 3' terminus of the miRNA are oxidized to dialhehyde with sodium periodate. Then they are made to react with and hydrazide derivative to covalently attach the label to the 3' end of each miRNA. For example, with biotin-X-hydrazide to biotinylate miRNAs (Figure 23A) and detect them with quantum dots functionalized with streptavidin (Figure 23B), this assay had a detection limit of 40

pM (0.4 fmol). Because 2',3'-diol is required, background signals from contaminant RNA which beares 3'-phosphate groups or DNA can be reduced [46, 48, 53].
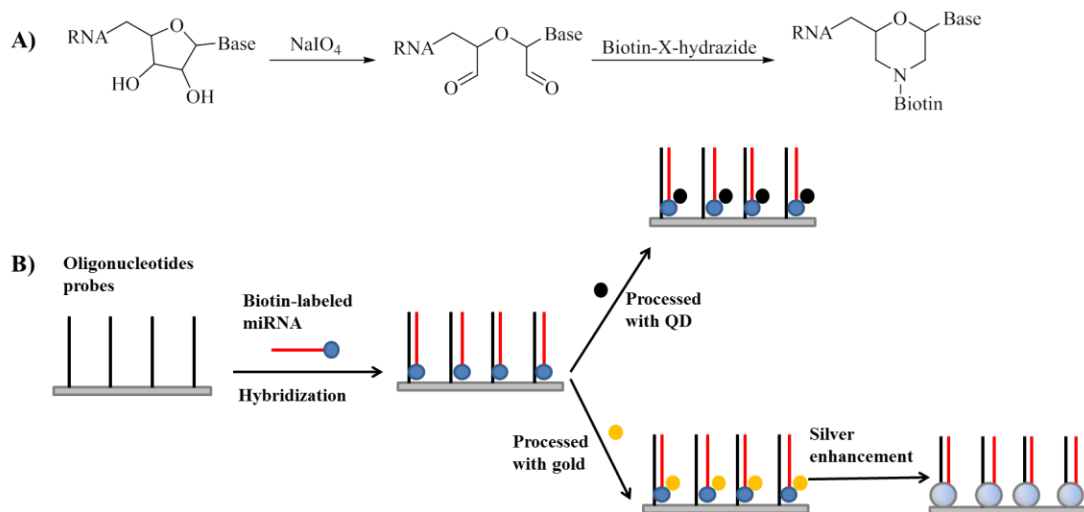
Figure 23: A) The target miRNA is biotinylated by converting the 3´ hydroxyls on the ribose ring into a dialdehyde, which then reacts with biotin–X-hydrazide. B) Immobilized oligonucleotide probes complementary to the target miRNA hybridized with the biotinylated miRNA; this event can be followed by addition of a streptavidin–quantum-dot (QD) or it might be processed with gold that later results in a buildup of metallic silver on the gold surface.

- **Labeling trough RNA-primed array-based Klenow enzyme assay (RAKE).** In these probes, three thymidine nucleotides are introduced between the linker and the capture segments. After hybridization, a heterogeneous duplex probe/miRNA is formed and it cannot be truncated by exonuclease I whereas the non-hybridized probes are. Then, Klenow-driven extension reaction occurs where miRNA and probe are primer and template, respectively. Biotin-labeled dATP is incorporated into the extended part of the miRNA which is then labeled by interacting with a streptavidin conjugated with a dye. Because of the need of an accurate match between the 3'ends of the miRNAs and the probes, this method can differentiate between sequences that differ at the 3' end [48, 54].

ii) Indirect Labeling

The advantages of this type of labeling are: that cDNA are more stable than miRNA and that the molecules derived from miRNA can be amplified and labeled simultaneously through PCR or in-vitro transcription [48].

- Labeling of the miRNA reverse transcript: this transcripts are acquired through random primer-driven reverse transcription. Different approaches have been done: Liu et al. used an eight-nucleotide random primer labeled with two biotin molecules (3'-(N)8-(A)12-biotin-(A)12-biotin-5') to reverse transcribe the total RNA into biotinylated cDNAs [55, 56]. Sun et al. labeled the obtained cDNAs with biotin-dideoxy-dUTP by terminal transferases action [57]. The probes used in this microarray target cDNA sequences, so they have the same sequence as the miRNA. Because of the low specificity of the random primer and the low miRNA content in total RNA, this method is prone to introduce errors.

- Labeling of RT-PCR products: two adaptor sequences are added to the 3' and 5' ends of the miRNA. Then, a biotinylated or fluorescent primer is designed considering the adaptor sequence to carry out the RT-PCR amplification to obtain the labeled PCR products. cDNAs can be amplified and labeling is done automatically in PCR so increasing the sensitivity. One disadvantage of this method is that the presence of the antisense strand may interfere with the hybridization between the sense strand and the probe. This problem was overcome by using two adapters of different length were the longer one was used for the sense strand and it was fluorescently-labeled; as a result, there was a length discrepancy between both strands and by doing a denaturing polyacrylamide gel electrophoresis, the sense strands can be isolated [48, 58].

- Labeling in vitro transcript: a promoter sequence is introduced into the adaptor sequence. The in vitro transcript can then be labeled with fluorescent nucleotides such as Cy3-CTP during the transcription reaction (labeled cRNA) [48, 59].

The main advantage of the microarray platform is its high-throughput screening capability which potentiates their use to characterize miRNA expression profiles. Although expensive the platform and the robotic for fabrication, microarrays can be cost-effective in large laboratories where many samples are analyzed daily. Other disadvantages are the low sensitivity because of the low sample-volume, the possibility of cross-hybridization between samples which differ in one only base, the absence of specific standard for data analysis or validation and that it does not provide quantitative data [41, 42, 47].

c) Electrochemical detection

Electrochemical detection methods are based on changes in circuit properties as a consecuence of target miRNA hybridization. A common type of electrical detection method involves the use of electrocatalytic moieties which are chemically attached to miRNAs. Then these moieties assist an oxidation reaction which is recorded amperometrically. The limit of detection of these assays is in the femtomolar range. Different catalytic or enzymatic moieties can be explored in order to improve the performance of the sensor [42]. One example is the use of PNA functionalized silicon nanowires whose resistance is monitored before and after miRNA hybridization. Zhan et al. got a limit of detection of 1fM and single base discrimination when detecting let7 by using an array of PNA-functionalized silicon nanowires [42, 60]. The target miRNA is conjugated to electrocatalytic moieties such as OsO_2 nanoparticles of $Ru(Pd)_2Cl_2$ where Pd is 1,10-phenantroline-5,6-dione [61, 62]. Oligonucleotide probes are immobilized on a glass slide and miRNAs are allowed to hybridize to the probe. The labeled-miRNA is detected by a current increase which can be correlated to the amount of target present in the sample (Figure 24). The limit of detection is in the high femtomolar to low picomolar range. It is limited in its ability to detect miRNA in vivo but its main advantage is its high sensitivity [41].
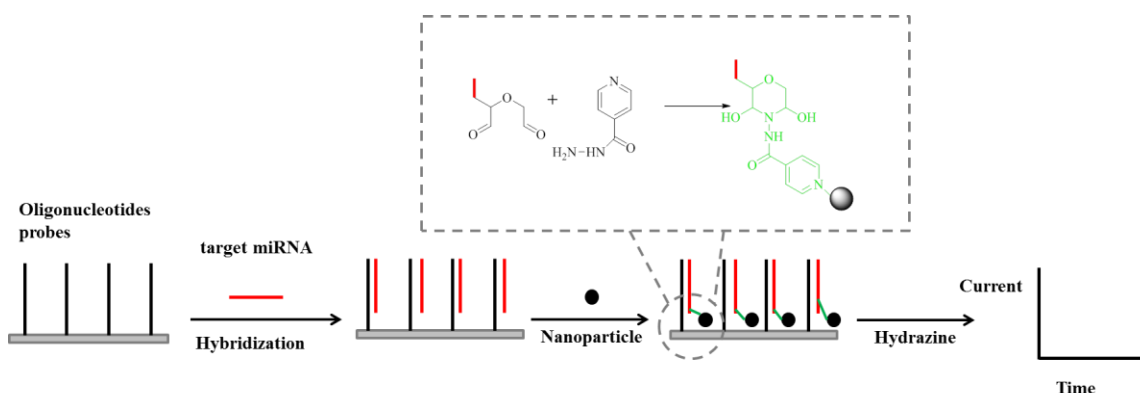
Figure 24: Solid-phase electrochemical miRNA detection. Probes targeting miRNA are immobilized on a slide, followed by the addition of the miRNA under study. Nanoparticles are then added, they will covalently attach to the miRNA and will be thus immobilized on the slide. Finally, the current generated from hydrazine oxidation catalyzed by the nanoparticle is measured [47].

d) Bioluminiscent detection method

It was developed by Cissell et al. Biotinylated-DNA complementary to the target miRNA (miR-21 in the example) is immobilized onto a neutravidin-coated well plate. Then, in a competitive assay, the target miRNA and a DNA probe labeled with Renilla luciferase (Rluc) compete to hybridize with the immobilized probe. Then, coelenterazine, a Rluc substrate, is added and it suffers an

oxidative decarboxylation resulting in light irradiation which can be measured with a luminometer. When the target miRNA is present in the sample, there is a luminescence decrease, whereas if there is no target, more Rluc-labeled probe hybridizes and a higher signal is generated (Figure 25). The drawbacks of this method are that it cannot be applied in vivo and that it relies on measuring a decrease in a signal [41, 63].
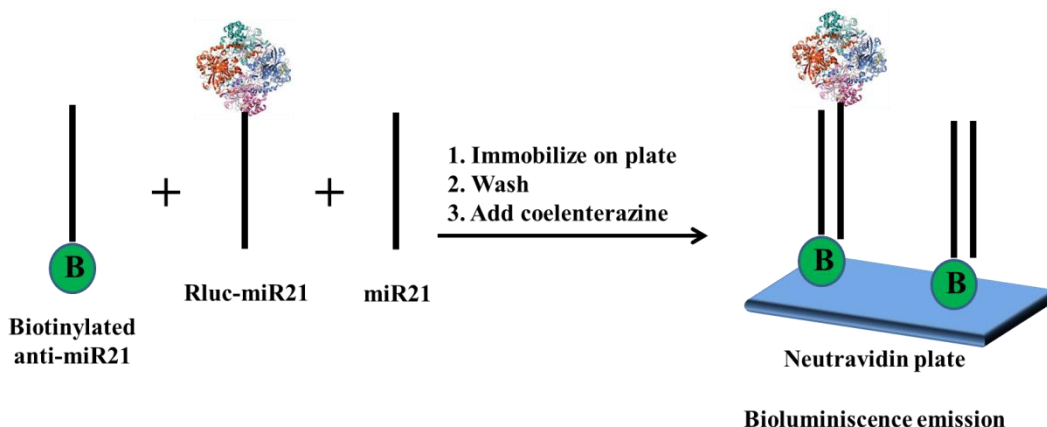
Figure 25: Solid-phase miRNA detection based on competitive hybridization. The miRNA has the same sequence as the Renilla luciferase (Rluc)-labeled oligonucleotide probe. Once the biotinylated anti-miRNA probe has hybridized, the Rluc-labeled oligonucleotide probe and miRNA compete to hybridize with the biotinylated probe [27].

e) Surface-enhanced Raman spectroscopy (SERS) method

Raman spectroscopy can be used to study the chemical state of the bonds in carbon materials. SERS enables the collection of Raman signals from a single molecule so increasing the utility of this technique to analyze molecules deposited onto metal surfaces [42]. This method was used by Driskell et al. [64].They adsorbed silver or gold nanorods onto a glass slide; then, miRNA are added to the nanorods and adsorbed to them. Finally, surface enhanced Raman scattering spectra are taken and the found peaks are used to identify the miRNAs. This method has good reproducibility and single-nucleotide specificity and the target does not need to be labeled. However, individual spectra of the target miRNAs should be obtained first in order to identify their characteristic Raman shift and miRNAs with overlapping peaks cannot be differentiated [41, 42]. The SERS technique is rather impractical in many laboratories since it requires a sophisticated read-out system, specific analytical skills and convoluted data interpretation and verification [42].

f) Surface plasmon resonance imagining (SPRI)-based methods

It is a label-free detection method that can be used to monitor molecular interactions on a surface. SPRI enhances the potential of SPR because it allows analyzing multiple interactions in an array

format [42]. This optical technique has been applied to monitor bioaffinity interactions such as DNA-DNA, RNA-DNA and peptide-protein at biopolymer layers formed on a thin gold film. The detection limit for DNA and RNA analysis is in the low nanomolar range. A two-component single-stranded DNA (ssDNA) microarray is exposed to the target RNA, only the perfect match elements form duplexes through hybridization adsorption what result in a positive increase in reflectivity. If the SPRI signal increase after hybridization adsorption is still below 10%, it is proportional to the relative surface coverage of complementary RNA [46]. Corn et al. applied this methodology to miRNA expression profiling, using a combination of a surface poly(A)- enzyme chemistry and gold nanoparticle-amplified SPRI measurements [65]. First, miRNAs hybridize with LNA probes, this process leaves an overhang at the 3'-end of the miRNA. Then, the SPRI response is amplified by the mass added through the hybridization of poly(T)-coated nanoparticles with the poly(A) tails (Figure 26). A 5 amol detection limit was achieved [42].

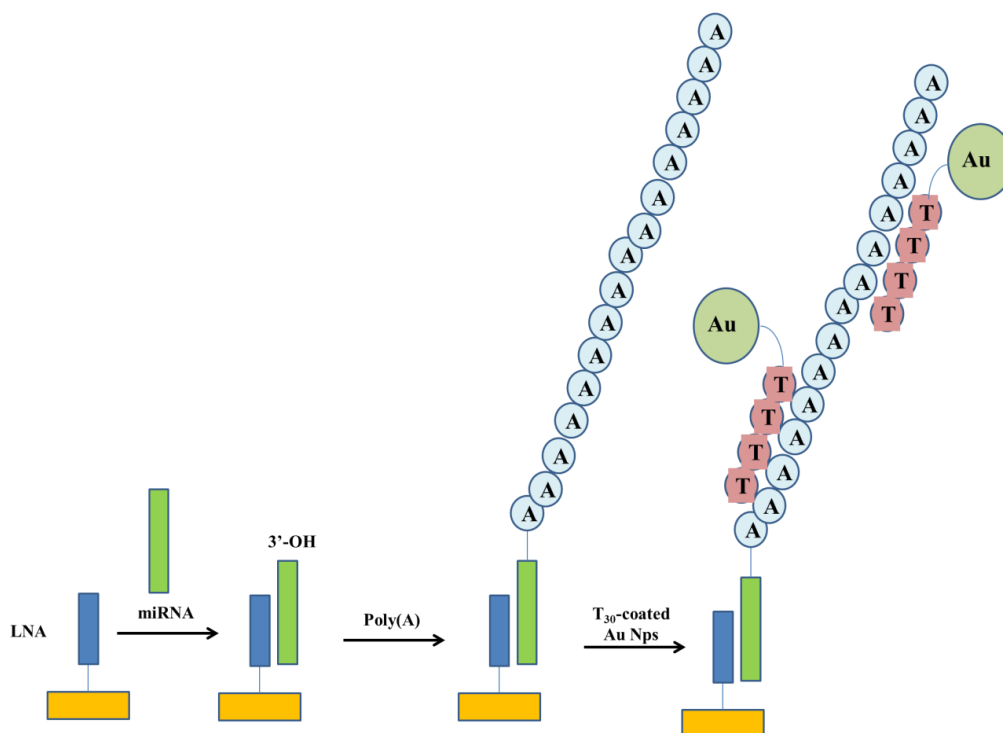**Figure 26:** Schematic representation of miRNAs detection using a combination of surface polyadenylation chemistry and nanoparticle amplified SPRI detection. (i) Hybridization of miRNA onto a complementary LNA probes on an array element, (ii) addition of poly(A) tails to the miRNAs bound to the surface (iii) hybridization.adsorption of nanoparticles coated with Thymine residues to the poly(A) tails [65].

2.1.2.2. Solution-phase methods:

a) RT-PCR

Real-time PCR is the gold standard method for gene expression quantification, it is highly sensitive and accurate. In this method, miRNA is modified for example by adding a poly(A) tail, then a primer is added and miRNA is reverse transcribed to form cDNA. After that, two primers are added to produce multiple copies of the cDNA, the forward primer is miRNA-specific whereas the reverse is universal. Amplification products can be detected in real-time; to do so, different strategies can be used, for example using a fluorescent intercalator such as SYBR Green which intercalates into dsDNA, using a dual labeled probe that can be cleaved by polymerase which releases the fluorophore and the quencher resulting in a fluorescence increase [41]. It is a high sensitive technique with good detection limits due to the amplification but it is partially limited by the cost of the equipment and materials needed [41, 42, 48]. The similar size of miRNAs and primers limits the application of traditional RT-PCR to miRNA detection. Applied Biosystems Co. solved this problem by using a stem-loop primer. First the stem-loop primer hybridizes with the miRNA and a reverse transcription is done. In a second step, a real time PCR with TaqMan probes is performed, primers were designed taking into account the sequences of the mature miRNA (forward) and the unfolded stem-loop primer (reverse). Some advantages of this technique are that the base stacking of the stem can enhance the thermal stability of the duplex primer/miRNA improving the RT efficiency of the short primers and 2) because of stem-loop primers are double stranded, the binding of non-specific RNA molecules is avoided and the specificity is increased [48].

To overcome the limitations of the traditional methods for miRNA detection, some techniques have been developed such as nanoparticle-derived probes, isothermal amplification, electrochemical methods…

b) Fluorescence correlation spectroscopy method

Different molecules in solution are distinguished based on their characteristic spectral properties, using a microfluidic, multicolor laser system which counts individual molecules as they flow at high velocity through the system [42]. It was developed by Neely et al.[66]. Two oligonucleotides probes labeled with organic fluorophores are added to the target miRNA. The probes hybridize with their targets and unbound probes hybridize with complementary oligonucleotides sequences which contain a quencher so decreasing background noise (Figure 27). The limit of quantification by this method was 500 fM [41, 42].
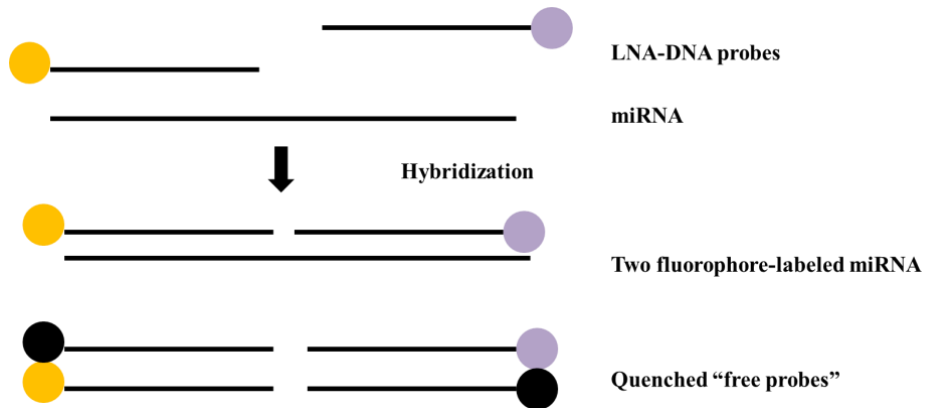
Figure 27: Schematic representation of the fluorescence correlation spectroscopy (FCS) method for miRNA detection. (A) miRNAs hybridize in solution with two fluorescent LNA-DNA probes which are spectrally distinguishable. Then, complementary DNA probes which bear a quencher molecule hybridize with the unbound probes [56].

c) Solution-phase bioluminescence methods

Bioluminiscence Resonance Energy Transfer (BRET) methods have also been developed. One developed by Cisell et al. consists of a Rluc-labeled oligonucleotide probe (Rluc-T1) whose sequence is the same than that of the target miRNA [67]. As a result, probe and target compete to hybridize with probe conjugated to quantum-dots (QD-CT1) whose sequence is complementary to the target miRNA. As a results, QD emission decreases when increasing target concentration (Figure 28). 2 pmol (10nM) of target could be detected in less than 30 minutes. A drawback of this method is that it relies on a decrease in a signal [41].
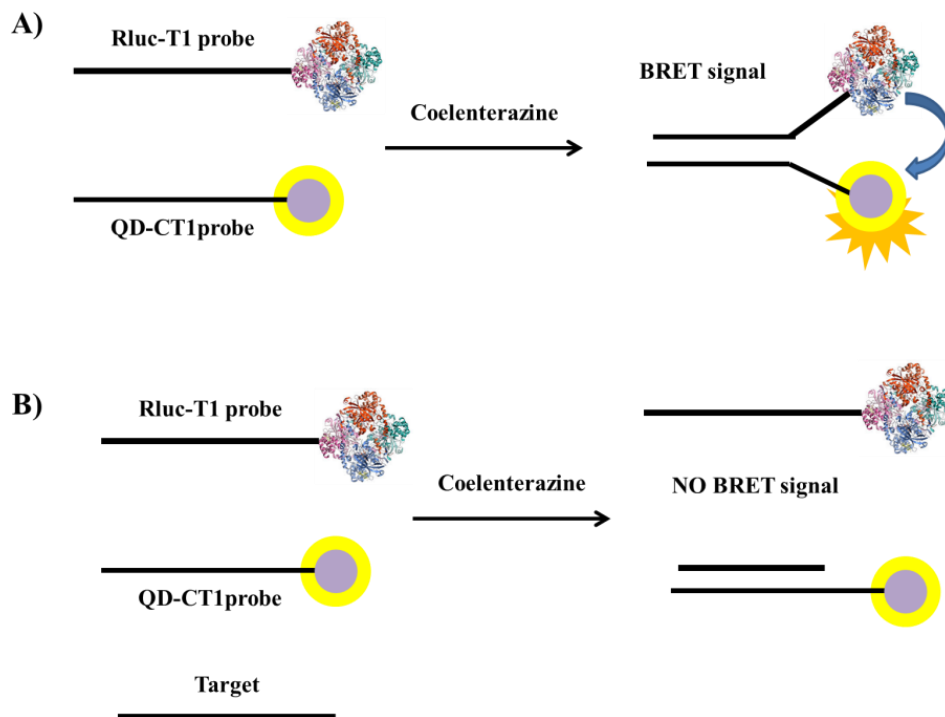
Figure 28: Bioluminescence resonance energy transfer (BRET)-based detection of nucleic acid in solution. The Rluc-labeled probe and the target nucleic acid compete to hybridize with quantum dots (QD) labeled with probes whose sequence is complementary to that of the target. As the levels of target increases, the QD emission decreases. A) In the absence of target, there is BRET signal. B) When the target is present, it hybridizes with the QD-probe and so there is no BRET [41, 67].

Another method developed by the same group uses protein complementation of the luminescent enzyme Rluc [68]. Two complementary oligonucleotides are conjugated to the N- and C-terminal fragments of Rluc, these fragments hybridize bringing together the two fragments of the protein and reassembling it into an active enzyme. If the target miRNA is present, the two Rluc-fragment probes compete with the target to hybridize which result in a luminescent signal decrease (Figure 29). It is a highly sensitive method, rapid and can be applied to in vivo measurement. However, it measures a decrease in a signal [41, 42].

Rluc-N-fragment   **Rluc-C-fragment**   **Active Rluc**

+   →

Probe 1   **Probe 2**
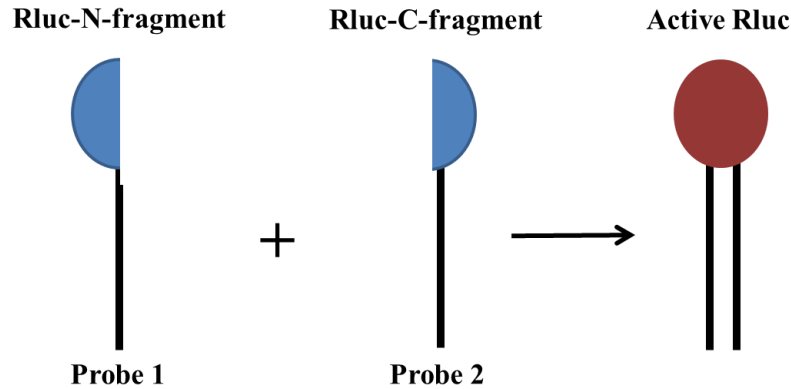
Figure 29: Schematic representation of the Rluc fragment reassembly by a probe hybridization proccess. [68].

2.1.2.3. Cloning

It is mainly used to discover new miRNAs. The frequency of cloning might indicate its abundance. Although there are different cloning methods, they have some common principles: small RNA molecules are first isolated using a denaturing polyacrylamide gel electrophoresis and the 3' and 5' ends are ligated with adaptor sequences that have restriction sites. Using theses adaptors, PCR primers are designed and the products are retrotranscribed (RT-PCR). Finally, the products obtained are transferred to a vector for further cloning and sequence analysis [48].

2.1.2.4. In-situ hybridization (ISH)

This technique uses labeled nucleic acid probes to detect nucleic acids in tissue section or fixed cells, which benefit from conserving the morphology [42]. The main advantage of using ISH for miRNA detection is the ability to monitor specific miRNA expression profiles at cellular or subcellular levels, thus identifying the type of cells which expresses each miRNA. It also gives a semiquantitative profile of miRNA expression. The small size of the targets and its low expression level is challenging and it has been partly overcome by introducing LNA probes which have higher binding affinity and are able to distinguish single nucleotide differences increasing thus the sensitivity and specificity of the assay. However, it cannot be used for high-throughput profiling [42].

2.1.2.5. High-throughput sequencing

Sequencing-based methods determine miRNA nucleotide sequence. They involve RNA isolation, ligation of linkers to the 3' and the 5' ends, reverse transcription to form cDNA and, finally, PCR amplification. Initially, they were used to detect low expressed miRNAs. Since 2007, deep-

sequencing methods allow the discovery of new miRNAs. These methods rely on next generation sequencing instrumentation and can process and simultaneously read thousands of sequences. They vary in the adapter, the primer sequences, the accuracy and the cost. The results obtained must be later validated by other methods because of the potential bias introduced during the sample processing: linker ligation, reverse transcription, PCR amplification…[42]

Although the number of methods for miRNA analysis is growing, they are not standardized. Standardized methods must be reproducible, accurate, robust and must have established normal miRNA levels in order to determine if the target miRNA is upregulated or downregulated. To develop more sensitive detection methods, it is needed to use markers with very low detection limits. Electrochemical- and bioluminescence-based methods are very sensitive and are seen as an alternative to fluorescence-based methods because an external energy source is not required; they have lower or no background noise and so higher sensitivity; and many bioluminescent proteins are similar in size to fluorescent proteins. Another attractive alternative is the use of quantum dots because of their high sensitivity and their strong photostability (a problem of many fluorophores) [41].

2.1.3. Use of miRNAs for determining disease conditions

miRNAs are present in biological fluids at relative constant levels, however when a pathological process occurs their expression is altered such that the expression patterns of circulating miRNAs can be used as fingerprints for various diseases [69, 70]. miRNAs possess some of the characteristics to be considered ideal biomarkers: they can be specific to the disease or pathology of interest -expression levels alteration-; they can indicate disease before clinical symptoms appear and are sensitive to changes in the pathological process (disease progression or therapeutic response); and, under appropriate conditions, they might also allow direct detection from biological fluids (e.g. blood, urine) [71-77]. In addition, circulating miRNAs are very stable in body fluids resisting enzymatic degradation and variations in physicochemical conditions such as pH [78].

Table 2 shows some diseases and indicates miRNAs whose expression is altered either up or down regulated. As it can be observed, the same miRNA can have a higher expression level in a disease condition and a lower one in another pathological process (for example miR-141 is down regulated in systemic lupus erythematosus and up regulated in ovarian cancer [38, 42-44].

Table 2: miRNAs associated with common human diseases [43, 44].

Disease type	miRNA	Up/Down regulation
Cardiac hypertrophy	miR-23a , miR-23b, miR-24, miR-195, miR-199a, miR-214	Up
Down síndrome	miR-99a, let-7c, miR-125b-2, miR-155, miR-802	Up
Alzheimer	miR-9, miR-128a, miR-125b	Up
Rheumatic arthritis	miR-155, miR-146	Up
Systemic lupus erithematosus	miR-189, miR-61, miR-78, miR-21, miR-142-3p, miR-342, miR-299-3p, miR-198, miR-298	Up
	miR-196a, miR-17-5p, miR-409-3p, miR-141, miR-383, miR-112, miR-184	Down
Psoriasis	miR-203	Up
Cancer		
Breast	miR-21, miR-155, miR-23, miR-191	Up
	miR-205, miR-145, miR-10b, miR-125b	Down
Ovary	miR-200a, miR-200c, miR-141	Up
	miR-199a, miR-140, miR-145, miR-125n1	Down
Endometrioid adenocarcinoma	miR-205, miR-155, miR-200a, miR-200b, 200c	Up
	miR-193a, 193b	Down
Colon	miR-let7g, miR-21, miR-20a, miR-17-19 family, miR-31, miR-135, miR-181b, miR-200c	Up
	miR-126	Down
AML	Has- miR-191, 199a, miR-155	Up
CML	miR-17-5p, miR-17-3p, miR-18a, miR-19a, miR-19b-1, miR-20a, miR-92a-1	Up
CLL	miR-21, miR-150, miR-155	Up
	miR-15a, miR-16, miR-29, miR-143, miR-45, miR-30d, miR-let7a, miR-181a	Down
Esophagus	miR-194, miR-192, miR-200c	Up
	miR-203	Down
Gastrointestinal	miR-106b-25	Up
	miR-15b, miR-16	Down
Lung	has-miR-21, has-miR-205, miR-17-92	Up
	has- miR-126*, miR-let7, hsa-let-7a-2, let-7f-1	Down
Bladder	miR-223, miR-26b, miR-221, miR-103-1, miR-185, miR-23b, miR-203, miR-17-5p, miR-23, miR-205	Up
	miR-29c, miR-26a, miR-30c, miR-30e-5p	Down

2.1.3.1. miR-122

miR-122 is a 22 nucleotide long single strand RNA highly expressed in liver where it constitutes 70% of the total miRNA pool [79]. The sequence of the mature has-miR-122-5p is: 5'-UGGAGUGUGACAAUGGUGUUUG-3' [80]. Recently, it has been reported that microRNA-122 (miR-122) levels are elevated in the plasma of patients with drug-induced liver injury (DILI); that the increase of miR-122 levels can be detected earlier than other widely used biomarkers such as alanine aminotransferase (ALT) and aspartate aminotransferase (AST) and with an enhanced hepatic specificity [81-83]. ALT and AST levels increase between 12 to 16 h after an overdose of drugs like acetaminophen, while miR-122 can indicate the corresponding liver injury within 4 h [84]. In other words, miR-122 might become a prospective biomarker of liver damage [81]. In addition, miR-122 has also been demonstrated to be an *in vitro* marker of drug-induced cellular toxicity for acetaminophen and diclofenac, with similar sensitivity to the one obtained in conventional assays based on the measurement of lactate dehydrogenase activity and intracellular adenosine triphosphate. Thus, miR-122 could be used as a biomarker during the first phases of the drug development processes [85, 86].

As a result of the potential applications and uses of miR-122 as a biomarker of liver injury, the development of a rapid test to detect miR-122 would be useful in healthcare and drug development [81, 87, 88]. However, advances in the development of an approved clinical diagnostic assay have been mainly blocked by the difficulties to carry out a robust and comparable profiling of circulating miRNAs [89, 90]. It is required to design a robust and reliable detection platform which removes laborious sample-preparation steps (e.g., enzymatic steps for PCR-based detections such as ligation, reverse transcription and real-time PCR); this would introduce miRNAs as part of the approved clinical diagnostic test arsenal.

As mentioned above, to date, direct detection of unlabeled nucleic acids is based on just hybridization events with tagged probes. Some of methods used are: the sandwich hybridization approach uses two probes [91] and can also uses ligases to elongate short sequences of miRNAs [92, 93]; methods based on triple-stem DNA probes [94] and methods which use a probe to create duplexes which can be then detected either by modified surfaces [95, 96], or p19 protein that specifically recognizes nucleic acid duplexes [97, 98]. These molecular assays are then integrated within different detection systems such as electrochemical sensors [32, 94, 95, 98, 99] and fluorescence-based platforms [92] with variable limit of detections. Regarding miR-122, there are three reports which uses electrochemical sensors to directly detect this miRNA with a limit of detection of 2.7 pmoles [99], 1 pmole [32] and sub-attomole [94] respectively.

Herein, it is described a proof of concept study for developing a chemistry-based diagnostic tool for the direct detection of unlabeled miR-122 in a sensitive and specific way. Chem-NAT technology (based on specific DGL probes and dynamic incorporation of SMART-NBs) is integrated within two platforms to develop two fluorescent assays: 1) LoC® from STMicroelectronics® for a microarray assay and 2) Magplex® microspheres from Luminex® for a bead-based assay.

2.2. Fluorescent direct detection of unlabeled miR-122 through "Single Nucleobase Labeling" (SNL) (Specific objective 1.1.)

2.2.1. Microarray LoC: In-Check™ platform

Biological assays have evolved from relatively large volume reactions to smaller volume, faster, highly automated tests. These assays are considered "arrays", they can be performed in a test tube rack, a microwell plate, or a micro-volume chip where samples are physically separated from one another [100].

Much progress has been made with molecular multiplexing. Microarray technology permits simultaneous detection of a given sequence in a sample by hybridization to thousands of defined probes. Amplification and microarray integrated assays have been developed [101]. In this sense, STMicorelectronics In-Check™ platform allows fast analysis of nucleic acids in a miniaturized silicon Lab-on-Chip (LoC) that integrates a Polymerase Chain Reaction (PCR) reactor together with a customable microarray[5]. The In-Check™ system, supplied by STMicroelectronics, is composed of a disposable silicon-based microelectromechanical system (MEMS), LoC; a Temperature Control System (TCS) for the accurate control of the thermal process; an optical reader (OR) for the fluorescence microarray image acquisition; and a software for the image analysis (experimental section 5.2.4.3., figure 85) [102].

The In-Check™ system is an open platform for fast and automated nucleic acids testing which integrates the sample preparation step with the PCR amplification and the multi-analytical capability of the microarray technology [101, 102]. The manufacturing process of the LoC was patented by STMicroelectronics. The LoC is composed of two silicon microreactors fluidically connected to a microarray chamber. Each silicon microreactor (maximum volume of 12 µL) contains resistors and sensors to control the thermal process. The microarray chamber consists on a 3.5 mm × 9 mm area where probes can be immobilized (Figure 30) [102].
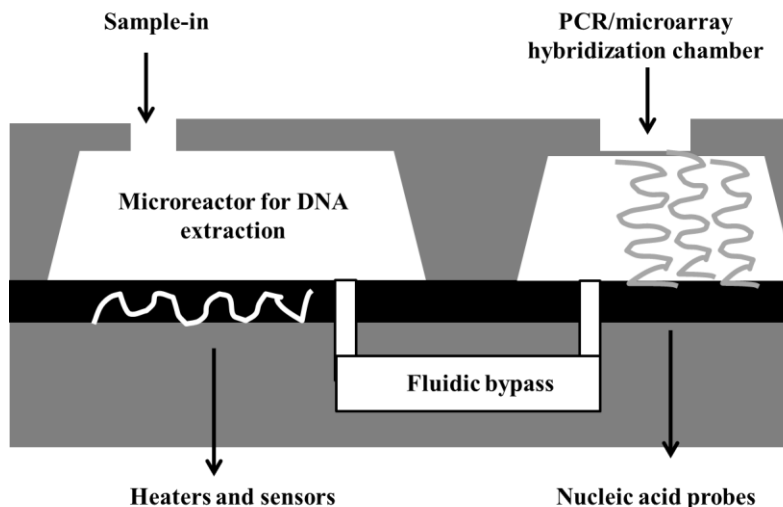
Figure 30: LoC cross-section[102].

In order to guarantee the microreactor sealing during the sample preparation, PCR amplification and hybridization reactions, it counts on PDMS-clamps. LoCs are chemically treated to allow for surface biocompatibility for the PCR amplification and the DNA microarray hybridization. After silicon standard cleaning, the surface is first modified using 3-glycidoxypropriltrimethoxysilane (GOPS) to obtain an epoxy derivative coating suitable for the microarray fabrication. Next, amino-modified probes are printed on LoC hybridization area. The Temperature Control System (TCS) is an electronic device to perform the enzymatic thermal cycling and hybridization reactions [102].

As an example, this system was used in a study where the microfluidic technology was combined with reverse transcription, PCR amplification, and microarray hybridization to develop an integrated LoC that can simultaneously detect and differentiate between 26 pathogen species (including bacteria, parasites and viruses) that cause 14 tropical diseases [101]. This and other examples provide proofs that LoCs were successfully applied for performing the PCR *in situ* and the subsequent nucleic acid testing. As a result, it was hypothesized that traditional probes might be replaced by DGL probes and merged the benefit of dynamic chemistry analysis of nucleic acids (Chem-NAT) with the ones of the microfluidic In-Check™ platform. As described above, an initial proof-of-concept was previously developed by our group using SMART-C-FITC as the SMART-NB for miR-122 detection (Figure 21) [34]. It was now intended to study the incorporation of a SMART-NB tagged with another fluorophore (sulfoCy5) and so evaluating the incorporation and fluorescence efficiency with this new SMART-NB and, therefore, questioning the possibility of expanding the test to a dual-color assay.

2.2.2. Results

2.2.2.1. DGL probes design

MiR-122 was selected as a model to perform the assay and study the integration between the platform and the dynamic chemistry approach for miRNA detection due to its potential application as prospective biomarker (see section 2.1.3.1.). Two different kinds of DGL probes were checked: with a neutral PNA-backbone (DGL-122-U for uncharged) and with 6 negative charges distributed along the sequence (DGL-122-C for charged) (see experimental section 5.2.1. and 5.2.2. for DGL probe sequences). This chiral and negatively charged DGL probe was achieved using PNA building blocks containing a propanoic acid side chain at gamma position (Figure 31B) (see experimental section 5.1.3. for PNA building monomers used for DGL probes synthesis).

A)   **B)**

PNA   **S-Propanoic-gamma PNA**
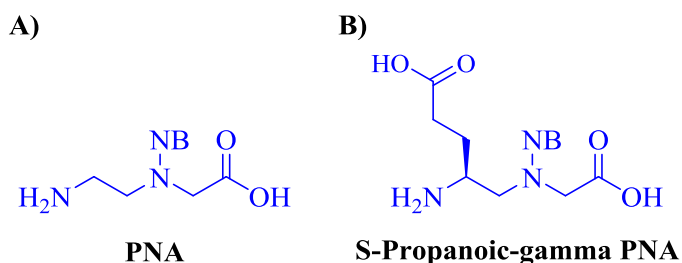
Figure 31: Chemical structure of neutral (A) and chiral and negatively charged PNA monomers having a propanoic acid chain at the γ-position (B).

DGL probes targeting miR-122 were used to validate and optimize this device for a chemistry approach for nucleic acid detection. Probe design was carried out using publicly available database (miRBase Accession Number: MIMAT0000421). They clamp the mature miR-122 sequence with their N-terminal facing the 3' end of the miR-122 sequence (antiparallel hybridization), meaning that the abasic position lined up opposite to a guanine (Figure 32).

Mature miR-122 5' UGG AGU GUG ACA AU G GUG UUU G 3'

C-term C TCA CAC TGT TA ? CAC AA N-term *DGL-122*

DNA-miR122 5' TGG AGT GTG ACA AT G GTG TTT G 3'

Figure 32: Alignment between mature miR-122 sequence, its mimic ssDNA (DNA-miR122) used for the assay development and the DGL probe sequence targeting both nucleic acid. The square G shows the templating nucleotide that lies opposite the blank position indicated by the squared question mark.

2.2.2.2. DGL probes immobilization on the In-Check™ platform LoC

Since DGL probes are going to be immobilized on a solid surface (Figure 33A), they need a nucleophilic group at their N-terminal. –NH2 and –SH groups were explored. Nucleophilic groups at the N-terminal of the DGL probes react chemoselectively with the epoxysilane groups that coat the silic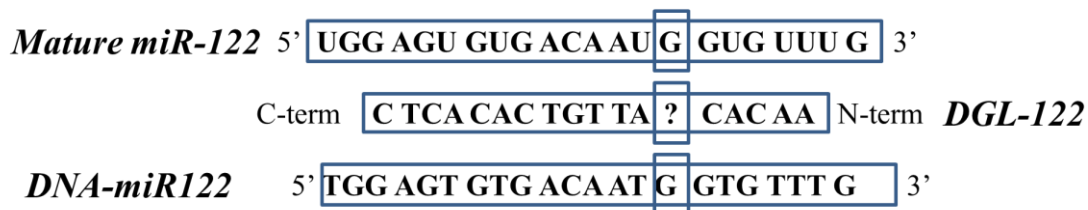on-based microarray surface of the In-Check™ LoC thus opening the epoxy ring of the surface and leading to the covalent immobilization of the DGL probe (Figure 33B).
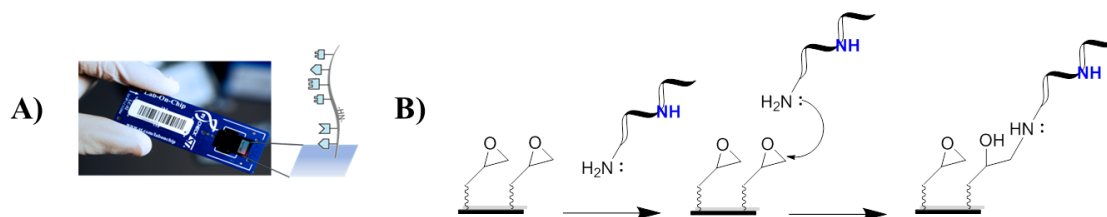

Figure 33: LoC reactive surface: A) highlight and scheme of the area where probes are immobilized; B) chemistry involved in the immobilization process: the epoxy-silanized LoC surface is attacked by the nucleophilic group on the N-terminal of the DGL probe, opening the ring and covalently immobilizing the probe.

A molecular spacer, poly(ethylene glycol) or PEG which is a polymer composed of repeating -CH$_2$CH$_2$O- units, was located at the N-terminal of the probes (Figure 34). This PEG spacer increases the distance between the DGL probes recognition area and the LoC surface so facilitating the interactions between the printed probes and their target nucleic acids in solution. It also increases the water solubility of the DGL probe by reducing their tendency to aggregate [103].
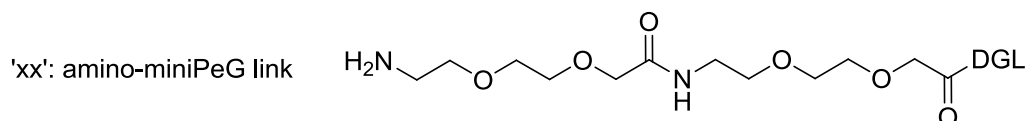
Figure 34: Amino-miniPEG spacer located at the N-terminal end of the DGL probes.

DGL probes were printed onto the array and arranged in 2 rows and 6 columns (12 features in total). They were deposited uniformly onto the LoC microarray area using a proprietary non-contact inkjet printer (Capital Bio PersonalArrayer16). The precise inkjet process enabled the delivery of small and accurate volumes of the probe (it has a dynamic volume capacity of 10 nl - 50 µl).

Different spotting buffers were tried in order to optimize the size and shape of the spot, minimize splashing and avoid contamination. 300 mM PBS with a 10% ethylenglicol was the selected one for neutral DGL probes (see experimental section 5.2.4.1.). It was also tried 40% of formamide in 300 mM PBS, 40% formamide in H$_2$O and Schott Spotting buffer. However, even though printing

improved, unspecificity issues were still happening. So, some changes in other part of the protocol needed to be arranged.

2.2.2.3. Blocking In-Check™ LoC reactive surface

Efficient blocking of reactive surface groups after arraying was critical for a reduced fluorescence background and avoiding non-specific SMART-NB reactions. The LoC was blocked with a 150 mM phosphate buffer containing 50 mM dimethylamine, pH 9 (60ºC 15 min, room temperature 15 min). The tertiary amines engendered prevented reactions with the aldehyde groups of the SMART-NBs (Figure 35) (see experimental section 5.2.4.1.). Standard SCHOTT blocking buffer (containing ethanolamine) was excluded as this would give rise to secondary amines on the surface which could react with the aldehyde groups of the fluorescently-labeled SMART nucleobase. Other compositions tried were 50 mM DMA in 150 mm Phosphate buffer pH 12 (60ºC 15min, room temperature 15 min), 50 mM Isopropanol in Acetate buffer pH 5 (room temperature 30 minutes).
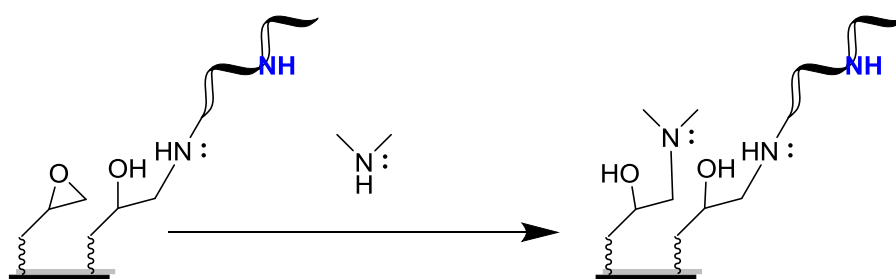
Figure 35: Blocking reaction where dimethylamine reacts opening the remaining epoxy-rings. The epoxy-rings would be thus functionalized either with a DGL probe or with dimethylamine which would avoid non-specific reactions.

2.2.2.4. Validation of the immobilized DGL probes

The performance of the DGL probes covalently linked to the LoC surface was checked: they have to maintain its ability to recognize and hybridize with a complementary nucleic acid strand forming a perfect duplex in order to allow the dynamic chemistry process to occur. Figure 36 schematizes the validation reaction that takes places on the LoC microarray area: A) probes non-complementary to the Cy5-labeled nucleic acid do not hybridize so there is no fluorescent signal. B) DGL-probes complementary to the target added hybridize with it being so fluorescently labeled.

A)

B)
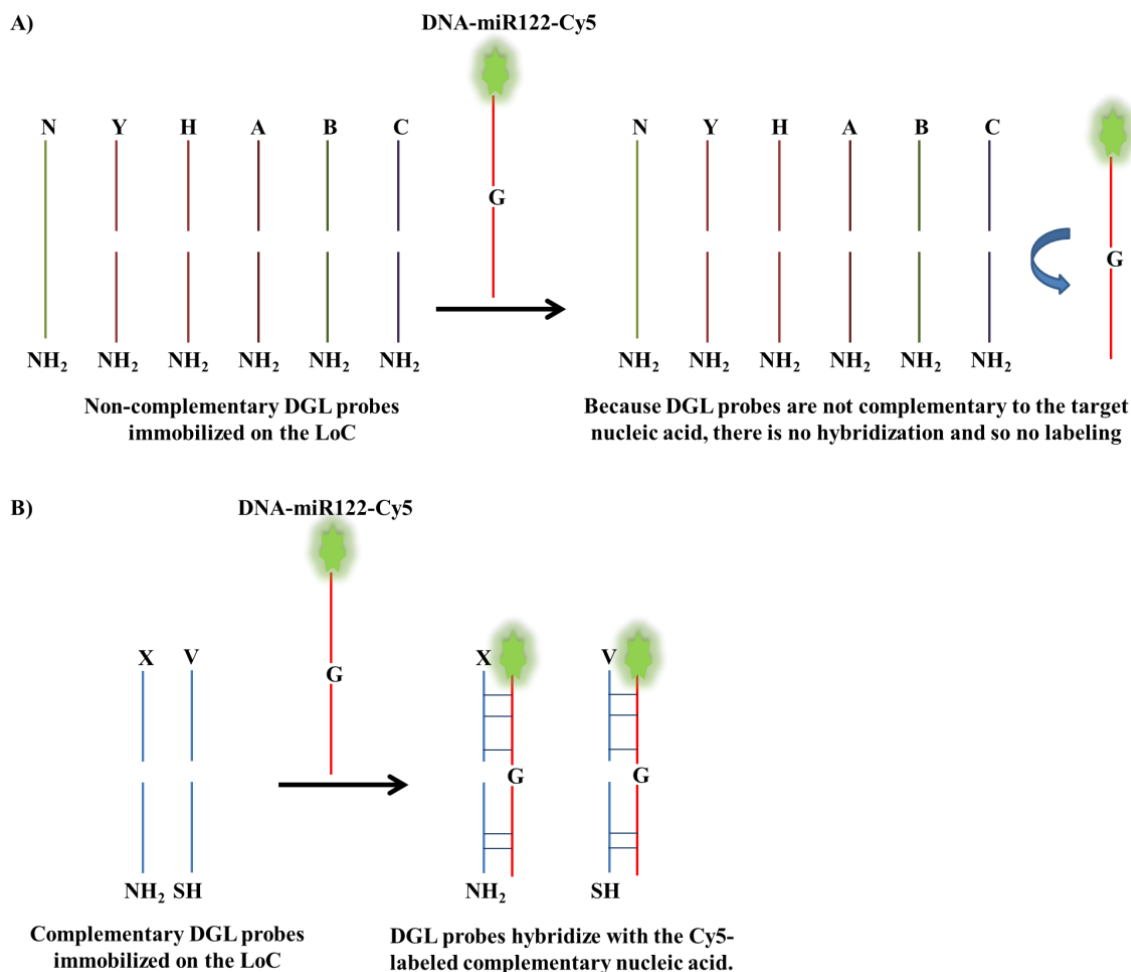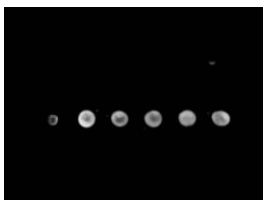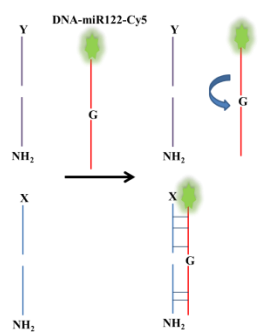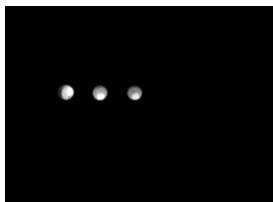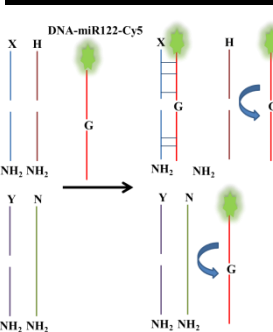
Figure 36: Scheme of the validation assay: A) One PNA strand (N) and several DGL probes (Y, H, A, B, C) non-complementary to the target nucleic acid, miR-122, are immobilized on the LoC surface which result in the absence of hybridization with the labeled target, DNA-miR122-Cy5 (no fluorescent signal). B) Two miR-122 DGL probes (X, V) complementary to the target nucleic acid spotted on the LoC. They both hybridize with the Cy5-labeled miR-122 (fluorescent signal).

Table 3 shows the results obtained after the validation reaction. It was carried out using a Cy5-labeled ssDNA, miR-122-Cy5, complementary to the miR-122 DGL probe (15 nM as final target concentration). After the hybridization, LoC are scanned and the bright spots that can be seen correspond to those places where a DGL probe –complementary to the ssDNA added- was spotted (Table 3). To check DGL probe specificity, different DGL probes and PNAs non-complementary to the target sequence miR-122 were also immobilized on the array area (DGL-G2Pr1-NH$_2$, DGL-G1Pr1-NH$_2$, PNA-Ana-NH$_2$, DGL-K12SRC-NH$_2$, DGL-K13SRC-NH$_2$, DGL-28S-NH$_{2;}$ schematized as probes Y; H; N; A; B; C, respectively) (see experimental section 5.1.6., table 35 for sequence details). Comparing the panel of immobilized DGL probes and where bright spots are

seen, it can be concluded that fluorescent signals are only observed in spots where DGL-miR122 (X) was immobilized and no fluorescent signals are observed for non-complementary probes (Y, H, N) so it can be confirmed that DGL probes selectively hybridize only with a complementary nucleic acid (Table 3).

Table 3: First and third columns show the panel of DGL printed: X: represent DGL probe for miR-122; Y and H correspond to DGL probe for bacteria whose sequence is not complementary to miR-122; N represents a PNA probe without abasic position and whose sequence targets another bacteria, Anaplasma. Second and fourth columns show the results of the spotted DGL-mir122-NH$_2$ LoC validation for which a complementary DNA labeled with Cy5 was used, DNA-miR122-Cy5 (15 nM final concentration). Fluorescent signal is only seen where the corresponding probe, X: DGL.122-NH$_2$, was immobilized.

DGL probe spotting map	Printing validation of DGL-miR122-NH$_2$	DGL probe spotting map	Printing validation of DGL-miR122-NH$_2$
Y Y Y Y Y Y X X X X X X Y = DGL–G2Pr1–NH$_2$ X = DGL–122–NH$_2$		X X X H H H Y Y Y N N N X = DGL–122–NH$_2$ H = DGL–G1Pr1–NH$_2$ Y = DGL–G2Pr1–NH$_2$ N = PNA–Ana–NH$_2$	

2.2.2.5. Base-filling reaction of Cy5-labeled SMART-NBs

After optimizing printing, blocking conditions and validating the capability of the DGL probes to efficiently hybridize only with complementary nucleic acids, the ability to achieve a Chem-NAT protocol on the LoC device was explored. The reactivity in the chemical pocket, being the templating power of the nucleotide under interrogation and the availability of the free secondary amine of the abasic position to react with the aldehyde group of the SMART-NBs, was analyzed. Figure 37 schematizes the dynamic incorporation process of SMART-C-Cy5 into DGL probes covalently linked to the LoC surface. Figure 37A shows DGL probes non-complementary to the target nucleic acid (N, H, Y, A, B, C), due to the absence of complementarity, do not hybridize with the target nucleic acid what prevents SMART-C-Cy5 incorporation into the abasic position of the

probes. On the other hand, Figure 37B shows the process where DGL probes (X, V) are complementary to the target nucleic acid what allow them to hybridize and so the templating guanosine drives the incorporation of SMART-C-Cy5 into the abasic position of the DGL probes.
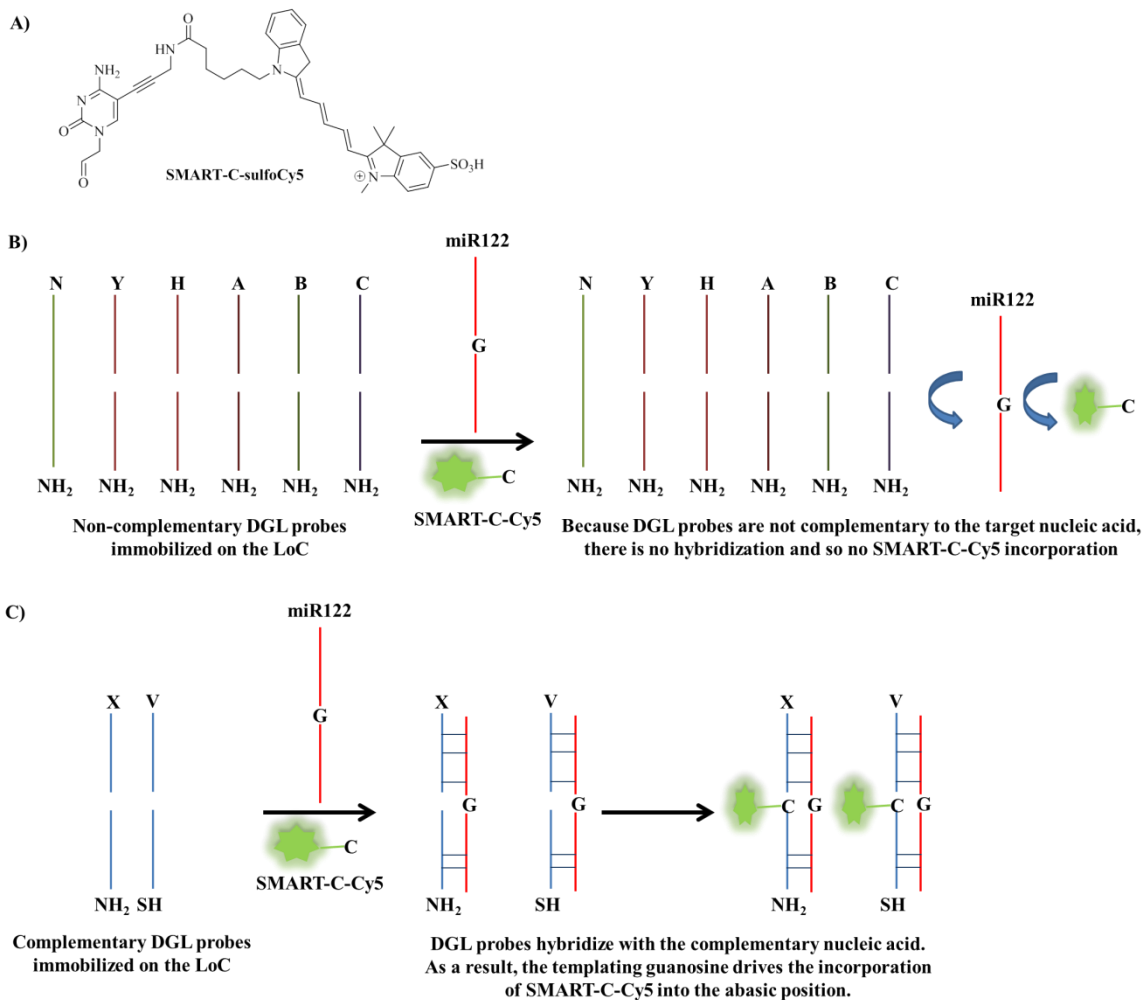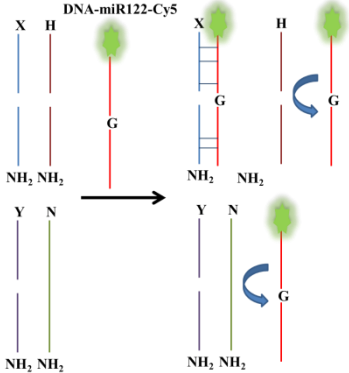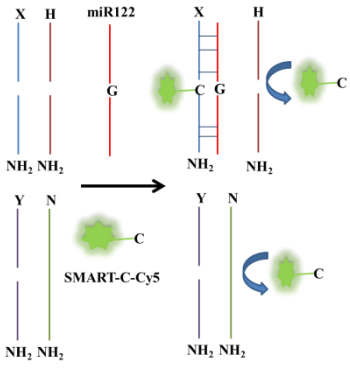
Figure 37: Scheme of the Chem-NAT technology on LoC: A) Chemical structure of SMART-C-sulfoCy5, the labeling nucleobase used for the fluorescence-based assay on the In-check™ LoC. B) One PNA strand (N) and several DGL probes (Y, H, A, B, C) non-complementary to the target nucleic acid are immobilized on the LoC. When the target nucleic acid, miR-122 is added, because of the absence of complementarity, there is no hybridization and so SMART-C-Cy5 incorporation is not templated (no fluorescence is observed). C) miR-122 DGL probes (X, V) complementary to the target are immobilized on the LoC surface. Upon miR-122 addition, they both hybridized with the target and so the guanosine that lies opposite the abasic site of the probe templates the incorporation of SMART-C-Cy5 (seen as a bright spot when scanning the LoC with the optical reader).

To simplify the assay and due to the one color detection, only one labeled SMART-NB is used, in this case SMART-C-Cy5. The first column of table 4 shows the DGL probe spotting layout. The

second column shows the validation results what indicates where signal should be seen when applying the dynamic chemistry approach. Finally, the third column corresponds to the base-filling reaction performed when using an unlabeled ssDNA, miR-122 (83.3 nM final concentration), complementary to DGL-miR122 probes (X, V) as target nucleic acid and SMART-C-Cy5 (5μM finmal concentration) as labeled SMART-NBs (see experimental section 5.2.4.3). Once DGL probes-DNA heteroduplex has been formed, the guanosine nucleotide that lies in front of the abasic position templates the incorporation of a SMART-C-Cy5 into the abasic position of the probe what when scanned were seen as bright spots.

Table 4: First column shows the panel of DGL probes printed: X: represent DGL probe for miR-122; Y and H correspond to DGL probe for bacteria whose sequence is not complementary to miR-122; N reprensents a PNA probe without abasic position and whose sequence targets another bacteria, Anaplasma.. Second column corresponds to LoC validation of DGL-mir122-NH$_2$ for which a complementary DNA labeled with Cy5 was used, DNA-miR122-Cy5 (15 nM). Fluorescent signal is only seen where the probe complementary to the labeled DNA added was immobilized. Third column shows LoC dynamic incorporation of SMART-C-Cy5. The reaction was done using SMART-C-Cy5 as labeled nucleobase and DNA-miR122 (83 nM) as target nucleic acid which templates the incorporation of SMART-NB. However, fluorescent signals are also seen for other DGL probes whose target DNA has not been added. A schema representing what is happening on the LoC is also shown.
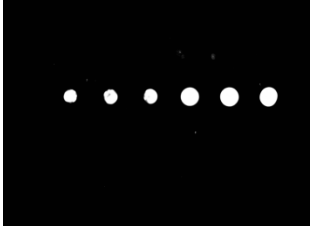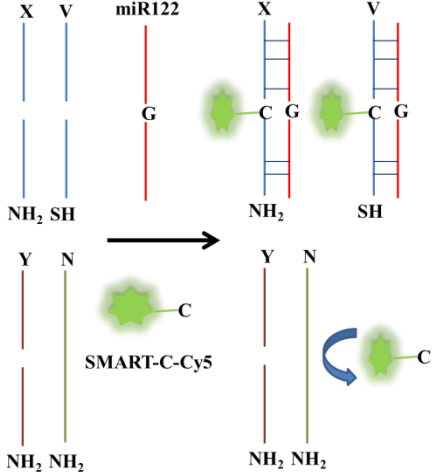
DGL spotting map	Printing validation of DGL-miR122-NH$_2$	Dynamic chemistry reaction on DGL-miR122-NH$_2$ using DNA-miR122 as template

Even though the validation assay worked well and signals could be only seen at those spots where DGL probes complementary to the DNA added were spotted, when doing the chemical reading reaction on LoC some unspecificity problems appeared. Fluorescent signals, due to Cy5-labeled SMART-NB incorporation, could be seen in spots where probe non complementary to the DNA added were immobilized (H, Y, N) (Table 4, third column, the last three spots of the first row). DGL probes and assay should be optimized. This might be related to the immobilization of probes on a solid platform, the reagents concentration, the assay itself.

Taking into account PNA features and considerations extracted when applying DGL probes and dynamic chemistry to other platforms, structural modification of DGL probes were tried: adding negative charges along the sequence assists in the hybridization process since it make the DGL probe to adopt a B-form similar to the one of the DNA and so easing the hybridization and it also should avoid the probes to fold on themselves once they have been spotted on the LoC (Figure 31B) [20, 104, 105]. This modification indeed improved DGL probe performance and removed some unspecificity problems as it can be observed in Table 5 where a new base-filling reaction was performed using miR-122 as target DNA and SMART-C-Cy5 as labeled SMART-NB. This LoC has four different DGL probes immobilized on the surface: two DGL probes complementary to the target nucleic acid [DGL-122-NH$_2$ (X) and DGL-122-SH (V) both having 6 negative charges distributed across the probe sequence and which differ in the nucleophilic group on the N-terminus being either an primary amine or a thiol group]; a non-complementary probe, DGL-G2Pr1 (Y); and a PNA strand non-complementary to the target and without abasic position, PNA-Ana (N). The target DNA, miR122, specifically hybridizes with their complementary probes what drives the specific incorporation of SMART-C-Cy5 into the abasic position of both probes DGL-122-NH$_2$ (X) and DGL-122-SH (V) being thus fluorescently labeled (bright spots observed in the LoC picture in Table 5). Bright spots were not observed for those non-complementary probes DGL-G2Pr1 (Y) and PNA-Ana (N) which highlights the benefitial effect of the chirality and negative charges introduced into the DGL probes sequences.

Table 5: First column shows the panel of DGL printed where X and V: represent DGL probe for miR-122 with an –NH$_2$ group (X) or an –SH group (V) at the N-terminal; Y corresponds to DGL probe for a bacteria so it is not complementary to miR-122 sequence and N reprensents a PNA probe without abasic position and whose sequence targets another bacteria, Anaplasma. Both DGL probes targeting miR-122 harbor six negative charges along the sequence. Second column corresponds to LoC dynamic incorporation of SMART-C-Cy5. The reaction was done using SMART-C-Cy5 as labeled nucleobase and DNA-miR122 (83 nM) as target nucleic acid which templates the incorporation of SMART-NB. Non-specific fluorescent signals are seen which confirms the fact that the negative charges and the chirality contributes to increase the specificity of the technology. It is also schematized the incorporation of SMART-C-Cy5 into the different DGL probes spotted on the LoD.

DGL spotting map	Dynamic chemistry reaction on negatively charged DGL probes: DGL-miR122-NH$_2$ and DGL-miR122-SH using DNA-miR122 (83nM) as template
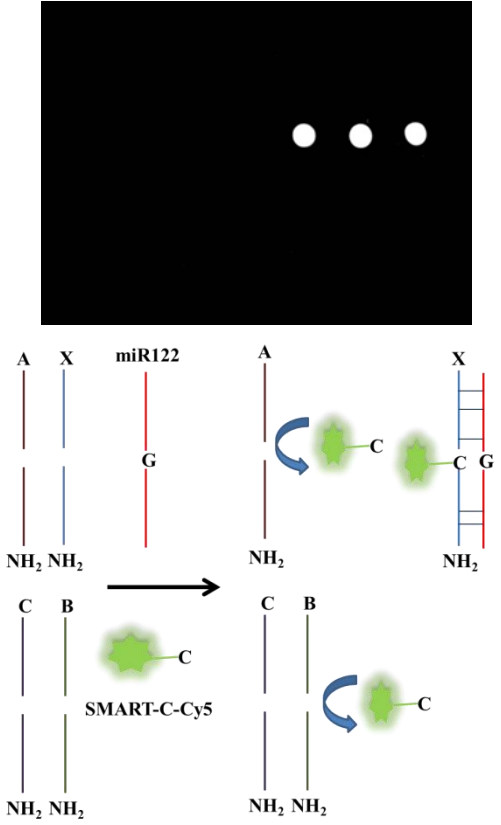
Template miR-122 (DNA-miR122) plus complementary DGL-122 attached to the array correctly hybridize and fluorescence due to SMART-C-sulfo-Cy5 incorporation; whereas spots where non-complementary DGL probes were immobilized, do not show fluorescence. These studies demonstrate that chemistry involved in the linkage between DGL probes and LoC silicon surfaces do not affect the dynamic chemistry reaction allowing thus the use of amino-modified probes. Moreover both amino and thiol N-terminal groups react with epoxy-modified silicon surfaces for

probe immobilization. Also PNA (without pocket) was used as control, demonstrating that SMART-NB incorporation did not happen.

Table 6 shows another miR-122 Chem-NAT assay carried out on a LoC with four different DGL probes immobilized: three non-complementary probes [DGL-K12SRC (A); DGL-K13SRC (B); DGL-28S (C)] and one probe complementary to the target, DGL-122 (X). As it can be observed in the picture of the second column of table 6, bright spots due to SMART-C-Cy5 incorporation into the abasic position of the DGL probes are only observed for DGL-122 (X) which highlight the selectivitiy and specificity of the Chem-NAT assay.

Table 6: First column shows the LoC layout: X is used to indicate the DGL for miR-122; A and B correspond to two DGL probes whose sequences target a region of KRAS gene; C refers to a DGL probe complementary to a gene of trypanosomatid parasites. Second columns show the result after the dynamic chemistry reaction. Even if 4 different DGL probes were immobilized, signals are only seen at those places where the probe immobilized is complementary to the DNA added which templates SMART-C-Cy5 incorporation. The second column also shown a schematic representation of the DGL probe labeling reaction where DNA only hybridizes with the complementary probe and then labels it *via* SMART-C-Cy5 incorporation

DGL spotting map	Dynamic chemistry reaction on DGL-miR122-NH$_2$ using DNA-miR122 as template
A A A X X X C C C B B B A = DGL-K12SRC-NH$_2$ X = DGL-122-NH$_2$ C = DGL-RNA28S-NH$_2$ B = DGL-K13SRC-NH$_2$	
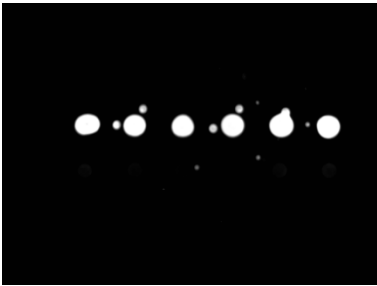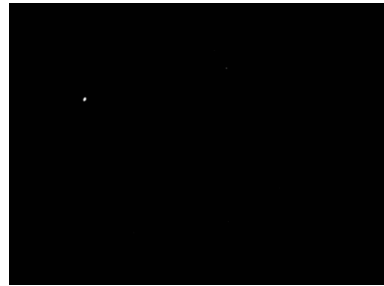
2.2.2.6. Specificity of the chemistry-based approach for nucleic acid reading on the In-Check™ LoC platform

A specificity study was carried out to evaluate the capacity of the chemical approach to recognize only complementary sequences and incorporate only the right SMART-NB according to Watson-Crick base pairing rules. To do so, a ssDNA mimicking miR-122 sequence, DNA-miR122 (with a Guanine as templating nitrogenous base in the chemical pocket) and a ssDNA representing a modified miR-122 sequence, DNA-miR122-A (with an Adenine instead of the real templating Guanine) were used. Two LoCs with two different DGL probes, DGL-122 (X) and DGL-RNA28S (C), immobilized on the surface were used. The hybridization was run in parallel but each LoC has a different templating ssDNA (Table 7). The second column of Table 7 shows the assay results when DNA-miR122 was added. Bright spots due to SMART-C-sulfoCy5 incorporation can be seen only where the complementary DGL probe had been immobilized. This confirms the selectivity of the assay and the high affinity of the designed molecular probes to recognize and hybridize only with fully complementary sequences.

On the other hand, the third column of Table 7 shows the assay in which DNA-miR122-A was used as template. Since there is an Adenine in front of the abasic position, it templates the incorporation of the unlabeled SMART-Thymine; as a result, no fluorescent signal is observed. This confirms the ability of the technology to follow Watson-Crick base pairing rules and fix into the abasic position only the right SMART-NB. To sum up, the absence of the signal in the Chem-NAT assay performed on the In-Check™ platform might be due to a) no complementarity and so, no hybridization between the target nucleic acid and the DGL probe and b) the absence of a G in front of the abasic position to template the incorporation of SMART-C-sulfo-Cy5 onto the pocket, since it is the only labeled SMART-NB used in this assay.

Table 7: Specificity of the Chem-NAT assay performed on the In-Check™ platform LoC. First columns shows the LoC layout: V correspond to DGL targeting miR-122 with an –SH at the N-terminal and C refers to a DGL probe complementary to a gene of trypanosomatid parasites Second and third column show the result of the dynamic incorporation of SMART-C-Cy5 using two different target nucleic acid: 1) when the target, miR-122 with a G as templating nucleotide, hybridizes with its probe, SMART-C-Cy5 incorporation occurs (second column). 2) Whereas when the target, miR-122-A having an A as templating nucleotide, complementary to the probe hybridizes, the templating adenosine avoids the fluorescent signal because there is no incorporation of the Cy5-labeled SMART-Cytosine (third column). An scheme of the process happening on the LoC is shown: DNA hybridize only with the complementary target and the templating nucleotide drives the incorporation of the complementary SMART-NB, being the DGL probe only labeled if SMART-C-Cy5 has been incorporated (second column).

2.2.2.7. Turnaround time

Once DGL probes have been immobilized and the LoC surface blocked, LoC can be stored until use. The process will last 1.5 hours between dynamic incorporation and washing steps. The Temperature Control System has capacity for 5 LoC so up to 5 analyses can be run at once.

2.2.2.8. Multiplexing capability

This assay shows the multiplex capability of the In-Check™ platform LoC to analyze different nucleic acids at the same time and its potential utility as a novel diagnostic tool. Multiplexing can be achieved just by designing and spotting a panel of probes targeting different features: SNPs, identification of a pathogen agent, miRNAs, and genes related to drug-resistance…Then, In-Check™ LoC with a specific panel of immobilized DGL probes can be prepared and stored until use. Knowing where DGL probes were immobilized and where bright spots can be seen, detection and identification of the nucleic acid under interrogation can be done. Up to 4 different DGL probes were analyzed when using Capital Bio PersonalArrayer16 as inkjet printing system.

2.2.3. Discussion

A "Proof of Concept" study for testing the integration of the dynamic chemical reading of nucleic acids on the In-Check™ platform LoC from STMicroelectronics has been described. This study represents a first step in the development of a medical diagnostic assay capable of delivering a novel biochip platform for the rapid detection of nucleic acids with high sensitivity and specificity.

As previously described [20, 104, 105] and also experimentally tested, standard PNAs tend to collapse when immobilized on surfaces because of their neutral backbone (Figure 3, 31A) and the hydrophobic interactions between nucleobases. In order to resolve this, anionic groups were added across the probe backbone. Since self-aggregation is reduced, polyanionic DGL probes were thus more readily available to hybridize with complementary nucleic acid strands and, hence, allow more efficient dynamic incorporation of the SMART-NBs. These modifications were introduced with PNA building blocks containing a propanoic acid chain at gamma positions with S-configuration (Figure 31B).

Background was at a very low level, demonstrating excellent blocking and the benefit of the proof reading step using the SMART-NB incorporation protocol.

Selective incorporation of SMART-C-sulfoCy5 into the DGL/DNA hybrid through dynamic chemical reactions can take place only when the nucleic acid, DNA-miR122 in this example, forms a perfect duplex with the designed DGL probe, DGL-miR122 (Table 5, 6 and table 7 second column). On the other hand, no fluorescence is observed when there is a non-complementary nucleic acid or when the nucleotide that lies opposite the abasic position templates the incorporation of a non-fluorescently-labeled SMART-NB (Table 7 third column). This demonstrated the selective incorporation of the "correct" base when the target nucleic acid forms a perfect duplex.

There were other possible fluorophores to be used for labeling at this wavelength such as the internally developed NNO650. However, its extinction coefficient (56,000 L mol−1 cm−1) was lower than the one for sulfoCy5, this implies that a higher concentration is required to achieve similar brightness than that obtained with SMART-C-sulfo-Cy5. So, it is important to assess the stability of the dyes (higher extinction coefficient lower stability) versus brightness (higher extinction coefficient higher brightness).

Optimizing printing performance allows many more DGL probes to be immobilized in the microarray reactive area improving the multiplexing capability of the LoC platform and so that of the assay.

On the other hand, a one-color detection assay has been presented what implies that each SMART-NB has to be interrogated individually. Using a cocktail of 4 different fluorescently-labeled SMART-NBs and an optical reader with filters for the corresponding 4 wavelengths would allow reading the four SMART-NBs simultaneously and so, analyzing as many targets as DGL probes had been immobilized in a single LoC.

As a result of optimizing the printing conditions to spot more DGL probes in a LoC reactive area and using 4 different fluorescently-labeled SMART-NBs, the multiplexing capability of the In-Check™ LoC platform would be increased.

The result confirms that the In-Check™ LoC could be used as a platform for a fluorescence-based assay to analyze nucleic acids. They also show the high fidelity of the chemical approach for testing nucleic acids. The reaction only takes place in the presence of a complementary-templating nucleic acid and it only incorporates the SMART-NB complementary to the one that lies opposite to the abasic position. The results further indicate that the Chem-NAT approach used for miR-122 herein could be extended to more generic, direct nucleic acid analysis such as allele-discrimination, SNP, miRNAs profiling, parasite identification...

However, some issues have to be considered in order to develop a diagnostic assay with good reproducibility, easy to be performed, at a low cost and with good multiplexing capacity. The In-Check™ platform constitutes a microarray platform (2-dimensional solid arrays). 'Multiplexing', or reading multiple test results in a single sample volume has been complicated primarily by spectral overlap -color from one assay detection channel which interferes with color in other detection channels-. This limited the assays only to a few analytes per sample [100]. In addition, even if this platform allows small-volume assaying of physically separated features, it might have limitations such as slow, solid-phase kinetics; instability of immobilized protein or nucleic acid capture molecules; and poor reproducibility what may limit its broader application in the clinical or research

laboratory. On the other hand, solution-phase multiplex assays benefits from reduced sample volume and other redundant consumables and faster results due to solution-phase kinetics [100]. This reasoning and potential limitations led to the search for other platforms which overcame the drawbacks of the microarray assays on surface.

2.3. Bead-based platform for direct detection of unlabeled miR-122 through "Single Nucleobase Labeling" (SNL) (Specific objective 1.2.)

2.3.1. Bead- based platform: Luminex® xMAP® technology

'Multiplexing', or reading multiple test results in a single sample volume has been complicated mainly because spectral overlap what has limited the number of analytes that could be studied per sample. In addition, 2-dimensional solid arrays follow solid-phase kinetics which might interfere with the reproducibility of the results and the performance of the assay. However, solution-phase multiplex assays benefits from reduced sample volume and other redundant consumables as in solid microarrays but they provide faster and more repoducible results due to solution-phase kinetics. A combination of the advantages of both methodologies was found in Luminex® xMAP® technology.

In the late 1990s, scientists at Luminex® invented xMAP® technology which conserves the strengths of solid-phase separation technology (adding magnetic properties to the microspheres what simplifies assay washings and allows each bead to be analyzed separately) without the limitations of solid-phase reaction kinetics (beads exhibit virtually solution-phase kinetics due to their microscopic size -6.5 µm- and low density) [100].

MagPlex® microspheres are the newest generation of Luminex® xMAP® beads. These are 6.5-micron superparamagnetic beads which are dyed with different ratios of two (Figure 38A) or three dyes (Figure 38C) allowing the generation of either 100 (Figure 38B) or 500 (Figure 38D) different colored beads, respectively, for the development of multi-analyte assays up to 500-plex. The surface of these beads is impregnated with iron-containing magnetite particles. This feature allows the use of magnets to rapidly remove the beads from reaction suspensions, to speed up processing protocols and to minimize bead loss, resulting in more reproducible data generation [100].
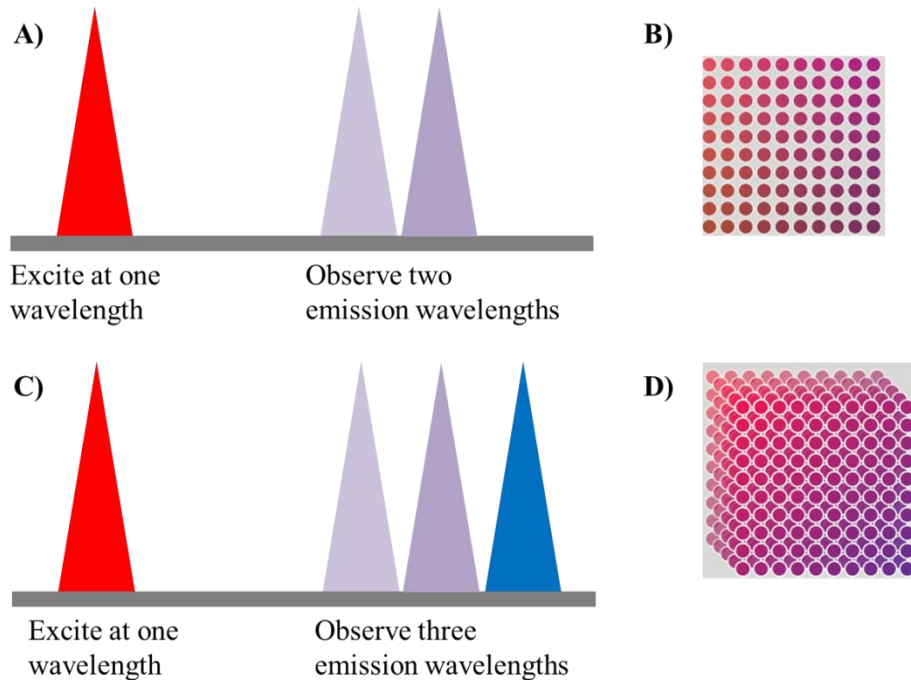
Figure 38: xMAP® microspheres include different combinations of two dyes where (A) one excitation wavelength allows observation of two separate fluorescence emission wavelengths, yielding (B) 100 unique microsphere sets (10x10 dye matrix); or three dyes where (C) one excitation wavelength allows observation of three separate fluorescence wavelengths, yielding (D) 500 unique microsphere sets. (10x10x5 dye matrix) [100].

There are two main light sources inside the Luminex analyzer: (1) one provides is the "classification" light which has a 635 nm emission wavelength and excites the dyes inside the microspheres allowing the identification of each microsphere particle (Figure 38 and 40) and (2) the second one summit analyte information, it excites samples at 532 nm recording signals from any fluorescent reporter molecules captured during the assay, commonly phycoeritrin (Figure 39 and 40). The instrument records dozens of readings for each bead set and produces a distinct result for each analyte in the sample. Using this process, xMAP® technology allows multiplexing of up to 500 unique bioassays within a single sample, using each color-coded bead for a different target molecule.
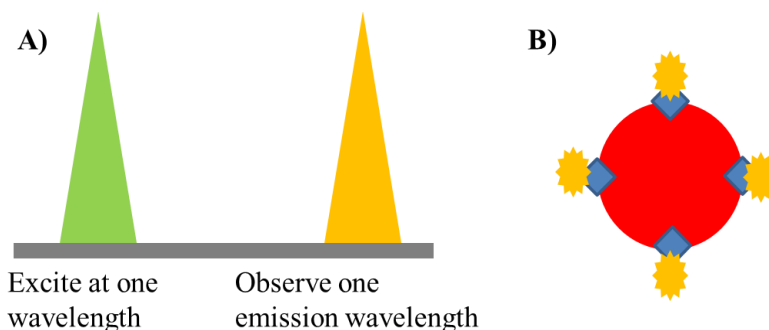
Figure 39: (A) A second excitation wavelength allows observation of a separate fluorescent reporter molecule (B) that allows detection of the analyte captured on the surface of the microsphere [100].
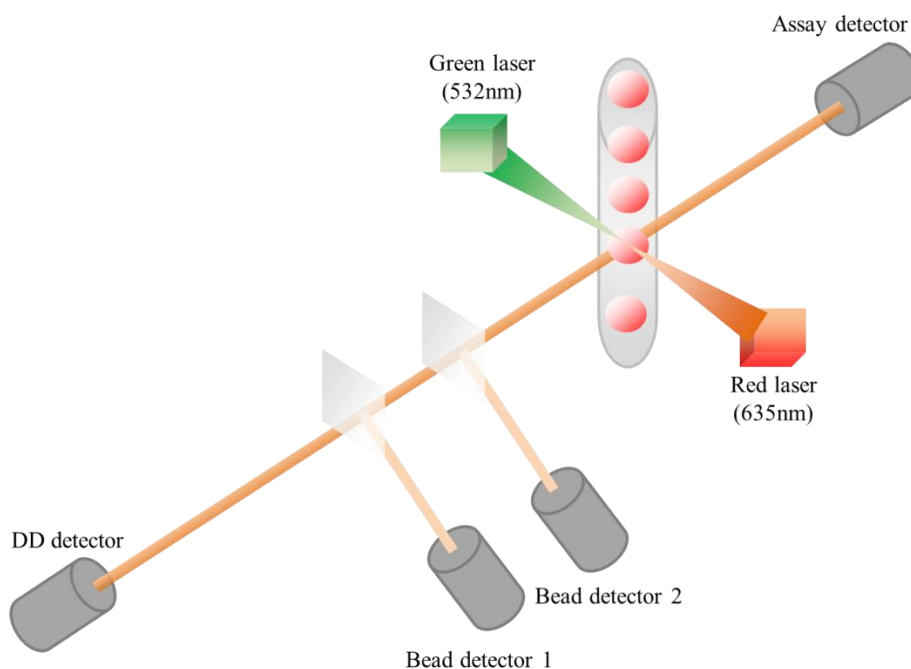
Figure 40: The reader has four detectors one for each of the optical paths shown in the figure. Detectors are used to measure the fluorescence of the assay, to determine the bead set (1-100 plex) and to discriminate between single and aggregate beads [106].

MagPlex® Microspheres are compatible with all Luminex instruments, including MAGPIX® (up to 50-plex), Luminex® 100/200™ with xPONENT® software (up to 80-plex) and FLEXMAP 3D® (up to 500-plex for MagPlex) [100].

xMAP® technology is adaptable to a number of biological assays, including immunoassays, nucleic acid assays and enzyme activity assays (Table 8). Common immunoassay formats are capture sandwich, competitive and indirect antibody assays. Nucleic acid assays are hybridization-based where a probe sequence captures a labeled complementary target from the sample reaction. Enzyme

activity assays typically involve labeling or cleaving a peptide substrate to introduce or release a fluorescent molecule [100].

Table 8: Types of biological assays performed with xMAP® technology

Immunoassay	Nucleic Acid	Enzyme Activity
Capture sandwich	TAG incorporation	Kinase/Phosphatase selectivity
Competitive	PCR based	
Indirect assay	Primer extension	
	Probe ligation	

Luminex® has licensed these multiplex biological assays to a number of kit developers in the clinical diagnostics, pharmaceutical and life science research markets. There are commercially available kits for molecular diagnostics, immunodiagnostics, kinase profiling, cytokine/chemokine, genotyping, gene expression, etc. In addition to commercial kits, Luminex® supports custom assay development.

A proof-of-concept study was carried out to analyze the potential combination of Chem-NAT technology with a bead-based platform (Luminex®) to develop a fluorescent assay to directly detect miRNAs, for which miR-122 was used as miRNA model. As it was previously described, nucleic acids are detected through its hybridization with high affinity DGL probes and the incorporation of the complementary SMART-NB onto the abasic position [32]. Relative quantification is also possible as the yield of the reaction depends on the amount of templating nucleic acid.

2.3.2. Results

2.3.2.1. Polyanionic DGL probes improve hybridization efficiency.

As described above, standard PNA molecules tend to adopt collapsed conformations, due to their neutral backbone (Figure 31A) and hydrophobic interactions between nucleobases [20, 107, 108]. When they are bound to polystyrene microspheres, these conformations were enhanced due to hydrophobic interactions between polymers and PNA oligomers. The strategy followed to resolve this was adding anionic groups across the PNA or DGL probe backbone since this might reduce this tendency and also reduce self-aggregation. Polyanionic DGL probes bound to microspheres would thus be more readily available to hybridize with complementary nucleic acid strands and, hence, allow more efficient dynamic incorporation of the SMART Nucleobases. To achieve this, PNA building blocks containing propanoic acid chains at gamma positions with S-configuration were used (Figure 31B) [105, 109, 110].

2.3.2.2. DGL probes design and bead functionalization

Two DGL probes, both containing the same sequence of nucleobases to allow hybridization to the mature miR-122 strand were prepared. As previously detailed, they were design so that once hybridized with the target; there will be a Guanine in front of the abasic positon acting as templating nitrogenous base (Figure 32). One DGL probe was built with unmodified PNA monomers (DGL-122-U) and the other one carried six PNA monomers containing the propanoic acid modifications at the gamma positions (DGL-122-C) (see experimental section 5.1.3. for PNA building monomers used for DGL probes synthesis and section 5.2.2. for DGL probe sequences). Both probes were conjugated to MagPlex® microspheres (MC10012) to give FB-1 (functionalized with DGL-122-U) and FB-2 (functionalized with DGL-122-C) respectively (see experimental section 5.2.5.1.for microspheres functionalization procedure).
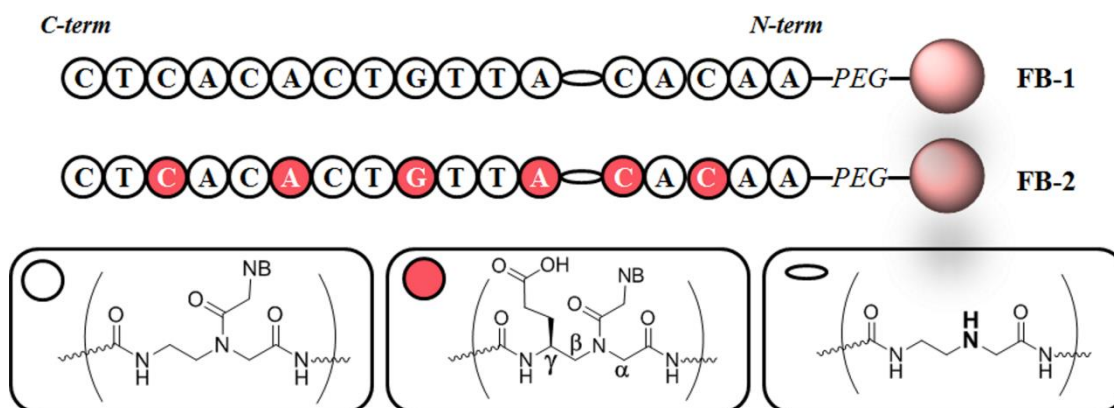
Figure 41: Sequence of the two DGL probes-functionalized microspheres (FB1 with DGL-122-U and FB-2 with DGL-122-C). Unmodified PNA monomers are represented with a white circle; chiral and negatively charged PNA monomers are shown with a red circle and the abasic site with a yellow ellipse. Reproduced with permission [111].

2.3.2.3. Validation of DGL probes immobilized on MagPlex® microspheres

In order to integrate Chem-NAT and xMAP® technologies, labeling with a reporter molecule is required; in this case, a biotin tag either on the target nucleic acid or on the SMART-NB was used. This tag will be later recognized by a fluorescent complex responsible for the generation of the fluorescent signal, in this case streptavidin-R-phycoerithrin conjugate (SAPE) was used. DGL probe performance and their capacity to recognize and join to their complementary target once they are immobilized on the microspheres was assessed by hybridization with biotin-tagged ssDNA oligomers mimicking the miRNA sequence. Fully complementary nucleic acid, DNA-miR122-biotin, or a non-complimentary control, DNA-miR21-biotin, (750 fmoles in a reaction volume of 50

µL, i.e., 15 nM) were used. Hybridization was followed by Streptavidin-R-Phycoeritrin (SAPE) labeling (see experimental section 5.2.5.2. for validation assay procedure). As it can be observed in figure 42, microspheres FB-2 (functionalized with the chiral and negatively charged DGL probe, DGL-122-C) showed better hybridization efficiency than FB-1 (functionalized with the neutral probe, DGL-122-U), they have a higher Median Fluorescence Intensity (MFI) and hence FB-2 were chosen for further experiments. Figure 42 also shows that fluorescence measurement similar to background or noise were obtained when adding the negative control DNA-miR-2-biotin what demonstrates the selectivity of the DGL probes to hybridize only with complementary nucleic acids. Propanoic acid groups improve the hybridization feature of DGL-122 probe due to (i) the chiral configuration which creates a right-handed duplex and (ii) the electrostatic repulsion provided by the negative charges distributed across its backbone [20, 104, 105].
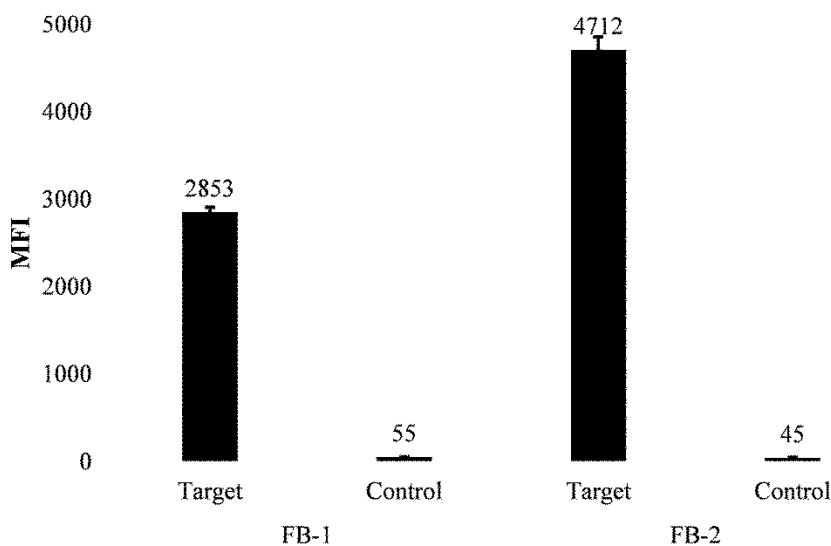
Figure 42: Median Fluorescence Intensities (MFI) obtained from MAGPIX® after hybridisation and SAPE treatment using FB-1 and FB-2. Target: miR122-biotin; control: miR21-biotin. n = 3. . Reproduced with permission [111].

2.3.2.4. Detection of miR-122 using Single Nucleobase Labeling (SNL) strategy and Limit of detection

The 'Single Nucleobase Labeling' (SNL) approach for miR-122 detection on the combined Chem-NAT&xMAP® platform involved several steps: First, DGL probes coupled to MagPlex® microspheres hybridize with their complementary target nucleic acid, DNA-miR122 (Figure 43, step 1 (i)), then a reversible reaction between the SMART-C-PEG-Biotin and the free secondary amine of the abasic position occurs leading to iminium ion formation (Figure 43, step 2 (ii)). This

process is driven by the templating Guanine on the target nucleic acid, which can just template the incorporation of the complementary aldehyde-modified cytosine, the other three iminium species are not stable enough to be reduced. The more thermodynamically stable iminium ions are then reduced by sodium cyanoborohydride yielding to a non-reversible tertiary amine within the DGL probe conjugated to the microspheres (Figure 43, step 1 (iii)) [33]. Once, the SMART-C-PEG-Biotin has been incorporated into the abasic position, the heteroduplex DGLprobe/DNA on the microsphere is fluorescently labeled with streptavidin-R-phycoerythrin conjugate (SAPE) *via* its interaction with the biotin tag on the SMART-NB (Figure 43, step 2). Finally, the fluorescence is measured using the Luminex® MAGPIX® platform (Figure 43, step 3) [111].
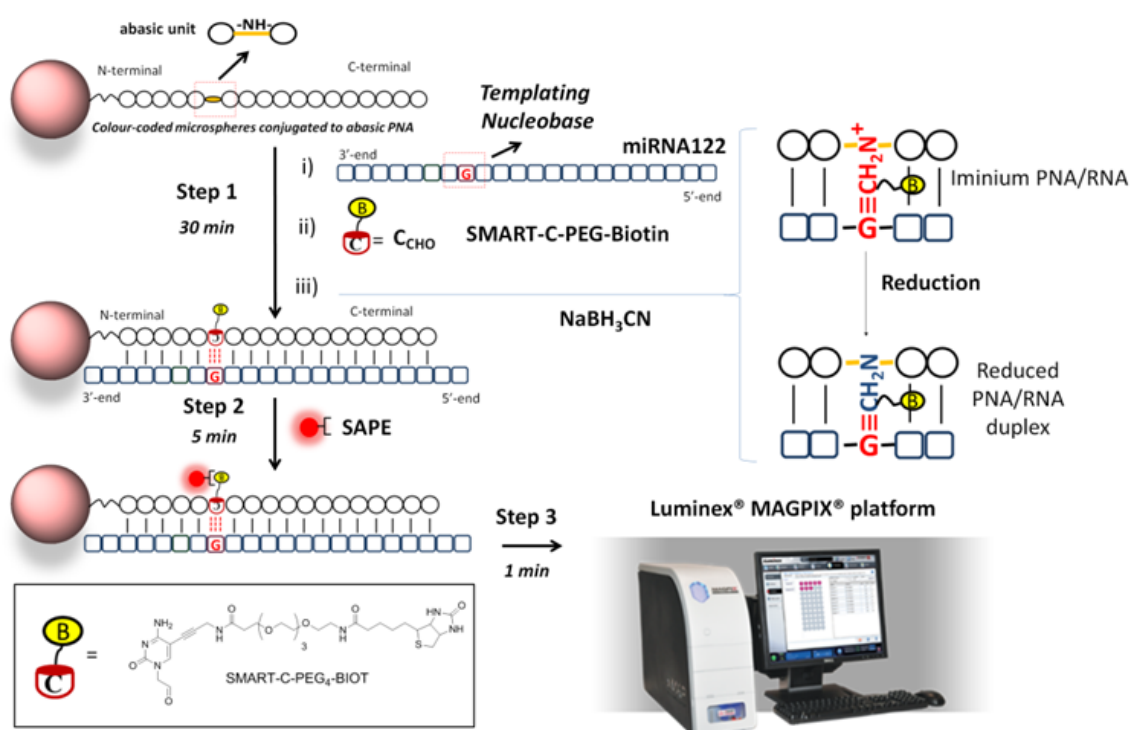
Figure 43: Merging of dynamic chemistry with Luminex® MAGPIX® platform for 'Single Nucleobase Labeling' (SNL) of miR-122. Step 1: it implies 3 substeps: i) miR-122 DGL probe conjugated to color-encoded microspheres (MagPlex® from Luminex®) perfectly hybridize with its target, miR-122; ii) formation of reversible iminium species between the free secondary amine of the abasic position of the probe and the aldehyde group of the SMART-C-PEG-Biotin; and iii) reduction of the iminium species by sodium cyanoborohydride (NaBH$_3$CN) resulting in a non-reversible tertiary amine within the DGL probe conjugated to the microspheres [33]. Step 2: Fluorescent-labeling with streptavidin-R-phycoerythrin Conjugate (SAPE) *via* its interaction with the biotin tag of the SMART-NB. Step 3: Fluorescent detection using Luminex® MAGPIX® platform (45 min total time, including washings). Reproduced with permission [111].

Once hybridization performance of DGL probes on the paramagnetic microspheres was established, SNL was conducted using FB-2 microspheres (functionalized with the chiral and negatively charged DGL probe, DGL-122-C), approximately 1250 microspheres were used per assay. Two different unlabeled nucleic acids were used, ssDNA mimicking miR-122 sequence, DNA-miR122, which fully matches the DGL probe sequence on the microspheres FB-2; and ssDNA mimicking miR-21 sequence, DNA-miR21, which is not complementary to the probe and so it shouldn't hybridize. Decreasing amounts of DNA-miR122 were tested: 7500, 750, 75 and 7.5 fmoles. The four quantities were combined with a fixed concentration of the negative control DNA-miR21 (7500 fmoles) in a total reaction volume of 50 µL (150, 15, 1.5 and 0.15 nM final concentration of target DNA-miR-122 respectively) (Table 9). According to the DGL probe design and because only one color can be analyzed, only one biotin-tagged SMART-NB was used, SMART-C-PEG$_2$-Biotin, at a final concentration of 40 µM. After SAPE labeling, microspheres samples were analyzed using Luminex$^{®}$MAGPIX$^{®}$ (see experimental section 5.2.5.3. for SNL procedure and experimental section 5.2.5.4. for fluorescence measurement on MAGPIX$^{®}$). Table 9 shows the obtained fluoresecence measurements (MFI). The experiments were repeated five times presenting coefficient of variant for each condition, ranging from 10% to 15% (Table 9). The obtained data of MFI versus miRNAs concentrations showed a linear correlation for the target, confirming the suitability of SNL to detect and semi-quantify unlabeled nucleic acids. No fluorescence was detected when analyzing DNA-miR21 samples which further corroborates the high specificity and selectivity of the presented technology avoiding false positives.

Table 9: Detection of miRNA122 using SNL approach, replicates (n=5). Reproduced with permission [111].

	Log miRNA concen (pM)	Median of the Fluorescence Intensity (MFI)					Mean of MFI	SD	CV	% CV
		1	2	3	4	5				
FB2 + miRNA122 (150 nM) + miRNA21 (150nM)	3,875	1576	1596	1709	1650	1201	**1546**	179	0,116	**11,6**
FB2 + miRNA122 (15nM) + miRNA21 (150nM)	2,875	1124	1081	1109	1240	901	**1091**	109,4	0,100	**10**
FB2 + miRNA122 (1.5nM) + miRNA21 (150nM)	1,875	491	469	468	490	345	**453**	54,6	0,121	**12,1**
FB2 + miRNA122 (0.15nM) + miRNA21 (150nM)	0,875	148	145	210	159	142	**161**	25,3	0,158	**15,8**

Signal corresponds to the MFI value of target, DNA-miR122; and background is the MFI of negative control, DNA-miR21. Signal to background ratios (S/N) were calculated dividing the MFI obtained with a miR-122 sample between the MFI obtained for a non-complementary nucleic acid sample, in this case miR-21. The average S/N obtained were 14.2 ± 1.5, 9.7 ± 0.7, 4.2 ± 0.6 and 1.6 ± 0.3, respectively for the four miRNAs concentrations. The assay showed that 15 fmoles (0.3 nM) of target could be detected.

In order to know if this limit of detection was low enough to analyze clinical samples, potential levels of miR-122 in patients were studied. Dear et al, the leading group proposing the use of miR-122 as biomarker of drug toxicity, reported a mean value of 71.3 million copies of miR-122 per mL of serum (95% confidence interval [CI] 29.3–113.2 million) in a group of 18 healthy volunteers. 71 million of copies of miR-122 per mL of non-intoxicated patients is equivalent to around 0.15 fmoles [112]. Dear's group previously reported [81, 82, 87] the increase of miR-122 level in patients with liver injury from acetaminophen toxicity, which are 100- to 10000-fold higher when compared with basal levels. Based on these reported data related to the amount of copies of miR122

per mL of serum and the ChemNAT limit of detection for this platform (15 fmol), just 3 mL of serum, wich would be obtained from 7.2 mL of blood, would be needed to be within its limit of detection.

2.3.2.5. Effect of PEG length on Signal to background ratios

To study the effect of the length of the polyethyleneglycol (PEG) chains on the incorporation of the SMART-NBs, two SMART Nucleobases were tested (i) (SMART-C-PEG$_2$-Biotin) having 2 ethylenglycol units (4 oxygen atoms) between the pyrimidine ring and the biotin group (Figure 44A) and (ii) (SMART-C-PEG$_6$-Biotin) with 6 units (12 oxygen atoms) (Figure 44B).

SMART-C-PEG$_2$-Biotin
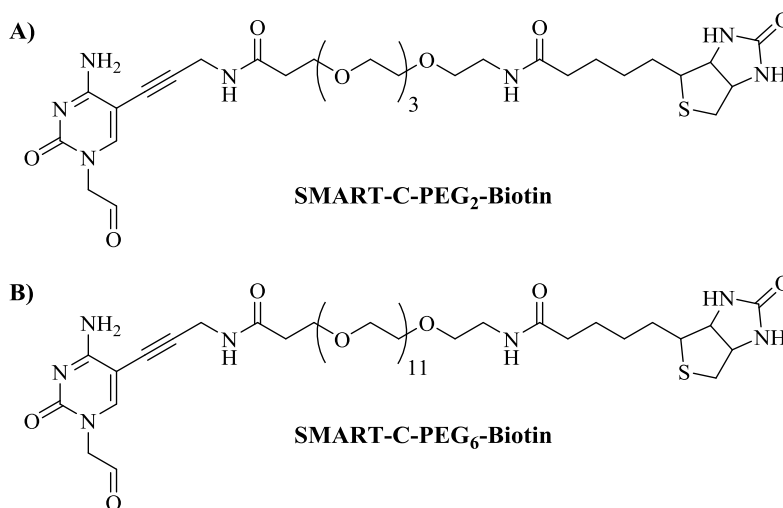
SMART-C-PEG$_6$-Biotin

Figure 44: Chemical structure of the two biotinylated SMART-Cytosines used for the SNL of miR-122. They differ in the length of the PEG spacer: A) two ehtylenglycol units, SMART-C-PEG$_2$-Biotin; or B) six units, SMART-C-PEG$_6$-Biotin.

Dynamic incorporation of both SMART-C-PEG-Biotin nucleobases was then studied using different quantities (7500, 750, 75 and 7.5 fmoles) of unlabeled complementary DNA-miR122 and non-complementary DNA-miR21. S/N ratios were then determined as described above (see section 2.3.2.4). While shorter PEG spacer (PEG$_2$) gave a better S/N at higher concentrations overall performance was very similar (Figure 45). So, it was concluded that the length of the PEG spacer chain in the SMART-NB did not have an influence on the detection limit.
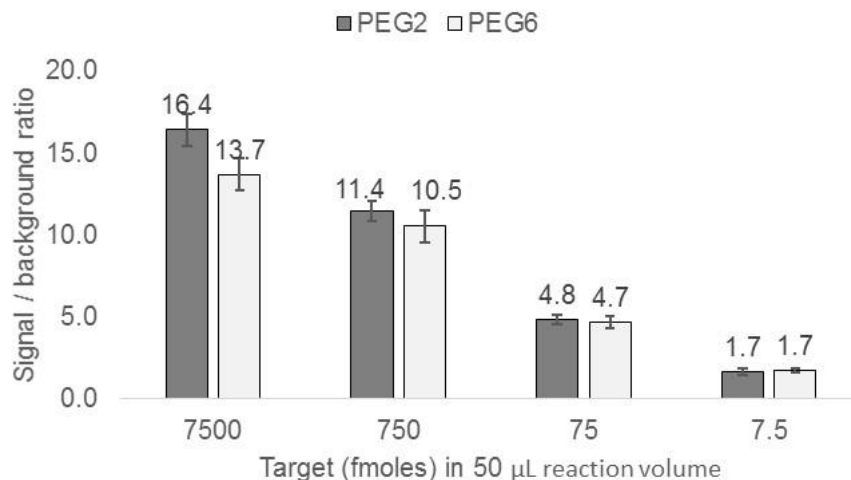
Figure 45: S/N ratios obtained after the SNL approach using two SMART-C-PEG-Biotin nucleobases which differ in the length of the PEG spacer: SMART-C-PEG$_2$-Biotin and SMART-C-PEG$_6$-Biotin. The S/N ratio was calculated dividing the MFI obtained from miR-122 by background - MFI obtained from miRNA-21. n =5. Reproduced with permission [111].

2.3.2.6. Specificity assessment of the Single Nucleobase Labeling (SNL) approach

To assess the level of specificity and selectivitiy of the SNL approach, an experiment was carried out using FB-2 microspheres, which are MagPlex® carboxylated microspheres functionalized with DGL-122-C. DGL probes coupled on the the microspheres hybridize with an unlabeled complementary nucleic acid sequence. Three different targets were studied and compared: When DNA-miR122 is used as target nucleic acid, it is fully complementary to the probe and templates the incorporation of SMART-C-PEG$_2$-biotin onto the abasic position which is subsequently labeled by SAPE (Figure 46A and 47). If DNA-miR122-A is used as target nucleic acid, it is also fully complementary to the probe and hybridizes with it; however, it does not template the incorporation of SMART-C-PEG$_2$-biotin so it is not labeled by SAPE (Figure 46C). Finally, when DNA-miR21 is used as target nucleic acid, it is not able to hybridize with the probe since it is not complementary (Figure 46B and 47).
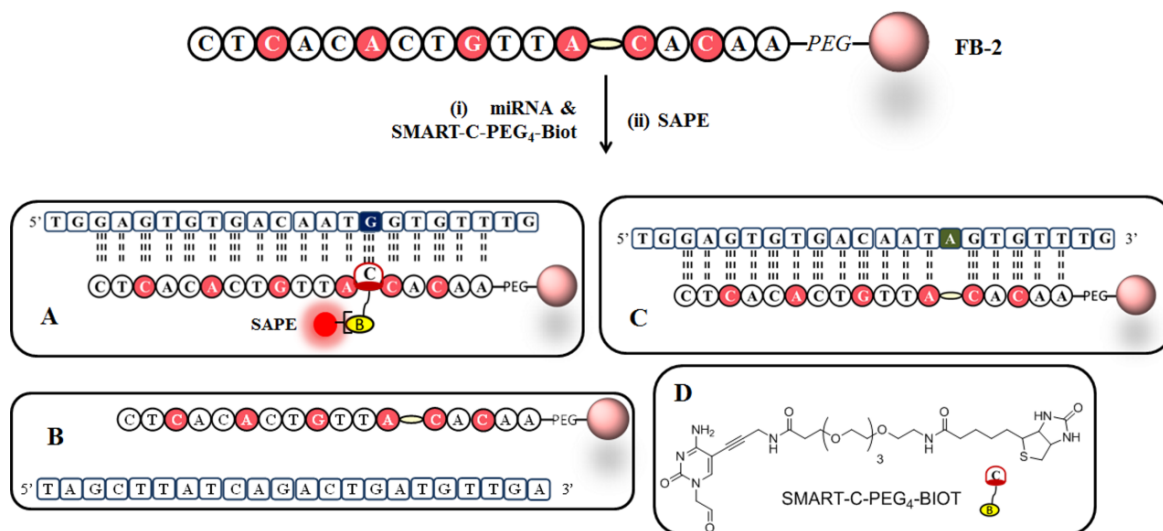
Figure 46: Representation of selectivity and specificity of the SNL approach using SMART-C-PEG$_2$-Biot and MagPlex® microspheres. (A) FB-2 (DGL-122-C functionalized MagPlex® carboxylated microspheres) hybridized with an unlabeled complementary nucleic acid sequence miR-122 which templates the incorporation of the SMART-C-PEG$_2$-Biot into the abasic position. After SAPE labeling, FB-2 microspheres become fluorescent and detectable by MAGPIX®. (B) FB-2 microspheres with a non-complementary nucleic acid, mirR-21, because of the absence of complementarity, no duplex is formed and so dynamic reaction is blocked. (C) FB-2 microspheres hybridized with an unlabeled complementary nucleic acid sequence, in this case miR-122-A, which templates the incorporation of SMART-Thymine, which does not hold a biotin-tag. Therefore, after SAPE labeling, even if the duplex has been formed, microspheres are not labeled by SAPE. (D) Structure of biotinylated SMART-Cytosine Nucleobase (SMART-C-PEG$_2$-Biot). Reproduced with permission [111].

Obtained results are shown in Figure 47. The graphic shows a positive linear correlation of the MFI values versus miRNAs concentration: MFI values increases as miR-122 concentration increases (Figure 47, blue dots and line for DNA-miR122). Moreover, it can be observed that no fluorescence was detected when the nucleic acid present in the sample is not complementary to the probe, such as miR-21 which was used as negative control, regardless the concentration used. The absence of complementarity avoids the duplex formation and so there is no templating power driving the dynamic reaction between the aldehyde group of the SMART-NB and the free secondary amine of the abasic position of the DGL probe (Figure 47, red dots and line for DNA-miR21).
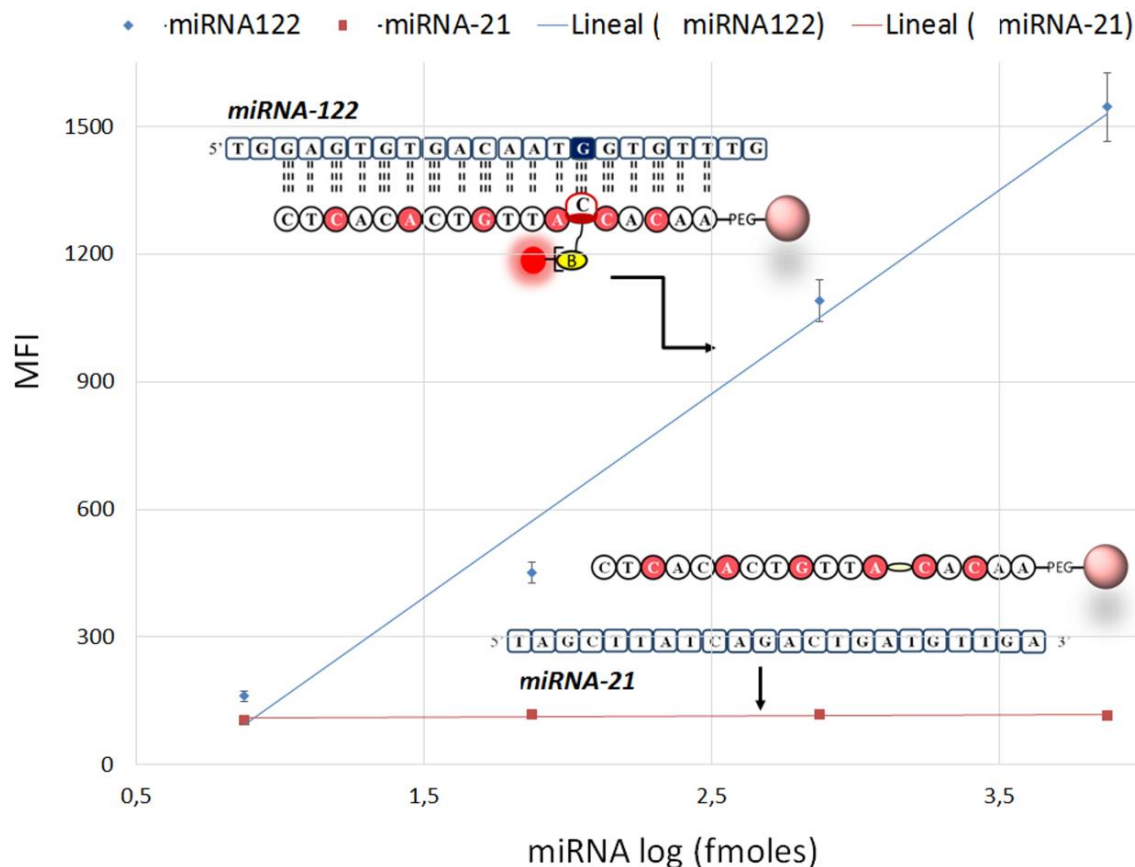
Figure 47: Direct detection of nucleic acids by dynamic chemistry. FB-2, SMART-C-PEG$_2$-Biotin, and four quantities (7500, 750, 75 and 7.5 fmoles) of unlabeled target (miR-122) and control (miR-21) were used. MFI obtained using MAGPIX$^®$ after SNL and SAPE treatment, reveal selective incorporation of the biotinylated SMART-NB, SMART-C-PEG$_2$-Biotin, only for the complementary target, miR-122. An increase in the MFI is observed as the amount of target increases. n =5. Reproduced with permission [111].

As schematized above, to evaluate the specificity of the dynamic incorporation of SMART-NBs on the DGL probes coupled to microspheres, two almost identical sequences were studied, miR-122 and miR-122-A. The only difference between the two sequences lies on the templating nucleotide, the one that lies opposite the abasic position. miR-122 mimics the original miR-122 sequence having a Guanine at that position and templating SMART-Cytosine incorporation (Figure 46A and Figure 48 with red dots and line for DNA-miR122), whereas miR-122-A has an Adenine instead and so it drives the incorporation of SMART-Thymine (Figure 46C and Figure 48 with blue dots and line for DNA-miR122-A). Because all the sequence except for the templating nucleotide that lies opposite the abasic site is the same, both nucleic acids are able to hybridize and formed a perfect heteroduplex DGLprobe-Nucleic Acid. However, only SMART-Cytosine is labeled with biotin, so fluorescent signals must only be observed when the target has a Guanine in front of the

abasic position. As a result, only fluorescent signal should and, indeed, were observed when the nucleic acid presents in the sample is miR-122 through the templated incorporation of SMART-C-PEG$_2$-Biotin and later biotin-streptavidin (SAPE) recognition (Figure 46A and Figure 48 with red dots and line for DNA-miR122). On the other hand, when miR-122-A was used as target nucleic acid; even if it fully matches with the DGL probe and formed a perfect heteroduplex; the templating nitrogenous base is an Adenine, so unlabeled SMART-Thymine was incorporated and, hence, no fluorescence was detected, the signals were unaffected and comparable to those of the non-complementary strand (Figure 46C and Figure 48 with blue dots and line for DNA-miR122-A). These results demonstrate the high discrimination capacity of the Chem-NAT technology what can be exploited to analyze iso-miRNAs, such as miR-10a and miR-10b.
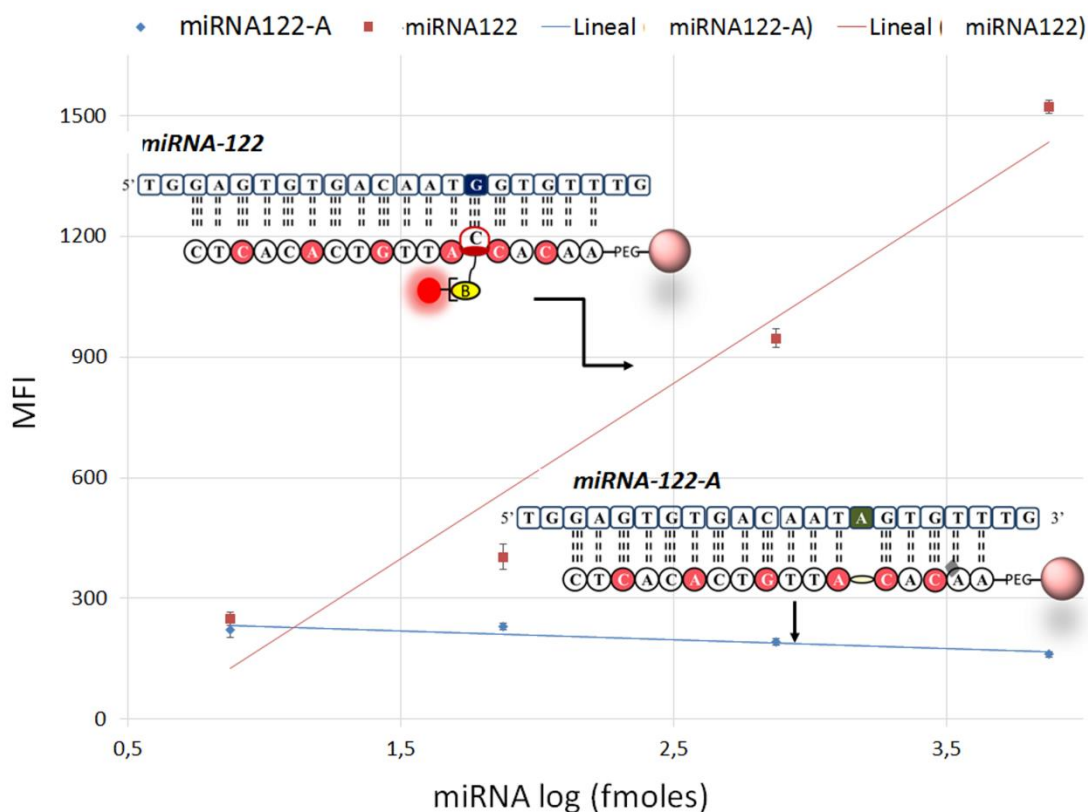
Figure 48: Direct detection of miR-122 by dynamic chemistry on MAGPIX® - specificity assessment. MFI obtained from MAGPIX® after SNL and SAPE treatment using FB-2, SMART-C-PEG$_2$-Biotin, and four different quantities (7500, 750, 75 and 7.5 fmoles) of unlabeled miRNAs (miRNA-122 and miRNA-122-A). Fluorescence is only detected when miR-122 is used since it templates the incorporation of the biotin-labeled SMART-Cytosine. MFI increases as miR-122 concentration increases. No fluorescence, similar intensity to negative controls, is observed when using miR-122-A which templates the incorporation of an unlabeled SMART-NB. n =5. Reproduced with permission [111].

2.3.2.7. Turnaround time

Once microspheres have been functionalized with a DGL probe, they can be stored until use. The SNL approach will last 45 minutes between dynamic incorporation and washing steps. The assay can be performed in a 96-well plate which can be directly introduced into the MAGPIX® analyzer for fuorescence analysis. So, up to 96 tests can be performed simultaneously and using different color-coded beads multiplexing can be achieved.

2.3.2.8. Validation of Single Nucleobase Labeling through flow cytometry

Flow cytometry was used to validate the results from MAGPIX®. The validation experiments also provide useful information to determine whether better discrimination could be achieved with Luminex® FLEXMAP 3D®, a more advanced multiplexing platform that uses flow cytometry-based technology [112]. SNL experiments were carried out with varying quantities (7500, 750, 75 and 7.5 fmoles) of DNA-miR122 (Figure 49, dot plots in the second column) and DNA-miR21 as negative control (Figure 49, dot plots in the first column). After SAPE labeling, samples were analyzed in parallel with MAGPIX® (Table 9 and Figure 47) and a flow cytometer (Figure 49). Flow cytometry assays were performed in a BD FACSCanto and dot-plots were obtained with Flowjo software (see experimental section 5.2.5.5.). Population shifts on the PE (phycoeritrin) channel were clearly seen even with the lowest amounts of miR-122 used (7.5 fmoles) (Figure 49, dot plots in the second column). In this case, better S/N ratio at the lowest concentration was achieved when compared with the data obtained using MAGPIX® indicating that a better detection limits might be achievable with the more advanced platform, FLEXMAP 3D®.
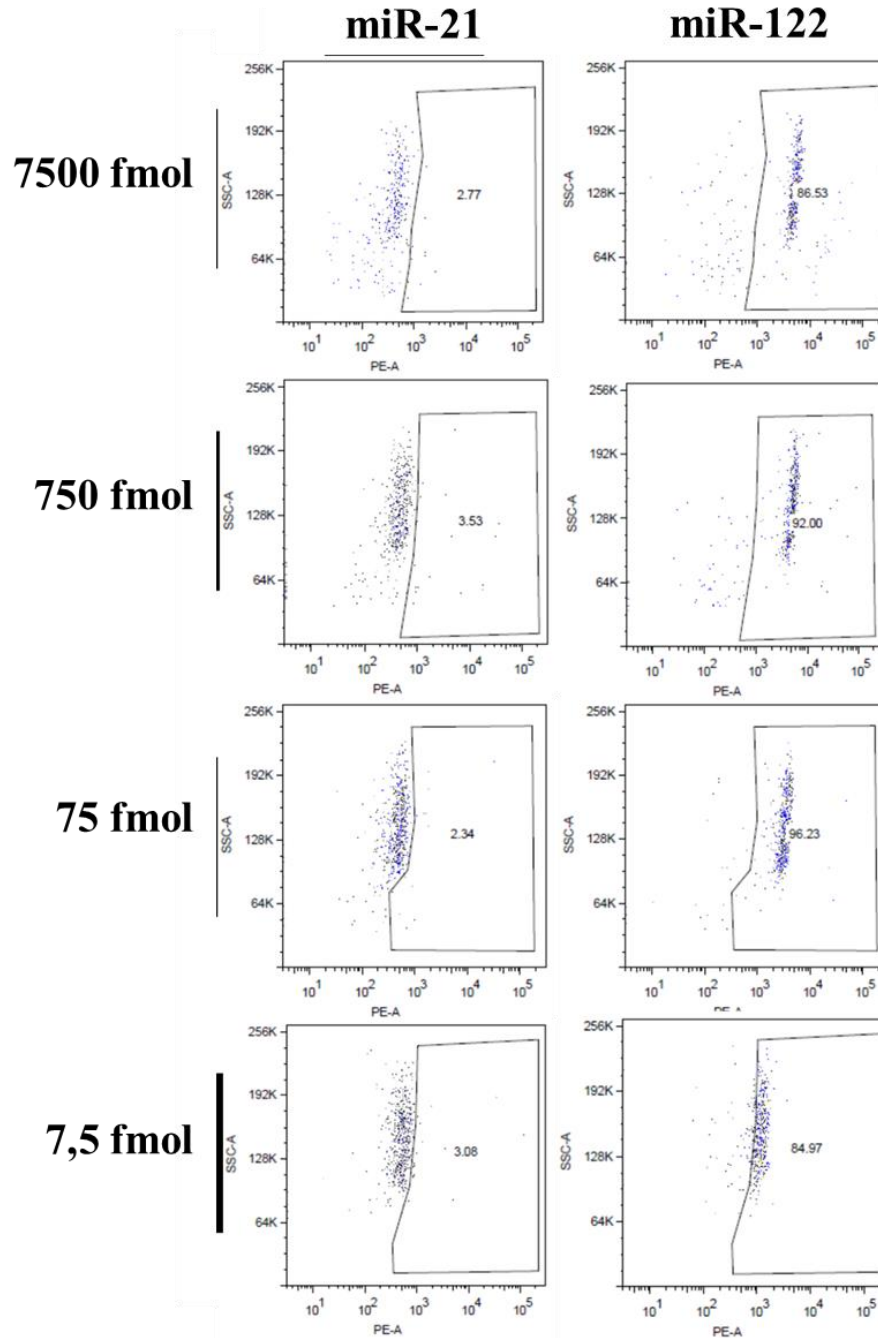
Figure 49: Flow cytometry analyses. SNL was conducted using FB-2, SMART-C-PEG$_2$-Biot and varying quantities (7500, 750, 75 and 7.5 fmoles) of DNA-miR21 as negative control (first column) and DNA-miR122 as target (second column). After SAPE incubation, samples were analyzed by BD FACSCanto II ™ using the PE channel. Dot plots were obtained with Flowjo (SSC in the Y-axis and PE in the X-axis). A fluorescence and population shift is observed when decreasing the concentration of the target nucleic aid (DNA-miR122, second column). No fluorescence was observed for samples containing DNA- miR21. Reproduced with permission [111].

2.3.2.9. Validation through confocal microscopy and analysis with ImajeJ

To provide a visual confirmation of selective dynamic incorporation of SMART-C-PEG$_2$-Biotin, samples of SNL conducted with 7500 fmoles of DNA-miR122 (target) and DNA-miR21 (negative control) were analyzed, after SAPE labeling, by confocal fluorescence microscopy (Figure 50). The images confirmed data previously obtained with MAGPIX$^®$ and by flow cytometry. FB-2 microspheres which hybridize with complementary DNA-miR122, incorporate SMART-C-PEG$_2$-Biotin and were fluorescently labeled by SAPE; while those samples treated with non-complementary DNA-miR21 were non-fluorescent. The images were then analysed using ImajeJ$^®$. The intensity of the beads was 81 and 0, for 7500 fmoles of DNA-miR122 and DNA-miR21 (negative control) respectively, confirming the specific incorporation of SMART-C-PEG$_2$-Biotin only when nucleic acids whose sequence is complementary to the DGL probe are present and template the incorporation of SMART-C-PEG$_2$-Biotin.
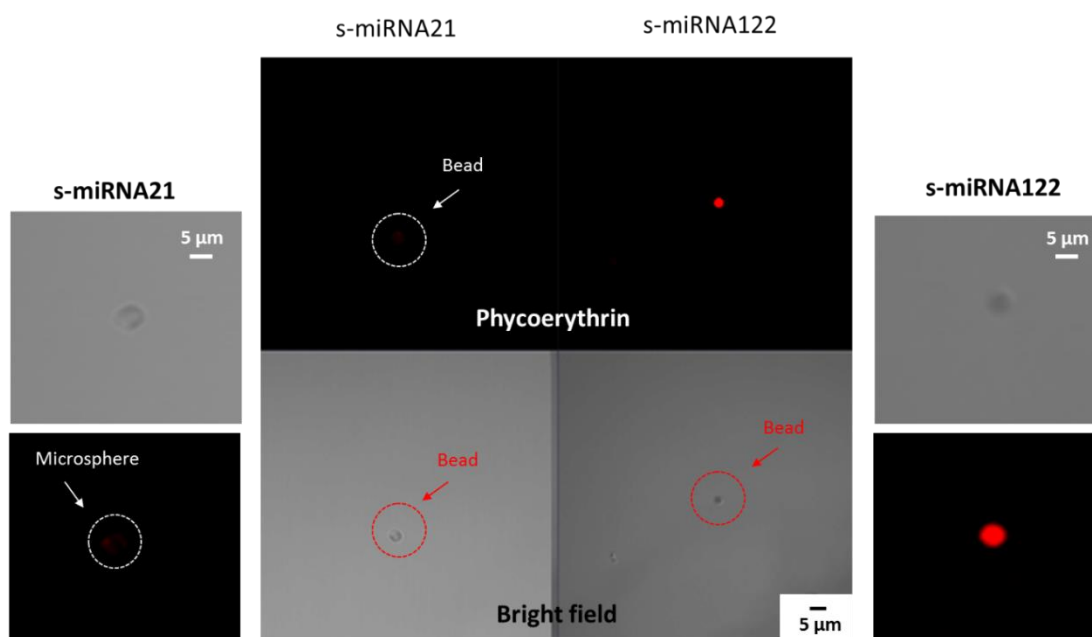
Figure 50: Confocal microscopy analysis: Confocal imaging was performed on a Zeiss LSM 710 confocal laser scanning microscope with Zeiss ZEN 2010 software. Emitted fluorescence was detected using a (PMT) and a filter with a 488 to 543-633 nm range. Fluorescence was only observed when miR-122 was used as templates since it hybridize with the probe and templates the incorporation of SMART-C-PEG2-Biotin which will be then labeled with SAPE leading to the fluorescence signal (red circle). Reproduced with permission [111].

2.3.3. Discussion

A "Proof of Concept" study for the integration of Single Nucleobase Labeling approach with Luminex® xMAP® technology for the detection of miR-122 has been presented. DGL probes were effectively conjugated to MagPlex® microspheres allowing the detection of miR-122 *via* dynamic incorporation of biotin-labeled SMART-NBs, SMART-C-PEG-Biotin in this case. This demonstrates the potential of the synergistic combination of both technologies for rapid and accurate profiling of miR-122 in particular and miRNAs in general with a detection limit of 15 fmoles (0.3 nM). This together with the high specificity and the capacity to differentiate sequences containing a single nucleobase difference opens the possibility for detecting miRNAs directly from biological fluids with neither pre-amplification nor pre-labeling.

The length of the PEG spacer on the SMART-NB did not improve detection; however, the introduction of negative charges and chirality (S-conformation) through the propanoic acid chain at the gamma position of some monomers of the DGL probes improved the hybridization efficiencies of DGL probes when coupled to microspheres. The results confirmed that these modified DGL probes have superior sequence selectivity and affinity when compared to unmodified DGL probes, matching previous studies [20, 107, 108].

The combination of these technologies provides a tool to profile miR-122. On the other hand, multiplexing can be achieved by coupling DGL probes targeting different nucleic acids onto microspheres with different spectral signatures. Hence the novel platform might provide a rapid, cost-effective and straight-forward method for clinical diagnostics and drug development by screening of miRNAs, not only associated with liver disease but also with genetic diseases, cancers, drug toxicology and heart diseases.

However, some of the limitations, such as the lack of reproducibility, found when using this platform are related to: 1) beads loss during the assay and washing steps, so beads that might have captured an analyte might not be read; 2) the analyzer provides a MFI from a few microspheres (a minimum count of 100 for the result to be considered) what implies that the fluorescence data might not be representative of the whole sample since analyte capture might not be uniform among the whole bead set. This is why the individual reading using more advanced platforms such as FlexMAP® might provide more reproducible and reliable results and with a lower limit of detection.

2.4. Industrial impact of "Single Nucleobase Labeling" (SNL) for miR-122 detection

Bead-based assay for SNL using a chemical approach for identifying nucleic acid sequences was first performed on Magplex® microspheres from Luminex®. Although the bead-based assay for SNL was successfully applied for the detection of miR-122, it showed several drawbacks that needed to be sorted out:

a) The limit of detection was not low enough, the sensitivity of the assay was not sufficient to detect miR-122 in clinical samples (the average behavior of the population was analyzed but not the contribution of its individual members. Flow cytometry experiments demonstrated that a better performance and lower limit of detection could be achieved with a FlexMAP® analyzer that analyzes fluorescence from each bead individually).

b) The reproducibility of the assays had to be improved. There was a huge variability in the fluorescence measurements of inter and intra experiment replicates. They might be due to pipetting errors, reagents performance, sample reading, loss of microspheres during washing, average reading of the fluorescence…

c) The lack of automation which contributes to errors and variability inter and intra experiments.

In order to overcome these problems, DestiNA Genomica S. L. found another platform on which develop a similar bead-based assay. This is Single Molecule array (SiMoA™) from Quanterix®.

2.4.1. Single Molecule Array (SiMoA™)-based digital ELISA from Quanterix® Corporation

The digital ELISA is performed in two stages. In the first stage, antigen capture occurs, the microscopic beads coated with capture reagent are mixed with samples followed by addition of biotin- labeled detection antibody and streptavidin–β-galactosidase. The beads are then loaded on a disc with an array of femtoliter-sized microwells. The diameter of each microwell (4.5 μm) can only accommodate zero to one bead with a diameter of 2.7 μm. The beads are resuspended in 15 μL of 100 μM resorufin-β-D-galactopyranoside (RGP) in PBS and loaded into the assembly through the fluidic inlet port using a pipette. Vacuum is then applied to the venting port to pull the bead suspension into the channel and over the array. The beads are then allowed to settle via gravity for 2 min. 50 μL of fluorocarbon sealing fluid is injected into the channel to displace the bead/RGP

suspension, remove excess beads on the surface of the array that did not fall into wells, and to seal the beads in the wells [113-115].

The biggest problem with capturing analyte molecules on a surface is the long time required to capture molecules at low concentration. To solve the inefficiencies with binding, microspheres with capture agents attached to the surface can be used to concentrate a dilute solution of molecules. Capture reagents (DNA probes or antibodies) are attached to the surface of microspheres. The beads are added to the sample solution such that there are more beads than molecules. There are two advantages for adding so many beads. First, at a roughly 10:1 bead to molecule ratio, which is in the Poisson regime, each bead captures either one or zero molecules. Second, with so many beads in solution, the bead-to-bead distance is short such that every molecule encounters a bead in less than a minute. Diffusion of the target analyte molecules occurs on a time scale such that with only a 30 min-incubation, all the molecules should have multiple collisions with multiple beads. In this manner, the slow binding to a fixed capture surface is avoided and the efficiency of binding increases dramatically [113, 116].

Beads are first washed to remove nonspecifically bound proteins and incubated with biotinylated detection antibody and then with β-gal labeled streptavidin. In this manner, it can be achieved that each bead that has captured a single protein molecule is labeled with an enzyme. Beads that do not capture a molecule remain label free. The beads are then loaded into the same microwells as described above, sealed with substrate, and then the substrate is converted to a fluorescent product by captured enzyme label [116].

One of the biggest challenges with these detection methods is non-specific binding (NSB), non-target molecules that bind and are counted. Consequently, many single molecule methods, while intrinsically able to detect a single molecule, cannot provide particularly sensitive detection limits because NSB is high. Techniques for reducing NSB include many surface modification approaches that attempt to passivate the surface so that it does not attract proteins. A related issue is the NSB of the analyte molecule to surfaces during the assay protocol. Glass and plastic adsorb proteins and many other molecules to some extent. When analyte concentrations are in the femtomolar and lower concentration range, loss of analyte to these surfaces can deplete the sample and produce erroneous results. Consequently, care must be taken to passivate these surfaces and to minimize transferring samples from one vessel to another. Another issue with single molecule detection is when a low absolute number of molecules is being detected, one encounters a serious problem with Poisson noise [116].

Simoa™ platform has several outstanding features:

- Digital readout. Because the final signal acquisition is done on a planar array with standard imaging, data acquisition is a much faster process compared with the digital readout with a fluidic system like the Erenna® [113, 117, 118].

- Broad dynamic range [115].

- Fully automated system. The instrument performs sample dilution (up to 1:10 dilution), mixing, washing, incubation, and data acquisition steps [113, 114, 118].

- Multiplexing: it is capable of measuring up to ten different analytes simultaneously. This multiplexing capability through a combination of bead encoded with dyes of different fluorescence properties and intensities. The single molecule signal (resorufin) remains the same for both singleplex and multiplex assays. Additional analysis steps are included at different excitation/emission wavelengths to identify assay-specific bead subpopulations labeled with different fluorescent properties [117, 118].

- Enhanced sensitivity. Every molecule encounters a bead. The ability of digital ELISA to measure much lower concentrations of proteins than conventional ELISA derives from two effects: (i) the high sensitivity of SiMoA™ to enzyme label and (ii) the low background signals that can be achieved by digitizing the detection of proteins. The enzyme−substrate reaction in analog immunoassays is conducted in relatively large reaction volumes (50–100 μL) that dilute product molecules during the signal generation step. Diffusion and dilution of signal molecules limit the sensitivity to the picomolar range. In contrast, SiMoA™ restricts this diffusion of the fluorescent product molecules from the enzyme−substrate reaction by confining individual labeled immunocomplexes and substrate to femtoliter-sized wells [113, 119]

- The required sample volumes are modest (generally 25 μL), and total assay times are approximately 1 h. With femtogram per milliliter sensitivity, the SiMoA™ HD-1 Analyzer is approximately 3 logs more sensitive than conventional fluorescence, chemiluminescence, and electrochemiluminescence immunoassay instrumentation [118].

- Washing steps to reduce nonspecific binding and background [118].

2.4.2. Implementation of Dynamic chemistry technology for nucleic acid reading (by DestiNA Genomica S. L.) on SiMoA™ platform [120]

The integration of the dynamic chemistry approach for nucleic acid testing *via* the SNL approach with the SiMoA™ system meets the limitations of the Luminex® bead-based assay presented technology since a) it can read individual beads, b) once the beads are functionalized (for which similar protocols to the ones already developed for the Luminex® assay will be applied), the rest of the process will be automatized so errors and bead-lost will be minimized.

Analysis of the bead-based assay for dynamic chemistry reading of nucleic acids carried out on the SiMoA™ HD-1 analyzer led to the development of a test for detecting miR-122 with a limit of detection of 500 fM. The assay combines the Biotin-labeling of a DGL-miR122 probe immobilized on beads, through the templating power of miR-122 molecules, with the detection, in arrays of femtoliter wells, of single enzymes that bind to the biotin tag. The SiMoA™ DNA assay was limited to relatively long target sequences (<100 bp) because of the requirement for a capture and multiple detection probes, each being 15-20 bases long. However, the combination of the dynamic chemistry and single molecule array approaches has enabled an assay with single label sensitivity and single base specificity using a single, short (<20 base) probe for detecting short RNA target molecules [120].

For the SiMoA assay, 2.8 μm diameter superparamagnetic beads with carboxylic acid groups were used as platform to immobilize the DGL probes. As described above (see section 2.3.2.2. and experimental section 5.2.2. for DGL probe sequences), DGL-122-C is built on a PNA backbone, having some chiral negatively charged monomers across the sequence. It is designed to clamp mature miR-122 so that the templating nucleotide is a Guanosine (Figure 32) and have a N-terminal free amine to allow its covalent binding to the beads [120].

Figure 51 shows that if the complementary miRNA, miR-122, is present in the sample, it hybridizes with the DGL probe and acts as template for the incorporation of complementary biotin-labeled SMART-NB into the abasic position. The dynamic reaction was done using 5 μM of SMART-C-Biotin and 1 mM of sodium cianoborohydride. Once beads were labeled by the biotin tag of the SMART-NB ('SNL'), they were analyzed on a SiMoA™ HD-1 Analyzer. The signal is generated by a Streptavidin-β-galactosidase (SβG) which binds to the biotin and then transforms the substrate, resorfurin-β-D-galactopiranoside (RGP) to give a fluorescent signal that is measured. The signal is proportional to the concentration of the target [120].
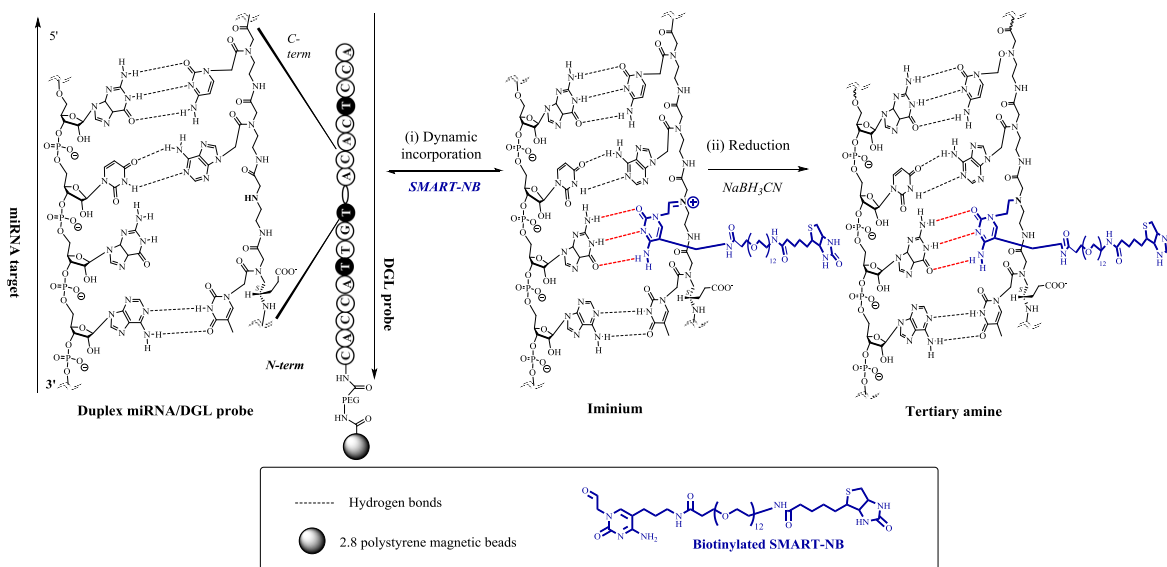
Figure 51: Chemical representation of the duplex miRNA-DGL probe highlighting the hydrogen bonds involved in this hybridization process. The incorporation of a biotinylated SMART-NB (shown in blue) is driven by the nucleotide that lies in front of the abasic position of the DGL probes, following Watson-Crick base-pairing rules, by forming first a reversible iminium intermediate which is then reduced to form the final tertiary amine. Reproduced with permission [120], CC BY license.

The array was fluorescently imaged and these fluorescent images were used to locate the beads within the wells and its enzyme activity. The analysis software determined the average number of enzymes per bead (AEB) and by interpolation in a linear curve made with the AEB values of calibrators of known concentration, the concentration of the target nucleic acid can be determined. The total assay time is 3.5 h. The limit of detection of the SiMoA assay was 500fM [120] whereas the limit of detection for the analog bead-based assay was 300pM [111] and the one for commercial RT-qPCR assay for miR-122 was 2.6 fM.

The SiMoA assay itself wasn't optimized so there is a scope for improving its sensitivity since it has been reported that the technique can detect 220 zM of SβG [119], subfemtomolar levels of proteins (0.6fM of PSA [119]) and 0.07 fM of DNA [121]. Moreover, the efficiency of the process described as the ratio between number of molecules captured and labeled and the total number of molecules in the sample was low, 0.08%.

Thanks to the implementation of the SNL concept within the SiMoA™ platform, the dynamic chemistry technology for nucleic acid testing has been licensed to Quanterix® Inc. This license is the first step to see the SNL concept as part of a molecular diagnostic assay. It will also allow bringing a SiMoA™ SR-X to Granada, being the first one of this equipment in Andalucia, and will allow creating highly qualified employment.

Chapter 3: Identification of Trypanosomatids by detecting Single Nucleotide Fingerprints using DNA analysis by Dynamic Chemistry (Objective 2)

Chapter 3: Identification of Trypanosomatids by detecting Single Nucleotide Fingerprints using DNA analysis by Dynamic Chemistry (Objective 2)

3.1. Introduction

3.1.1. Trypanosomatid parasites

Parasitic diseases are responsible of millions of morbidities and mortalities, and they impose serious health and economic consequences. Specifically, protozoan parasites of the family *Trypanosomatidae* are the causative agent of devastating diseases in humans and livestock that range from self-curing dermal lesions to fatality if not treated [122-124]. Among trypanosomatids, there are three main classes of human pathogens: *Trypanosma cruzi*, *Trypanosoma brucei* and *Leishmania* spp. which are the causative agents of Chagas disease, sleeping sickness and leishmaniasis, respectively [125]. These diseases were mainly found in tropical and sub-tropical regions; however, in the last decade, there has been a global spread of these diseases reaching also developed countries [122]. The increasing numbers of patients, migrations, and individuals traveling overseas from/to countries with high prevalence of tropical/sub-tropical infectious diseases are leading to a growing number of *Trypanosomatidae* infections reports [122, 126].

An accurate and rapid diagnosis is crucial for an effective clinical management of these diseases. However, diagnosis is affected by the lack of expensive and specialized diagnosis equipment and trained personnel in developing countries [127].

Microscopy-based diagnosis of these diseases can be hindered by the low number of parasites and their similar appearance. The clinician can assist the technologist providing clinical and/or epidemiological information that help choose the right test and guide the interpretation of results. Sensitivity can be improved using concentration techniques such as centrifugation and filtration. Microscopic examination and/or culture of ulcer, bone marrow, tissue aspirates and biopsy samples, are useful for the diagnosis of African trypanosomiasis, leishmaniasis, onchocerciasis and trichinosis. Serologic assays can also be used; however, they are not sensitive and specific enough as to be used alone [128].

Parasitological culture, PCR and serological assays have drawbacks that make difficult for them to be implemented and used for routine diagnosis: (i) they are time-consuming (an average of 15 days for culture and several hours for PCR and serologic assays); (ii) they might require special and expensive equipment and reagents and skilled technicians; (iii) they are susceptible to microbiologic

contamination; (iv) some of them are expensive; (v) differentiation between present and past infection can be difficult [129]. Other issues to be considered are cross-reactivity and false-positive results of serological tests because of the phylogenetic similarity between T. cruzi and Leishmania spp. [130].

3.1.1.1. *Leishmania spp.* and leishmaniasis

Leishmaniasis is a vector-borne disease caused by different species of the protozoan parasite *Leishmania*. It has been stated by the World Health Organization (WHO) as one of the most neglected diseases. There are between 12 and 15 million infected people in the world, approximately 1.5 to 2 million new cases occur each year and it causes 70.000 deaths per year [122-125, 131, 132]. The genus *Leishmania* belongs to the family *Trypanosomatidae* (order *Kinetoplastida*). The parasite is categorized in two main groups: the Old World species (*L. tropica*, *L. major*, *L. aethiopica*, *L. donovani*, and *L. infantum)* in Europe, Africa and Asia and the New World species (the complexes *L. mexicana* and *L. braziliensis)* in America [133].

Many of the *Leishmania* sp. infecting humans are zoonotic (with mammal reservoir host) and other are anthroponotic (having human-to-human transmission through the vector). The disease is transmitted through the bite of an infected sand fly vector (various species of the genus *Phlebotomus* in the Old World and *Lutzomyia* in the New World). It is rarely transmitted by other routes such as blood transfusions, needle sharing or congenitally. Each sand fly species transmits only one parasite specie and each parasite provoke a specific clinical form of the disease [133].

Amastigotes are the form that parasites are found inside the human phagolysosomes of macrophages. When the sand fly feeds from human blood, a wound is formed resulting in the release of skin macrophages into the blood and its uptake by the vector. Once in the vector, the parasite multiplies and differentiates to metacyclic promastigote, the mammalian infective stage, which are left on the skin of the mammalian when the fly feeds again [133].

There are three type of leishmaniasis:

1) **Cutaneous leishmaniasis** is the less severe form of the disease whose main symptom is self-healing ulcers. Localized cutaneous leishmaniasis was first described in the Old World by Lewis and Cunningham in 1876; it is mainly caused by *L. tropica.* It is characterized by a local increase in temperature and swelling; an erythematous papule is formed at the site of the bite which turns into a pustule and after breaking it results in a rounded ulcer. Diffuse cutaneous leishmaniasis is characterized by anergy (absence of cellular immune response to parasite antigens) which allows parasite dissemination through tissue, lymph and blood

pathways resulting in lesions in most of the skin. It is caused by *L. mexicana* complex (*L. amazonensis*, *L. braziliensis* and *L. pifanoi*). It starts with erythematous nodules and reddish-brown infiltrative smooth or verrucous plaques which usually starts in the face and then progresses through extremities, buttocks and mucous membranes [132, 133].

2) **Mucocutaneous leishmaniasis or "Espundia"** is caused by the complex *L. braziliensis*, which includes the species *L. braziliensis*, *L. guyanensis*, and *L. panamensis.* It starts with the invasion and destruction of nasopharyngeal mucosa which then spread to the oral and pharynx mucosa, the larynx and the skin of nose and lips [132, 133].

3) **Visceral leishmaniasis or Kala-azar** is the most severe form of the disease with 100% mortality if untreated. It is caused by *L. donovani*, *L. infantum*, and *L. chagasi*, *L. amazonensis*, and *L. tropica.* It causes lymphadenopathy, hepatomegaly, splenomegaly, pallor, anemia, leukopenia, thrombocytopenia, fever, night sweats, weakness, anorexia, asthenia, cutaneous pigmentation, and weight loss [132, 133]

Leishmaniasis diagnosis is based on the epidemiological context, although laboratory confirmation and specie identification are important.

- Histopathological data: in LCL, sections stained with hematoxylin-eosin show epidermal atrophy or hyperplasia with inflammatory infiltrate (macrophages, lymphocytes and plasma cells). In early phases, parasites are found within cytoplasmatic vacuoles in histiocytes (Leishman bodies); and in late phases, there are less infected macrophages with less amastigotes and some lympho-histiocytic infiltrates. Lesions of patients with diffuse CL have highly parasitized macrophages and few dermal lymphocytes. The sensitivity is approximately 85% [132].

- Culture is performed by the inoculation of triturated tissue in Novy–McNeal–Nicolle medium. It has a sensitivity of 85% [132].

- Laboratory data: the Montenegro skin test is positive for localized forms and negative for anergic forms. A negative result does not exclude the disease. The parasites are observed in the smear or in the imprint stained with Giemsa or Wright. Serological assays to determine serum anti-Leishmania IgG and the determination of anti-K39 antibodies are also used and have a sensitivity of 90-100%. Antibodies can also be detected by direct agglutination, direct immunofluorescence and enzyme-linked immunosorbent assay. PCR can also be used in LCL with 100% specificity [132].

The standard method for visceral leishmaniasis diagnosis is histopathologic microscopy of Giemsa- or hematoxylin-eosin stained and fixed aspirate samples of bone marrow or spleen or biopsies of bone marrow or liver. The standard method for cutaneous and mucocutaneous leishmaniasis is microscopy of Giemsa- or hematoxylin-eosin-stained scrapings, aspirate samples, or biopsy samples of skin ulcers or mucosal lesions. With the addition of culture, the diagnosis sensitivity can increase up to 85%. Serologic assays used for the diagnosis of visceral leishmaniasis are not sensitive and/or specific for the diagnosis of cutaneous leishmaniasis [128, 132].

The only effective leishmaniasis treatment is intravenous pentavalent antimonials in the form of sodium stibogluconate or meglumine antimoniate [132].

3.1.1.2. *Trypanosoma brucei* and sleeping sickness

Human African Trypanosomiasis (HAT) or sleeping sickness is a vector-borne parasitic disease caused by different subspecies of *Trypanosoma* (genus) *brucei* (specie). *Trypanosoma brucei brucei* (*T.b.b.*) transmits Nagana to domestic animals and it is not pathogenic to humans. *T. b. gambiense* is an anthroponotic parasite, it is a slow-progressing form and causes a chronic syndrome with a mean duration of 3 years. *T. b. rhodesiense* is zoonotic, it is a fast-progressing form and causes an acute syndrome which progresses to second-stage within a few weeks and death in 6 months. HAT is endemic in sub-Saharan Africa and it is considered a Neglected Tropical Diseases, those that occur mainly in poor populations. Indeed, HAT together with other diseases such as Malaria, HIV is among the 17 priority Neglected Tropical Diseases [134, 135].

It is transmitted by the bite of an infected tse-tse fly, genus *Glossina,* which has metacyclic trypomastigotes in the salivary gland. During its blood meal, the tse-tse fly injects saliva to prevent blood coagulation, and while doing so, trypomastigote trypanosomes are injected subdermally into the host. These parasites proliferate and transform into blood-stream trypomastigotes form (first stage of the disease). They multiply by binary fission and can move to the cerebrospinal fluid (CSF) (second stage of the disease) [134]. Other routes of transmission might be possible but very rare (sexual, laboratory accidents, blood transfusion, organ transplantation) [135].

The symptoms of HAT caused by the two subspecies are the same but they vary in the frequency, the severity and the kinetic appearance. The first stage is the hemolymphatic or bloodstream stage and its symptoms can be intermittent fever, headaches, pruritus, lymphadenopathy, asthenia, anemia and hepatosplenomegaly. The second or meningoencephalic stage starts when crossing the blood-brain barrier, the symptoms are neuropsychiatric (sleep disturbances, limb paralysis, hemiparesis,

irritability, aggressive behavior, abnormal movement, psychotic reactions) and it can be fatal if not treated [134, 135].

The standard method for Chagas diagnosis during the acute phase is microscopy examination of thick and thin blood or buffy coat films stained with Giemsa or other stains. The diagnosis in latent and chronic stages is established serologically or by microscopic examination and culture of tissue aspirate samples or biopsies [128]. Early diagnosis should be done in order to avoid disease progression to the neurological stage. The diagnosis of HAT is mainly based on an active screening to detect either antibodies or parasites [134].

- **Antigen detection:** CATT (Card-Agglutination Trypanosomiasis Test): it is a serological test used for initial population screening. The antigen used is complete bloodstream forms of *T. b. gambiense* variable antigen LiTat 1.3. Although a high specificity (97%) is achieved, false-positives can be obtained in patients with other parasitic diseases (malaria, transient infection with *T. b. brucei)* and false-negatives might be obtained if the parasite strain do not express the gene coding for LiTat 1.3 [134, 135].

- **Parasite detection:**

(i) Lymph Node Examination. Lymph node palpation is done on positive CATT patients. The fluid is examined after puncture. The sensitive varies 40-80% depending on the parasite strain, the stage of the diseases and the prevalence of other lymphadenopathy-causing diseases [134].

(ii) mAECT (Mini Anion Exchange Centrifugation Technique): since patients' blood cells are negatively charged and trypanosomes' ones are neutral they can be separated with an anion-exchange chromatography at pH 8. The eluent contains the trypanosomes and can detect 30 trypanosomes/mL which shows the high sensitivity of the technique (77%) [134].

(iii) CTC (Capillary Tube Centrifugation). A capillary tube containing an anticoagulant is filled with finger-prick blood. Trypanosomes are concentrated on the same layer as the white blood cells, between plasma and erythrocytes by high-speed centrifugation. Capillary tubes are observed looking for mobile parasites. The limit of detection is about 500trypanosomes/mL, the sensitivity is 56% [134].

- **Proteomics studies** to analyze the protein profiles of the CSF and linked them to the disease stage have also been done; osteopontin and beta-2-microglobulinn were found as accurate markers of first and second stage HAT [134].

- Polysomnography: Due to the alteration of the sleep-wake cycle, polysomnography studies have also been carried out where variables such as respiratory and heart rate are measured and results combined with other tests like electroencephalogram, electromyogram and electrooculogram. A high number of Sleep Onset Rapid Eye Movement Periods (SOREMP) is found. However, polysomnogrphy requires high-tech, bulky material, trained personnel and long examination periods and the results are not specific of HAT [134].

- DNA amplification: blood, CSF, urine or saliva samples are used to amplify parasite DNA sequences by PCR. Loop-mediated isothermal amplification (LAMP) is an alternative to PCR which requires minimal equipment and can be performed in laboratories of HAT endemic countries, the positive result can be analyzed by fluorescence, white precipitates or color change and several samples can be analyzed simultaneously. Another alternative is Trypanozoon-specific real-time nucleic acid sequence-based amplification (NASBA) which allows detecting 18S rRNA. However, the presence of DNA or RNA in the CSF of HAT patients has to be considered carefully because of the poor of already existing molecular test (sensitivity and specificity depend on the target and primer sequences). In addition, molecular biology is not considered a good marker for the post-treatment follow-up [134, 135].

Disease stage identification can only be done by examination of the CSF obtained in a lumbar puncture. The microscopic detection of the parasite in the CSF has limited sensibility since the number of circulating parasites can be very low and so induce false-negative results. On the other hand, an increase in the white blood cells count in the CSF (a consensus of 10 cells per μL has been adopted) is an indicator of meningitis; although this result is not exclusive of sleeping sickness [134].

Many of the existing diagnostic procedures are difficult to be implemented because they need specialized mobile teams, trained to do rapid testing and using invasive protocols. So novel approaches are being developed such as lateral flow immunochromatographic devices which detect anti-trypanosome antibodies (this represent a simple to use device with easy to read results); or analysis of parameter indicative of immune response and inflammation in the brain like an increased concentration of immunoglobulin in the CS; the absence of a switch between IgM and IgG; an early activation of macrophages and astrocytes; the presence of Mott cells (plasma cells with IgM) [134].

Pentamidine (for *T. b. gambiense)* and Suramin (for *T. b. rhodesiense)* are used in the first stages of the disease; however, they can have severe reactions (Suramin can induce allergic reactions,

hypersensitivity, nephrotoxicity, hematuria and peripheral neuropathy). In the second stage, Melarsoprol, Eflornithine and Eflornithine/Nifurtimox combination are used. Melarsoprol can provoke fatal enephalopatic syndrome and Eflornithine cause the same kind of adverse reactions as antineoplasic agents. These treatments usually require clinical surveillance which is a disadvantage for people with no access to health structures [134].

3.1.1.3. *Trypanosoma cruzi* and Chagas disease

Chagas disease is caused by the protozoan parasite T. cruzi. It was discovered in 1909 by Chagas [136]. This disease has been recognized by the WHO as one to the 13 most neglected tropical diseases. It is endemic in 21 American countries and migration of infected people has brought the disease to other areas in the world. It affects approximately 8 million people and causes around 12.000 deaths/year [137]. *T. cruzi* is transmitted by the inoculation of infected feces of the triatomino vector through a bite site or an intact mucous membrane of the mammalian host [136]. It can also be transmitted through other routes, which are especially important in non-endemic countries, such as blood and blood products, solid organ transplantation, congenitally from the mother to the unborn child, consumption of contaminated food and drink and laboratory accidents [137, 138]. Approximately 1.7 million people from Chagas disease endemic countries live in Spain and around 50% are women of reproductive age [139]. *T. cruzi* is present in two forms in the human body: the trypomastigote which does not divide in blood but carries the infection and the amastigote which multiplies within cells mainly of mesenchymal origin. Chagas disease usually comprises two stages: 1) the acute phase with fever, inflammation at the inoculation site, unilateral palpebral oedema (Romaña sign), lymphadenopathy and hepatosplenomegaly. It can last 4-8 weeks and parasitaemia decreases from 90 days onwards. 2) The chronic phase, 30-40% of chronically infected patients can develop organ involvement within 10-30 years after the acute infection (cardiomyopathy or megaviscera megaesophagus, megacolon), being cardiac involvement the most frequent and severe. Gastrointestinal involvement is less common. Chagas disease can also provoke cardioembolic stroke and neuropathy [138].

Diagnosis is made mainly by direct microscopic observation of trypomastigotes in blood and, sometimes, in other body fluids such as CSF. In the chronic phase, parasitaemia is low and intermittent which makes PCR-based methods unreliable. Moreover, diagnosis by PCR has variable sensitivity (50-90%) which depends on the blood volume, the methodology, the target genes, the infection stage, the presence of immunosuppression, genetic variability of *T. cruzi*. Instead, serological testing through the detection of IgG antibodies against T. cruzi is used. Serological techniques can use whole parasite antigens and purified extracts (conventional tests) or recombinant

antigens and synthetic peptides (non-conventional tests). The most common tests are indirect fluorescent assay, indirect haemagglutination and ELISA [138]. Because no gold standard method has been identified for an accurate and reliable diagnosis of *T. cruzi*, WHO recommends the use of two tests based on different principles and/or antigens, for example two serological assays with two different antigens [136]. Additionally, visceral complications must be assessed by doing a resting electrocardiography, cardiac ultrasonography (cardiac involvement), barium swallow and enema (gastrointestinal involvement) [138]. Regarding diagnosis in the newborn, during the first weeks of life, diagnosis is based on microscopic visualization of bloodstream parasites after concentration techniques like microhaematrocrit; however, it can miss up to 50% of infected infants. Molecular techniques might improve early diagnosis since parasitaemia is at maximum level one month after birth and at that time false positives due to parasite DNA transmitted from the mother are avoided. It must be noticed that a positive RT-PCR result from one month onwards confirms *T. cruzi* infection whereas a negative one does not exclude it, being necessary to do another test at 9 months to confirm the diagnosis [139].

Benznidazole and nifurtimox are the only licensed drugs for the treatment of Chagas disease. Although their bad safety and efficacy profile, they are the mainstay of parasiticidal treatment. It must be highlighted that early detection and treatment are essential because drug effectiveness decreases with time from primary infection [138].

3.1.1.4. NATs and pathogen detection

The detection and identification of human pathogens is an important function in medical laboratories for example for setting an effective drug treatment. Molecular diagnostic techniques based on nucleic acid tests (NATs) are commonly used due to its sensitivity and specificity. However, NATs require continuous adaptation in order to prevent microorganism to evade detection because of the appearance of novel, drug-resistant, mutated or recognized microorganisms in unexpected situations. They also offer some advantages such a quick turnaround time, improved biosafety due to pathogen inactivation during the sample preparation step [7, 140].

Each microorganism has unique nucleic acid sequences that can be used to determine the presence of that specific microorganism. Nucleic acid based diagnostics refers to the use of theses sequences to detect the presence of a pathogen in a clinical sample. Nucleic acid-based systems exist in a wide range of formats from probe hybridization to amplification of a genomic target by one of the wide range of amplification technologies. NATs require a nucleic acid target sequence specific or the microorganism of interest that should be present in a relative high copy number and should be heterologous enough to allow differentiation from other related species. Different genomic targets

have been used such as genes related to metabolism, genes coding for toxins or virulence factors, multicopy genes like rRNA, etc. RNA represents an alternative to DNA as target for NAT; although it is more labile it permits differentiate between viable and non-viable microorganism. These NATs can be used for microbial identification, identification of susceptibility to antibiotic, monitoring treatment, monitoring surveillance routes to improve drug treatment [3].

Most molecular diagnostic procedures are usually chosen as a result of a presumptive diagnosis to detect single organisms or a small panel of them. These assays can fail to identify the etiological agent if it is not part of the panel or when it is a mutated variant that, due to the sequence changes, is no longer recognized by the probe [140].

There are 3 main levels of diagnosis based on the level of confidence about the etiological agent [140]:

> a) **Specific identity of the infectious agent is suspected.** The diagnosis can be carried out by approaches that include: targeted multiplex real-time PCR, a suited of targeted multiplex PCRs, PCR-microsphere panels, etc.
>
> b) **Identity of the agent is suspected at the level of genus, family or group** because of the main medical condition they cause (e.g. encephalitis, hemorrhagic fever, respiratory infections…). The diagnosis can be performed using tools that incorporate degenerated PCR (for example targeted at the genus level), complemented with sequencing, simple chip/array, microsphere detection, mass-spectrometry, etc.
>
> c) **Unknown identity of the etiological agent.** The diagnosis might be done with tools that incorporate metagenomics, random PCR, pyrosequencing, array-based detection, etc.

3.1.1.5. Evolution of parasitic diagnostic methods: introduction of molecular diagnostic methods

The symptomatology amongst Chagas disease, sleeping sickness and Leishmaniasis are very similar but their treatments are not just highly toxic but also completely different, so a rapid and accurate diagnosis is essential to deal with this disease effectively [123]. Hence, the necessity to have rapid and accurate results which enable more precise and appropriate use of treatments, better individualized patient management, and more efficient epidemiological and public health surveillance [141].

The primary tests currently used to diagnose many parasitic diseases have not changed much since the development of the microscope in the 15th century [142] so *Trypanosomatidae* diagnosis is

normally undertaken by microscopic examination of either tissues or parasite cultures. Immunological techniques, which detect antibodies in response to parasitic infections, are also used [123, 124, 142].

However, with the completion of the genome sequencing of many pathogenic species, the demand for other molecular diagnostic methods has increased. Thus, molecular diagnostics in clinical parasitology have seen a rapid development during the last years, and have been introduced in the majority of laboratories as a new way for diagnosis [123, 124]. Although a considerable amount of work has been published reporting novel and promising molecular detection methods for the diagnosis of parasites either in blood or tissue biopsies, only a few have reached clinical application [123]. Several molecular techniques for detecting nucleic acids have been introduced in the clinical laboratories for routine diagnosis bringing vast improvements in parasite detection [123, 124]. Over all, the use of nucleic acid amplification techniques (NAATs) such as polymerase chain reaction (PCR), real-time PCR or nucleic acid sequence-based amplification (NASBA) have demonstrated their potential key role in detecting infections and post-treatment monitoring [124, 143]. However, currently molecular tools available present lots of difficulties since they are not sensitive enough which generates a great deal of false-positive results for cross-reactivity [124].

Conventional DNA sequencing has arisen as a diagnostic tool able to detect parasitic infections with high sensitivity and specificity. It is based on PCR amplification that amplifies highly conserved ribosomal gene sequences from several parasites using generic primers. DNA sequencing analysis is carried on the amplified fragment to identify the specie. Although the DNA sequencing methods currently used have some disadvantages such as high cost and complex protocols which require an expert operator [144].

Some of the single base resolution methods developed for detecting and distinguishing between parasites are based on single base extension (SBE). These methods, through oligonucleotide primer extension, allow single nucleotide analysis. These primers are design to hybridize with a complementary nucleic acid region so that the 3' end of the primer finish immediately before the nucleotide under interrogation. Although, SBE methods have in general good diagnostic utility, there are some concerns related to the generation of false readings because of mis-priming in amplification reactions [145]. When analysing DNA by dynamic chemistry, mis-priming is not a problem.

Minicircle kinetoplast DNA (kDNA) and a repeat tandem sequence of nuclear DNA (stDNA) of the parasite are the most used molecular targets for diagnosis via PCR because of their high number of copies [146]. rRNA genes are also used since they are highly conserved between different

eukaryotic organisms and the gene copy number is maintained at a constant level characteristic for each organism [124, 125, 147]. The eukaryotic ribosome is composed of two subunits with four rRNA molecules and more than 70 proteins. The large subunit (LSU) contains the 28S, the 5.8S and the 5S rRNAs. The small subunit (SSU) contains the 18S rRNA (SSU rRNA). There is a wide variation in the rDNA and 5S rDNA gene copy number that exists among eukaryotes: 110 copies of the rDNA are present in the genome of the kinetoplastid *T. cruzi*, 56 copies of the rDNA in *T. brucei*, 63 in *L. major* and 166 in *L. donovani* [148, 149]**.** The highly conserved sequences and the high copy number of rRNA genes makes them ideal targets for almost every molecular diagnostic method.

Herein, a proof of concept study for developing a chemistry-based detection tool for the rapid diagnostic of *Trypanosomatidae* diseases with high sensitivity and specificity is presented. It integrates Chem-NAT technology (based on highly specific DGL probes and SMART-NBs) [32, 33] with Matrix-Assisted Laser Desorption Ionization – Time-of-Flight Mass Spectrometry (MALDI-TOF MS) for a mass-based assay and with DNA-flow through technology for a colorimetric assay. The novel tool was evaluated and validated for the analysis of the delta subunit of the 28S rRNA (rRNA) coding gene of *Trypanosome cruzi*, *Trypanosome brucei* and *Leishmania* spp. to identify parasites by the screening of Single Nucleotide Fingerprint (SNF) markers. SNF is a new term that our group has coined to describe a single nucleotide variation which may occur at some specific position in the conserved target nucleic acid sequences of the pathogens. The rRNA 28S sequences are highly conserved except for a few SNF markers that are thus interrogated using DGL probes. So, the application of the dynamic chemistry approach fo nucleic acids 'reading' to trypanosomatid identification might create an innovative product with a true diagnostic potential and utility for rapid detection of SNFs with benefits in terms of result consistency, time, cost, and ease of use.

Although dynamic chemistry has already been validated as an approach for the analysis of single-base changes in human genomic DNA (gDNA) [33], the question remained as to whether dynamic chemistry could be reliably applied as a means of identifying 'Single Nucleotide Fingerprint' and so identifying the trypanosomatid species related to a specific SNF. To answer this, a study was planned in which samples containing gDNA from the three trypanosomatid species under study would be identified via their unique SNFs in the gene coding for the rRNA 28S-delta.

The novel molecular method is based on a singleplex PCR that amplifies a highly conserved region of the 28S rRNA gene of *Trypanosomatidae* species (*Leishmania* spp. (*L. major*), *Trypanosoma cruzi* (*T. cruzi*), *Trypanosoma brucei* (*T. brucei*)) [147, 148, 150-153]. This target was chosen so

that it is present in a high copy number and it was homologous enough between the three species except for a few nucleotides. SNFs are similar to 'Single Nucleotide Polymorphism' (SNP) but nucleotide differences occur between different species and are related to their identity what is harnessed to differentiate them. The high homology allows amplifying the target region with a unique pair of primers regardless the species present in the sample to study and to design two DGL probes able to hybridize with all of the possible amplification products. The pattern of SMART-NB incorporation will thus vary depending on the *Trypanosomatidae* species present, allowing their identification.

Two different assays and read-out approaches were studied:

1) A mass-based assay which uses Matrix-Assisted Laser Desorption Ionization – Time-of-Flight Mass Spectrometry (MALDI-TOF) [154-161]. This approach was first used for developing the molecular probes and validating the assay itself.

2) A colorimetric-based assay which uses nylon membranes and colored spots to identify the region where the dynamic incorporation of a biotinylated SMART-NB has taken place.

3.2. Identification of Trypanosomatids by detecting Single Nucleotide Fingerprints using DNA analysis by Dynamic Chemistry with MALDI-TOF (Specific objective 2.1.)

3.2.1. Introduction

3.2.1.1. Mass spectrometry

Mass spectrometry (MS) is an analytical technique in which chemical compounds are first ionized becoming then charged molecules and measuring their mass to charge (m/z) ratio. Although it was discovered in the early 1900s, it was mainly applied on chemical sciences. However, when electron spray ionization (ESI) and matrix assisted laser desorption ionization (MALDI) were developed in 1980s, MS started to being used on large biological molecules like proteins. In both techniques, peptides capture or loss one or more proton to ionize. They are "soft ionization" methods so sample integrity is not lost due to ionization. MALDI- TOF MS generates singly charged ions, thus data analysis is easier compared with ESI-MS [162].

MALDI-MS was developed in 1988 by Hillenkamp and Karas. It has now become a widespread analytical tool for peptides, proteins and other biomolecules such as oligonucleotides, carbohydrates, natural products, and lipids. MALDI provides a non-destructive vaporization and ionization of biomolecules. The analyte is co-crystallyzed with a matrix compound; this mixture is then radiated and vaporized. The matrix is essential since it absorbs the laser energy and makes the analyte vaporize. It can also act as a proton donor or receptor, helping in the ionization of the analyte [163]. High amounts of ions from the analyte are generated because of an efficient and directed energy transfer during the desorption process (matrix-assisted and laser-induced). Because many ions are generated it allows to measure substances with high accuracy and sensitivity (subpicomole range) [163].

There are three types of mass analyzers typically used with the MALDI ionization source: a linear time-of-flight (TOF), a TOF reflectron, and a Fourier transform mass analyzer. In a linear TOF mass analyzer ions are accelerated to a detector; since all ions have the same energy, each ion reaches the detector at different times depending on their mass-to charge ratio (m/z), smaller ions reach the detector first because of their higher velocity (Figure 52) [163].
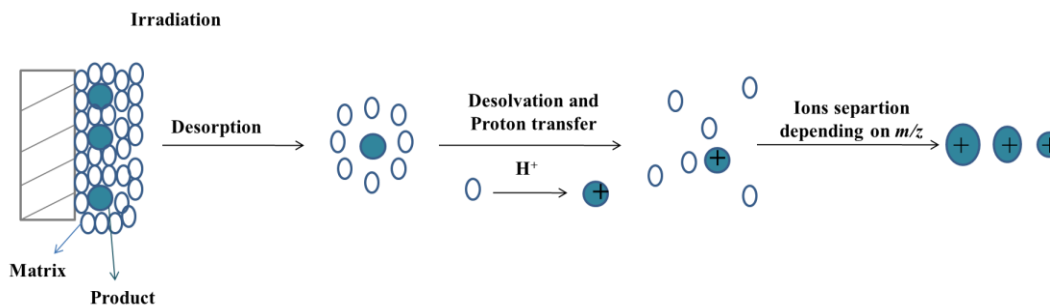
Figure 52: MALDI-TOF ionization scheme: Sample mix with matrix, ionization by proton transfer: MALDI (Matrix-assisted Laser Desorption Ionization), ion separation according to their mass-to-charge ratio: TOF (Time-of-Flight).

The TOF reflectron combines TOF technology with an electrostatic analyzer, the reflectron. The reflectron increases the amount of time ions need to reach the detector, reducing the temporal distribution. Since resolution results from dividing the mass of a peak divided by its width $m/\Delta m$ (or $t=\Delta t$ since *mass* is related to *time*), increasing t and decreasing Δt results in higher resolution. Increasing resolution might lead to a loss of sensitivity and a relatively low mass range, typically $<10\,000\ m/z$ [163].

3.2.1.2. Applications of mass spectrometry in diagnostic

The ability of MALDI to analyze complex mixtures makes it a promising method for the diagnostic screening of biological fluids (serum, cerebral spinal fluid, urine). However, low analyte concentrations and signal suppression due to large amounts of host protein (e.g. hemoglobin in blood) often hinder the screening of such complex natural fluids this is why isolation of the analyte is usually needed [163].

Mass spectrometric immunoassays (MSIA), developed by Nelson et al., are based on the capture of an analyte from the biological matrix prior to mass spectrometric analysis. It pre-concentrates the analyte and isolates it. First, it is captured by antibodies immobilized on a solid support and then the binding is disrupted by the acidic matrix. Unlike ELISA, any non-specifically bound molecules can be differentiated from the analyte due to their characteristic m/z values; moreover, incubation times are shorter than in traditional ELISA [163].

Immunoassays generally have low reproducibility and reliability, and poor or no selectivity between related compounds such as a drug and its metabolites. HPLC is relatively selective and accurate but the sensitivity depends on the compound and it requires time to develop a method. As a result, although both techniques are useful, they suffer when compared to Mass spectrometry speed, sensitivity, and accuracy [163].

Mass spectrometric analysis of DNA samples, either directly or with a probe offers an attractive advantage from a highthroughput perspective. However, the polyanionic and fragile nature of DNA usually results in poor sensitivity and difficult mass spectra [36].

Peptide nucleic acids (PNA) have been used as probes for DNA sequence determination, including SNP genotyping. Because it resistance to fragmentation and lower tendency to form adducts, PNAs are a good strategy for mass spectrometric analysis of DNA sequences [164-166]. Because of their efficient ionization in the positive ion mode, PNAs can be detected without separating them from the DNA target. Apart from the uses of PNA in DNA fingerprinting [167] and in the determination of CpG methylation levels [168] no other major breakthrough in the field has been reported; although there are many indirect uses of PNA in combination with mass spectrometry for SNP typing [169-171].

A mass spectrometric method for DNA sequence analysis using PNA probes was developed [172]. It is based on an ion-exchange capture technique for the isolation of PNA·DNA hybrids and on the use of a conformationally restricted pyrrolidinyl PNA as a probe to differentiate complementary and single-base mismatched 9-15-mer DNA targets at room temperature. They have also been used for detecting unpurified and unlabeled DNA samples obtained from standard PCR mixtures, including the simultaneous multiplex SNP typing[36].

3.2.1.3. Previous results of base-filling reactions using MALDI-TOF as readout tool

As previously mentioned, the capability of the proposed chemistry-based technology for nucleic acid "reading" (Chem-NAT) was first developed and explored [32] using synthetic DNA sequences and MALDI-TOF as readout tool. Once optimized and confirmed the ability of the presented methodology to read any sequence without mis-incorporation, it was applied and validated for the genotyping of 12 cystic fibrosis patients [33]. Now, it is presented a new application of MALDI-TOF where it was used as readout tool of the dynamic chemistry reaction for trypanosomatid nucleic acid testing. Herein, three trypanosomatid parasites: *L. major*, *T. cruzi* and *T. brucei* were differentiated by using two DGL probes targeting two positions which differ among the high homologous sequence of the gene coding for the 28S rRNA (see section 3.1.1.5.). Each parasite will give a unique SMART-NBs incorporation pattern analyzed by MALDI-TOF which would allow their unmistakable identification.

3.2.2. Results

3.2.2.1. Target nucleic acid selection

28S rRNA delta gene sequence was chosen as target nucleic acid for the dynamic chemistry approach for the identification and differentiation of the three trypanosomatid species studied (*Leishmania major*, *Trypanosoma brucei*, *Trypanosoma cruzi*). *L. major* (Lm, LmjF.27.rRNA.31)*, T. brucei* (Tb, Tb927.2.1407) and *T. cruzi* (Tc, TcCLB.419169.10). Figure 53 shows the multiple sequence alignment of 28S rRNA delta gene sequences. The three sequences were aligned using EMBL-EBI tool for multiple sequence alignment Clustal Omega [173]. This sequence was chosen for three main reasons:

1) It is present in a high copy number.

2) It is homologous enough to design a unique set of primers and DGL probes able to hybridize with any of the three parasites.

3) It holds a few SNFs –shown by the absence of a star- to be targeted by the DGL probes.

```
Tb   GTGAGATTGTGAAGGGATCTCGCAGGCATCGTGAGGGAAGTATGGGGTAGTACGAGAGGAA
Lm   GTGAGATTGTGAAGGGATCTCGCAGGTATCGTGAGGGAAGTATGGGGTAGTACGAGAGGAA
Tc   ----GATTGTGAAGGGATCTCGCAGGTATCGTGAGGGAAGTATGGGGTAGTACGAGAGGAA
     ********************** ************************************

Tb   CTCCCATGCCGTGCCTCTGGTTTCTGGAGTTTGTCGAAGGGCAAGTGCTCCGACGCTATCG
Lm   CTCCCATGCCGTGCCTCTAGTTTCTGGGGTTTGTCGAACGGCAAGTGCCCCGAAGCCATCG
Tc   CTCCCATGCCGTGCCTCTGGTTTCTGGAGTTTGTCGAACGGCAAGTGCTCCGACGCTATCG
     ****************** ******** ********** ********* **** ** ****

Tb   CACGGTGGTTCTCGGCTGAACGCCTCTAAGCCAGAAACCAGTCCCAAGACCGGGTGCCCGT
Lm   CACGGTGGTTCTCGGCTGAACGCCTCTAAGCCAGAAGCCAATCCCAAGACCAGATGCCCAC
Tc   CACGGTGGTTCTCGGCTGAACGCCTCTAAGCCAGAAGCCAGTCCCAAGACCAGATGCCC-A
     ************************************ *** ********** * ***** *
```

Figure 53: Multiple sequence alignment of the 28S rRNA delta gene sequences of the three trypanosomatid species: *L. major* (Lm)*, T. brucei* (Tb) and *T. cruzi* (Tc). The absence of "star" shows where the SNFs in the 28S rRNA delta gene sequences occur. EMBL-EBI tool for multiple sequence alignment Clustal Omega [173] was used. (Reproduced with permission [161]).

3.2.2.2. Multiple sequence alignment of several species of the genre Leishmania

28S rRNA delta gene sequences of different *Leishmania spp*. were aligned using EMBL-EMI tool for multiple sequence alignment Clustal Omega [173] to study which *Leishmania* species are prone to be submitted and detected by the proposed assay. *L. major* (Lm, LmjF.27.rRNA.31*)* was the selected specie and was used as a model of *Leishmania spp*. for validating the assay. Although, as it can be observed in figure 54, multiple sequence alignment analysis confirmed that the assay could

be also used for detecting other *Leishmania* species such as *L. braziliensis*, *L. amazonensis* and *L. donovani*.

```
Lmajor          --------GTGAGATTGTGAAGGGATCTCGCAGGTATCGTGAGGGAAGTATG
Lamazonensis    --------GTGAGATTGTGAAGGGATCTCGCAGGTATCGTGAGGGAAGTATG
Lbraziliensis   --------GTGAGATTGTGAAGGGATCTCGCAGGTATCGTGAGGGAAGTATG
Ldonovani       TATATGTAGTGAGATTGTGAAGGGATCTCGCAGGTATCGTGAGGGAAGTATG
                **************************************************

Lmajor          GGGTAGTACGAGAGGAACTCCCATGCCGTGCCTCTAGTTTCTGGGGTTTGTC
Lamazonensis    GGGTAGTACGAGAGGAACTCCCATGCCGTGCCTCTAGTTTCTGGGGTTTGTC
Lbraziliensis   GGGTAGTACGAGAGGAACTCCCATGCCGTGCCTCTAGTTTCTGGGGTTTGTC
Ldonovani       GGGTAGTACGAGAGGAACTCCCATGCCGTGCCTCTAGTTTCTGGGGTTTGTC
                **************************************************

Lmajor          GAACGGCAAGTGCCCCGAAGCCATCGCACGGTGGTTCTCGGCTGAACGCCTC
Lamazonensis    GAACGGCAAGTGCCCCGAAGCCATCGCACGGTGGTTCTCGGCTGAACGCCTC
Lbraziliensis   GAACGGCAAGTGCCCCGAAGCCATCGCACGGTGGTTCTCGGCTGAACGCCTC
Ldonovani       GAACGGCAAGTGCCCCGAAGCCATCGCACGGTGGTTCTCGGCTGAACGCCTC
                **************************************************

Lmajor          TAAGCCAGAAGCCAATCCCAAGACCAGATGCCCAC
Lamazonensis    TAAGCCAGAAGCCAATCCCAAGACCAGATGCCCAC
Lbraziliensis   TAAGCCAGAAGCCAATCCCAAGACCAGATGCCCAC
Ldonovani       TAAGCCAGAAGCCAATCCCAAGACCAGATGCCCAC
                ***********************************
```

Figure 54: Multiple sequence alignment of different species of *Leishmania*. Although the assays were carried out using *L. major* as the parasite species representative of the Leishmania genre, the multiple sequence alignment study shows that the approach (primers and DGL probes) could be used for other *Leishmania spp.*, such as *L. donovani, L. braziliensis and L. amazonensis* (Reproduced with permission [161]).

3.2.2.3. Primers design

L. major (Lm, LmjF.27.rRNA.31)*, T. brucei* (Tb, Tb927.2.1407) and *T. cruzi* (Tc, TcCLB.419169.10) 28S rRNA delta gene sequences were aligned using EMBL-EBI tool for multiple sequence alignment Clustal Omega [173]. The outcome of the multiple sequence alignment of the three trypanosomatids (Figure 53) allowed us to design the 'primers' for the amplification step so that they hybridize with the gDNA of any of the three parasites strains under study without needing to suspect in advance the trypanosomatid specie present in the sample. Figure 55 shows the result of the msa where forward and reverse primer target sequences for the PCR amplification step are highlighted in yellow and green, respectively.

```
Tb  GTGAGATTGTGAAGGGATCTCGCAGGCATCGTGAGGGAAGTATGGGGTAGTACGAGAGGAA
Lm  GTGAGATTGTGAAGGGATCTCGCAGGTATCGTGAGGGAAGTATGGGGTAGTACGAGAGGAA
Tc  ----GATTGTGAAGGGATCTCGCAGGTATCGTGAGGGAAGTATGGGGTAGTACGAGAGGAA
        ********Fw*********** ****************************************

Tb  CTCCCATGCCGTGCCTCTGGTTTCTGGAGTTTGTCGAAGGGCAAGTGCTCCGACGCTATCG
Lm  CTCCCATGCCGTGCCTCTAGTTTCTGGGGTTTGTCGAACGGCAAGTGCCCCGAAGCCATCG
Tc  CTCCCATGCCGTGCCTCTGGTTTCTGGAGTTTGTCGAACGGCAAGTGCTCCGACGCTATCG
        ****************** ******** ********** ********* **** ** ****

Tb  CACGGTGGTTCTCGGCTGAACGCCTCTAAGCCAGAAACCAGTCCCAAGACCGGGTGCCCGT
Lm  CACGGTGGTTCTCGGCTGAACGCCTCTAAGCCAGAAGCCAATCCCAAGACCAGATGCCCAC
Tc  CACGGTGGTTCTCGGCTGAACGCCTCTAAGCCAGAAGCCAGTCCCAAGACCAGATGCCC-A
        ***********************Rv*********** *** ********** * ***** *
```

Figure 55: Multiple Sequence Alignment of the 28S rRNA coding gene of *T. brucei* (Tb), *L. major* (Lm) and *T. cruzi* (Tc), the region highlighted in yellow and green correspond to the Forward (Fw) and Reverse (Rv) primer respectively.

Some pieces of advices were followed when designing them for a better performance of the PCR such as a GC content between 40 and 60%, similar melting temperature for both forward and reverse primers (no more than 5ºC of difference), between 18-30 nucleotides length…[174]. Analysis of primer self-dimers and heterodimers formation was carried out using the Oligo analyzer 3.1 tool (IDT) [175].

Primers were purchased from Sigma-Aldrich Inc. Table 10 shows primer sequences and related information.

Table 10: Primer sequences and information about length, GC content and melting temperature.

Primers	Sequence 5'---3'	Length (nucleotides)	GC content (%)	Melting temperature (ºC)
Forward	GATTGTGAAGGGATCTCGCAG	21	52.4 %	55.6 ºC
Reverse	TCTGGCTTAGAGGCGTTCA	19	52.6 %	55.9 ºC

3.2.2.4. PCR Amplification

It is known that standard PNAs can invade dsDNA but only when composed by homopurine stretches [104]. Preliminary studies also demonstrated that standards DGL probes were unable to invade dsDNA [33]. Therefore, different attempts to generate ssDNA and/or disrupt the double helical structure were made: 1) direct asymmetric PCR, 2) thermal denaturalization -heating dsDNA at 96ºC for 10 minutes and then keeping the sample in ice until DGL is added for 2 minutes-, 3) mechanical denaturalization –sonication- and 4) chemical denaturalization –betaine-. However, when doing the liquid phase assay for MALDI-TOF detection, just the unreacted DGL probes were detected. As a result, a two-stage PCR amplification had to be performed; the first one, a symmetric

PCR (sPCR) to generate dsDNA amplicon, followed by an asymmetric PCR (aPCR) (with higher concentration of the forward primer) to give rise to ssDNA and so make the dynamic chemistry assay possible.

PCR amplification reactions were performed on a Veriti® 96-well Thermal cycler (Thermo Fisher Scientific). Different attempts trying to optimize PCR yield were done: a gradient of annealing temperatures (61ºC was chosen), adding DMSO, a range of concentrations of gDNA, higher concentrations of primers, Mg^{+2} and/or dNTPs. Increasing the amount of DNA template seemed to improve PCR yield, but slight difference were seen between 50 and 100 ng of gDNA so the lowest one was chosen to perform most of the assays. Despite the different modifications performed on the PCR reaction, standard conditions and concentrations from the PCR master mix (Thermo Fisher Scientific [176]) were finally used (2 mM $MgCl_2$, 0.2 mM each dNTP, 1.25 U Taq DNA polymerase). Table 11 shows the cycling conditions used for both sPCR and aPCR reactions.

Table 11: Cycling conditions for both sPCR and aPCR:

PCR step		Number of cycles	Temperature (ºC)	Time
Initial denaturation		1	96ºC	3 minutes
Amplification	Denaturation	40	96ºC	30 seconds
	Annealing		61ºC	30 seconds
	Extension		72ºC	30 seconds
Final extension		1	72 ºC	10 minutes
Final hold		1	4 ºC	∞

Regarding the PCR template, optimization experiments were initially carried out using gBlocks® Gene Fragments which mimic the coding DNA sequences (CDS) for the 28S rRNA delta genes of *L. major* (183 bp), *T. brucei* (183 bp) and *T. cruzi* (178 bp) (see experimental section 5.3.5.) before using gDNA from parasites (see experimental section 5.3.6.). Either $1.5 \cdot 10^9$ copies of synthetic dsDNA (gBlocks® Gene Fragments) or 50 ng of ATCC® gDNA solution for *L. major* or *T. cruzi* and gDNA extracted from *T. brucei* in culture were used as DNA template.

For the sPCR, either 3 µL of synthetic dsDNA at $5 \cdot 10^8$ copies/µL (gBlocks® Gene Fragments) or 5 µL with different amounts of ATCC® gDNA solution for *L. major* or *T. cruzi* and gDNA extracted from *T. brucei* in culture were amplified using 1X PCR master mix (Thermo Fisher Scientific), 0.15 µM forward and reverse primers per reaction with a final volume of 50 µL. DNA templates were replaced with water for negative controls. aPCR was performed as for sPCR but using 2 µL of the first sPCR crude mixture as DNA template and a lower concentration of the reverse primer -0.15

µM forward primer and 0.015 µM reverse primer- to favor synthesis of only the sense strand (see experimental section 5.3.7. for PCR amplification reation details).

An aliquot (1 µL) of all sPCR and aPCR samples was used to run a capillary electrophoresis and so check that the PCR reaction has worked. Figure 56 shows the capillary electrophoresis result after running sPCR and aPCR samples using gBlocks® Gene Fragments as template for the amplification reaction. A band at 154 bp was observed for the sPCR samples (Figure 56, lines 1, 3, 5), which agrees with the expected amplicon length. A faint band of the right length is detected for the aPCR (Figure 56, lines 2, 4, 6) which might be due (i) to the dsDNA template from the previous sPCR that has been added to the aPCR reaction as template and (ii) to the dsDNA amplicons still generated during the aPCR amplification. However, the main product formed during aPCR is ssDNA toward which intercalating agents have lower affinity when compared with dsDNA.
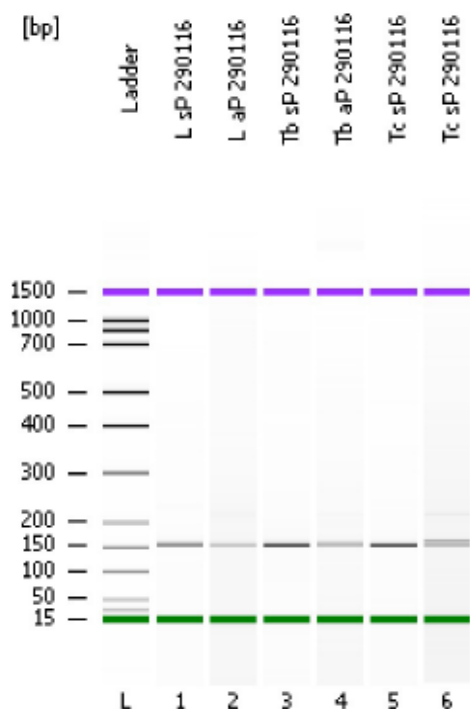
Figure 56: PCR product analyses by capillary electrophoresis (2100 Bioanalyzer). sPCR and aPCR using synthetic double-strand DNA as template (gBlocks® Gene Fragments). L: ladder; 1: *L. major* sPCR; 2: *L. major* aPCR; 3: *T. brucei* sPCR; 4: *T.brucei* aPCR; 5: *T.cruzi* sPCR; 6: *T.cruzi* aPCR. (Reproduced with permission [161]).

Then, amplification reactions were performed using gDNA as template. The fidelity of the PCR reaction when amplifying the target gDNA was confirmed by sequencing analyses using capillary electrophoresis (Sanger method 3130 Genetic Analyzers, Applied Biosystems, US) [131].

Moreover, PCR reactions were double-checked by using the Agilent 2100 Bioanalyzer and DNA 1000 Kit (Agilent Technologies Inc.) (Figure 57). As described above for PCR reaction in which gBlocks® Gene Fragments were used as template for the amplification reactions (Figure 56), a band of the right length (154bp) was observed for the sPCR samples (Figure 57, lines 2, 3, 4). No band was observed for the the negative controls in which either water for the sPCR or negative sPCR for the aPCR reaction were used as template (Figure 57, lines 1, 5); this confirmed the absence of contamination. The software also provides an estimation of the amplicon concentration. Regarding the aPCR reaction and as mentioned above, a faint band of the expected length was detected (Figure 57, lines 6, 7, 8) but it might be amplicon from the previous sPCR and the slightly dsDNA generated during the aPCR but the main product formed during aPCR is ssDNA.
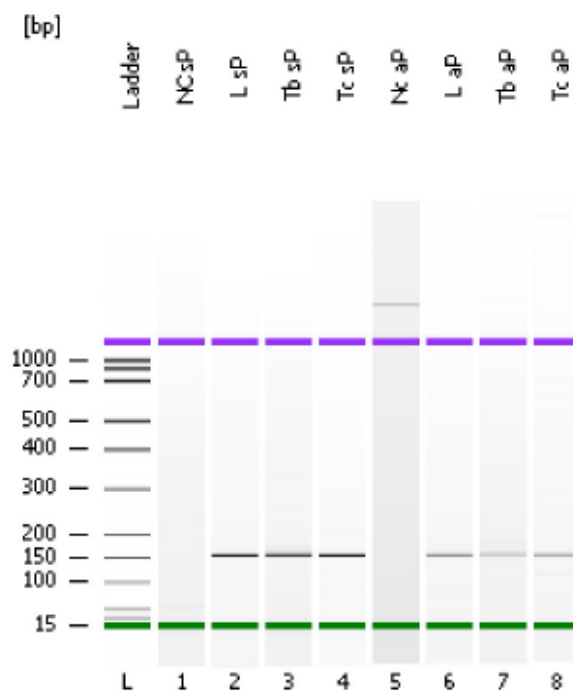
Figure 57: PCR product analyses by capillary electrophoresis (2100 Bioanalyzer). sPCR and aPCR using gDNA as template (ATCC® gDNA solution for *L. major* or *T. cruzi* and gDNA extracted from *T. brucei* in culture). 1*:* Negative control sPCR; 2: *L. major* sPCR; 3: *T. brucei* sPCR; 4: *T.cruzi* sPCR; 5: Negative control aPCR; 6: *L. major* aPCR; 7: *T.brucei* aPCR; 8: *T.cruzi* aPCR.

3.2.2.5. DGL probes design for the mass-based assay

The result of the multiple sequence alignment of the of 28S rRNA delta gene sequences of the three trypanosomatids was used to design DGL probes which targeted the Single Nucleotide Fingerprints (SNFs), the nucleotides that differ between the three species. As it can be observed in figure 58, these SNFs are surrounded by an identical sequence between the three parasites. As a result, two

DGL probes were designed (figure 58, DGL#1 in bue and DGL#2 in grey) which targeted two of these SNFs (highlighted in bold white in figure 58). After DNA/DGL probe hybridization, a 'chemical pocket' composed by the SNF under interrogation in the target DNA and the abasic position of the DGL probe is formed. These SNFs drive the incorporation of the complementary SMART-NB into the abasic position of the DGL probe. The combined analysis of just this two DGL probes enabled the unequivocal identification of the parasite present in the sample, since each parasite gives a unique pattern of SMART-NB incorporation for each DGL probe.

Figure 58: Multiple sequence alignment of the 28S rRNA delta gene sequences of the three *Trypanosomatidae* species. The absence of "star" shows where the SNFs in the 28S rRNA delta gene sequences occur. Forward and reverse primers are highlighted in yellow and green, respectively. The two SNFs under interrogation when using the MALDI approach are highlighted in white bold and the surrounding sequence which is the target for the corresponding DGL is highlighted in blue (DGL#1) and grey (DGL#2).

In other words, according to the templating nitrogenous base in the DNA coming from each parasite, specific SMART-NBs would be incorporated into the abasic position of the two DGL probes, allowing thus trypanosomatid identification. Figure 59 shows a scheme of the expected SMART-NB to be incorporated into each DGL probe depending on the parasite. *L. major* templates the incorporation of SMART-T into DGL#1 and SMART-G into DGL#2; when *T. brucei* is present, SMART-C is incorporated into both DGLs; and *T. cruzi* drives the incorporation of SMART-C into DGL#1 and SMART-G into DGL#2.
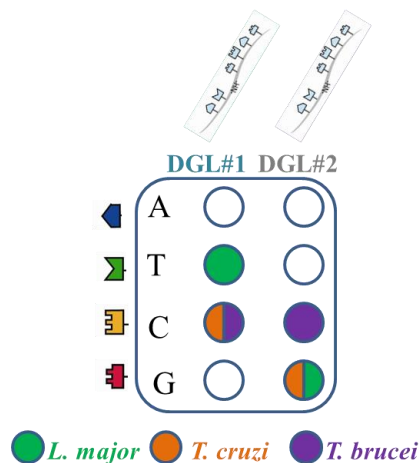
Figure 59: Scheme of the pattern of SMART-NB incorporation for the mass-based approach. The colored spots indicate the SMART-NB incorporated into the abasic position of the DGL probe. Each parasite is identified with a different color to follow the specific parasite-pattern of SMART-NB incorporation (green for *L. major*, orange for *T. cruzi* and purple for *T. brucei*).

When MALDI-TOF is used as readout tool, the assay characterizes because: 1) DGL probes bears a triphenyl phosphonium tag to at the N-terminal to improve the limit of detection. This group offers a permanent positive charge hence helping to detect molecular ions by the TOF detector. And 2) the four SMART-NBs (A, T, C and G – Figure 18B) can be simultaneously interrogated in a single assay. Therefore, the two DGL probes can identify any of the SNFs found within the selected region. The nucleobases highlighted in white and bold (Figure 58) are the SNFs targeted by the two DGL probes (DGL#1 and DGL#2). Table 12 shows the sequence of the two DGL probes used for the mass-based assay.

Table 12: Sequences of the DGL probes used for the mass-based approach.

DGL probes	DGL probe sequence (N-C)*
DGL#1	$(Ph)_3P^+$-CCA GAA AC_ AGA GGC ACG-$CONH_2$
DGL#2	$(Ph)_3P^+$-GCA CTT GCC _TT CGA CAA AC-$CONH_2$

* DGL probes are written from the N-terminal end (left) to the C-terminal end (right). DGL probes are capped at their N-terminal with 3-(carboxypropyl)triphenylphosphonium bromide and have a C-terminal primary amide. "_" represents a blank site.

Once the probe and the target DNA hybridized, what creates "the chemical pocket", the nitrogenous base in the SNFs guides the incorporation of a specific SMART-NB into the abasic position of a DGL probe, giving rise to different products each of which have different masses. In DGL#1, SMART-T is incorporated when it is *L. major* and SMART-C when the parasite is either *T. cruzi* or

T. brucei. Whereas in DGL#2, SMART-G is incorporated if it is *L. major* or *T. cruzi* and SMART-C when the parasite is *T. brucei* (Figure 59 and 60).
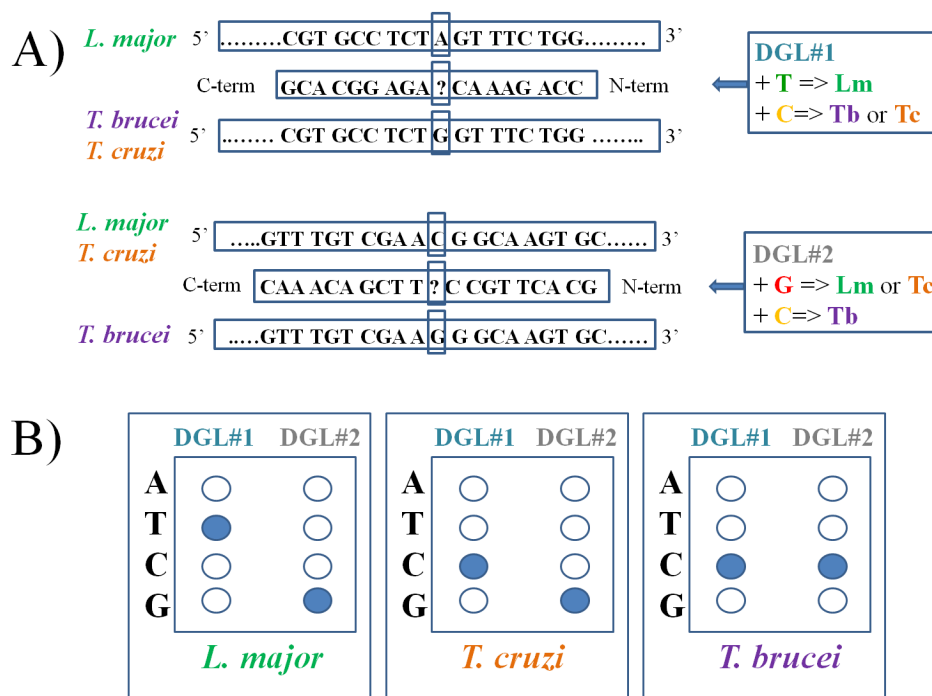
Figure 60: Scheme of SNF-mass-based detection. A) The three trypanosomatids can be distinguished using two DGL probes (DGL#1 and DGL#2). The squared question mark shows where the abasic position is. The square within the DNA sequence shows the templating nitrogenous base. The unique pattern of SMART-NB incorporation into each DGL probe indicates unequivocally the DNA coming from a given parasite: SMART-T incorporation into DGL#1 and SMART-G incorporation into DGL#2 indicates the presence of *L. major*; SMART-C incorporation into both DGL#1 and DGL#2 calls for *T. brucei*; and SMART-C incorporation into DGL#1 and SMART-G incorporation into DGL#2 relates to *T. cruzi.* B) Graphical representation of the unique pattern created by a specific parasite when interrogated with DGL#1 and DGL#2 and SMART-NBs. The blue dot indicates the incorporation of that SMART-NB onto the abasic site of a DGL probe. (Reproduced with permission [161]).

3.2.2.6. Trypanosomatids discrimination by dynamic chemistry and MALDI-TOF

Figure 61 shows a scheme of the mass-based assay procedure. Reaction takes place in solution, DGL probes, target nucleic acids and SMART-NBs are mixed and allowed to hybridize and the SMART-NBs to be incorporated into the abasic site of the DGL probe forming the iminium intermediate. Then, the reducing agent, sodium cianoborohydride, is added to reduce the more stable iminium ion and generate a tertiary amine. After that, samples are purified using an anion exchange resin, Q-sepharose®, and spotted onto the stainless steel MALDI-TOF plate using

sinapinic acid matrix (see experimental section 5.3.8.1.) [32]. Finally, a mass spectrum is obtained in which different mass peaks can be observed, knowing the difference between these peaks allows determining the SMART-NB that has been incorporated and so the nucleotide under interrogation, in this case the SNF.
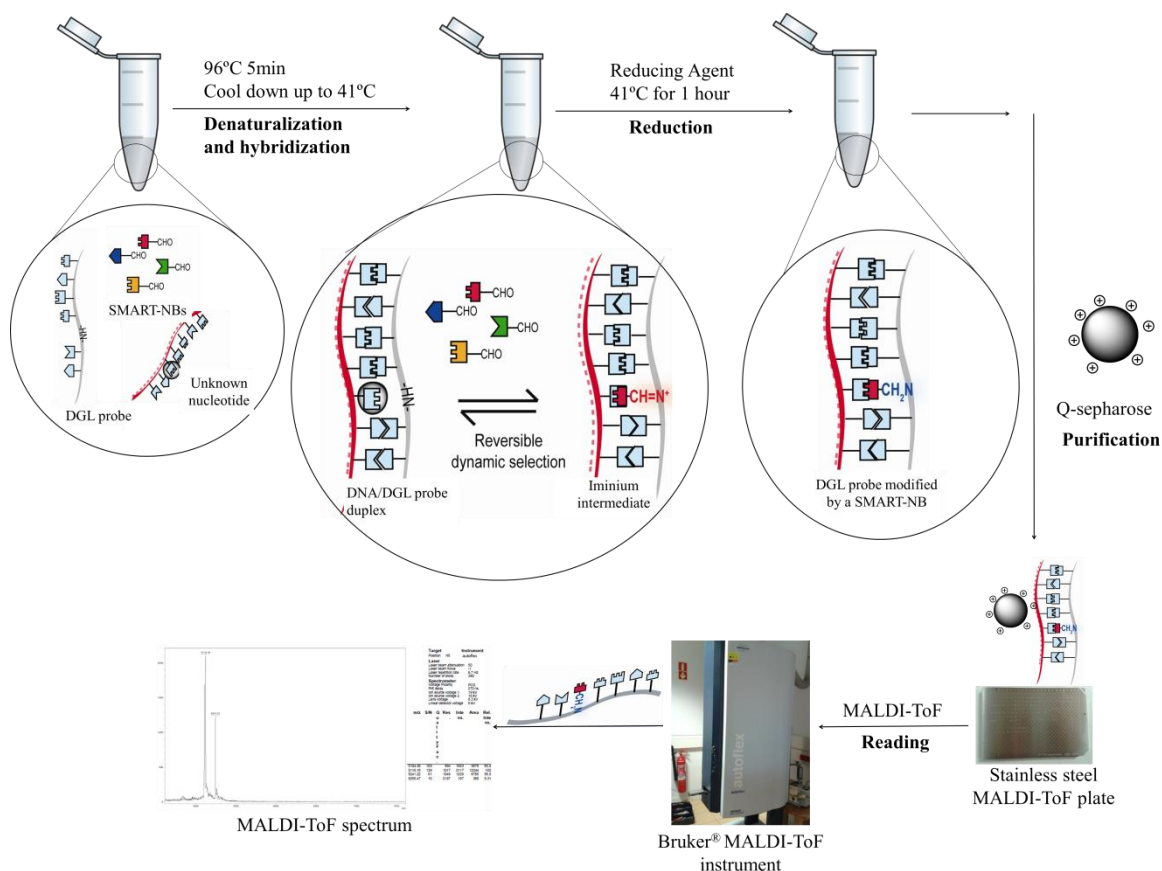
Figure 61: Steps of the dynamic chemistry reaction when using MALDI-TOF as readout tool: First, DGL probe and target nucleic acid hybridizes, then, the SMART-NBs incorporate into the chemical pocket and the one with the right hydrogen binding motifs is reduced and fixed into the position. The duplex DGLprobe/DNA is purified with an ion exchange resin Q-sepharose. The sample are finally spotted onto the MALDI-TOF plate and ionized. (Reproduced with permission [161]).

3.2.2.6.1. Base-filling reaction using synthetic ssDNA oligos

Initially, synthetic ssDNA representative of the target sequences of the three parasites for both DGL probes were purchased. Table 13 shows the DNA oligos sequences and the expected SMART-NB to be incorporated according to the templating nucleotide. The standard protocol developed previously [32] was applied to the analysis of these synthetic oligomers, using equimolar concentrations of the four SMART-NBs (see experimental section 5.3.8.1.1.). This experiment was used to validate the performance of the DGL probes and the protocol for the chemical reading of the

target nucleic acids. Figure 62 shows the obtained MALDI-TOF spectra in which the assignment of each peak is specified.

Table 13: DGL probes #1 and #2, with the two possible target ssDNA sequences complementary to each DGL probe taking into account the SNF of each parasite (highlighted in bold) and the SMART-NB that has to be incorporated into the abasic position.

DGL probes	Target DNA	Target DNA sequences (5'-3') complementary to the DGL probe	SMART-NB to be incorporated
DGL#1	DNA-1Lm	CGT GCC TCT **A**GT TTC TGG	SMART-T
	DNA-1TbTc	CGT GCC TCT **G**GT TTC TGG	SMART-C
DGL#2	DNA-2LmTc	GTT TGT CG A A**C**G GCA AGT GC	SMART-G
	DNA-2Tb	GTT TGT CGA A**G**G GCA AGT GC	SMART-C

Data analysis was carried out by measuring the mass difference between the two main peaks of the MALDI-TOF spectra: (i) peaks which correspond to unreacted DGL probes (sometimes borane adducts were also detected), which act as internal calibrator, and (ii) peaks which correspond to a DGL probe plus a specific SMART-NB, which was covalently bound to the abasic position forming a tertiary amine. By identifying that SMART-NB, the target nucleic acid under interrogation can be easily identified as it has to contain the nitrogenous base complementary to the incorporated SMART-NB.
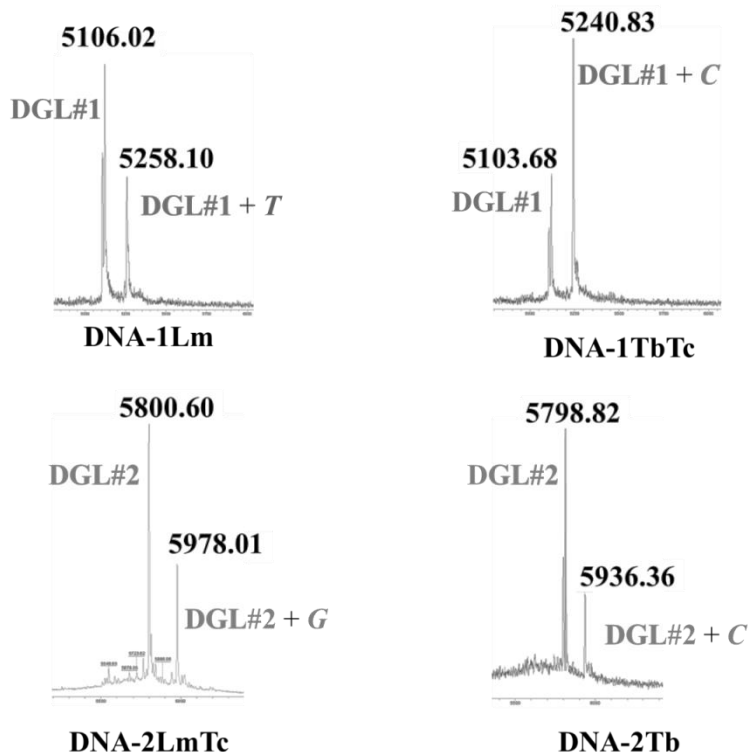
Figure 62: MALDI-TOF spectra for the validation of the two DGL probes using oligo DNAs. Two main peaks are seen for each combination of DGL probe-target ssDNA. The mass of the peaks and the peaks assignment are highlighted: by calculating the difference between the two mass-peaks, peak identity is attributed. (Reproduced with permission [161]).

The main peaks found in the MALDI-TOF spectra that are involved in the final outcome are registered in the table 14, where each mass peak is identified with its identity (either a DGL probe, a DGL probe boron adduct or a DGL plus the SMART-NB incorporated). It was so confirmed that the incorporated SMART-NB coincided with the complementary to what was the templating nucleotide in the target nucleic acid (in this test ssDNA oligomers complementary to the probes).

Table 14: Main mass peaks found in the MALDI-TOF spectra for each dynamic chemistry reaction that was carried out using oligo ssDNAs. First column shows every DGL probe and target ssDNA pair. The second column shows the mass peaks and in brackets their correspondence. Third and fourth columns indicate the relative intensity and the S/N ratio of each peak in the spectrum. (Reproduced with permission [161]).

Sample	Mass peak observed in the MALDI-TOF spectra	Peak relative intensity (%)	S/N
DGL#1+DNA-1Lm	5106.02 (unreacted DGL#1)	63.7%	35
	5119.52 (boron adduct DGL#1)	100%	56
	5258.10 (DGL#1+SMART-**T**)	54.2%	29
DGL#1+DNA-1TbTc	5104.79 (unreacted DGL#1)	30.1%	15
	5118.87 (boron adduct DGL#1)	51.1%	27
	5242.14 (DGL#1+SMART-**C**)	100%	55
DGL#2+DNA-2LmTc	5800.60 (unreacted DGL#2)	100%	212
	5814.59 (boron adduct DGL#2)	23%	38
	5978.01 (DGL#2+SMART-**G**)	49.1%	102
DGL#2+DNA-2Tb	5798.82 (unreacted DGL#2)	52.3%	15
	5812.85 (boron adduct DGL#2)	100%	32
	5936.36 (DGL#2+SMART-**C**)	38.6%	11

3.2.2.6.2. Trypanosomatids identification using aPCR product (from gBlocks® Gene Fragments)

Once the ability of the DGL probes to hybridize with complementary ssDNA and the ability of the SMART-NBs to covalently bind into the abasic position of a DGL probe were checked, a synthetic dsDNA which mimics the gene targeted by the primers and DGL probes was used as template. Since it is shorter than the whole genome, it will provide information regarding the amplification step and the dynamic chemistry reading of a sequence longer than the DGL probe length. For the reasons mentioned above, a two-step amplification reaction –sPCR followed by an aPCR- was done using these synthetic dsDNAs (gBlocks® Gene Fragments) as template (see section 3.2.2.4). In previous studies, the product of this second aPCR was purified using commercially available spin-columns (Quiagen) [33]. However, due to the short length of this amplification product, the recovery was very low. So, aPCR was used directly without any further purification step, just an acidification step to neutralize PCR buffer components and lower the pH to an optimal value to allow reductive amination to occur. Therefore, the ssDNA amplicon generated after the aPCR was analyzed by the chemistry-based approach for nucleic acid reading using the combination of two DGL probes and the SMART-NBs ((see experimental section 5.3.8.1.2.). The resulting MALDI

spectra (Figure 64) allowed clear calling of the three parasites studied, demonstrating that the two DGL probes designed were suitable for the analysis of the region of interest.
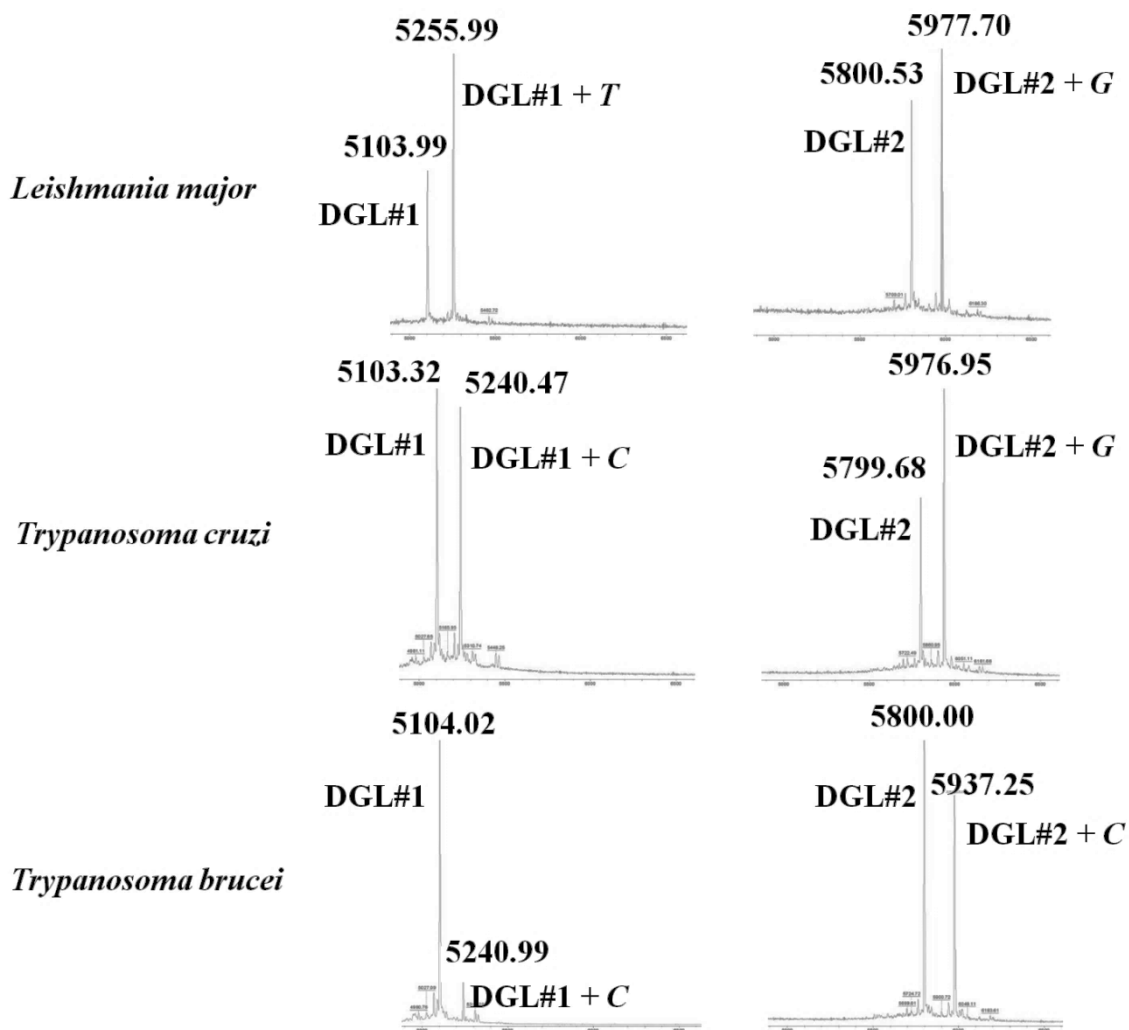
Figure 64: MALDI-TOF spectra obtained after the dynamic chemistry reaction that was carried out using synthetic aPCR product (from synthetic dsDNA gBlocks® Gene Fragments) as templating nucleic acid. It confirmed that the proposed chemical-based approach is suitable to distinguish the three trypanosomatid using a singleplex PCR and two DGL probes.

The peaks highlighted in the MALDI-TOF spectra obtained after the dynamic incorporation, on which synthetic aPCR products were detected, are summarized in table 15. As previously mentioned, sometimes a third peak corresponding to the DGL probe boron adduct appears. These results confirmed the ability of the probes to hybridize with a longer nucleic acid sequence and incorporate the right SMART-NB according to the templating nucleotide.

Table 15: Main mass peaks found in the MALDI-TOF spectra when reading the results of the dynamic chemistry reactions that were done from aPCR products obtained from synthetic dsDNA gBlocks® Gene Fragments. The first column indicates the DGL probes and the parasite DNA used. The second column shows the three main mass-peaks observed: DGL probe, boron adduct (not always detected) and DGL probe plus a SMART-NB. The third and fourth columns are the relative intensity and S/N ratio of the peaks.

Sample	Mass peak observed in the MALDI-TOF spectra	Peak relative intensity (%)	S/N
DGL#1 + *L. major* synthetic aPCR product	5103.99 (unreacted DGL#1)	56.5%	50
	5117.27 (boron adduct DGL#1)	7.23%	3
	5255.99 (DGL#1+SMART-**T**)	100%	92
DGL#2 + *L. major* synthetic aPCR product	5800.53 (unreacted DGL#2)	80.0%	67
	5814.25 (boron adduct DGL#2)	14.8%	6
	5977.70 (DGL#2+SMART-**G**)	100%	87
DGL#1 + *T. brucei* synthetic aPCR product	5104.02 (unreacted DGL#1)	100%	140
	5118.50 (boron adduct DGL#1)	15.6%	13
	5240.99 (DGL#1+SMART-**C**)	95.7%	136
DGL#2 + *T. brucei* synthetic aPCR product	5800.00 (unreacted DGL#2)	64.4%	105
	5813.48(boron adduct DGL#2)	10.0%	10
	5937.25 (DGL#2+SMART-**C**)	100%	169
DGL#1 + *T. cruzi* synthetic aPCR product	5103.32 (unreacted DGL#1)	100%	626
	(boron adduct DGL#1)		
	5240.47 (DGL#1+SMART-**C**)	16.6%	98
DGL#2 + *T cruzi* synthetic aPCR product	5799.68 (unreacted DGL#2)	100%	191
	(boron adduct DGL#2)		
	5976.95 (DGL#2+SMART-**G**)	78.9%	152

3.2.2.6.3. Trypanosomatids identification using aPCR product (from gDNA)

Once all reagents and protocols were validated, analysis of aPCR products obtained from 1 ng/µL of parasite gDNA was performed. Experiments for each specie were carried out in triplicate (see experimental section 5.3.8.1.2.). Figure 64 shows one representative mass spectrum for each pair specie-DGL probe.
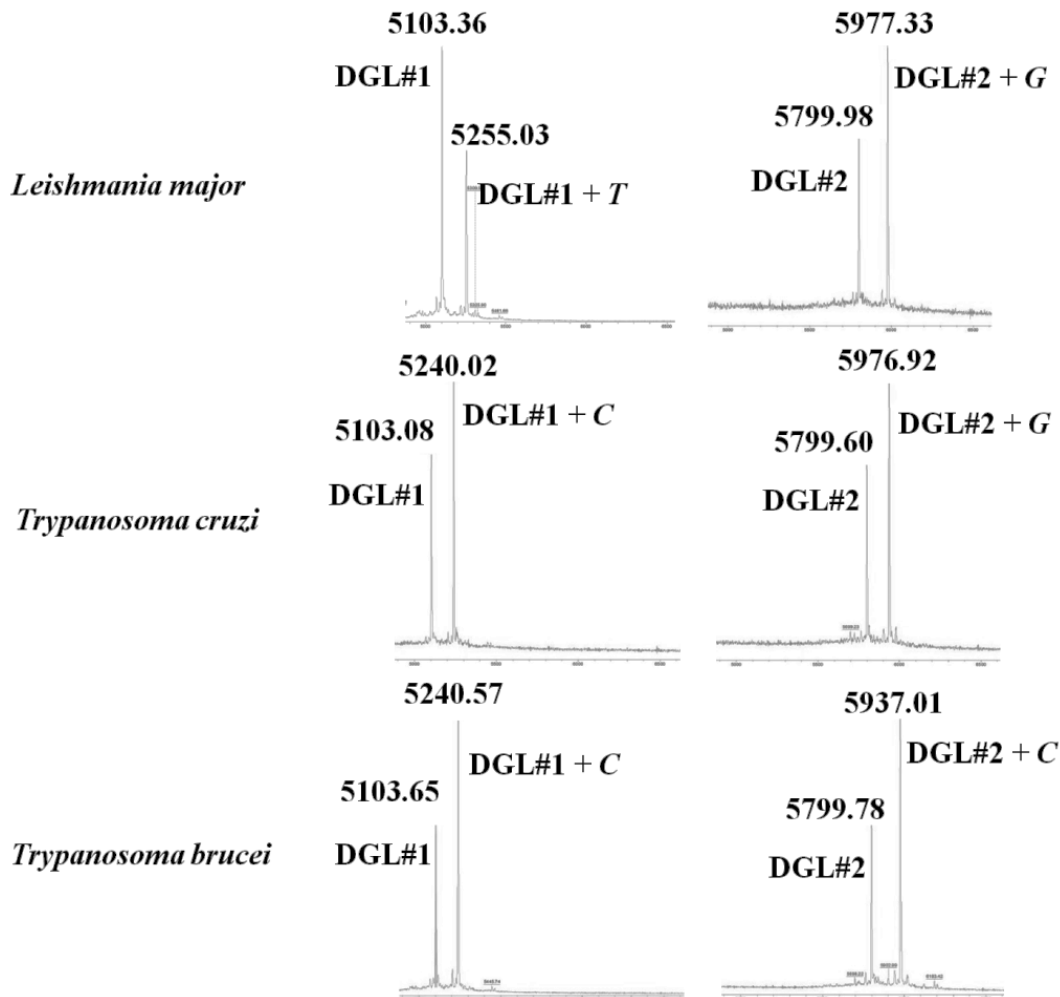
Figure 64: Representative MALDI-TOF spectra obtained when analysing aPCR products prepared from parasite gDNA by dynamic chemistry with DGL #1 and #2 and SMART-NBs. The difference between the mass of the two main peaks confirms the incorporation of the right SMART-NB for each aPCR product. (Reproduced with permission [161]).

Table 16 shows the main mass peaks found in the MALDI-TOF spectra after the dynamic incorporation reaction on which aPCR products generated from gDNA were used as template. The results further confirmed the previous experiments: 1) the DGL probes are able to hybridize with a complementary sequence; 2) the incorporation of the right SMART-NB occurs upon the templating power of the target nucleic acid according to Watson-Crick base-pairing rules; 3) the SMART-NB incorporation pattern into DGL#1 and DGL#2 allows unequivocal identification of the trypanosomatid specie.

Table 16: Main mass peaks found in the MALDI-TOF spectra when reading the results of the dynamic chemistry reactions that were done from aPCR product with gDNA as template. The first column indicates the DGL probes and the parasite DNA used. The second column shows the three main mass-peaks observed: DGL probe, boron adduct and DGL probe plus a SMART-NB. The third and fourth columns are the relative intensity and S/N ratio of the peaks (Reproduced with permission [161]).

Sample	Mass peak observed in the MALDI-TOF spectra	Peak relative intensity (%)	Signal/Noise
	5103.36 (unreacted DGL#1)	100%	368
DGL#1 + *L. major* aPCR product	(boron adduct DGL#1)		
	5255.03 (DGL#1+SMART-**T**)	62.4	232
	5799.98 (unreacted DGL#2)	69.5%	38
DGL#2 + *L. major* aPCR product	5816.35 (boron adduct DGL#2)	12.0%	3
	5977.33 (DGL#2+SMART-**G**)	100%	58
	5103.65 (unreacted DGL#1)	73.4%	72
DGL#1 + *T. brucei* aPCR product	5116.82 (boron adduct DGL#1)	9.70%	4
	5240.57 (DGL#1+SMART-**C**)	100%	102
	5799.78 (unreacted DGL#2)	71.0%	58
DGL#2 + *T. brucei* aPCR product	5813.48 (boron adduct DGL#2)	12.5%	5
	5937.01 (DGL#2+SMART-**C**)	100%	84
	5103.08 (unreacted DGL#1)	62.1%	163
DGL#1 + *T. cruzi* aPCR product	5117.79 (boron adduct DGL#1)	7.25	12
	5240.02 (DGL#1+SMART-**C**)	100	273
	5799.60 (unreacted DGL#2)	63.3%	115
DGL#2 + *T. cruzi* aPCR product	5812.99 (boron adduct DGL#2)	7.53%	8
	5976.92 (DGL#2+SMART-**G**)	100%	189

3.2.2.7. Mass peaks assessment

The unreacted DGL probe of lowest mass was used as an internal calibrator. SNFs were determined by both visual inspection, and also by input of the peak table data into a Microsoft Excel file. Raw mass-peak data obtained from the MALDI spectra was analyzed using a 'LOOKUP' formula, which converted numerical mass-to-charge ratio peak values (m/z) within a set range and above a certain intensity threshold into an output parasite specie. Presented below is the output from spreadsheets after the input of raw mass peaks data into Microsoft Excel file (see appendix section 6.4 for excel file tables). The formula used selected just peaks with S/N>10 and relative intensity >15% (see appendix section 6.3 to see the formula used to convert these data into an output parasite) [33]. Similar results to those with synthetic DNA oligomers were obtained for both aPCRs generated

from synthetic dsDNA and gDNA, which were in full agreement with the expected data. In all cases, every specie was unequivocally assessed using the mass spectra coming from the two DGL probes used in this study.

3.2.2.8. Turnaround time

In terms of time to results, once DNA is isolated, the work-flow lasts around 5 hours and 30 minutes. However, many samples can be run in parallel, depending on the instrument availability in the testing laboratory: thermomixers have a capacity of 24, 48 or 96 tubes and centrifuge capacities vary from 12 up to 96 tubes. The stainless steel MALDI-TOF plate has 386 wells for samples to be analyzed. The process itself is very simple, and very suited for automatic liquid handling. Finally, analysis of the MALDI-TOF spectra is straightforward thanks to the LOOKUP formula we have developed (see appendix section 6.3.), which automatically assigns the parasite species after introducing the mass peak from the spectra. This process can be also automatized by programming a simple macro.

3.2.2.9. Limit of detection of the mass-based assay: Sensitivity and specificity

A sensitivity test was done, *T. cruzi* was the selected trypanosomatid to perform the assay. sPCRs using decreasing amounts of *T. cruzi* gDNA as starting material were carried out. Six concentration points (50, 5, 0.5, 0.05, 0.005, 0.0005 ng of gDNA as template) plus negative controls (H$_2$O as template) were used in triplicate. A Thermofisher application from its website [177] was used to calculate the concentration of ATCC$^{®}$ gDNA of *T. cruzi*, expressed as number of copies per µL, for the sPCR amplification step. To do so, the website uses 650 g/mol as average molar mass per base-pair and the length of the target nucleic acid -106.4 Mb is the estimated diploid genome size for *T. cruzi* [149]- to provide a DNA concentration expressed as number of copies/µL is given.

Additionally, six more reactions, three for each parasite (*L. major* -32.8 Mb genome length [178] and *T. cruzi* –whose genome account for 26 Mb [179]-) using 50 ng of gDNA as starting template amount for the sPCR reaction were carried out to assess the specificity of the assay. In total, 27 PCR reactions were analyzed by this method. There were 3 negative controls, 18 *T. cruzi* positive – with decreasing amount of gDNA for sPCR-, 3 *L. major* positives and 3 *T. brucei* positives. PCR products were then analyzed by capillary electrophoresis to confirm the amplification reaction and determine the amount of amplicons generated (see Figure 65 for capillary electrophoresis result and table 17 for numeric data of starting material and amplification products). As it can be observed in figure 65, amplicons of the expected size were detected when using the four highest amounts of gDNA; however, when using 0.005 ng and 0.0005 ng of *T. cruzi* gDNA, no bands were identified.

A faint band, which may be due to the primers, can be seen for these two lowest amounts of DNA template. No band appears in the negative control sample which indicates the absence of contamination.
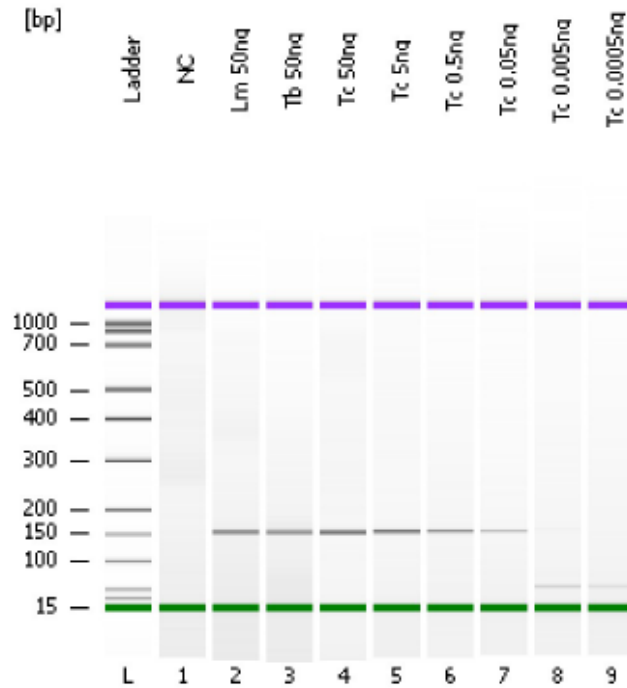

Figure 65: Capillary electrophoresis of *T. cruzi* sPCRs used for the limit of detection experiment. 1*:* Negative control sPCR; 2: *L. major* sPCR 50 ng; 3: *T.brucei* sPCR 50 ng; 4: *T.cruzi* sPCR 50 ng; 5: *T.cruzi* sPCR 5 ng; 6: *T.cruzi* sPCR 0.5 ng; 7: *T.cruzi* sPCR 0.05 ng; 8: *T.cruzi* sPCR 0.005 ng; 9: *T.cruzi* sPCR 0.0005 ng. (Reproduced with permission [161]).

Table 17: Amount of ATCC® gDNA of *T. cruzi* used for the sPCR done for the limit of detection analysis: it is shown the amount of gDNA (ng), the final concentration of gDNA in the sPCR reaction (expressed in ng/µL and in number of copies/µL for which it was taking into account that the length of the gDNA of *T. cruzi* is 106.4 Mb, 26 Mb for *T. brucei* and 32.8 Mb for *L. major*) and the yield of the PCR (expressed ng/µL and nanomolarity of dsDNA amplicon detected by bioanalyzer). (Reproduced with permission [161]).

Amount (ng) of gDNA in sPCR reactions	Concentration (ng/µL) of gDNA in sPCR reactions	Nº copies/µL of gDNA in sPCR reactions	ng/µL of amplicon detected by Bioanalyzer	Molarity (nM) of amplicon detected by Bioanalyzer
Lm-50 ng	1	28246	2.28	22.3
Tb-50 ng	1	35633	1.97	19.3
Tc-50 ng	1	8707	3.41	33.5
Tc-5 ng	0.1	870.7	2.34	22.8
Tc-0.5 ng	0.01	87.07	1.35	13.1
Tc-0.05 ng	0.001	8.707	0.61	5.9
Tc-0.005 ng	0.0001	0.87	0.1	0.9
Tc-0.0005 ng	0.00001	0.087	---	---
H₂O-Negative Control-0 ng	0	0	---	---

Each of these products were then amplified by aPCR and analyzed by dynamic chemistry and MALDI-TOF as described above (see experimental section 5.3.8.1.2.). 0.25 µM of DGL probe was used to avoid a large excess of probe compared with the amplification product to be detected and so avoid masking the incorporation mass-peak. Figure 66 shows an example of a MALDI-TOF spectrum obtained when analyzing each aPCR reaction with DGL#1 (Figure 66A) and DGL#2 (figure 66B). Moreover, Spectra were assessed semi-automatically, following mass-peaks assignments of MALDI-TOF spectra using the LOOKUP formula (see appendix section 6.3.). The method presented 0 false positives, 21 true positives, 3 true negatives and 6 false negatives. *T. cruzi* samples which started from the four highest amounts of gDNA (12 samples) were unequivocally called as *T. cruzi*. However, as it can be observed in Figure 66 samples where gDNA concentrations were 0.0001 and 0.00001 ng/µL, (0.005 and 0.0005 ng of gDNA, respectively) which is also equivalent to 0.87 and 0.087 copies/µL were called as parasite free, hence being false negatives. This correlates with the fact that sPCR product using these amounts of gDNA could not be detected by Agilent 2100 Bioanalyzer and DNA 1000 Kit (Agilent Technologies Inc.) (Figure 65, line 8 and 9). Samples starting from 50 ng of either *L. major* or *T. brucei* gDNA were unequivocally identified as *L. major* or *T. brucei* (data shown above, figure 64). Replicates of negative controls were all called as parasite free, these results emphasized the role of nucleic acids in templating the base-filling reactions. In none of the assays, mis-calls between the three species occurred. False negatives

were linked to the inability of the PCR amplification step to create enough copies of amplicons. Therefore, the limit of detection of this assay is linked to the sensibility of the PCR amplification of gDNA, being 1 pg/µL -equivalent to 8.7 copies/µL- of gDNA, the lowest starting concentration that could be analysed by the presented method.
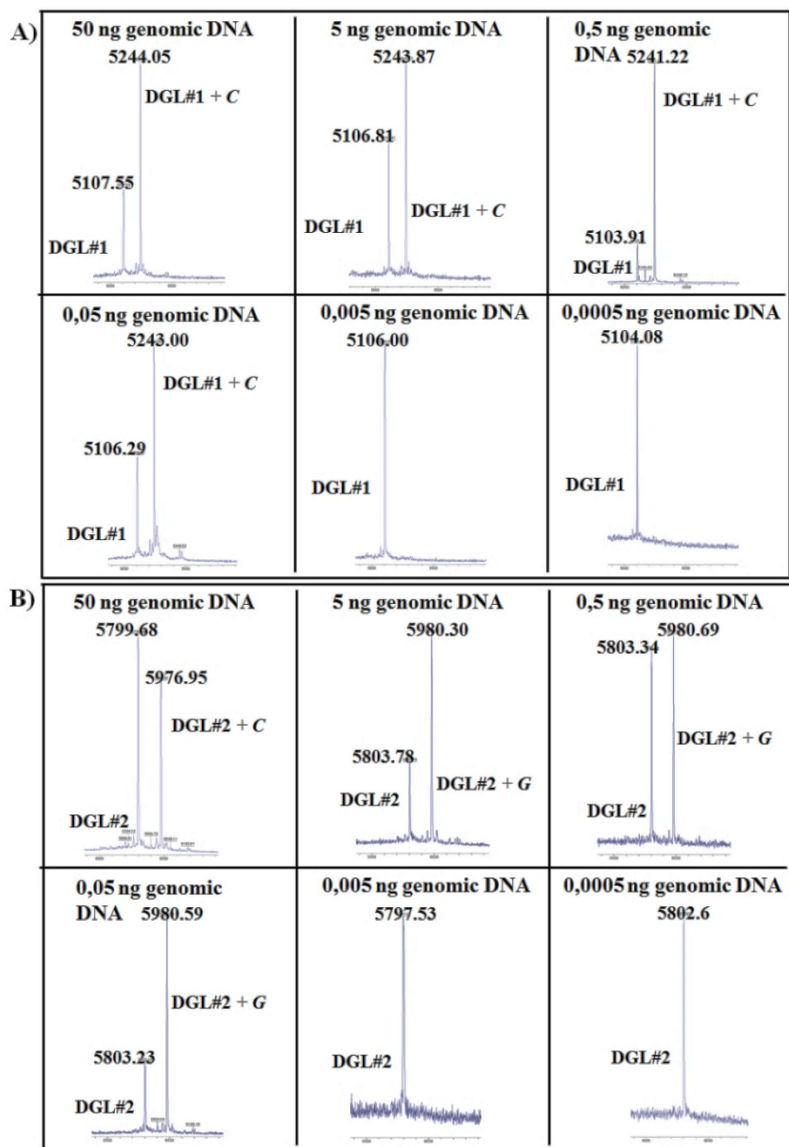
Figure 66: MALDI-TOF spectra obtained in the limit of detection experiment. Decreasing starting concentrations of *T. cruzi* gDNA were used for the sPCR amplification, the product was then amplified by an aPCR and finally analyzed by dynamic chemistry using MALDI-TOF as read-out tool. It is shown the MALDI-TOF spectra generated for the different aPCR amplicons interrogated using DGL#1 (A) and DGL#2 (B). (Reproduced with permission [161]).

3.2.3. Discussion

Trypanosomatids can cause diseases that can be fatal if not treated [122-124]. Clinical symptoms associated with the infection are fairly unspecific, reported as fever and malaise, so doctors are unable relying on the clinical symptoms alone to accurately diagnose trypanosomatids diseases [123]. Moreover, diagnostics tests have changed little, being microscopic observation or immunological tests to detect antibodies the main methods used [123, 142, 180]. It is proposed a unique molecular approach that with a single test quickly differentiates *T. cruzi*, *T. brucei* and *L. major*. The assay thus allows rapid and accurate diagnosis what could improve treatment decisions, as well as suitable aftercare. The method is based on a singleplex PCR amplification followed by the interrogation of the generated amplicon *via* dynamic chemistry and MALDI-TOF spectroscopy for reading the results [33]. Dynamic chemistry can be thus added to the group of genotyping methods which generates allele-specific product. It was successfully applied for the genotyping of cystic fibrosis patients [33]. Now, it is introduced a novel term "Single Nucleotide Fingerprinting" (SNF), which identifies single nucleotide differences within highly conserved regions of different species, such as *L. major*, *T. brucei* and *T. cruzi*. Target regions entitled to be detected by this method must have the following features (i) be highly conserved among the different species under interrogation (ii) be susceptible to be amplified with a single set of primers (forward and reverse) regardless the parasite specie, (iii) contain SNF responsible which drive a unique SMART-NB incorporation pattern characteristic of each parasite and (iv) must not have homology with human gDNA. 28S rRNA delta coding gene fulfilled all the criteria [148, 150-152, 180]. Identification and differentiation of the three parasite species studied was possible using the SNF approach (Figure 59). One of the advantages of this method is the use of just a single set of primers to amplify a target highly homogenous sequence of three difference species and then identified each one by the dynamic chemistry approach (Figure 55). Briefly, *T. cruzi* and *T. brucei* template the incorporation of SMART-C on DGL#1, as they both have a guanosine opposite the abasic position; whereas *L. major* has an adenosine and so templates the incorporation of SMART-T on DGL#1. In the case of DGL#2, *T. brucei* templates SMART-C incorporation, while if either *L. major* or *T. cruzi* are present in a sample, SMART-G is incorporated. The unique combinations of SMART-NB incorporation allow the identification of these three Trypanosomatids in a single tube (Figure 59). Dynamic chemistry is thus successfully applied to the identification and differentiation of these three trypanosomatid species (*L. major*, *T. brucei*, *T. cruzi*) using a singleplex PCR in a single tube (Figure 64).

This distinct method has some advantages over other allele discrimination assays. 1) There is no need for the tight optimization and control of conditions associated with the hybridization of ASO probes and subsequent washing steps [181]. As DGL probes hybridize across the SNF regardless the trypansomatid specie, so the tight optimization and control of conditions associated with ASO probes is no needed. 2) Dynamic reading of nucleic acid for allele-discrimination does not need enzymes unlike other methods that rely on enzymatic extension. This is specially convenient in methods that use ddNTPs, since these unnatural nucleotides triphosphates are incorporated less selectively than dNTPs by natural enzymes and, therefore, modified enzymes are required to overcome this [182]. Moreover, other assays like iPLEX and SPC-SBE [183] need enzymatic steps with shrimp alkaline phosphatase (SAP) and exonuclease I to degrade nucleic acids, dNTPs and primers, before being finally extended with ddNTPs. Obviating these enzymatic reactions, like in dynamic chemistry assays, provides benefits in terms of cost and analysis time.

On the other hand, when compared to other single base resolution technologies there are some features that stand the value of this dynamic chemistry approach:

1) The target nucleic acid does not have to be tagged, as it is the technology itself through the dynamic chemistry process that allows the detection of the target. As a result, amplicons do not have to be labeled unlike other methods of probe hybridization and primer extension which need labeled primers, dNTP or ddNTPs to create the labeled amplicons, this also means that the PCR step should be very accurate to avoid final reading errors. This assay so falls within the category of molecular assays which provides the highest specificity, relying on a third level of sequence detection of the products. For example, TaqMan®, Molecular Beacons and Scorpions technologies which require of 3 binding events (2 primers and a probe) to create a signal.

2) The unique combination of SMART-NBs that has to be incorporated into each customized DGL probe depending on the parasite present in a sample and this is done using just a single set of primers regardless the parasite. This is particularly important when compared to SBE technologies where the complexity of the assay is increased since an allele specific primer extension is required for each possible variant. In this case, the four possible variants can be read in a single tube using a singleplex PCR.

3) The four nucleobases can be read in a single tube. Even though there are platforms with very high multiplexing capacity, being able of detecting large number of analytes per sample such as microarrays, not many of them can look at the four possible nitrogenous bases in a single position. Many approaches use fluorescence reading, several of them rely

on third molecules, i.e TaqMan and Scorpion, but they mostly only read two variants per position. More sophisticated fluorescence readers allow having four fluorescence channels. On top of that, these technologies are limited in their multiplexing capacity. Next Generation Sequencing (NGS) can have the multiplexing and capability of reading the four bases, but this is more expensive and so it would be difficult to be adapted for parasite detection in developing countries, even if the cost per patient can be economically sustained.

If compared to other nucleic acid analysis that use MALDI-TOF, dynamic chemical allele-discrimination with DGL probes benefits from the PNA backbone of the probes which is particularly well suited for detection by MALDI [17]. DNA and RNA are more difficult to be analysed; for example, the GOOD assays requires an additional alkylation step and a permanent charge tag to address this. The use of PNAs for MALDI-TOF genotyping has previously been reported, but these assays use ASO probes for discrimination, with the associated disadvantages described above [36].

There are tree features of the presented technology can be potential hurdles to the analysis of gDNA:

1. The DGL probe concentration must always be approximately equal to or less than that of the DNA template. If a large excess of DGL probe is used, then any signal for the templated products can be masked by unreacted probe. The sensitivity of this method is in a certain way limited by the detection limit for the DGL probes, which we set at 0.25 μM.

2. The detection limit for the DGL probe following dynamic incorporation was established to be on the order of 8.7 copies/μL of *T. cruzi* sPCR amplicon (Figure 66). In the absence of a charge tag the limit of detection is usually lower.

3. Only ssDNA can be analysed because canonical PNAs (containing all four bases) are unable to invade linear (B-form) dsDNA [104]. However, gDNA is double stranded, which provides a further barrier to direct analysis making necessary to either denaturalize the dsDNA or to do a second aPCR to transform dsDNA into ssDNA.

The assay described here relies upon PCR, with all of its inherent problems, for DNA amplification. Since SMART-NB incorporation will only occur in the presence of templating DNA, any false positives or negatives will arise from the enzymatic amplification stage, as it was demonstrated in the sensitivity study were samples with less than 8.7 copies/μL of gDNA were mis-called as parasite free (Figure 65 for capillary electrophoresis result line 8 and 9 were no amplification

product was observed, and figure 66 for MALDI-TOF spectra when using 0.005ng and 0.0005ng of gDNA as template where no SMART-NB incorporation was observed). However, this dependence on PCR is shared by virtually all genotyping technologies currently available. A notable exception is the INVADER assay [184], although this method requires the input of a huge amount of gDNA. The requisite of ssDNA necessitates an additional step, which is also a drawback if compared with other assays. An example is the solid-phase capture-single base extension (SPC-SBE) method, which overcomes this through the use of biotinylated primers and streptavidin-functionalized solid supports. aPCR may be performed in a single step as opposed to the two reported here [185], although it might be harder to be achieved. Direct analysis of dsDNA may be possible through the use of conditions which favor PNA/DNA over DNA/DNA hybridization (such as low salt concentrations) [186], or modifications to the PNA backbone which makes it to adopt an helical organization which favours duplex invasion [104].

The need for a PCR step in genotyping by dynamic chemistry is dependent on the sensitivity of the detection method and the concentration of the templating nucleic acid. It is reasonable to predict, for example, that a realistic lowering of the detection limit to the 10^{-15} mol (1femtomole) level would allow direct profiling of the high copy number nucleic acids, such as some miRNAs, by this dynamic chemical approach [187].

The resulting MALDI-TOF mass spectrum after the DNA base-filling reaction permitted clear identification of the trypanosomatid. LOOKUP and IF formula used to translate mass peaks into a trypanosomatid species were adjusted to take into account peaks with a S/N ratio higher than 10 and a relative intensity higher than 15%, since some dynamic reactions gave poorer yields. In general, no peaks corresponding to nucleobase incorporation were observed with lower intensities.

Some of the assays described or the instrumentation required to run the experiments are significantly challenging in terms of cost and adaptation of the parasite detection routine in developing countries laboratories. So, once the dynamic chemistry assay for trypanosomatids identification was validated by MALDI-TOF, it was intended to implement it into a more economic, handy and easy to perform platform which does not require sophisticated instrumentation or expert operators. It was thought about a colorimetric-based assay which relies on DNA-flow through and reverse-dot blot technologies and where results can be easily observed and interpreted with the naked eye.

3.3. Colorimetric-based assays for the identification of Trypanosomatids by detecting Single Nucleotide Fingerprints using DNA analysis by Dynamic Chemistry (Specific objective 2.2.)

3.3.1. Colorimetric-based platform

3.3.1.1. Dot blot and Reverse-dot blot

The detection of DNA sequences with nucleic acid probes can be done using different techniques such as quartz crystal microbalance (QCM), surface plasmon resonance (SPR) and MALDI-TOF mass spectrometry, etc. However, to do so, complex instrumentation, well-equipped laboratories and clinical experts are needed, so they are not suitable for remote, rural or low-income areas [94].

Dot-blot hybridization has been proposed as an alternative technique. It is a simple technique to identify a target nucleic acid molecule, detect genetic mutations and polymorphisms in a biological sample The sample containing the biological target (usually proteins or nucleic acids) is spotted on a membrane (such as nitrocellulose, Nylon 66, poly(vinylidene Fluoride) (PVDF)) without prior electrophoretic separation. The target will be detected through binding with a probe and generation of a radioactive, fluorescent, chemiluminescent or colorimetric event (Figure 67). Some of the advantages of dot-blot hybridization are that multiple samples can be analyzed inexpensively, accurately and in a high-throughput fashion [94, 188].

When designing a dot-blot hybridization assay, three components must be considered: the membrane, the probe and the detection method. Commercial membranes for DNA blotting are made of nitrocellulose, poly(vinylidene) fluoride (PVDF) ,Nylon 6.6, etc, They are generally hydrophobic, which may originate non-specific adsorption, so this undesirable effect is avoided by treating the membrane with a buffer solution containing metal ion (MgCl2), organic solvent (acetonitrile, formamide), anionic detergent (sodium dodecyl sulfate), etc. [94].

This method of nucleic acid analysis has been simplified thanks to the polymerase chain reaction (PCR) which can selectively increase the number of copies of a particular DNA segment in a sample [188, 189]. Once the target has been amplified, it is fixed onto nylon membranes and hybridized with a labeled oligonucleotide probe. However, because each probe must be individually hybridized to the amplified DNA, the process can become difficult if many different mutations or polymorphisms have to be interrogated [188].

One approach to overcome this procedural difficulty is to "reverse" the assay by attaching the probes to the support and then hybridizing the amplified DNA (Figure 67) [188, 189]. Thus, in a

single hybridization reaction, an entire series of sequences could be analyzed simultaneously. All the bound oligonucleotides must be sequence-specific under the same hybridization conditions. If not, it can be achieved by adjusting the length, position, and strand specificity of the probes or by varying the amount applied to the membrane. The presence of tetramethylammonium chloride in the hybridization buffer can also help to minimize the differences among immobilized oligonucleotides caused by their different sequences [188].

Comparing the sensitivity of reverse-dot blot with the conventional dot blot format where the PCR products are immobilized to the membranes and hybridized to a ^{32}P or biotin labeled probe, even if similar sensitivity could be achieved, the background is usually higher. With the probes covalently bound at the N-terminal or 5' ends, they should all hybridize with equal efficiency to the PCR products. In contrast, in the dot blot format, the PCR product is immobilized randomly so that all target sequences may not be available for hybridization [189]. In addition, the amount of PCR product applied to the filter is almost variable, since the PCR cannot be controlled to synthesize the same amount of target sequences and this may be reflected in variable hybridization signals; whereas the reverse-dot blot has a precise amount of probe at each spot [189].
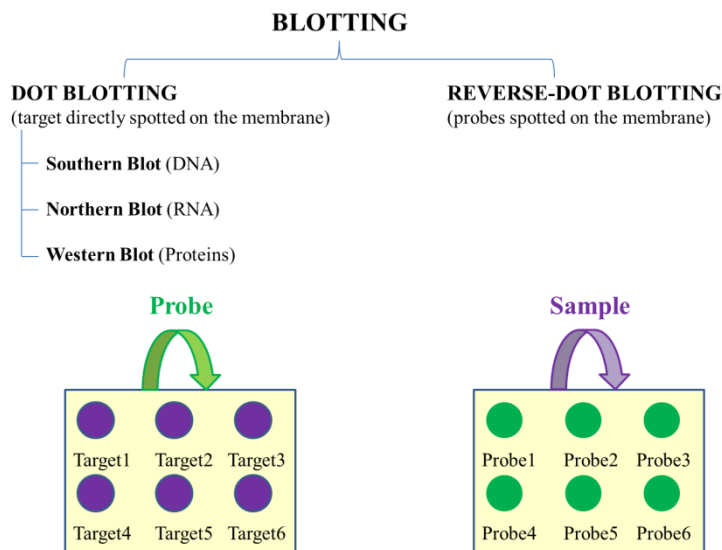
Figure 67: Scheme highlighting the differences between dot-blot (samples are spotted on the membrane and probes are later added) and reverse dot-blot (probes immobilized on the membrane and then a sample is added).

Although it requires some initial effort, the end result is a simple, robust, and potentially automatable system that can be completed (amplification, hybridization, and color development) in 3-4 hr. Reverse-dot-blot technology is especially valuable for assays where several sequence

variations have to be tested and, more importantly, it can be prepared in a ready-to-use format where probes are immobilized on many support at one time and then store until use [188].

3.3.1.2. Flow-through hybridization technology

The membrane-based "Flow-through Hybridization Platform" by Diagcor Bioscience Inc. Limited, Hong Kong SAR (China) (US Patent number 5741647) is capable of developing low cost membrane-based macro-arrays for use in molecular diagnostic applications [190].

With the flow-through process, a detectable signal is observed with an incubation time of 1 minute. Within 5 minutes of the flow-through hybridization process, 71% of the signal intensity was achieved in comparison to an overnight conventional method; with 8-10 minutes incubation, similar sensitivity is reached and with an extended hybridization time to 15 minutes, flow-through process has an increased sensitivity. So, flow-through process showed to be superior by shortening the hybridization time and giving higher sensitivity. In a comparable intensity assay pair, flow-through hybridization process implies around a 10-fold time reduction which is very important for diagnosis purposes because reporting time is often a limiting factor. The overall volume of reagent and cost are also reduced in Flow-through hybridization processes [190].

The speed of the diffusion and concentration of the target molecules moving through the solid matrix is the rate limiting step resulting in a long incubation step. The Flow-through method eliminates this diffusion process by directing the target DNA to the complementary capture probes that are immobilized on and inside the membrane pores. This effectively changes the hybridization action from a passive random diffusion action to an active channeling process, speeding up the reactions. The reasons for the slow rate of the annealing process in conventional hybridization are:

1) The need for large reagent volume to cover the whole area which results in a lower effective concentration available for binding to the immobilized probe.

2) During the incubation process, the majority of the non-contacted target DNA are self-annealed which reduced the effective concentration of the denatured target DNA and so the efficiency of the hybridization.

3) Membranes are characteristically porous and DNA molecules of <500bp can readily diffuse through a 0.45 micron membrane [190].

4) In membrane preparation, 24-30-mer probes are immobilized inside the matrix pores. In conventional hybridization, only a small portion of the total probes immobilized on the surface of the membrane are accessible for binding to the target DNA molecules.

The flow-through hybridization method eliminates these intrinsic defects. It generates higher signal intensities with reduced processing time and reagent volumes. In washing, a clean solution front moving forward is anticipated each time a new wash is done, making it the most effective washing mechanism possible, so a cleaner background can also be expected [190].

3.3.1.3. Membranes used for the Reverse-dot blot

PALL Life Sciences offers a variety of membranes with different properties and chemistries for use in transfer and immobilization procedures. They can be used for a wide variety of applications: nucleic acid and protein transfer and detection (Northern, Southern and Western transfers; colony and plaque lifts, replica plating, dot-blots, DNA firngerprinting), microarrays, macroarrays, solid phase ELISAs, protein sequencing, affinity separations [191].

PALL Nylon membranes are cast from nylon 6,6 (Figure 68A) whose polymer structure is mostly non-polar with terminal amino and carboxyl groups. When formed into a membrane, hydrophobic regions fold away from the surface of the pores so that the terminal polar groups are exposed leading to hydrophilic membranes (Figure 68B) [191].
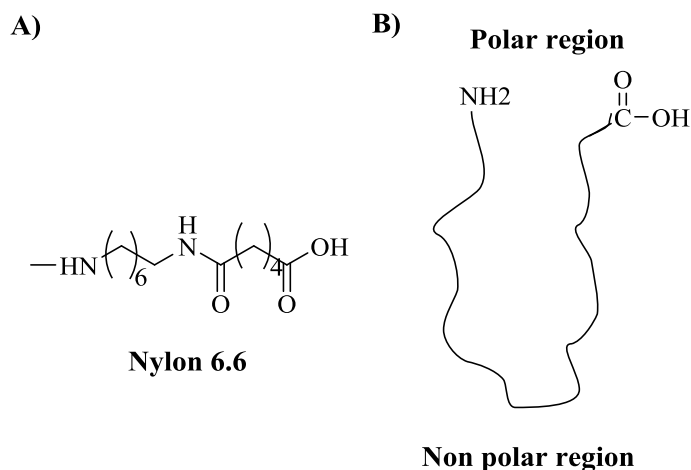
Figure 68: A) Nylon chemical structure and B) schematic representation of the folding to give a hydrophilic surface on the membrane.

Immunodyne ABC® membranes are nylon 6,6 membranes structure formed around a non-reactive, non-woven, polyester fabric matrix which confers high tensile strength, toughness, flexibility, and resistance to tearing, cracking, and puncture. These membranes, thanks to their pre-activation, have improved retention and stability of immobilizing ligands because of the covalent linkage with nucleophilic groups found on proteins and other biological macromolecules. Indeed, their primary reactivity is with amine groups at neutral pH. The narrow pore size distribution of Immunodyne ABC® membranes ensures uniform binding of biologically active macromolecules across the

membrane surface. The 75-85% void volume provides for minimal flow resistance and high diffusion rates [192].

3.3.1.4. Equipment for the Flow-through&Reverse-dot blot assay

Vitro group has developed 3 tools for DNA-hybridization: HibriSpot24™, HibriSpot12™ and e-BRID system™. They have some features in common: all of them are based on DNA-flow technology, they use reverse-dot blot as hybridization system, they count on the hybrisoft software to analyze and control the samples. HibriSpot12™ was used for the initial development of the colorimetric-based assay for trypanosomatid identification. It is a semiautomatic DNA-flow hybridization system with capacity for 12 samples and which allows controlling time and temperature.

The Vitro group has developed different assays based on this DNA-Flow through technology where probes are immobilized on the membranes and a biotinylated PCR product is then detected. The biotin tag is recognized by a streptavidin-alkaline phosphatase conjugate which first bind to the biotin products and then the enzyme transform a colorless substrate (NBT/BCIP, Nitro blue tetrazolium chloride/ 5-Bromo-4-chloro-3-indolyl phosphate) into a blue precipitate. Figure 69 shows the chemical structure of the reagents involved in the color development reaction. A positive control, biotin, is immobilized on the membrane to confirm that the test was carried out correctly and no problems occur during the assay development and it is also used to quantify the signal. In order to remove variability (performance errors, background, different batches of reagents and membranes…) and thus provide a more accurate measurement, signal intensities are related to the one obtained for the positive control spotted on that membrane.
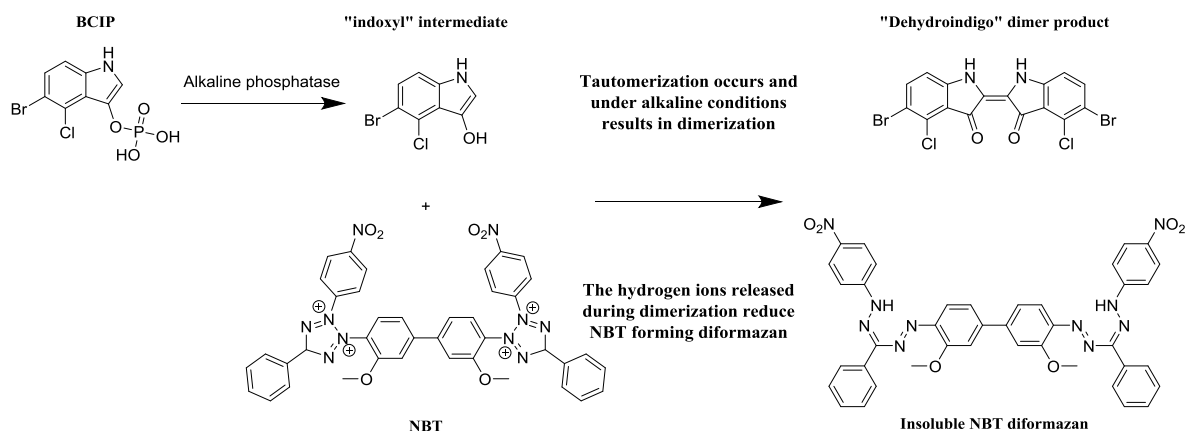

Figure 69: Chemical reaction of alkaline-phosphatase on NBT/BCIP, Nitro blue tetrazolium chloride/ 5-Bromo-4-chloro-3-indolyl phosphate to form the blue precipitate of the colorimetric detection on membranes.

Different kits are already commercialized by the Vitro group using this technology:

- HPV Direct Flow CHIP, an in vitro diagnostic kit which targets the human papiloma virus. The infection by HPV is related to cervical and anogenital cancer. According to the degree of the lesion the HPV can be classified in high risk-oncogenic or low risk. This system detects and genotypes 36 types of HPV [193].

- Sepsis Flow CHIP, it allows the simultaneous detections of bacterias responsible of sepsis together with their antibiotic resistant forms. Among others it detects, Gram positives such as *Staphylococcus aureus, Streptococcus pneumoniae, Streptococcus agalactie, Listeria monocitogenes…*Gram negatives such as *Pseudomonas aeruginosa, Escherichia coli, Serratia marcescens, Neisseria meningitides…*and also some fungus such as *Candida albican* [194].

- Viral CNS Flow CHIP, it detects virus which cause neurological infections such as *Epstein-Barr virus, Varicela-zoster, Herpes simplex 1 and 2 virus, Citomegalovirus…*[195]

- Bacterial CNS Flow CHIP, it detects meningitis causing bacteria such as *H. influenza, Neisseria meningitides, Streptococcus pneumoniae, Mycobacterium tuberculosis, Coxiella burneti* [196].

- Tick-borne bacteria Flow CHIP, it detects pathogen bacteria transmitted by arthropods from the genre Anaplasma, Ehrlichia, Borrelia, Bartonela, Coxiella, Rickettsia and Francisella [197].

3.3.2. Results

3.3.2.1. DGL probes design for the colorimetric-based approach (membranes)

As previously explained for the mass-based approach, two DGL probes were needed for the assay targeting the 28S rRNA delta coding gene.

Two special considerations must be taken into account when doing the dynamic chemistry assay on solid surfaces:

1) As it was previously described, when working on surface (membranes, microspheres, LoC), DGL probes require several modifications:

i) A nucleophilic group at the N-terminal to allow its immobilization on the surface. The Immunodyne ABC® membranes used characterizes because they have activated carboxylic acid groups on the surface to facilitate the immobilization of any desired

biomolecule. In this case, DGL probes through their N-terminal $-NH_2$ group are covalently immobilized by an amide bond formation. Figure 70 schematizes the DGL probe immobilization process.
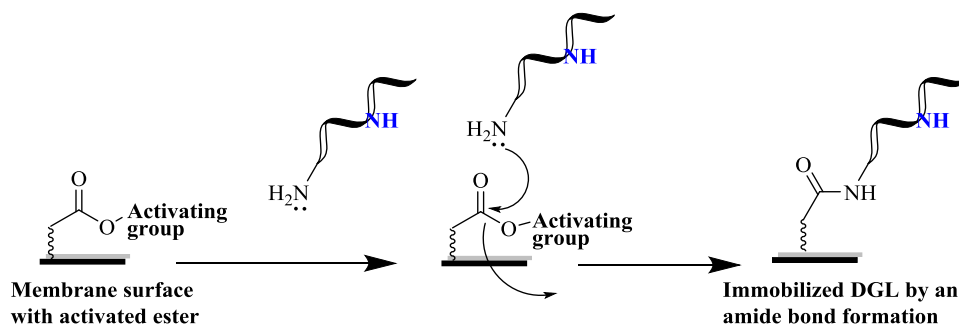
Figure 70: Scheme of the reaction involved in the covalent immobilization of the DGL probes on the membrane surface. The activated carboxylic acid groups easily react with the nucleophilic group –NH2 of the DGL probe linking thus the probe to the surface.

ii) Some chiral and negatively charged monomers distributed along the sequence since it was previously described that this charge and chirality avoid PNA backbone to collapse [20, 107, 108]. These changes led to the second generation of DGL probes which are easily available to be recognized and join to a complementary DNA strand and so allow a better SMART-NB incorporation. This was achieved by using PNA monomers containing propanoic acid chains at gamma positions with S-configuration (Figure 31B)[105, 109, 110]. For this dynamic chemical approach for nucleic acid reading, it was not only previously reported but also experimentally confirmed with the assay carried for the detection of miR-122 on the LoC from STmicroelectronics® (see section 2.2.) and on Magplex® microspheres from Luminex® (see section 2.3.) [111]. Additionally, modifications in the chemical structure of the abasic site were also carried out what led to a third generation of DGL probes which have not only the charges and chirality along the sequence but also on the abasic site (*GL*, Figure 71B) what allows a better dynamic incorporation of the SMART-NB because of the spatial orientation of the free secondary amine of the "blank" position. (See experimental section 5.1.3. to see the chemical structure of each PNA building monomers used for DGL probes synthesis).

A)

B)

"_"= Neutral abasic PNA monomer

***GL*= Chiral and negatively charged abasic PNA monomer**
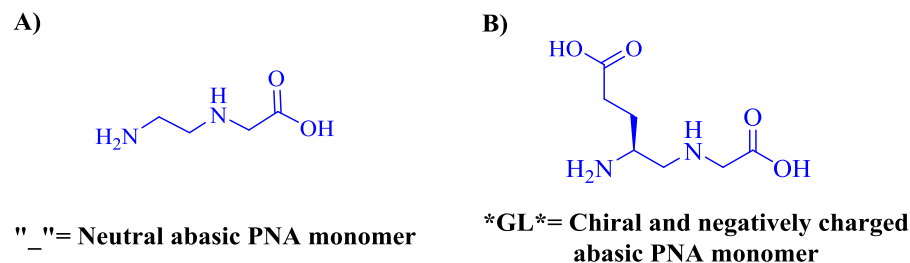
Figure 71: Chemical structure of the abasic monomers: A) neutral abasic postion ("_") and B) chiral and negatively charged abasic monomer (*GL*).

2) SMART-NBs have to be labeled with a biotin tag because the reaction for color development relies on the biotin-tag recognition by a streptavidin-alkaline phosphatase complex. This conjugate binds to the biotin-tag and transforms a chromogenic reagent (NBT/BCIP, Nitro blue tetrazolium chloride/ 5-Bromo-4-chloro-3-indolyl phosphate) into a blue precipitate any time there is a biotin tag attached to the membrane (Figure 69). In other words, the blue spots correspond to places where immobilized DGL probes have hybridized with a complementary nucleic acid which templates the incorporation of a biotinylated SMART-NB into the abasic position. Therefore, since color development depends on the same tag, biotin, each SMART-NB has to be interrogated separately.

In order to simplify the assay and because each biotin-labeled SMART-NB has to be interrogated separately, only one biotinylated SMART-NB is used, in this case SMART-C-Biotin. This means that a positive signal observed as a blue spot, would be only obtained when the nucleotide under interrogation is a guanosine. Any other nucleic acids, including those ones with the same sequence but a nitrogenous base different from guanine in front of the abasic position, do not create any signal. Moreover, following clinicians' advice, the assay was adapted and focused on the differentiation of just *L. major* and *T. cruzi*. Taking into account these modifications (the use of SMART-C-Biotin and the differentiation of *L. major* and *T. cruzi*), the approach for trypanosomatid colorimetric differentiation was redesigned: DGL#1 was maintained, DGL#2 was removed and a new DGL probe (DGL#3) was added to the panel. Figure 72 shows the multiple sequence alignment result of the 28S rRNA delta gene of the two target trypanosomatids, primers and DGL probes target sequences are highlighted. Table 18 shows the sequences of the DGL probes used for the colorimetric assay, they have some chiral and negatively charged PNA monomers ("Xglu") as well as chiral and negatively charged abasic site (*GL*) and a free amine at the N-terminal to immobilize them onto the membranes.

Figure 72: Multiple sequence alignment of *L. major* and *T. cruzi*. Forward (yellow) and reverse (green) primers and DGL#1 (blue) are maintained from the MALDI-TOF assay. The new probe, DGL#3, is highlighted in red and the guanosine templating nucleotide in white bold.

Table 18: Sequences of the DGL probes for the colorimetric assay. They have a free primary amine at the N-terminal and a C-terminal primary amide (-CONH$_2$). xx: PEG spacer; "Xglu" chiral negatively charged PNA monomers; *GL* chiral and negatively charged abasic site.

DGL probes	DGL probe sequence (N-C)
DGL#1-memb	NH$_2$- x x C Cglu A G A A A Cglu *GL* A G A G G Cglu A Cglu G-CONH$_2$
DGL#3-memb	NH$_2$- x x C C A Tglu A C T Tglu C *GL* C Tglu C A Cglu G A T-CONH$_2$

The new probe, DGL#3, gives a positive result for both parasites confirming thus the presence of a trypanosomatid in the sample under study, either *T. cruzi* or *L. major*. Both, *L. major* and *T. cruzi*, template the incorporation of SMART-C-Biotin into the abasic position of the DGL#3 since it clamps a homologous region for both parasite where there is a guanosine as templating nucleotide. On the other hand, DGL#1 will be the probe responsible for the trypanosomatid identification: *L. major* templates the incorporation of SMART-Thymine (not labeled with biotin so there won't give a positive signal after incorporation) whereas *T. brucei* incorporates SMART-C-Biotin which bears the biotin tag and will result in a blue spot after the incorporation (Figure 73).
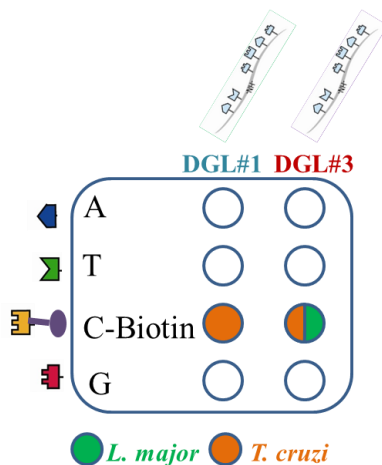
Figure 73: Scheme of the SMART-C-Biotin incorporation and so the blue spots that should be observed on the membranes. Each parasite gives rise to a specific pattern, due to their SNF. *T. cruzi* gives a positive result for both DGL probes, whereas *L. major* only shows a positive result in DGL#3.

3.3.2.2. Trypanosomatids discrimination by dynamic chemistry and DNA-flow through technology: colorimetric assay design

Figure 74 shows a scheme of the colorimetric assay. First, DGL probes are immobilized on the membranes used to develop the assay. Then, everything needed for the dynamic incorporation reaction (target nucleic acid, SMART-NBs one of them labeled with biotin and reducing agent) is added in one-step. After DNA/DGL probe hybridization, the dynamic incorporation of the SMART-NBs into the abasic site occurs. Only the SMART-NB complementary to the templating nucleotide is fixed into this positon. When it is a biotinylated SMART-NB, this tag is later recognized by the streptavidin-alkaline-phosphatase conjugate which binds to it and, after adding the chromogenic mixture (NBT/BCIP), a colorless substrate is transformed into a blue precipitate.
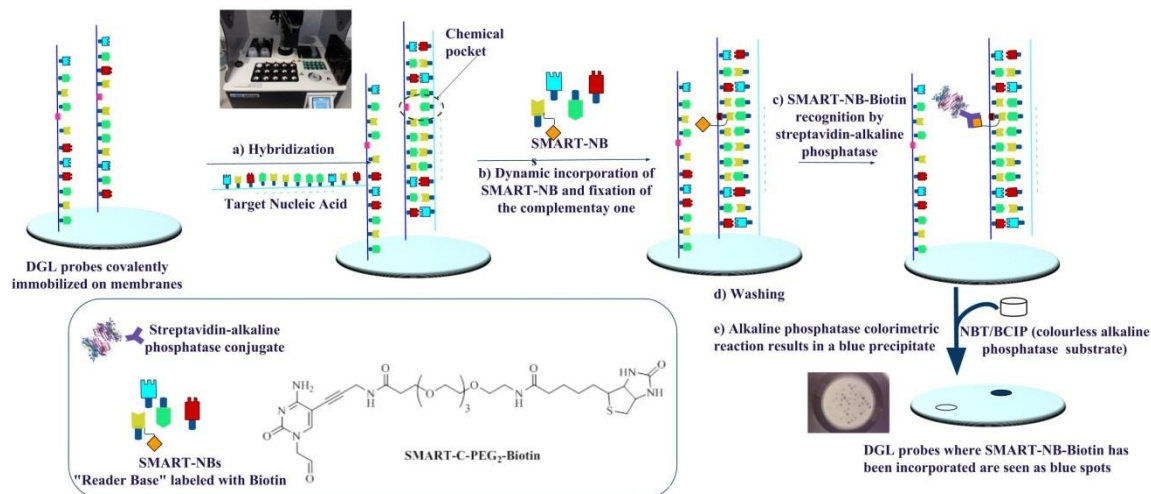
Figure 74: a colorimetric assay for the chemical reading of nucleic acids: DGL probes are covalently immobilized on the membrane. When a nucleic acid is added, if there is complementarity, they hybridize creating the 'chemical pocket'. This would promote the thermodynamically driven reaction of a SMART-NB with the free secondary amine of the abasic position. When a biotinylated SMART-NB is incorporated, the streptavidin-alkaline phosphatase conjugate binds to that position and transform a colorless chromogenic reagent into a blue precipitate.

Synthetic ssDNA representative of the target sequences of both DGL probes were purchased (Table 19). The standard protocol described by Vitro group for the HibriSpot12™ system [198] was slightly modified to combine the hybridization step of the reverse-dot-blot technology with the dynamic chemistry reaction. It was firstly applied to the analysis of synthetic short DNA oligomers so that it will allow ascertaining if the dynamic chemistry assay could be performed on the nylon surface. Synthetic ssDNAs were thus used to modify and optimize protocols and reagents concentrations and to validate the performance of the DGL probes and the Chem-NAT protocol after turning the mass-based assay into a colorimetric one.

Applying this hypothesis to our target nucleic acid for trypanosomatid identification, gene coding for rRNA 28S delta: *L. major* should only give signal on DGL#3 (it templates unlabeled SMART-T incorporation on DGL#1 and SMART-C-Biotin incorporation on DGL#3) and *T. cruzi* should give a blue spot for both DGL probes, DGL#1 and DGL#3 (it templates SMART-C-Biotin incorporation on both DGL probes). By identifying the spot pattern created by the blue spots, the parasites can be identified (Figure 75).
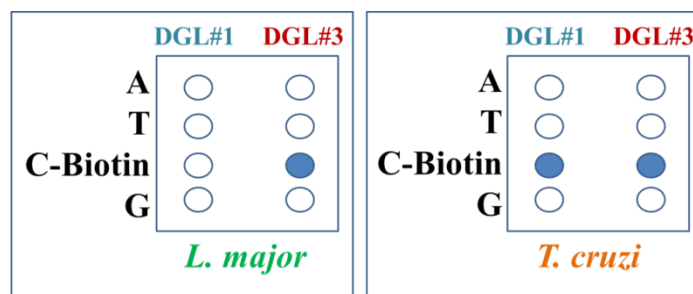
Figure 75: Graphic scheme of the spot patterns that have to be seen on the membranes for *L. major* (only positive for DGL#3) and *T. cruzi* (positive for both DGL#1 and DGL#3).

As previously described for the mass-based assay, synthetic ssDNAs oligomers (Table 19) were used to set experimental conditions and confirm the ability of performing the dynamic chemistry incorporation of SMART-NBs followed by the subsequent colorimetric detection by streptavidin-alkaline-phosphatase conjugate on the membrane surface. There were three features that these assays had to fulfil:

1) Immobilized DGL probes must be able to hybridize with a complementary ssDNA.

2) SMART-NBs must be correctly incorporated into the abasic position of the DGL probes.

3) The biotin tag of the SMART-C-Biotin must be recognized by the streptavidin-alkaline-phosphatase and the enzyme has to then react and transform the chromogenic substrate into a blue precipitate.

Table 19: Target DNA complementary to each DGL probe and SMART-NB that has to be incorporated into the blank position according to the parasite specie. Target SNF nucleotides are highlighted in bold.
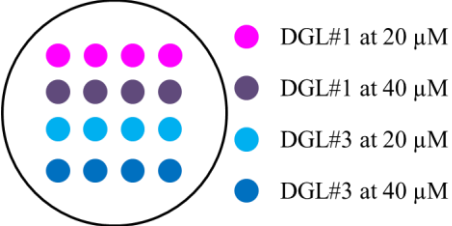
DGL probes	Target DNA	Target DNA sequences (5'----3') complementary to the DGL probe	SMART-NB to be incorporated
DGL#1-memb	DNA-1Lm	CGT GCC TCT **A**GT TTC TGG	SMART-T
	DNA-1Tc	CGT GCC TCT **G**GT TTC TGG	SMART-C-Biotin
DGL#3-memb	DNA-3LmTc	ATC GTG AG**G** GAA GTA TGG	SMART-C-Biotin

3.3.2.3. Base-Filling reaction on membranes and comparison between manual and automatic spotting

In order to immobilize DGL probes onto nylon surfaces, a manual as well as an automatic spotting could be done. Most of the initial set-up experiments were done using membranes manually spotted, synthetic ssDNA oligomers as target nucleic acid and SMART-C-Biotin as labeling nucleobase (see experimental section 5.3.9.2. and 5.3.9.3.). Following final washing, pictures of the nylon membranes are taken straightforward. Different rounds of optimization took place.

Firstly, spotting of DGL probes on nylon membranes was reviewed. It was observed that the manual spotting could strongly affect the results: signal intensity, spot features and reproducibility. As it can be observed in table 20, different spots of the same DGL probe, even when they have theoretically the same concentration, gave different results -different color intensities of the spots-. There were problems when printing the probe solution such as solution spread –bigger spots and so less concentration in a specific area-, "doughnut" effect –a hole in the middle of the spot-, signal intensity –spots of the same probe with the same concentration provide different results. Manual spotting can be used as a daily routine to quickly check an assay, but for making decisions, an automatic spotting must be used since it would remove this variability.

Table 20: Dynamic incorporation of SMART-C-Biotin on DGL probes manually spotted: Two DGL probes, DGL#1 and DGL#3, were spotted manually at 20 and 40 µM. Each spot has a different size, and different intensity. This kind of spotting can be used to check conditions, but to do a reproducible test and to extract conclusions, an improvement in the DGL probe immobilization should be applied.

DGL probe spotting layout	Dynamic incorporation of SMART-C-Biotin on DGL#1 (ssDNA-1Tc)	Dynamic incorporation of SMART-C-Biotin on DGL#3 (ssDNA-3LmTc)
DGL#1 at 20 µM / DGL#1 at 40 µM / DGL#3 at 20 µM / DGL#3 at 40 µM		

In order to remove this variability source, automatic spotting using PersonalArrayer[TM]16 (CapitalBio Corporation) was carried out (Figure 76).

Figure 76: PersonalArrayer[TM]16 (CapitalBio Corporation, China) used for the automatic spotting.
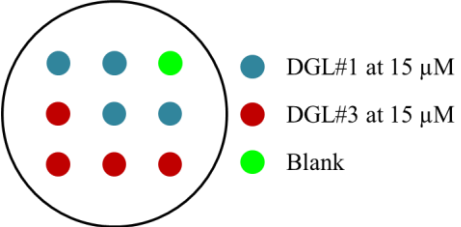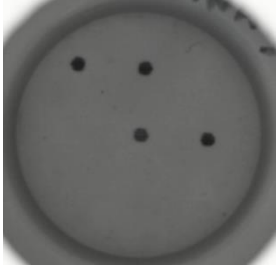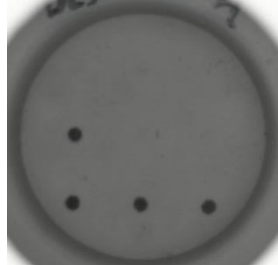
Different concentrations of DGL probes were also tested (5, 10, 15, 20, 40 µM). To find the best concentration, different factors have to be taken into account (i) signal intensities (to avoid reaching saturation), (ii) background levels and (iii) unspecificity (high concentrations of immobilized probe

could contribute to this problem). Following different tests, the two DGL probes were finally immobilized at a final concentration of 15 μM. In addition to the 4 spots for each DGL probe, DGL#1 and DGL#3, a blank spot was added. It contains all the reagents used in the spotting solution except for the DGL probe that has been replaced by water (see first column of table 21 for DGL probe spotting layout). The combination of several DGL probes and a blank spot on the same membrane is used to check (i) unspecificity issues (if signals where there is no probe or the probe is not complementary to the DNA added are observed, then the DGL probe should be redesigned) and (ii) contamination problems (carry over in the automatic spotting system that can cause that in the spots for a DGL probe there is also some DGL probe solution left over from the previous spotting, in this case a stronger washing of the needle should be introduced).

Second and third columns of table 21 shows the colorimetric assay results obtained after the dynamic incorporation of SMART-C-Biotin on automatically spotted membranes. The assay was done following standard coditions 50 μM of each SMART-NB and 1 mM of sodium cianoborohydride at 41ºC for 20 minutes (see experimental section 5.3.9.2. and 5.3.9.3.). The biotinylated SMART-Cytosine bears a PEG spacer (SMART-C-PEG$_2$-Biotin, the one used for the bead-based assay, see figure 44A for chemical structure) to increase water solubility and distance the nitrogenous base involved in the hydrogen bonding recognition from the biotin tag responsible for the color development. Some tests to improve yield were carried out.

Table 21: the first column schematizes the spotting layout of membrane. Second and third columns show the dynamic incorporation on both DGL probes which is templated by ssDNA, DNA-1Tc and DNA-3LmTc complementary to the probe. The spots observed coincides with the spots where the corresponding DGL was immobilized. No unspecificity issues where observed.
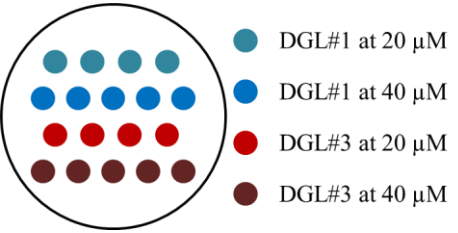
3.3.2.4. Acidic washing step to remove background

In addition to the standard protocol for the HybriSpot12™ system, an acidic washing step after the hybridization and dynamic incorporation reaction was introduced. After trying different

concentrations, 1mM of hydrochloric acid for 5 minutes at 41ºC was selected. The benefial effect of the introduction of an acidic washing step can be observed in the third columns of table 21 when compared to a membrane without this acidic washing (second column of table 21). This acidic washing contributed to increase signal intensity by reducing background intensity, as a result brighter membranes with darker spots are obtained.

Table 22: the first column schematizes the spotting layout of membrane. Second and third columns show the dynamic incorporation of SMART-C-PEG$_2$-Biotin on DGL#1 templated by ssDNA-1Tc. The second column corresponds to the standard hybridization protocol which usually lead to a higher background and the third column reproduces the same procedure but introducing the acidic washing after the reaction what contributes to a lower background, clearer membranes and so darker spots. Manual spotting were used in these optimization studies.
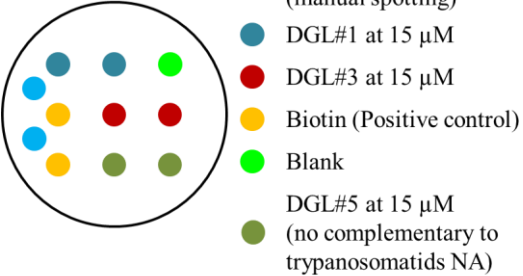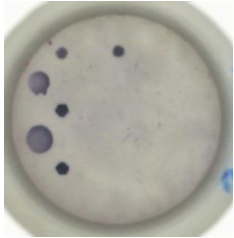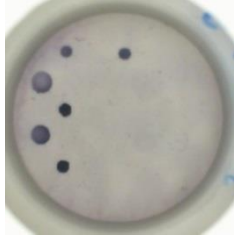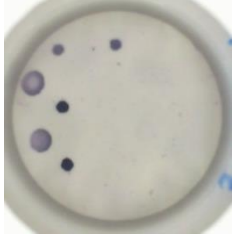
DGL probe spotting layout	Dynamic incorporation of SMART-C-PEG$_2$-Biotin on DGL#1 (ssDNA-1Tc)	Dynamic incorporation of SMART-C-PEG$_2$-Biotin on DGL#1 (ssDNA-1Tc) with HCl washing
DGL#1 at 20 µM DGL#1 at 40 µM DGL#3 at 20 µM DGL#3 at 40 µM		

3.3.2.5. Optimizing reagents concentration for the base-filling reaction

DNA-1Tc was used to carry out these improving experiments. Different concentrations of reducing agent (sodium cianoborohydride at 1, 2, 4, 5 mM) and SMART-C-PEG$_2$-Biotin (5, 10, 50, 100 µM) were tested. Dynamic incorporation reaction time was also increased to 40 minutes. Additionally to the automatic spotting, two manual spots for DGL#1 at 13 µM were added to observe the influence of the spotting in the final outcome and remove the variability source. Table 23 shows some of the best results obtained using 1 and 2 mM of reducing agent and 5 and 10 µM of SMART-C-PEG$_2$-Biotin either alone or in combination with the other unlabeled SMART-NBs (TAG).

Table 23: Dynamic incorporation of SMART-C-PEG$_2$-Biotin using different combinations of biotinylated SMART-C and reducing agent concentrations. Different DGL probes, DGL#1 DGL#3 and DGL#5, a blank and a positive control (biotin) are spotted. The blank and the non-complementary probes to the target DNA are used to check unspecificity. The positive control is used to assure the good performance of the assay and can also be used to semi-quantify the signal intensity.

DGL probe spotting map	Dynamic incorporation of SMART-C-PEG$_2$-Biotin on DGL#1 (ssDNA-1Tc) with 1 mM of Reducing Agent	Dynamic incorporation of SMART-C-PEG$_2$-Biotin on DGL#1 (ssDNA-1Tc) with 2 mM of Reducing Agent
	SMART-C-PEG$_2$-Biotin 5µM	SMART-C-PEG$_2$-Biotin 5µM
	SMART-C-PEG$_2$-Biotin:TAG 5µM	SMART-C-PEG$_2$-Biotin:TAG 5µM
	SMART-C-PEG$_2$-Biotin 10µM	SMART-C-PEG$_2$-Biotin 10µM

DGL probe spotting map legend:

- DGL#1 at 13 µM (manual spotting)
- DGL#1 at 15 µM
- DGL#3 at 15 µM
- Biotin (Positive control)
- Blank
- DGL#5 at 15 µM (no complementary to trypanosomatids NA)

1 mM of Reducing agent and 5µM of SMART-C-PEG$_2$-Biotin were selected since the signal is high enough and has a low background. The addition of the unlabeled SMART-NBs (TAG: SMART-T, SMART-A, SMART-G) does not contribute to increase the signal and because there is no unspecificity issues, they can be removed from the reaction mixture. Since the technology works when doing the dynamic incorporation with synthetic ssDNA as target, it opens up the opportunity
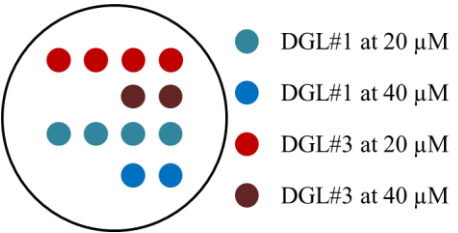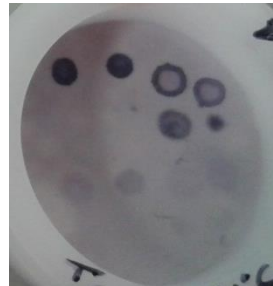
to wide the application of the assay and use it to distinguish trypanosomatid parasites based on their DNA.

3.3.2.6. Base-filling reactions using PCR product as template

Once DGL probes immobilization and dynamic incorporation of SMART-C-PEG$_2$-Biotin were checked; *L. major* and *T. cruzi* sPCR and aPCR products were tested on membranes (see experimental section 5.3.9.2 and 5.3.9.3. for assay procedure and table 24 for Chem-NAT results when using sPCR and aPCR products as template). Interestingly, even if aPCR product gives higher signal intensities; SMART-C-PEG$_2$-Biotin incorporation could also be observed when using the sPCR products. This notably differs from the mass-based assay in which SMART-NBs could only been incorporated when using ssDNA as template, being in that type of assay the ssDNA generated from aPCR reactions. Table 24 shows the obtained results which coincided with what was expected: 1) *T. cruzi* templates the incorporation of SMART-C-PEG$_2$-Biotin on both DGL probes, so all spots for DGL#1 and DGL#3 were positive. 2) *L. major,* which templates SMART-T incorporation into DGL#1 and SMART-C-PEG$_2$-Biotin into DGL#3, only give blue spots at those places where DGL#3 was immobilized. However, the signal intensities were lower if compared with the ones observed when using synthetic ssDNAs oligomers as templates (i.e. DNA-1Tc, DNA-3LmTc; see for example membranes in table 23).

Table 24: the first column schematizes the spotting layout of membrane. Second and third columns show the results obtained after the dynamic incorporation of SMART-C-Biotin when using *T. cruzi* and *L. major* PCR product as target nucleic acid, respectively. All spots are positive, when using a *T. cruzi* amplicon since it templates the incorporation of the SMART-C-PEG$_2$-Biotin on both DGL probes, DGL#1 and DGL#3. On the other hand, only spots where DGL#3 was immobilized are positive for L. major since it only templates SMART-C-PEG$_2$-Biotin incorporation on DGL#3. It is also show the results for both sPCR and aPCR amplicons. Positive results are obtained with both reactions; although signal intensities are higher with aPCR products.

DGL probe spotting layout	Dynamic incorporation of SMART-C-Biotin using *T. cruzi* PCR product	Dynamic incorporation of SMART-C-Biotin using *L. major* PCR product
DGL#1 at 20 µM / DGL#1 at 40 µM / DGL#3 at 20 µM / DGL#3 at 40 µM	*T. cruzi* sPCR *T. cruzi* aPCR	*L. major* sPCR *L. major* aPCR

As mentioned above, the fact that sPCR products could be used as template significantly differs from the mass-based assay where no incorporation peaks were observed when using double stranded amplicon. This feature represents an advantage for this platform since it would simplify the assay by removing the aPCR amplification step and adding instead a simple dsDNA denaturalization. Unlike the MALDI assay, denaturalization of the dsDNA generated from the sPCR reaction provides ssDNA able to hybridize with its complementary DGL probes immobilized on the membranes. It was achieved with a thermal denaturalization process by heating the sPCR product at 96ºC for 10 minutes to separate the double DNA strand, followed by 2 minutes incubation in ice to prevent rehybridization of both ssDNA strands.

The results confirmed that each sPCR templates the incorporation of the expected SMART-NBs (table 24) and so according to DGL probe spotting panel and where the blue spots are obtained, the trypanosomatid can be identified. Moreover and as previously demonstrated for the dynamic incorporation assay using MALDI-TOF as readout tool, the detection is related to the PCR yield (see section 3.2.2.9. for the limit of detection mass-based assay experiments). Despite the fact that the designed assay works and both species can be identified, there was certain variability in signal intensity intra and inter experiments, when manual spotting is used. All this sustained the fact that an automatic spotting should be used. Furthermore, some other changes need to be done in order to obtain higher signal intensities what is especially important when working with real samples since the parasitaemia load can be very low.

3.3.2.7. Turnaround time

In terms of time to results, once DNA is isolated, the work-flow lasts around 3.5 hours (2 hours for the PCR amplification and 1.5 hours for the color-development assay). However, up to 24 samples can be run in parallel, depending on the instruments used: Hibrispot12™ (12 samples, e-BRID™ (15 samples), Hibrispot 24™ (24 samples). The process itself is very simple and the system can be semi-automatic (Hibrispot12™) or completely automatic (e-BRID™ and Hibrispot 24™). Finally, analysis of the results is straightforward having the map of where each DGL probe was spotted and the pattern of SMART-C-Biotin incorporation that each parasite should give (Figure 73 and 75), which would correspond to the potential blue spots to be obtained. This process is also going to be automatized by programing the software which takes the picture of the membranes and analyze them. This is already done for the tests provided by the Vitro group.

3.3.3. Discussion

Once the MALDI-TOF assay for trypanosomatids identification was validated, translating the assay into a potential commercial product by integrating the dynamic chemistry technology to an easier, handier, cheaper and faster platform was needed. The approach taken was to design a colorimetric assay by combining Chem-NAT and DNA-flow through technologies which was carried out on the HibriSpot12™ system commercialized by Vitro group. The system is based on DNA-flow-through and reverse-dot-blot technologies and uses three dimensions porous nylon membranes on which probes are immobilized. Sample solutions are then made to go through the membrane thanks to the pumping system. After that, if a biotin tag (SMART-NB-Biotin) is present on the membrane, it is identified by a streptavidin-alkaline-phosphatase conjugate *via* the high affinity binding between biotin and streptavidin, being the enzyme conjugate to streptavidin the one which transforms a

colorless substrate (NBT/BCIP) into a blue precipitate. The system was adapted to the dynamic chemistry technology by introducing a few modifications:

> 1) Sample composition: unlabeled target nucleic acids, labeled SMART-NBs (SMART-C-PEG$_2$-Biotin) and a reducing agent were used.

> 2) Reaction temperature: 41ºC for hybridization and dynamic reaction between the aldehyde group of the SMART-NB and the secondary amine of the abasic position of the DGL probe.

> 3) Washing steps: an additional acidic washing was added to reduce background due to the reagents used for the dynamic reaction.

Successful tests were carried out with synthetic ssDNA and PCR products. However, there are some procedural problems that need to be sorted out: low signal intensities, signals were not always seen, results were not reproducible… They are mainly due to the manual spotting and were potentially solved when using an automatic printing system. On the other hand, it has to be considered the fact that there might be also printing defects that can affect the color measurement such as pinholes, missing dots, deformed dots, inaccurate printed dots, halo effect, and doughnut effect... The colorimetric characterization is constrained when these effects occur within the measurement area because it can induce an increase in the brightness as if the ink intensity were too low [199].

As a result, the printing system might be responsible for this variability from one membrane to another. 1) Even when all spots have the same concentration of DGL probes, using a manual spotting might imply that it wasn't deposited the same volume of DGL probe solution in every spots. 2) The solution deposited spread and so DGL probe was more diluted (same concentration in a bigger area). 3) The "doughnut effect" where spots adopted a double circle shape where no DGL probe was in the inner one (spots with a hole or a dark center) [200].

HybriSpot™12 is a new semi-automatic platform that provides a quick, cheap and easy diagnostic tool. The platform is based on the principle of the "flow-through" hybridization technology where nucleic acids, by means of a pumping system, goes through a tri-dimensional porous membrane on which there have been previously immobilized probes complementary to the target nucleic acid. This system has been used as platform for the dynamic chemistry assay presented. Slight modifications are made to the MALDI-TOF-based assay to adapt it to the HibriSpot™ system and so make it not only easier and faster to be performed but also doable almost anywhere since the HibriSpot™ system is smaller and cheaper than MALDI-TOF. This colorimetric assay could successfully distinguish between *Leishmania spp.* (being *L. major* the species used as a representative model) and *T. cruzi* infections. The designed assay is based on just two DGL probes

and a biotinylated SMART-NB (SMART-C-PEG$_2$-Biotin was used). DGL#3 is the probe responsible for the confirmation that there is a parasite present in the sample. It targets a homologous region for both parasites so that when they form the heteroduplex DGL-DNA, the abasic site lies in front of a guanosine which templates the incorporation of SMART-C-PEG$_2$-Biotin. On the other hand, DGL#1 acts as the distinction probe, since it should only give a positive result due to SMART-C-PEG$_2$-Biotin incorporation when *T. cruzi* is present in the sample; whereas if it is *L. major*, it should incorporate SMART-T, the absence of a biotin tag leads to no dark spots. Having this in mind, *T. cruzi* is present if it is positive for both probes whereas if only DGL#3 is positive, it is *Leishmania spp*.

Despite the fact that it represents an attractive and easy system for developing a colorimetric-based assay on membranes, there are some performance issues that might affect signal development. The vacuum applied to pump off the solutions was not uniform so membranes were not evenly washed off what might be affecting the final results because some were too dried between steps and other were slightly wet and so impregnated with reagents and solutions from previous steps which were not completely removed.
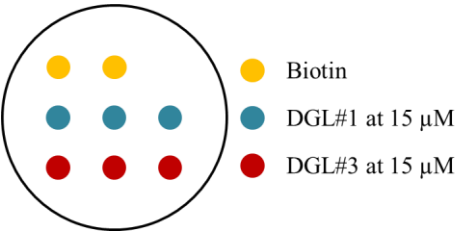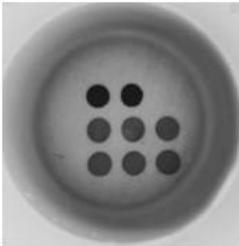
3.4. Industrial impact of the colorimetric assay for trypanosomatids identification

The problems found make necessary to introduce some changes into the system to improve its performance and make it more reproducible. In collaboration with DestiNA Genomica S.L., a new assay format has been developed. It takes advantage of all the previous technologies and combines them in an even simpler format that does not require any special system for the reaction to be developed. This new platform for the colorimetric assay is called "DestiNA spin-tube" and might become the first DestiNA commercial product. This product holds important differences if compared to the HybriSpot™ system:

1) Membranes size are reduced in order to adapt them to a support inserted into an 1.5mL tube, this also means that DGL probes are immobilized in a smaller area and so reactions take place in a smaller volume and on a smaller area. All these changes mean that reagents are more concentrated and so higher signal intensities might be achieved.

2) Instead of the vacuum system, the spin-tubes are centrifuged and so, due to the centripetal force, the different solutions and reagents are washed off the membrane.

3) An automatic spotting is done using PersonalArrayer™ 16 (CapitalBio Corporation, China).

4) This new assay format is even easier to perform since it is only needed a water bath set at 45ºC and a microcentrifuge to pump out the membrane the different solutions and reagents.

5) A smartphone application has also been developed in collaboration with EC sensor (University of Granada). It consists on a software program that analyzes the membrane picture after the reaction and transforms the outcome into a parasite strain by using an off-the-shelve smartphone.

Table 25 shows the expected results membranes to be obtained when using SMART-C-PEG$_2$-Biotin as labeling nucleobase and depending on which trypanosomatid, either *L. major* or *T. cruzi*, is present in the sample. Moreover, a positive control, biotin, is also spotted on the membrane. This control can be used 1) to check the assay performance –it must always give a blue spot- and 2) to relatively quantify the signal intensity –it normalizes variation between different membranes and it is considered the maximum signal intensity (100%) that any other spot can reach-.

Table 25: Expected results of the membrane after the dynamic incorporation of SMART-C-PEG$_2$-Biotin on DGL#1 and DGL#3. Positive results for both DGL probes indicate *T. cruzi*; positive results just for DGL#3 call for *L. major*.
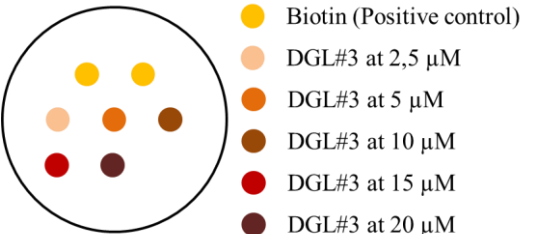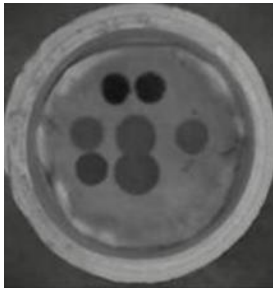
DGL probe spotting layout	Dynamic incorporation of SMART-C-PEG$_2$-Biotin when *T. cruzi* is present in the sample	Dynamic incorporation of SMART-C-PEG$_2$-Biotin when *L. major* is present in the sample
Biotin — DGL#1 at 15 µM — DGL#3 at 15 µM		

Different parameters were optimized:

3.4.1. Spotting conditions

When optimizing the concentration of the spotted DGL probes it must be taken into account that each DGL probe might have a different optimal concentration depending on its sequence, its ability to hybridize with a complementary target nucleic acid and the position and spatial organization of the abasic site regarding the templating nucleotide. Using a lower than optimal concentration might provide lower signal intensities; whereas a higher concentration might lead to unspecific signals. Table 26 shows the results obtained after SMART-C-PEG$_2$-Biotin incorporation on DGL#3 using ssDNA-3LmTc as template. Different DGL probe concentrations (2.5µM, 5µM, 10µM, 15µM y 20µM) were spotted on the same membrane and signal intensities were compared.

Table 26: Results obtained after SMART-C-incorporation onto DGL#3 printed on membranes at different concentrations. Synthetic ssDNA-3LmTc was used as target nucleic acid which templates the incorporation of SMART-C-PEG$_2$-Biotin on DGL#3.

DGL probe spotting layout	Dynamic incorporation of SMART-C-PEG$_2$-Biotin on DGL#3 (ssDNA-3LmTc)
Biotin (Positive control) — DGL#3 at 2,5 µM — DGL#3 at 5 µM — DGL#3 at 10 µM — DGL#3 at 15 µM — DGL#3 at 20 µM	

The signal intensity increases as the DGL probe concentration increased up to a point where there are no significant changes, almost no difference is observed between 15μM and 20μM. Having in mind a potential commercial product –low price- and avoiding unspecificity issues, 15μM was selected.
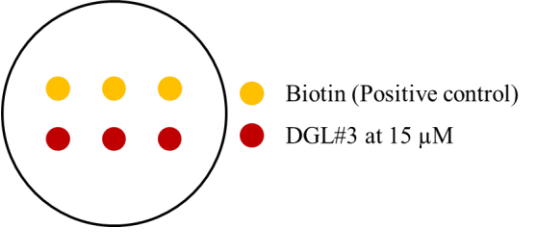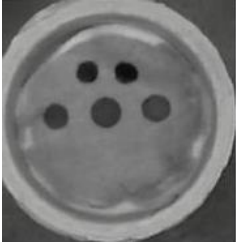
3.4.2. Automatic spotting

Most experiments were initially done using a manual spotting of the probes. However, as explained above, automatic immobilization of the probes on the membranes will be essential for a commercial product because:

1) It provides a nicer presentation –rounded and small spots-.

2) It can increase the number of probes spotted per row what implies the possibility of including other DGL probes targeting different nucleic acids and so expanding the application of a single membrane.

3) It helps to optimize the performance of the spotted DGL probes. The automatic spotting contributes to increase the signal intensity and balance the intensity obtained from different spots of the same DGL probe solution. This is achieved by fixing the volume and so the concentration of probe in every spot which is also localized in a smaller area compared with a manual spotting.

To do so, PersonalArrayer^{TM} 16 (CapitalBio Corporation, China) was used, which released a fixed volume of spotting solution at every spot. The automatic spotting allows increasing the number of spots per row. Table 27 shows the result of SMART-C-PEG$_2$-Biotin incorporation when using sPCR product from *L. major* as template, as a result, positive signals should only be seen for DGL#3. The reaction were done on both manually (table 27, second column) and automatically (table 27, third column) spotted membranes.

Table 27: Results obtained for the SMART-C-PEG$_2$-Biotin incorporation comparing manual versus automatic spotting. *L. major* sPCR was used as template which should give only positive results in DGL#3. Automatic spotting provides nicer spot and with higher signal intensities when compared to the positive control, biotin, which is assumed as the maximum signal intensity.

DGL probe spotting layout	Dynamic incorporation of SMART-C-PEG$_2$-Biotin using *L. major* sPCR product	Dynamic incorporation of SMART-C-PEG$_2$-Biotin using *L. major* sPCR product
	Manual spotting	**Automatic spotting**

As expected, automatic spotting was not only visually nicer what is important when designing a comercial product but also the signal intensity was higher due mainly to the concentration of the probe in a smaller area.
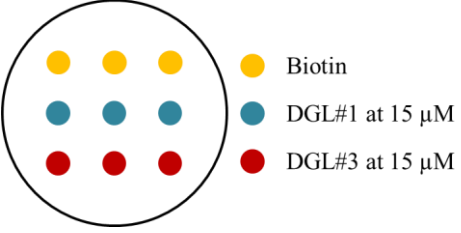
3.4.3. Optimizing the conditions for the chemical reading of nucleic acids on membranes

Different factors have to be taken into account when optimizing the assay:

1) Reaction time: It should be long enough to allow the dynamic incorporation of the SMART-C-Biotin but at the same time it should be kept at the minimum to avoid high background and reduce the time-to-results which will be important for a higher commercial demand.
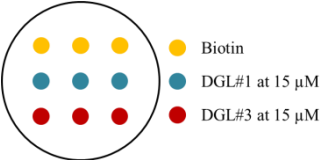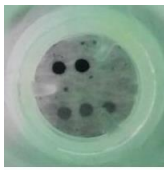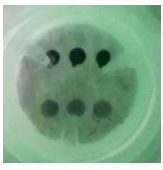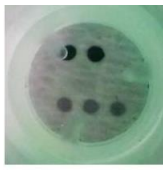
Reaction time experiments were done fixing 20µM of SMART-C-Biotin and 2mM of reducing agent. Table 28 show the results of the SMART-C-PEG$_2$-Biotin incorporation after 30 minutes (second column) and 1 hour (third column) of hybridization and dynamic incorporation reaction.When reducing reaction time from 1 hour to 30 minutes the signal intensity decreased but the background did not so 1 hour was chosen as reaction time.

Table 28: Results obtained for SMART-C-PEG$_2$-Biotin incorporation when using different reaction times: 30 minutes and 1 hour. *L. major* gDNA is used as template. Signal is only seen for DGL#3.

DGL probe spotting layout	Dynamic incorporation of SMART-C-PEG$_2$-Biotin using *L. major* sPCR product	
	30 minutes	**1 hour**
Biotin · DGL#1 at 15 µM · DGL#3 at 15 µM		

2) Reagents concentration: SMART-C-PEG$_2$-Biotin and reducing agent –sodium cianoborohydride-. Looking for a concentration where even if experimental errors happen, the signal is not affected. After selecting 1 hour as reaction time, reagents concentration was varied. Table 29 shows the results obtained after the colorimetric assay when using *L. major* sPCR product as template and different reagents concentrations: two different concentrations of SMART-C-PEG$_2$-Biotin -20 and 10 µM- and sodium cianoborohydride -2 and 1 mM- . Comparing the pictures shown in table 29, it can be observed that even if reagents concentration is reduced, the signal intesity is good enough and the background is reduced. As a result, 10µM of SMART-C-PEG$_2$-Biotin and 1 mM of reducing agent were selected as final concentrations for the assay.

Table 29: Results obtained when modifying reagents concentration for the chemical reading of nucleic acid. sPCR product generated from *L. major* gDNA is used as template. Signal is only seen for DGL#3. Four conditions were tried 20 and 10 µM of SMART-C-Biotin and 1 and 2 mM of reducing agent.
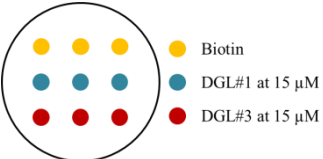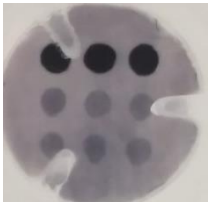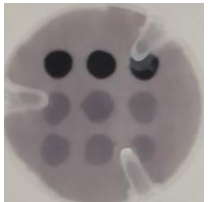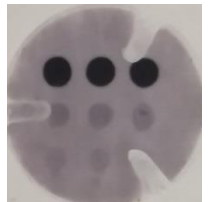
DGL probe spotting layout	Dynamic incorporation of SMART-C-Biotin using *L. major* sPCR product			
	20µM of SMART-C-PEG$_2$-Biotin and 2mM of reducing agent	20µM of SMART-C-PEG$_2$-Biotin and 1mM of reducing agent	10µM of SMART-C-PEG$_2$-Biotin and 2mM of reducing agent	10µM of SMART-C-PEG$_2$-Biotin and 1mM of reducing agent
Biotin · DGL#1 at 15 µM · DGL#3 at 15 µM				

3.4.4. Limit of detection of colorimetric assay: Sensitivity

As previously done for the mass-based assay, a sensitivity test was carried out using *T. cruzi* as trypanosomatid model specie. aPCR products were used as template for the dynamic chemistry reading of nucleic acids when using MALDI-TOF as readout tool. As described in section 3.2.2.9., to obtain these aPCR products, a first sPCR was done. These sPCR products were used 1) as template for the aPCR reaction for the mass-based assay and 2) also as template for the base-filling reaction for the colorimetric assay using DestiNA spin-tube as platform. As described above different sPCR amplification reactions were done using decreasing amounts of *T. cruzi* gDNA as starting material. Six concentration points (50, 5, 0.5, 0.05, 0.005, 0.0005 ng of gDNA as template) plus negative controls (H_2O as template) were done. Amplification was confirmed by capillary electrophoresis except for the two lowest amounts of template 0.005 ng and 0.0005 ng of *T. cruzi* gDNA where no amplification was detected (Figure 65, capillary electrophoresis result for the sPCR reactions). MALDI-TOF spectra were in line with capillary electrophoresis results, no SMART-NB incorporation was detected for these two samples. These sPCR products were later used as template in the base-filling reaction for the colorimetric assay, using previously optimized conditions (10µM of SMART-C-PEG$_2$-Biotin and 1mM of reducing agent and 1 hour of reaction). Table 30 shows the result of the limit of detection experiment.

A semi-quantification of the signal intensity was done using ImageJ software. Signal intensity for background was subtracted to all the measurements. Biotin signal intensity (positive control) of each membrane is used as the 100% of signal to be obtained; then, average signals for each DGL probe are taken and expressed as a percentage of the biotin signal. Almost no difference is observed for the membranes which had 50 and 5 ng of T. cruzi gDNA sPCR as template. Then, the signal intensity decreased, blue spots cannot be observed and so it cannot be quantified further. Relative quantification results expressed as percentage are shown for each quantificable experiment and for each DGL probe.

Table 30: Limit of detection experiment on the colorimetric assay: Results obtained after the dynamic incorporation of SMART-C-PEG$_2$-Biotin using decreasing amounts of gDNA from *T. cruzi* as template for the sPCR reaction. Results confirmed the presence of *T. cruzi* since it is positive for both DGL probes, DGL#1 and DGL#2. They were positive up to 0.05ng or 8.7 copies/μL of template what coincides with the LoD obtained for the mass-based assay and the last PCR reaction that could be detected by capillary electrophoresis. There were two false negatives when using the two lowest amounts of templates which is also in agreement with previous results both MALDI-TOF and bioanalyzer. A percentage of the relative intensity signal (using the positive control of each membrane, biotin, as 100% intensity) is shown.

DGL probe spotting layout	Dynamic incorporation of SMART-C-PEG$_2$-Biotin using decreasing amounts of gDNA from *T. cruzi* as template for the sPCR		
	50 ng	**5 ng**	**0.5 ng**
	DGL#1 32.9 % DGL#3 32.9%	DGL#1 37.5% DGL#3 29.9%	DGL#1 24.5 % DGL#3 19.5%
	0.05 ng	**0.005 ng**	**0.0005 ng**
	DGL#1 24 % DGL#3 14.7%	DGL#1 N/A DGL#3 N/A	DGL#1 N/A DGL#3 N/A

Results agreed with all previously obtained, up to 8.7 copies/μL of *T. cruzi* gDNA (i.e. sPCR in which up to 0.05 ng of gDNA were used as template) can be detected. This further confirmed that the limit of detection of the assay depends on the PCR yield to provide enough amount of template, leading to reactions where no enough copies were created and so they were mis-called as parasite free, being false negatives. Negative control was called as parasite free.

3.4.5. Different tube formats

Different tube formats were developed and then evaluated taking into account issues such as the S/N ratio obtained, the ease of handling, the adaptability to a commercial format, the cost, the support for the membrane…Two prototypes has been previously selected (Figure77). Dynamic incorporation of SMART-C-PEG$_2$-Biotin on sPCR products from *L. major* and *T. cruzi* were tested

on both prototypes using the previously fixed conditions 1 hour of reaction, 10µM of SMART-C-PEG$_2$-Biotin and 1 mM of reducing agent (Table 31).

Figure 77: Two prototypes for the *DestiNa Spin-Tube*

Table 31: Results obtained after the dynamic incorporation of SMART-C-PEG$_2$-Biotin on the two prototypes. sPCR product from *L. major* and *T. cruzi* were used as template which allow to see the different spot panel that each trypanosomatid should give on the final assay. *L. major* will be positive only for DGL#3 and *T. cruzi* will give signal in both DGL probes.

DGL probe spotting layout	Prototype 1		Prototype 2	
	Dynamic incorporation of SMART-C-PEG$_2$-Biotin using *L. major* sPCR	**Dynamic incorporation of SMART-C-PEG$_2$-Biotin using *T. cruzi* sPCR**	**Dynamic incorporation of SMART-C-PEG$_2$-Biotin using *L. major* sPCR**	**Dynamic incorporation of SMART-C-PEG$_2$-Biotin using *T. cruzi* sPCR**

Both preselected prototypes are easy to handle and provide reproducible results. However, slight changes are being made to improve the format such as removing the flanges that support the membrane on the type 1 and removing the color in the prototype 2. The porous support of the membrane on the second format seems to decrease the background so that this is going to be an essential part in the final format. It is likely that the final format would be chosen by the laboratories which validate the technology with clinical samples taking into account not only the results obtained but also the easiness of performing the assay and getting the results.

3.4.6. Base filling-reaction using RNA as template

Since the target nucleic acid of the assay is the gene coding for the 28S rRNA delta unit, RNA might also be used as template being readily detected by the dynamic chemistry approach. This would avoid PCR amplification and denaturalization steps what would simplify and shorten the protocol and reduce contamination possibilities. It should be considered that although RNA is an interesting target, caution should be taken when working with it since it is prone to degradation.

First, RNA was extracted from one million parasite cells in culture following a Trizol® protocol. The integrity of the extracted RNA was checked by running an eukaryote total RNA nanochip on a 2100 Bioanalyzer (Agilent). Figure 78 shows the RNA capillary electrophoresis results, total RNA from the three trypanosomatid species was checked, several replicates were run. Table 32 shows the electropherogram of one RNA sample of each trypanosomatid. The appearance of 3 bands indicates that the quality of the extracted RNA is good and it could be used for further experiments.
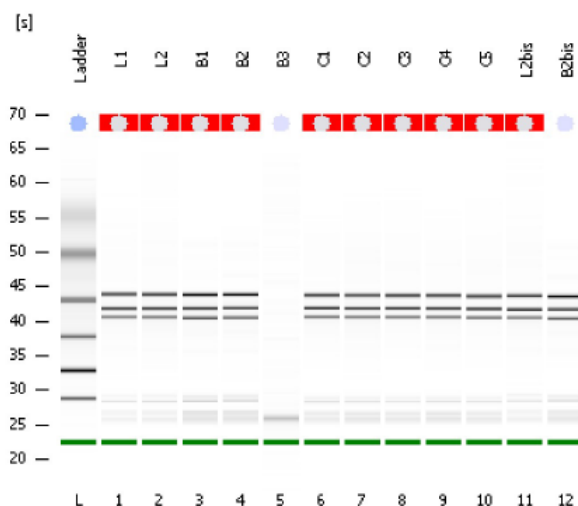
Figure 78: Capillary electrophoresis run summary: Total RNA from L, major (row 1, 2, 11), T. brucei (row 3, 4, 5, 12) and T. cruzi (rows 6-10). 3 bands can be mainly observed, which correspond to the ribosomal subunits and confirms that the quality of the extracted RNA is good.

Table 32: Three total RNA electropherogram from *L. major*, *T. brucei* and *T. cruzi*, respectively, are shown.
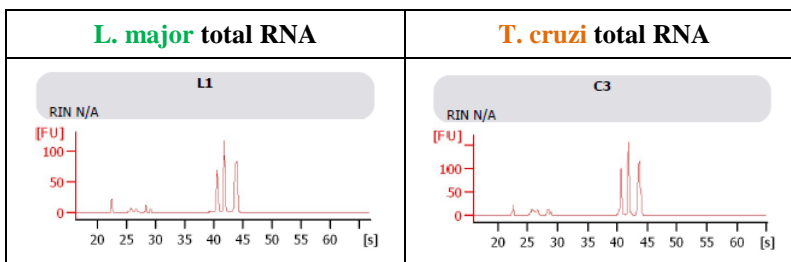
Once RNA was extracted and its integrity was checked, it was fragmented to break long strand and prevent the target sequence to be hidden, thus easing the hybridization with the probes. NEBNext® Magnesium RNA Fragmentation kit (BioLabs Inc. New England) was used. A 2100 Bioanalyzer using a total RNA pico chip was run to analyze the state of the RNA after the fragmentation protocol. Table 33 shows the electropherogram of the fragmented RNA sampes. It can be observed that the three peaks of the total RNA disappeared whatich confirmed that RNA was fragmented and potentially easily available to hybridize with the complementary DGL probe.

Table 33: Electropherogram of the fragmented RNA samples
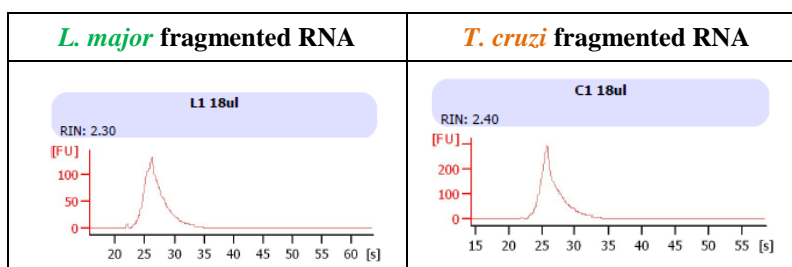
Finally, dynamic incorporation of SMART-C-PEG$_2$-Biotin was performed. The previously optimized conditions were used: 10 μM of SMART-C-Biotin and 1 mM of reducing agent for 1 hour. The remaining steps for the color development assay were followed. Table 34 shows the results of the Chem-NAT approach when using fragmented RNA as target nucleic acid. The results obtained coincide with the previous ones when using sPCR product as template. *L. major* gave positive for DGL#3 and *T. cruzi* provided a positive signal for both DGL probes. This is an essential achievement, since direct trypanosomatids identification from RNA samples avoids the PCR step shortening thus the protocol and reducing the possibility of contamination.

Table 34: Results of the membrane after the dynamic incorporation of SMART-C-PEG$_2$-Biotin on DG#1 and DGL#3 using RNA as template. Positive results for both DGL probes indicate *T. cruzi*, Positive results just for DGL#3 call for *L. major*.
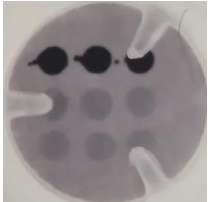
DGL probe spotting layout	Dynamic incorporation of SMART-C-Biotin using fragmented RNA from *T. cruzi*	Dynamic incorporation of SMART-C-Biotin using fragmented RNA from *L. major*

Chapter 4: Conclusions

Chapter 4: Conclusions/ Conclusiones

4.1. Conclusions

1. The selectivity and specificity of the chemical-based method for nucleic acid testing (ChemNAT technology) has been further ratified highlighting its unique features:

> 1) The higher binding affinity and selective hybridization between DGL probes and target DNA or RNA, compared with duplex DNA/DNA or DNA/RNA hybridizations. A single mis-match destabilizes the duplex.

> 2) DGL probes through their abasic position implies a proof-reading step so that the rapid and selective incorporation of complementary SMART-NB (with or without tag) into the DGL/RNA or DGL/DNA hybrid can only occur if the target nucleic acid forms a perfect duplex with the designed probe. A single mismatch would destabilize the duplex.

> 3) The flexibility to design "personalized", simple, quick and low cost multiplex assays for nucleic acids detection.

2. The dynamic chemistry approach for nucleic acid reading has been succesffully applied for the detection of two different target nucleic acids –miR-122 and trypanosomatids rRNA 28S delta coding gene- and combined with four different platforms –for fluorescent detection, ST's In-Check™ LoC and Luminex®MagPlex® microspheres (fluorescent); for mass-based detection , MALDI-TOF and for colorimetric detection, membranes.

3. The technological development that has been carried out and optimized for miR122 detection finally resulted in the integration of ChemNAT with SiMoA™ platform creating an assay which successfully detects miR-122 in serum samples.

4. The assay development and optimization performed for trypanosomatid identification end up in the platform, DestiNA-spin tube, in which trypanosomatids differentiation assay was successfully achieved in a cost-effective, easy-to-use way which does not required any special equipment nor skilled technician.

5. The limit of detection depends on the platform and the assay itself being the lowest ones those obtained when working on the final platform: SiMoA and DestiNA-spin tube. Moreover, when detecting PCR products, the sensitivity of the assay is related to the PCR yield. The SiMoA™ platform, when detecting miR-122, provides more accurate measurement thanks to its ability to read single bead fluorescence. The colorimetric assay performed on the DestiNA-spin tube, when

detecting trypanosomatids, concentrates the sample in a smaller area and improves washing what efficiently removes the backgroung and increases the signal intensity.

6. It has been demonstrated the versatibililty of the ChemNAT technology which can not only be applied to the detection of different nucleic acid targets but also integrated on different platforms with different readout.

4.2. Conclusiones

1. La selectividad y especificidad del método químico para el análisis de ácidos nucleicos (Chem-NAT) ha sido nuevamente ratificada destacándose las características únicas tales como:

> 1) Una mayor afinidad de unión y una hibridación más selectiva entre las sondas DGL y las dianas ADN o ARN, en comparación con los dúplex homólogos DNA/DNA o DNA/RNA. Un apareamiento erróneo es capaz de desestabilizar el dúplex.

> 2) La posición abásica de las sondas DGL que permite realizar un paso de "comprobación" de forma que sólo se produzca la incorporación selectiva (en función de las normas de apareamiento de bases) de una SMART-NB (con o sin marcaje) en el híbrido DGL/ADN or DGL/ARN si el ácido nucleico diana forma un dúplex perfecto con la sonda DGL (mayor desestabilización por apareamientos erróneos).

> 3) La flexibilidad para diseñar ensayos para la detección de ácidos nucleicos que sean "personalizados", sencillos, rápidos, de bajo coste, con capacidad para analizar varias dianas al mismo tiempo y que no requieran personal especializado para su realización.

2. La estrategia basada en la química dinámica para el análisis de ácidos nucleicos ha sido validada con éxito para la detección de dos ácidos nucleicos diana diferentes –miR-122 y el gen que codifica para el ARN ribosomial 28S delta-. Además, dicha tecnología ha sido integrada en 4 plataformas diferentes –para la detección fluorescente -In-Check™ LoC de STMicroelectronics y microesferas magnéticas fluorescentes MagPlex® de Luminex®; para la detección basada en la diferencia de masas, MALDI-TOF; y para la detección colorimétrica, membranas-.

3. El desarrollo tecnológico llevado a cabo y optimizado para la detección de miR-122 ha resultado en un proyecto final consistente en la integración de la tecnología Chem-NAT con la plataforma SiMoA™ dando lugar a un ensayo que ha detectado con éxito niveles de miR-122 en suero de pacientes.

4. El desarrollo y la optimización de los ensayos para la identificación de parásitos tripanosomátidos ha dado lugar al desarrollo de una nueva plataforma, DestiNA-spin-tube, en la que

se ha realizado la diferenciación de estos parásitos satisfactoriamente y de una forma costo-eficiente, fácil y sin necesidad de equipos ni personal especializados.

5. El límite de detección depende de la plataforma utilizada y del propio ensayo, obteniéndose los mejores datos cuando los ensayos se realizaron en la plataforma final: SiMoA™ y DestiNA-spin-tube. Además, cuando los ácidos nucleicos diana son productos de PCR, la sensibilidad del ensayo está relacionada con el rendimiento de dicha PCR. La plataforma SiMoA™, utilizada para la detección de miR-122, proporciona medidas más precisas gracias a su capacidad para analizar la fluorescencia de cada microesfera. El ensayo colorimétrico llevado a cabo en el DestiNA-spin-tube, para la detección e identificación de parásitos tripanosomátidos, permite concentrar la muestra en un área más pequeña y mejorar los lavados lo que contribuye a reducir el color del fondo de la membrana y mejorar así la intensidad de las señales.

6. Se ha demostrado la versatilidad de la tecnología Chem-NAT que puede aplicarse a la detección de una gran variedad de ácidos nucleicos, integrarse en diferentes plataformas y ofrecer diferentes métodos de observación y análisis de los resultados.

Chapter 5: Experimental

Chapter 5: Experimental

5.1. General

All synthetic DNA oligomers were purchased in a desalted form from Microsynth AG (Balgach, Switzerland).

All chemicals (sodium cyanoborohydride ($NaBH_3CN$) and dimethylamine (DMA), HCl…) were obtained from Sigma Aldrich and used as received. Streptavidin-R-phycoerythrin conjugate (SAPE, 1 mg/mL) was purchased from Thermo Fisher Scientific. SCD buffer was prepared from 2× saline sodium citrate (SSC) and 0.1% sodium dodecyl sulfate (SDS) with the pH adjusted to 6.0 using HCl.

STMicroelectronics In-Check™ LoC platforms were fabricated as described previously [201] and provided by STMicroelectronics.

Hybridisation (ST Hyb buffer) and washing buffers for LoCs assay were provided by STMicroelectronics® and used as recommended. Carboxylated paramagnetic microspheres (MagPlex®, MC10012) were obtained from Luminex® Corporation (Netherlands) and stored at 4°C in the dark.

SMART-NBs (SMART-A, SMART-C, SMART-T, SMART-G, SMART-C-sulfoCy5, SMART-C-PEG_2-Biotin, SMART-C-PEG_6-Biotin) and monomers for DGL probes synthesis were provided by DestiNA Genomica S. L.

5.1.1. Instrumentation

DGL probe concentrations were determined using a Thermo Fisher NanoDrop 1000 spectrophotometer. Hybridization and SNL reactions were conducted in a: a) Temperature Control System (TCS from ST microelectronics), b) Techne Thermal cycler (TC-5000) (for bead-based and mass-based assay), c) water bath (for colorimetric assay). Flow cytometry was conducted using a BD FACSCanto II™ λex 488 nm and emission collected with a 585/42 band pass filter. Confocal imaging was performed with a Zeiss LSM 710 confocal laser scanning microscope using the Zeiss ZEN 2010 software. A Petroff-Hausser Counting Chamber (Hausser Scientific) was used to count the microspheres.

5.1.2. General Solid-Phase Synthesis (SPS) Procedures and Information

DGL probes were prepared by standard solid-phase synthesis techniques on polymer supports by repeated rounds of coupling of activated (amino-protected) PNA monomers followed by

deprotection of the terminal amino group, with washing steps after each stage. Reactions were performed at room temperature in microscale columns with PTFE filter (Intavis, Germany). Figure 79 shows a general scheme of the steps involved in the DGL probe synthesis.
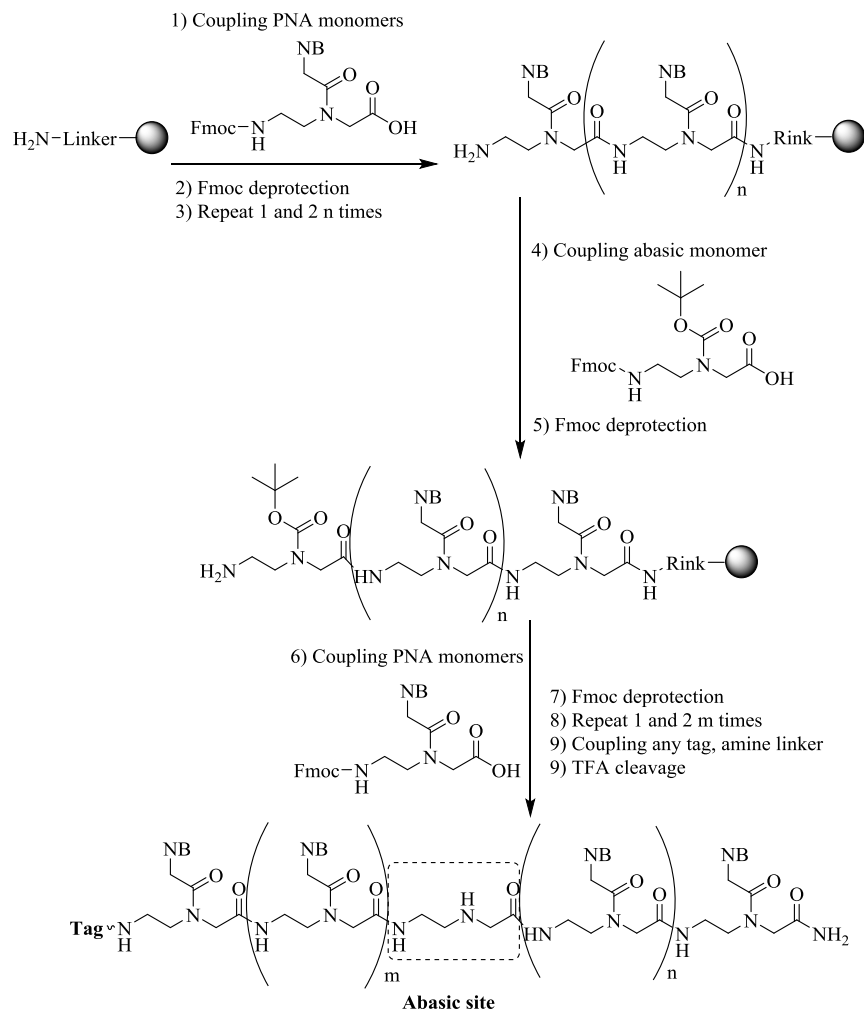
Figure 79: Scheme of the general steps involved in the synthesis of DGL probes by solid-phase chemistry. DGL probes are synthesized from the C- to the N-terminal. First PNA monomer is coupled first to the resin, then Fmoc deprotected and the next monomers following DGL probe sequence is coupled. The abasic PNA monomer is introduced across the synthesis. The final coupling is the introduction of any label to the DGL probe such as the tryphenylphosphonium tag, a dye or an amino-mini-PEG-linker. Once the DGL probe is synthesized, it is cleaved from the resin using an acidic mixture, mainly trifluoroacetic acid, which not only separates the probe from the resin but also removes the acid-labile protecting groups from the monomers such as Boc, Bhoc, ^{t}Bu.

Cleavage of full length DGL probes with concomitant Bhoc and Boc deprotection were carried out using a TFA:TIS:H$_2$O (92.5:5:2.5 v/v) cocktail for 2 h. The resulting cleavage mixtures were precipitated by addition (1.5 mL) of cold diethyl ether (-20ºC). The precipitated DGL probe was

collected by centrifugation, the supernatant removed, washed again centrifugally with cold ether (750 μL) and solubilized in 1 mL of water. DGL probes crude were analyzed and purified by High Performance Liquid Chromatography. Fractions were collected, liophilized and analyzed by MALDI-TOF mass spectrometry.

5.1.3. Synthesis of DGL probes

DGL probes (DGL-122-U, DGL-122-C, DGL#1, DGL#2, DGL#1-memb, DGL#2-memb, DGL#3-memb) were synthesized at DestiNA Genomica S.L. (Spain) following standard solid phase chemistry on an Intavis Bioanalytical Instruments MultiPrep CF Synthesiser (Intavis AG GmH, Germany). They were synthesized on Tentagel resin (loading 0.24 mmol/g) (Polymer Labs, UK). Fmoc/Bhoc protected PNA monomers (synthesized by DestiNA Genomica S. L.) were employed alongside (Figure 80). Chiral negatively charged monomers were synthesized and provided by DestiNA Genomica S.L. as Fmoc/Bhoc/^{t}Bu protected PNA monomers (Figure 81). Both neutral and negatively charged abasic monomers (Figure 82) were provided by DestiNA Genomica S.L. and used to insert the two types of 'blank' positions: neutral ("_") and chiral-negatively charged (*GL*). When using MALDI-TOF as readout tool a triphenylphosphonium tag is added and when working on solid surfaces a mini-PEG linker is introduced (Figure 83).

C= Cytosine PNA-COOH

G= Guanine PNA-COOH

A=Adenine PNA-COOH

T=Thymine PNA-COOH
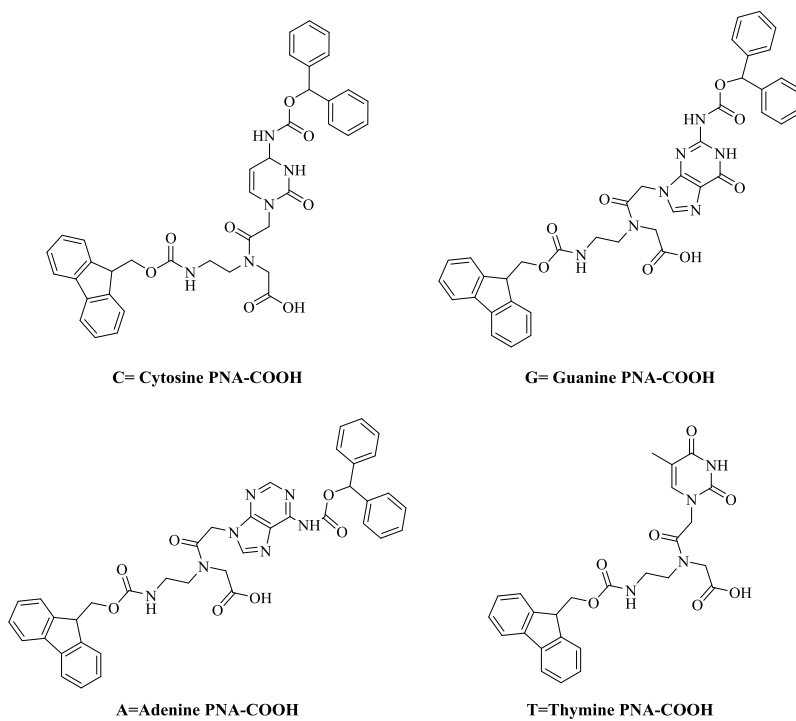
Figure 80: Chemical structure of neutral PNA monomers used for the synthesis of DGL probes. They all are N-Fmoc protected to allow the synthesis on solid phase. Additionally, if necessary to avoid secondary reactions, they carry a second orthogonal protecting group, Bhoc, as for the one protecting the –NH$_2$ of adenine, cytosine and guanine.

Cglu= Cytosine gamma-modified PNA-COOH

Gglu= Guanine gamma-modified PNA-COOH

Aglu= Adenine gamma-modified PNA-COOH

Tglu= Thymine gamma-modified PNA-COOH
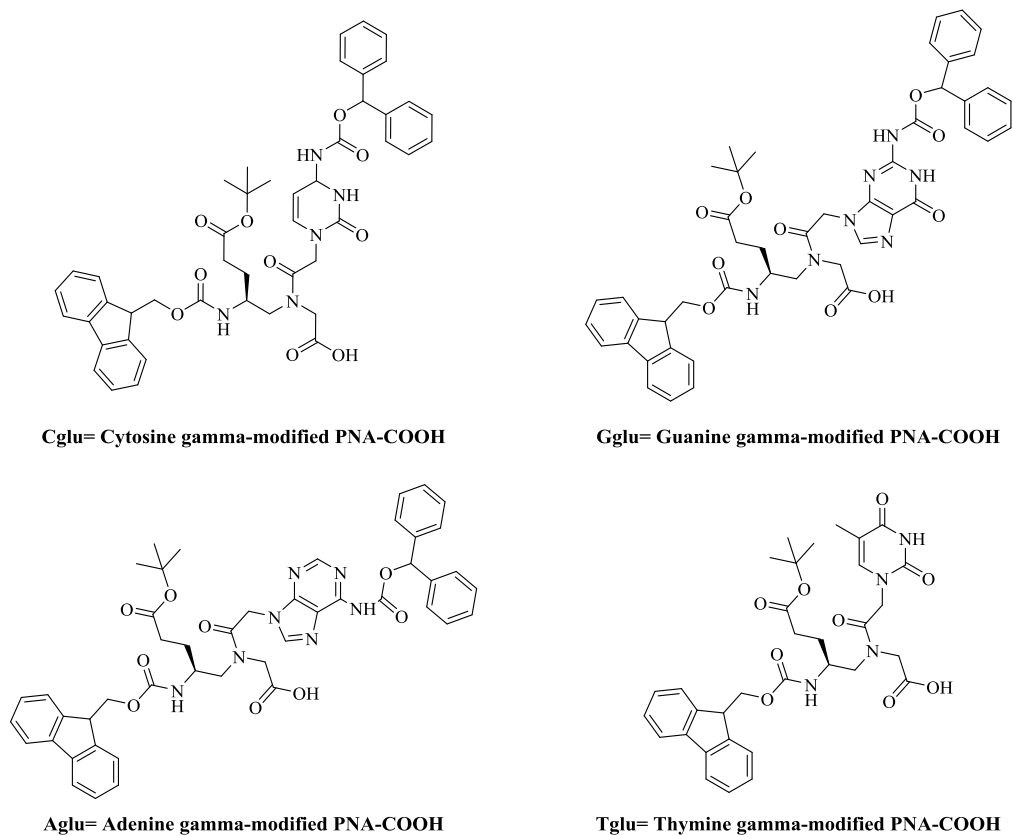
Figure 81: Chemical structure of the chiral and negatively charged PNA monomers used for the synthesis of the DGL probes. They are N-Fmoc protected to allow the synthesis on solid phase and they also have a propionic acid group (^{t}Bu protected) at γ-position to make the monomers chiral and negatively charged. Additionally, if necessary to avoid secondary reactions, they carry a second orthogonal protecting group, Bhoc, as for the one protecting the –NH$_2$ of adenine, cytosine and guanine.

"_"= Neutral abasic PNA monomer

GL= Chiral and negatively charged abasic PNA monomer
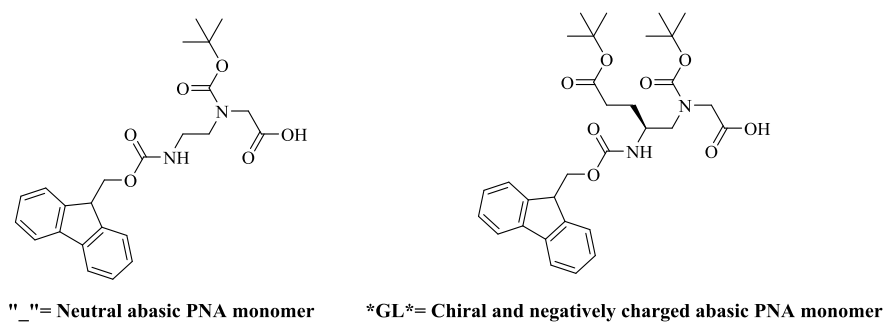
Figure 82: Chemical structure of the two kinds of abasic PNA monomers used to introduce the 'blank' site or abasic position. The amine groups are protected to control the synthesis: the N-terminal amine is Fmoc protected and the amine group of the glycine is Boc protected. The chiral and negatively charged monomer also carries a propionic acid group (^{t}Bu protected) at γ-position.

xx= amino-miniPEG-linker   (Ph)₃P⁺= Phosphonium tag
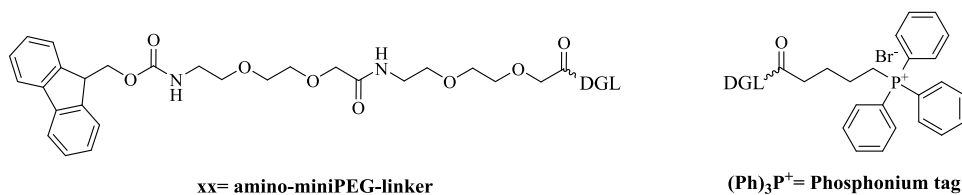
Figure 83: Chemical structure of the amino-miniPEG-linker (generally coupled to all DGL probes to provide the spacer and the free amine N-terminal group to allow its immobilization on any surface) and the phosphonium tag (added only to the DGL probes used for the mass-based-MALDI-TOF approach to enhance their limit of detection).

Couplings were carried out using 4 equivalents of each reagent (protected PNA monomers, DIC and Oxyma, all solubilized in NMP). They were left at room temperature for 20 minutes. Then resin was washed with DMF and fresh coupling reagents were added to repeat the coupling. A capping step after the second coupling was added. A solution of 5% of Luteidin and 5% of acetic anhydride in DMF was used. Fmoc deprotection was achieved by three washing steps (5, 5 and 8 minutes, respectively) with a 20% solution of piperidine in DMF. Phosphonium tags were added using (4-carboxybutyl)triphenylphosphonium bromide and N-Fmoc protected PEG units, PEG2, were purchased from Sigma-Aldrich Inc. and used to add the phosphonium tags and the PEG spacer, respectively.

5.1.4. HPLC characteristics

HPLC analyses were performed on an Agilent 1260 infinity.

Analytical HPLC analyses were performed with an Agilent Poroshell 120® EC-C18, 2.7 μm, 50 x 4.6 mm column. Detection was by UV absorbance at 260 nm. The following eluents were used: (A) H2O + 0.1% TFA; (B) MeCN + 0.1% TFA. HPLC grade eluents were employed, at a flow rate of 1 mL/min and filtered prior to injection. The following HPLC method was used: 5% to 25% B over 8 min, 25% to 95% B over 4 min, then 95% B over 4 min.

Preparative HPLC runs were done with an Agilent Eclipse XDB-C18, 5 μm, 250 x 9.4 mm column. HPLC grade eluents were employed, at a flow rate of 2.5 mL/min with samples prepared to a concentration of approximately 10-20 mg/mL and filtered prior to injection of a volume containing up to 10 mg. The following eluents were used: (A) H2O + 0.1% TFA; (B) MeCN + 0.1% TFA. The following methods were used:

Method 1: 5 % to 17.5 % B over 10 min, then 17.5 to 20% B over 6 min, then 20% to 95% over 4 min, then 95% B over 4 min (for general DGL probes).

Method 2: 5 % to 30 % B over 12 min, then 30 to 95% B over 3 min, then 95% B over 4 min (for phosphonium tag-DGL probes).

5.1.5. Resuspension of liophilized DGL probes

Aqueous solutions of DGL probes were prepared and concentrations determined by measuring the absorbance at 260 nm on a Nanodrop® ND-1000 Spectrophotometer version 3.3.1 (Thermo Fisher Scientific) using as extinction coefficient values (ϵ_{260}) either 6.6, 8.8, 13.7, 11.7 and 2.5 (mM^{-1} cm^{-1}) for C, T, A, G and the triphenylphosphonium tag, respectively, for the probes synthesized or using the extinction coefficient provided by the manufacturer (Panagene) for the purchased probes. DGL probes were characterized by MALDI-TOF mass spectrometry and HPLC. SMART-NBs C, T, A and G were provided by DestiNA Genomica S.L. (Spain) and prepared as reported elsewhere [5].

5.1.6. DGL probes

Table 35 shows DGL probes sequences used alongside. They were synthesized as described in experimental section 5.1.2. and 5.1.3. and characterized by HPLC and MALDI-TOF.

Table 35: DGL probes and PNAs sequences

DGL probe name	Sequence N---C	MALDI-TOF MS	HPLC Retention time (minutes)
DGL-122-U	H_2N-xx-AAC AC__ ATT GTC ACA CTC-$CONH_2$	4997	7.301
DGL-122-C	H_2N-xx-AACglu ACglu__ AgluTT GgluTC AgluCA CgluTC-$CONH_2$	5356.9	9.44
PNA-Ana	H_2N-TATTCTTTATAGCT-$CONH_2$		
DGL-miR-21	H_2N-xx-CgluAT CgluAG Tglu__Tglu GATglu AAGglu CT-$CONH_2$	5178	9.673
DGL-RNA28S	H_2N-xx-CCgluA GAgluA ACglu__ AgluGA GGgluC ACgluG-$CONH_2$	5482	9.081
DGL-G1Pr1	H_2N-xx-ATY GCG RT__ TCC TGT CCA C-$CONH_2$	5217.6/5201.9	9.3/9.6
DGL-G2Pr1	H_2N-xx-CGglu A TCGglu CCC Tglu__Cglu CAC GgluTG CTglu-$CONH_2$	5882	9.361
DGL-K12SRC	H_2N-xx-CTAglu CGCglu CACglu __AgluG CTgluC CAgluA-$CONH_2$	5344.8	8.9
DGL-K13SRC	H_2N-xx-TTGglu CCTglu ACG Cglu__Aglu CCAglu GCTglu-$CONH_2$	5368.3	9.5
DGL#1	$(Ph)_3P^+$-CCA GAA AC_ AGA GGC ACG-$CONH_2$	5103	14.271
DGL#2	$(Ph)_3P^+$-GCA CTT GCC _TT CGA CAA AC-$CONH_2$	5801	13.256
DGL#1-memb	H_2N-x x C Cglu A G A A A Cglu *GL* A G A G G Cglu A Cglu G-$CONH_2$	5409	15.984
DGL#2-memb	H_2N-x x G C A Cglu T T G Cglu C *GL* T Tglu C G A Cglu A A A C-$CONH_2$	5839	15.5
DGL#3-memb	H_2N-x x C C A Tglu A C T Tglu C *GL* C Tglu C A Cglu G A T-$CONH_2$	5252	15.683

* DGL probes are written from the N-terminal end (left) to the C-terminal end (right). R is an A/G mixture and Y is a C/T mixture. For MALDI-TOF experiments, DGL probes are capped at their N-terminal with 3-(carboxypropyl)triphenylphosphonium bromide. "_" represents the neutral abasic position. For surface assays, DGL probes have two miniPEG groups (xx) and -NH_2 group at the N-terminal to allow their immobilization on membranes. *GL* represents the chiral blank site. 'Xglu' represents the chiral and negatively charged PNA monomers. All of them have a C-terminal primary amide.

5.2. Experimental part of chapter 2: miR-122 detection by dynamic chemistry

5.2.1. DGL probes design

Two DGL probes (DGL-122-U and DGL-122-C) targeting miR-122 sequence and terminated with an amino-pegylated group were designed and synthesized by standard solid phase chemistry on an INTAVIS MultiPep Synthesiser (Intavis AG GmH, Germany) as described above. The 18-mer DGL probe sequences were designed to allow anti-parallel hybridization with miR-122 strands (N-terminal end of DGL probes align with the 3'-end of nucleic acids). The abasic site was positioned at +13 from their C-terminal end so that after hybridization with mature miR-122 strands, there will be a Guanine at that position (+15 from the 5′-terminus) thereby templating the incorporation of a cytosine into the abasic position (section 2.2.2.1., Figure 32).

5.2.2. DGL probes

Table 36: DGL probes used for the miR-122 detection assay. It is shown probe sequences and characterization by HPLC and MALDI-TOF.

DGL probe name	Sequence N---C	MALDI-TOF MS (*m/z*)	HPLC Retention time (minutes)
DGL-122-U	H_2N-xx-AAC AC__ ATT GTC ACA CTC-$CONH_2$	4997	7.301
DGL-122-C	H_2N-xx-AACglu ACglu__ AgluTT GgluTC AgluCA CgluTC- $CONH_2$	5356.9	9.44

* DGL probes are written from the N-terminal end (left) to the C-terminal end (right). xx- = amino-miniPEG spacer (Ethylene Glycol Linker); "__" = neutral abasic position; "Xglu"= negatively charged monomer. All of them have a C-terminal primary amide

5.2.3. DNA oligonucleotides

Unlabeled, Cy5-labeled and biotin-labeled ssDNA oligonucleotides were purchased from Microsynth AG.

Table 37: ssDNA oligonucleotides sequences: complementary to the DGL probe for miR-122. Cy5 labeling at 5´terminus allows the validation of the immobilized probes.

Reference	Oligonucleotides sequences (5'-3')	5'-modifications
miRNA122-Cy5	TGG AGT GTG ACA AT**G** GTG TTT G	Cy5
miRNA122	TGG AGT GTG ACA AT**G** GTG TTT G	-
miRNA122-A	TGG AGT GTG ACA AT**A** GTG TTT G	-
miR122-biotin	TGG AGT GTG ACA AT**G** GTG TTT G	Biotin
miR21-biotin	TAG CTT ATC AGA CTG ATG TTG A	Biotin
miR21	TAG CTT ATC AGA CTG ATG TTG A	-

'In bold and underlined': The nucleobase at +15 from the 5′-terminus of miRNA122 under interrogation *via* dynamic chemistry with Cy5-labeled SMART nucleobases.

5.2.4. Experimental part of section 2.2.: Fluorescent direct detection of unlabeled miR-122 through Single Nucleobase Labeling: In-Check™ LoC platform (specific objective 1.1.)

5.2.4.1. DGL probes immobilization on In-Check™ LoC platform

DGL probe stock solution is denaturalized by heating at 96ºC for 5 and then kept in ice for 2 minutes. Then, the printing solution is prepared by mixing 50% of 300mM-pH 9 sodium phosphate buffer with 50% of enough volume of denaturalized DGL probe solution to reach the desired concentration and water (final printing solution composition 10 μM DGL probes in 150mM Phosphate Buffer, pH9). The solution was spotted onto the epoxysilane-functionalised LoC using an automatic printing system –PersonalArrayer16™ (Capital Bio)- (2 rows with 6 spots per row). Once the printing solution has been spotted on the LoC surface, LoC are left at room temperature with 70% of relative humidity for 2 hours.

After that, LoC are washed to remove unbound DGL probe molecules and buffer substances: a) Rinse 1 x 5 min in 0.1 % Triton® X-100 at room temperature; b) Rinse 2 x 2 min in 1 mM HCl solution at room temperature; c) Rinse 1 x 10 min in 100 mM KCl solution at room temperature; d) Rinse 1 x 1 min in diH2O at room temperature.

Then, the remaining epoxide reactive groups on the LoC surface are blocked with a 50 mM DMA in 150 mM phosphate buffer, pH 9.0. Two incubation steps of 15 minutes each, the first one at 50ºC, the second one at room temperature, followed by 1 minute incubation in H_2O.

Finally, LoC are dried by centrifugation (3000 x rpm for 2 min) to avoid any water stains on the slide surface. LoC are stored at room temperature until use.

5.2.4.2. Validation of DGL probes immobilization on In-Check™ system LoC

Features on the LoCs were hybridized with complementary Cy5-labeled synthetic ssDNAs. In short, in a 0.2 mL Eppendorf, 15 µL of ST Hybridization buffer, 1 µL of 500 nM Cy5-labeled synthetic ssDNAs, DNA-miR122-Cy5 and 14 µL of of diH2O are mixed. This solution was loaded into LoCs (through the two inlets to reach the microarray area). The array is sealed inserting the "2IN" clamp first and the Outlet clamp last (Figure 84) and inserted into Temperature Control System (TCS) for hybridization. Hybridization was standardized by treatment at 55 °C for 1 h. Thereafter, clamps were removed, and the LoCs were washed for 10 min each in $2 \times SSC + 0.1\%$ SDS, $2 \times SSC$ and then $0.2 \times SSC$ (all wash steps were performed at room temperature). LoCs were dried centrifuging at 3000 rpm for 2 minutes and then scanned with the ST optical reader using 1000 ms as exposure time and emission and detection filters appropriate for Cy5.

Figure 84: Reaction area sealing clamps

5.2.4.3. Base filling reaction on ST's In-Check™ "LoC" device: 'Single Nucleobase Labeling' with SMART-C-sulfoCy5

In a 0.2 mL Eppendorf, 15 µL of ST Hybridization buffer, 5µL of 500 nM unlabeled miRNA122 oligomer aqueous solution (final concentration 83 nM), 5µL of 36 µM SMART-C-sulfoCy5 (final concentration 6 µM) and 5µL of freshly prepared 1 mM sodium cianoborohydride (final concentration 166 µM) are mixed. The reaction mixture is loaded on the LoC and sealed as described above. Then, it is placed in the Temperature Control System (TCS). The reaction is carried out at 40ºC for 1 h. Once finished, LoCs are washed, dried and scanned as described above (Figure 85).
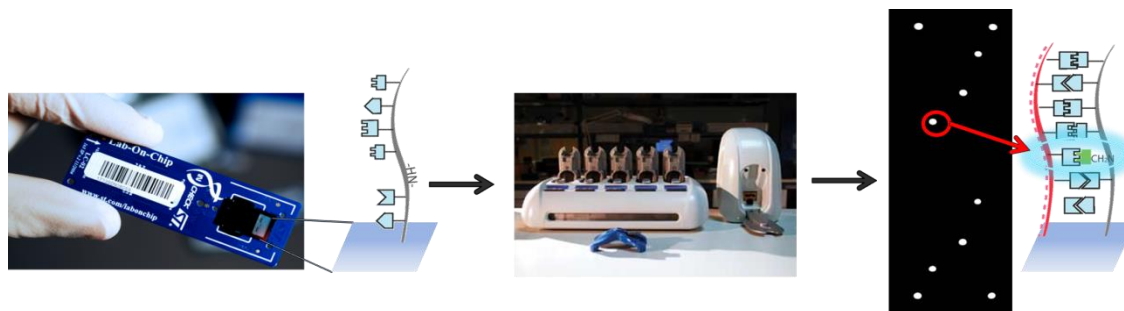
Figure 85: LoC work-flow: a) immobilization of DGL probes on the epoxide-silanized reactive area of the In-Check™ LoC, b) STMicroelectronics Temperature Control System and optical reader, c) example of a positive result observed in a LoC, the bright spots correspond to those areas where there has been a SMART-C-Cy5 incorporation reaction, as it is schematized on the drawing.

5.2.5. Experimental part of section 2.3.: Bead-based platform for direct detection of unlabeled miR-122 through Single Nucleobase Labeling: Luminex (specific objective 1.2.)

5.2.5.1. Functionalization of Luminex® MagPlex® microspheres with DGL probes DGL-122-U and DGL-122-C

DGL-122-U and DGL-122-C were coupled to MagPlex® carboxylated microspheres (MC10012) to give the functionalized beads, FB-1 and FB-2 respectively.

85 μL of a 1.25×10^7 microspheres/mL suspension of MagPlex® carboxylated microspheres (MC10012), approximately 1.0625×10^6 microspheres, were placed in a 1 mL Eppendorf tube. The supernatant is removed using a magnet and microspheres were re-suspended in MES Buffer (100 μL, pH ~ 4.5), then stirred, decanted magnetically and the supernatant removed. They were washed once more leaving approximately 20 μL of MES buffer and adding freshly prepared coupling reagents solutions EDC (10 μL of 10 mg/mL EDC in deionized water) and DGL probe solution (100 μM, 5 μL) were added and vortexed, followed by incubation (30 min at room temperature shaking in the dark). Then 10 more μL of feshly prepared EDC solution were added and left stirring in the dark for 30 min. Once coupling has finished, the microspheres were washed (×2 0.02% Tween- 20, 200 μL and ×2, 0.1% SDS, 200 μL), re-suspended in water (100 μL, ~1×10^4 microspheres per μL). The microspheres working solution is prepared by diluting them in SCD buffer pH 6 (10 μL of functionalized microspheres stock solution are added to 990 μL of SCD buffer pH6, ~100 microspheres per μL).

5.2.5.2. Hybridization assessment of FB-1 and FB-2 microspheres.

The performance of FB-1 and FB-2 were confirmed by hybridizing a complementary oligonucleotide modified at their amino-5′-terminus with a biotin tag (miR122-biotin) (Table 2), followed by labeling with SAPE and analyzing on a MAGPIX®. Briefly, 12.5 µL of either FB-1 or FB-2 (100 microspheres per µL, ~1250 microspheres per assay), 30 µL of SCD buffer and 7.5 µL of 100 nM miRNA122-biot (final concentration 15 nM), were mixed in a 200 µL eppendorf tube. Hybridization was conducted at 41° C for 20 min, followed by addition of 10 µL of SAPE (working solution 20 µg / mL, prepared by adding 10 µL of SAPE at 1 mg/mL to 490 µL of SCD buffer pH 6, final assay concentration 3.3 µg/µL), vortexed for 1 sec and incubated at 41°C for 5 min in a thermal cycler prior to analysis. The same protocol is followed for the negative control where a non-complementary biotinylated synthetic oligonucleotide (miR21-biotin) was used as a target.

5.2.5.3. Base filling reaction on functionalized microspheres: Single Nucleobase Labeling (SNL) with SMART-C-PEG-Biotin

23.5 µL of SCD buffer, 12.5 µL of the functionalized microspheres (dispersed in SCD buffer, containing 100 microspheres per µL, 1250 microspheres per assay), 4 µL of SMART-C-PEG$_2$-Biotin (500 µM, final concentration 40 µM), 7.5 µL of either miR122 or controls miR21 and miR122-A (to give final concentrations of 1 µM, 100 nM, 10 nM or 1 nM) and 2.5 µL of reducing agent, sodium cyanoborohydride (20 mM, final concentration 1 mM) were added in a 200 µL Eppendorf tube, vortexed and incubated (41° C for 30 min in a thermal cycler). The microspheres were then washed twice with SCD buffer, re-suspended in 50 µL of SCD buffer (pH 6), followed by addition of 10 µL of SAPE (20 µg/mL, prepared as described above, final concentration 3.3 µg/mL). They were vortexed and incubated in a thermal cycler (41° C for 5 min) before being analyzed with the MAGPIX® instrument or prepared for flow cytometry or confocal microscopy analysis.

5.2.5.4. Single Nucleobase Labeling analysis using Luminex® MAGPIX®

The MAGPIX® instrument was calibrated (once a week) and verified (every day) using the verification and calibration kit and following manufacturer standard instructions. Phycoerythrin (PE) was detected using a LED (λex 511 nm ± 27 nm) and a CCD camera. Microspheres post hybridization or SNL and streptavidin-R-phycoeritrine (SAPE) incubation, were vortexed (1 sec) and analyzed in the MAGPIX® System (injection volume 20 µL) with a threshold of 100 as minimum microsphere count for the experiment to be considered.

5.2.5.5. Single Nucleobase Labeling analysis by Flow cytometry

Following SNL with 7500, 750, 75 and 7.5 fmoles of miR-122 or miR-21 as a negative control and SAPE incubation, the microspheres were washed twice with SCD buffer, resuspended in 150 µL of SCD. The results of flow cytometry were analysed with Flowjo (version 7.2.4).

5.3. Experimental part of chapter 3: Identification of Trypanosomatids by detecting Single Nucleotide Fingerprints using DNA analysis by Dynamic Chemistry

5.3.1. Target nucleic acid selection

28S rRNA delta gene sequence was chosen as target nucleic acid for the dynamic chemistry approach for the identification and differentiation of the three trypanosomatid species studied (*Leishmania major*, *Trypanosoma brucei*, *Trypanosoma cruzi) (*Table 38).

Table 38: Trypanosomatids 28S rRNA delta information and sequences for multiple sequence alignment from Tritryp database. (Reproduced with permission [161].

	Leishmania major	*Trypanosoma brucei*	*Trypanosoma cruzi*
Tritryp link	http://tritrypdb.org/tritrypdb/app/record/gene/LmjF.27.rRNA.31#Sequences	http://tritrypdb.org/tritrypdb/app/record/gene/Tb927.2.1407	http://tritrypdb.org/tritrypdb/app/record/gene/TcCLB.419169.10
Reference	LmjF.27.rRNA.31 28S rRNA (LSU-delta, M2)	Tb927.2.1407 M2 rRNA	TcCLB.419169.10 rRNA large subunit delta (M2), 5' partial
Type	rRNA encoding	rRNA encoding	rRNA encoding
Chromosome	27	02	Not Assigned
Location	LmjF.27:996,895..997,077(+)	Tb927_02_v5.1:261,083..261,265(-)	Tcruzi_13557:571..748(-)
Species	*Leishmania major*	*Trypanosoma brucei*	*Trypanosoma cruzi*
Strain	strain Friedlin	brucei TREU927	strain CL Brener
Status	Curated Non-Reference Strain	Curated Reference Strain	Curated Non-Reference Strain
Genomic sequence	(183bp) GTGAGATTGTGAAGGGATCTCGCAGGCATCGTGAGGGAAGTATGGGGTAGTACGAGAGGAACTCCCATGCCGTGCCTCTGGTTTCTGGAGTTTGTCGAAGGGCAAGTGCTCCGACGCTATCGCACGGTGGTTCTCGGCTGAACGCCTCTAAGCCAGAAACCAGTCCCAAGACCGGGTGCCCGT	(183bp) GTGAGATTGTGAAGGGATCTCGCAGGCATCGTGAGGGAAGTATGGGGTAGTACGAGAGGAACTCCCATGCCGTGCCTCTGGTTTCTGGAGTTTGTCGAAGGGCAAGTGCTCCGACGCTATCGCACGGTGGTTCTCGGCTGAACGCCTCTAAGCCAGAAACCAGTCCCAAGACCGGGTGCCCGT	(178bp) GATTGTGAAGGGATCTCGCAGGTATCGTGAGGGAAGTATGGGGTAGTACGAGAGGAACTCCCATGCCGTGCCTCTGGTTTCTGGAGTTTGTCGAACGGCAAGTGCTCCGACGCTATCGCACGGTGGTTCTCGGCTGAACGCCTCTAAGCCAGAAGCCAGTCCCAAGACCAGATGCCCA

5.3.2. DGL probes design

DGL probes were designed according to multiple sequence alignment results Figure 86. DGL#1 and DGL#2 target two sequence fragment which have a nucleotide which does not align between the three trypanosomatids, so according to the SMART-NB incorporation the species can be identified (for DGL#1 *L. major* incorporates SMART-T, *T. brucei* and *T. cruzi* incorporates SMART-C; for DGL#2, *L. major* and *T. cruzi* incorporates SMART-G and *T. brucei*, SMART-C). When transferring the experimental design to a colorimetric assay which used only one labeled SMART-NB, SMART-Cytosine some changes need to be done: 1) a third DGL probe, DGL#3 was added, it targets a sequence identical for the three species thus confirming the presence of a parasite in a sample; 2) positive results are due to the incorporation of a labeled SMART-Cytosine, so *L. major* gives positive only in DGL#3; *T. cruzi* show positive results in DGL#1 and DGL#3; *T. brucei* gives positive results in the three probes (Figure 87).

Figure 86: Multiple sequence alignment. The absence of star shows the lack of homology. DGL probes target sequences are highlighted in color, templating nitrogenous base are highlighted in bold white.
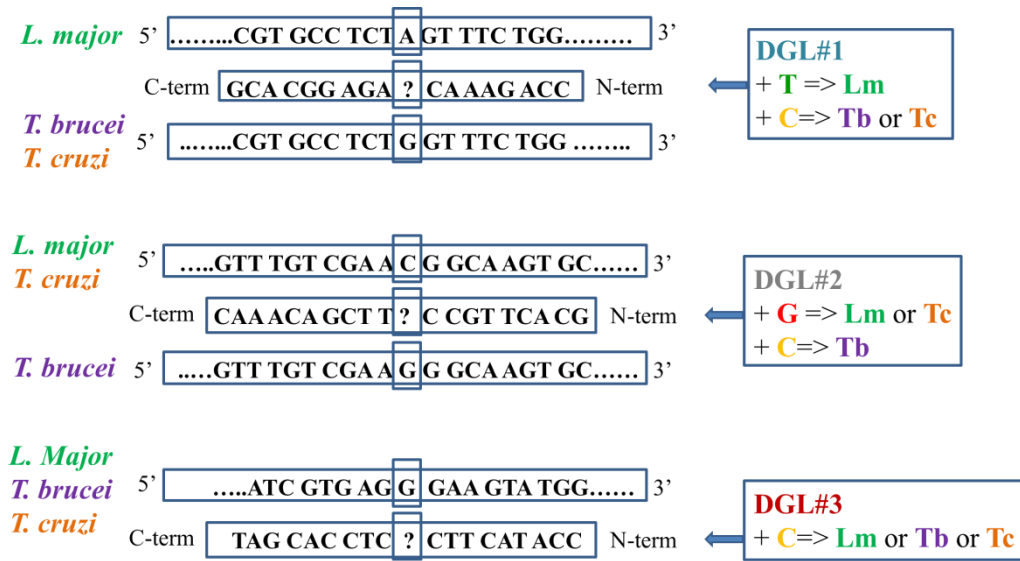
Figure 87: Alignment between the DGL probes for the trypanosomatid identification assay and their target nucleic acids. The square letter indicates the templating nucleotides that lie opposite the abasic position shown by the question mark. The SMART-NB that should be incorporated into each DGL probe depending on the templating nitrogenous base and so the parasite it indicated on the right.

5.3.3. DGL probes

Table 39: DGL probes sequences for trypanosomatid identification assays and their characterization by MALDI-TOF and HPLC.

DGL probes	DGL probe sequence (N-C)	Found mass MALDI-TOF MS (*m/z*)	HPLC Retention time (minutes)
DGL#1	$(Ph)_3P^+$-CCA GAA AC_ AGA GGC ACG-NH_2	5103	14.271
DGL#2	$(Ph)_3P^+$-GCA CTT GCC _TT CGA CAA AC-NH_2	5801	13.256
DGL#1-memb	x x C Cglu A G A A A Cglu *GL* A G A G G Cglu A Cglu G-NH_2	5409	15.984
DGL#2-memb	x x G C A Cglu T T G Cglu C *GL* T Tglu C G A Cglu A A A C-NH2	5839	15.5
DGL#3-memb	x x C C A Tglu A C T Tglu C *GL* C Tglu C A Cglu G A T	5252	15.683

* DGL probes are written from the N-terminal end (left) to the C-terminal end (right). For MALDI-TOF experiments, DGL probes are capped at their N-terminal with 3-(carboxypropyl)triphenylphosphonium bromide. "_" represents the neutral abasic position. For colorimetric assays, DGL probes have two miniPEG groups (xx) and -NH_2 group at the N-terminal to allow their immobilization on membranes. *GL* represents the chiral blank site. 'Xglu' respresents the chiral and negatively charged PNA monomers. All of them have a C-terminal primary amide

5.3.4. Oligo ssDNAs

All DNA oligomers (DNA-1TbTc, DNA-1Lm, DNA-2LmTc, DNA-2Tb, DNA-3LmTbTc) were purchased in desalted form from Sigma-Aldrich Inc. (Table 40).

Table 40: Sequences of the ssDNA oligomers complementary to DGL probes: the nucleotides that will lie opposite the abasic position are highlighted in bold and underlined.

Reference	Oligo DNAs sequences (5'-3')
DNA-1Lm	CGTGCCTCT**A**GTTTCTGG
DNA-1TbTc	CGTGCCTCT**G**GTTTCTGG
DNA-2LmTc	GTTTGTCGAA**C**GGCAAGTGC
DNA-2Tb	GTTTGTCGAA**G**GGCAAGTGC
DNA-3LmTbTc	ATCGTGAG**GG**AAGTATGG

5.3.5. Synthetic dsDNAs (gBlocks® Gene Fragments)

Synthetic dsDNAs (gBlocks® Gene Fragments): Lm rRNA28S-delta, Tb rRNA28S-delta and Tc rRNA28S-delta were purchased from Integrated DNA Technologies (IDT) (Table 41).

Table 41: Sequences of the synthetic double strand DNAs (gBlocks® Gene Fragments): the targeted SNFs are highlighted in bold and underlined.

Name	Sense DNA strand sequence (5'-3')
Lm rRNA28S-delta	GTGAGATTGTGAAGGGATCTCGCAGGTATCGTGAGGGAAGTATGGGG TAGTACGAGAGGAACTCCCATGCCGTGCCTCT**A**GTTTCTGGGGTTTGT CGAA**C**GGCAAGTGCCCCGAAGCCATCGCACGGTGGTTCTCGGCTGAA CGCCTCTAAGCCAGAAGCCAATCCCAAGACCAGATGCCCAC
Tb rRNA28S-delta	GTGAGATTGTGAAGGGATCTCGCAGGCATCGTGAGGGAAGTATGGGG TAGTACGAGAGGAACTCCCATGCCGTGCCTCT**G**GTTTCTGGAGTTTGT CGAA**G**GGCAAGTGCTCCGACGCTATCGCACGGTGGTTCTCGGCTGAAC GCCTCTAAGCCAGAAACCAGTCCCAAGACCGGGTGCCCGT
Tc rRNA28S-delta	GATTGTGAAGGGATCTCGCAGGTATCGTGAGGGAAGTATGGGGTAGT ACGAGAGGAACTCCCATGCCGTGCCTCT**G**GTTTCTGGAGTTTGTCGAA **C**GGCAAGTGCTCCGACGCTATCGCACGGTGGTTCTCGGCTGAACGCCT CTAAGCCAGAAGCCAGTCCCAAGACCAGATGCCC

5.3.5.1. Synthetic dsDNAs (gBlocks® Gene Fragments) resuspension

The dried contents of gBlocks® Gene Fragments tubes, normally a translucent film or a white powder was resuspended following manufacturer's instruction. Briefly, tubes were centrifuge for 3-5 second at a minimum of 3000 x g to ensure the material is in the bottom of the tube. Enough volume of TE pH 8 was added to the tube to reach a desired final concentration, we set 10 ng/µL, which correspond to approximately 5×10^{10} copies/µL. The tubes were briefly vortexed and then incubated at 50ºC for 20 minutes. They were briefly vortexed and centrifuged. Finally, the working solution was prepared, it was a 100-fold dilution which contained 5×10^{8} copies/µL.

5.3.6. Genomic DNA from parasites

Two gDNAs (gDNA) were purchased from ATCC®: a) gDNA from *T. cruzi* strain Tulahuen with ATCC® ID 30266D™ and b) gDNA from *L. major* with ATCC® ID 30012D™. gDNA from *T. brucei* was isolated from parasites.

5.3.6.1. Genomic DNA extraction from T. cruzi parasites culture

gDNA from *T. cruzi* and L. major were bought from ATCC®, whereas gDNA from *T. brucei* was extracted from parasites in culture. *T. brucei* 427 MIT at 1.2 bloodstream forms were cultivated in HMI-9 medium with 10% fetal bovine serum (Sigma- Aldrich) at 37°C and 5% CO2. Parasites were quantified by counting in a Neubauer chamber.

T. brucei parasites were counted and approximately 2×10^{7} were put in a 15 mL centrifuge tubes and centrifuged at 2,500 r.p.m. for 10 minutes at 4ºC. After removing the supernantant, the pellet was resuspended in 1 mL of sterile PBS and transferred to a new 1.5 mL Eppendorf. The solution was

centrifuged at 13,000 r.p.m. for 1 minute at 4ºC and the supernatant was removed. 70 µL of buffer A (10 mM Tris, 10 mM E.D.T.A., 10 mM E.G.T.A.), 80 µL of buffer B (10 mM Tris, 10 mM E.D.T.A., 10 mM E.G.T.A., 2% S.D.S.) and 40 µL of NaCl 5M were added to the pellet and mixed by pipetting up and down a couple of times and left overnight on ice. The solution was centrifuged at 10,000 r.p.m. for 10 minutes at 4ºC, the supernatant transferred to a new 1.5 mL Eppendorf and an equal volume of phenol:chloroform:isoamyl alcohol (25:24:1) solution was added for a first extraction. After centrifuging at 14,000 r.p.m. for 5 minutes at 4ºC, the aqueous phase (upper one) was transferred to a new 1.5 mL Eppendorf. The same extraction procedure was repeated two more times. After the third extraction, all the aqueous solution was transferred to a new 1.5 mL Eppendorf and a new extraction was performed by adding chloroform:isoamyl alcohol (24:1). The solution was centrifuged at 14,000 r.p.m. for 5 minutes at 4ºC. The aqueous phase was transferred to a new 1.5 mL Eppendorf. DNA was precipitated by adding twice the volume of the aqueous phase of cold absolute ethanol. The solution was left for 2 hours at −20ºC, centrifuged at 14,000 r.p.m. for 5 minutes at 4ºC, and the supernatant removed. 1 mL of 70% ethanol was added and the Eppendorf was centrifuged at 14,000 r.p.m. for 5 minutes at 4ºC. The supernatant was removed and the pellet left drying. Approximately 20 µL of miliQ water and 1 µL of RNase A at 10 mg/mL were added, the DNA solution was left for 1 hour at 37ºC and then stored at 4ºC until their use.

5.3.7. PCR Amplification

PCR primers were purchased from Sigma-Aldrich Inc (Table 42).

Table 42: Primer sequences and GC content and melting temperature information

Primers	Sequence 5'---3'	Length (nucleotides)	GC content (%)	Melting temperature (ºC)
Forward	GATTGTGAAGGGATCTCGCAG	21	52.4 %	55.6 ºC
Reverse	TCTGGCTTAGAGGCGTTCA	19	52.6 %	55.9 ºC

PCR amplifications were performed on a Veriti® 96-well Thermal cycler (Thermo Fisher Scientific). Two consecutive PCR amplifications were performed; the first one, symmetric PCR (sPCR) to generate dsDNA amplicon, followed by an asymmetric PCR (aPCR) (with higher concentration of the forward primer) to afford ssDNA. Cycling conditions for both sPCR and aPCR were as follows: 1) initial denaturation at 96ºC for 3 min; 2) 40 cycles of a) denaturation 96ºC for 30 sec, b) annealing at 61ºC for 30 sec, and (c) extension at 72ºC for 30 sec; 3) final extension at 72ºC for 10 sec; 4) final hold at 4ºC.

sPCR: either 3 µL of synthetic dsDNA at $5\cdot10^8$ copies/µL (gBlocks® Gene Fragments) or 5 µL with different amounts of ATCC® gDNA solution for *L. major* or *T. cruzi* and gDNA extracted from *T.*

brucei in culture were amplified using 1X PCR master mix (Thermo Fisher Scientific), 0.15 µM forward and reverse primers per reaction with a final volume of 50 µL. DNA templates were replaced with water for negative controls.

aPCR: 2 µL of the first sPCR crude mixture was amplified using the 1X PCR mastermix (Thermo Fisher Scientific), 0.15 µM forward primer and 0.015 µM reverse primer per reaction with a final volume of 50 µL. Negative controls were performed using 2 µL of the negative controls from the first sPCR.

PCR products were confirmed by sequencing analyses using capillary electrophoresis (Sanger method 3130 Genetic Analyzers, Applied Biosystems, US) [131] and analyzed using the Agilent 2100 Bioanalyzer and DNA 1000 Kit (Agilent Technologies Inc.).

5.3.8. Experimental part of the section 3.2.: Identification of Trypanosomatids by detecting Single Nucleotide Fingerprints using DNA analysis by Dynamic Chemistry with MALDI-TOF (specific objective 2.1.)

5.3.8.1. Base-Filling reactions in solution for mass-based assays (MALDI-TOF)

Prior to use, Q Sepharose® Fast Flow (GE Healthcare; 1 mL of a suspension in ethanol) was centrifuged and the supernatant removed. The resin was subsequently washed centrifugally with H_2O (1 mL) and 10 mM phosphate buffer, pH 7 (2 x 1 mL), before re-suspending in the same buffer (0.5 mL). Then a 10-fold dilution was made by adding 100 µL of pre-equilibrated Q Sepharose® to 900 µL of 10 mM phosphate buffer, pH 7. Immediately before use, the pre-equilibrated Q Sepharose® was agitated to resuspend the resin beads [32, 33]. This anion exchange resin carries quaternary ammonium functionality and binds the negatively charged sugar phosphate backbone of the DNA template. In doing so, any hybridized PNA probe is also bound, permitting a washing step to remove any inorganic salts (which constitute the pH buffer and reducing reagent) that may give rise to adducts in the mass spectrum, together with any unbound PNA [36].

MALDI-TOF mass spectra were recorded on a BRUKER AUTOFLEX MALDI-TOF MS using a weight range from 4,500 to 10,000 Da. Spectra were acquired for each sample in positive ionization reflector mode (delay 270 ns, 19 kV accelerating voltage, variable laser intensity, typically more than 200 shots). Sinapinic acid matrix consisted of a saturated solution of sinapinic acid in acetonitrile:water with 0.1% v/v TFA in a ratio 1:2. Samples were diluted in 50% v/v acetonitrile in water with 0.1% v/v TFA.

5.3.8.1.1. Reactions with synthetic short Oligo DNA as target

DGL probe performance and dynamic chemistry assay was validated following previous stablished protocols [32]. A DGL probe (2.5 µL, 40 µM, final concentration 5 µM), DNA template (1 µL, 100 µM, final concentration 5 µM), SMART-NB mixture containing equimolar concentrations of the four nucleobases (5.5 µL, each SMART-NB at 500 µM each, final concentration 137.5 µM each) and pH 6 phosphate buffer (11 µL, 10 mM aq) were combined in a 1.5 mL Eppendorf tube (Eppendorf AG) and placed in a Thermocycler (TC-312 Techne) at 80 ºC for 5 min, shaking at 1,400 r.p.m. The reaction was then cooled to 41ºC at 3ºC/min without agitation and once the temperature was reached, sodium cyanoborohydride (NaBH3CN) (2 µL, 1 M. final concentration 100 mM) was added and the reaction was left at 41ºC for 60 min while shaking at 1,400 r.p.m. Pre-treated Q Sepharose® Fast Flow resin (5uL, see above) was then added and the mixture was kept shaking at room temperature (25ºC) for 20 min. The reaction tube was centrifuged, the supernatant removed, and the resin washed centrifugally with 3% aqueous acetonitrile (3 x 200 µL; 3 min at 13,400 rpm). Finally, 20 µL of OS buffer (Acetonitrile: 2.5% TFA in water, 1:1) were added to the resin. 2 µL of sinapinic acid matrix (saturated solution of sinapinic acid in Acetonitrile: 0.1% TFA in water, 1:2) were mixed with 2 µL of resin. 2 µL of the resulting mixture were spotted onto the Bruker® 384 stainless steel MALDI-TOF plate for analysis.

5.3.8.1.2. Reactions with aPCR product as target

Similar protocol to the one described above for short oligo DNAs as targets was followed but introducing some changes in reagents concentration and denaturalization temperature. 45 µL of aPCR product, without any further purification steps, were placed in a 1.5 mL Eppendorf tube and acidified to pH 6 using HCl. Then, a DGL probe (1.5 µL, 10 µM, final concentration 0.25 µM) and SMART-NB mixture containing the four nucleobases (6 µL, each SMART-NB at 500 µM each, final concentration 50 µM each) were added. The resulting mixtures were heated in a Thermocycler (TC-312 Techne) at 96 ºC for 5 min, shaking at 1,400 r.p.m., then cooled to 41ºC at 3ºC/min without agitation and once the temperature was reached, sodium cyanoborohydride (NaBH3CN) (6 µL, 100 mM, final concentration 10 mM) was added and the reaction was left at 41ºC for 60 min while shaking at 1,400 r.p.m.

Once the reaction was completed, 5 µL of pre-treated Q Sepharose® Fast Flow resin (10-fold dilution from the pre-treated stock solution, see above) was added and the mixtures were kept shaking at room temperature (25ºC) for 20 min. The solution was centrifuged, the supernatant removed, and the resin washed by centrifugation (3 min at 13,400 rpm) with 3% aqueous acetonitrile (3 x 200 µL; acetonitrile (Fisher Scientific)). Finally, 20 µL of OS buffer (Acetonitrile:

2.5% TFA in water, 1:1) were added to the resin. 2 μL of sinapinic acid matrix (saturated solution of sinapinic acid in Acetonitrile: 0.1% TFA in water, 1:2) were mixed with 2 μL of resin. 2 μL of the resulting mixture were spotted onto the Bruker® 384 stainless steel MALDI-TOF plate for analysis. Sinapinic acid matrix was chosen following references of previously settled methods [1, 2].

This region contains different Single Nucleotide Fingerprint (SNF) markers, defined as specific positions within conserved nucleic acid regions of different species where single nucleotide variations occur. When these regions are analysed by dynamic chemistry using two DGL probes and the four SMART-NBs then each of the PCR products create a unique mass pattern which is used to identify each parasite species (Figure).

5.3.9. Experimental part of the section 3.3.: Colorimetric-based assays for the identification of Trypanosomatids by detecting Single Nucleotide Fingerprints using DNA analysis by Dynamic Chemistry (specific objective 2.2.)

5.3.9.1. DGL probes spotting solution

Spotting solution is prepared from a mixture of reagents plus the DGL probe to be printed on the membrane: Amaranth dye at 0.2025 mg/mL, Sodium bicarbonate at 0.125 M, 30% of DMSO, DGL probe at the desired concentration and H_2O.

Enough volume of a stock solution of amaranth dye at 15 mg/mL is added to reach a final concentration of 0.2025 mg/mL (dilution factor 74). A solution of Sodium bicarbonate at 0.5 M is added to reach 0.125 M (dilution factor 40). Dimetilsulfoxide is added to have 30% of DMSO in the final solution (dilution factor 3.33). DGL probe from a stock solution, normally around 100 μM, is added to the spotting mixture to reach the desired concentration. The remaining volume of the mixture is completed with H_2O.

5.3.9.2. Reagents for the colorimetric assay for the dynamic chemistry reaction on membranes:

a) Buffer and dilution reagents (unknown buffer composition, it is property of the Vitro group): Reagent A (2X SSC and 0.1% SDS, for suiting the membranes to the reaction buffer and conditions); Reagent A* (2X SSC and 0.1% SDS, acidified to pH 5 by adding hydroclorhidric acid, for washing after dynamic reaction); Reagent B (for blocking); Reagent C (for enzymatic reaction it contains Streptavidin- alkalin phosphatese conjugate); Reagent D (it contains tris-HCl, for washing after the enzymatic reaction); Reagent E (it is formed by the mixture of reagents E01 and E02, 50%

each, prepared immediately before use, it contains the chromogenic reagent); Reagent F (for washing after the chromogen).

Reagents A, D, F are kept at room temperature. Reagents B, C, E are stored at -4 ºC. Before being used reagents are set in a water bath at 41ºC (the same temperature as the one used in the hybridization step).

b) Samples used for positive controls (using synthetic ssDNAs oligomers) and negative controls (ssDNA is replaced by H_2O):

> b1) Stock of ssDNAs for positive controls: it is prepared by mixing 684 µL of H2O, 666 µL of reagent D and 150 µL of ssDNA at 1 µM. This makes a final concentration of 100 nM.

> b2) Negative control: it is prepared by mixing 834 µL of H2O and 666 µL of reagent D.

c) Dynamic chemistry mixture: 30 µL of SMART-NBs master mix and 20 µL of Reducing agent.

> c1) SMART-NBs master mix: It contains SMART-C-Biotin and the other three unlabeled SMART-NBs. There is an excess of the SMART-NBs with lower incorporation yield, so that they are in a ratio 1: 1: 3: 5 for SMART-G: SMART-C-Biotin: SMART-A: SMART-T, being their final concentrations in the SMART-NBs master mix 50: 50: 150: 250 µM, respectively. A working solution containing the three unlabeled SMART-NBs is prepared by mixing 450 µL of a 1 mM stock of SMART-T, 270 µL of a 1mM of stock SMART-A, 180 µL of a 500 µM stock of SMART-G. This solution is mixed with an equal volume (900 µL) of SMART-C-Biotin at 100 uM.

> c2) Reducing agent: a 15 mM stock solution of sodium cianoborohydride in H2O is prepared. It is aliquoted in vials and Kept at -20ºC until used. Once the working solution has been thawed, it is disregarded.

5.3.9.3. Base-filling reaction on membranes for the colorimetric assay: SMART-C-Biotin incorporation

Samples mixtures for a final volume of 300µL:

> a) For positive control (ssDNA): 45 µL of ssDNA at 100 nM prepared as described above, 50 µL of dynamic chemistry reagents, 205 µL of Reagent A* (pH 5).

> b) For negative control (H_2O): 45 µL of negative control samples prepared as described above, 50 µL of dynamic chemistry reagents, 205 µL of Reagent A* (pH 5).

c) For PCR reactions (dsDNA obtained from sPCR): 45 µL of sPCR product prepared as described previously, 50 µL of dynamic chemistry reagents, 205 µL of Reagent A* (pH 5).

1) Membranes are incubated for 2 minutes at 41ºC with 300 µL of a solution of reagent A (composed of 2X SSC and 0.1% SDS).

2) The dynamic chemistry step is done all at once, 300 µL of the dynamic chemistry mixture are added to the membranes and left at 41ºC for 20 minutes.

3) Membranes are incubated with 1mM of hydrochloric acid for 5 minutes at 41ºC

4) Three post-hybridization washing steps at 41ºC using 300 µL of reagent A for each one.

5) Blocking step where membranes are incubated with reagent B for 5 minutes. During this time temperature is lower from 41ºC to 29ºC.

6) Enzymatic reaction, 300 µL of reagent C are added and left at 29ºC for 5 minutes.

7) Four post-enzymatic reaction washing steps with 300 µL of reagent D. In the meantime, the temperature is increased from 29ºC to 36ºC.

8) Chromogen, incubation with 300 µL of reagent E at 36ºC for 5 minutes.

9) Three post-chromogen washing steps, each one with 300 µL of reagent F.

Once finished the reaction, membranes are visually analyzed.
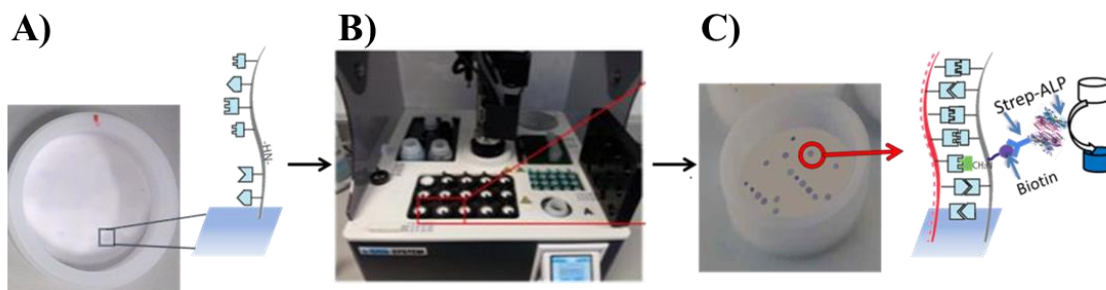
Figure 88: Colorimetric-based detection on membranes: A) Immobilization of DGL probes on membranes, B) automatic e-BRID™ system for temperature and time control, for adding reagents and doing the washing steps, C) example of the result to be obtained on a membrane: when SMART-C-Biotin has been incorporated, it will bind to a streptavidin-alkaline-phosphatase complex which transforms a colorless substrate into a blue precipitate.

5.3.10. Experimental part of the section 3.4. Industrial impact of the colorimetric assay for trypanosomatids identification

Some modifications with regard to the traditional reverse-dot blot&DNA-flow through assay are made.

5.3.10.1. Reagents for the colorimetric assay for the dynamic chemistry reaction on DestiNA-spin tube:

a) Buffer and dilution: 0.1M citrate buffer with 0.1% SDS (pH 6, is used for conditioning the membranes to the reaction buffer and conditions and for hybridization). Before being used, citrate buffer and reagents A and E are set in a water bath at 45ºC (the same temperature as the one used in the hybridization step).

b) Dynamic chemistry reagents: 15 µL of 200 µM SMART-C-Biotin and 20 µL of 15 mM sodium cianoborohydride in H_2O (reducing agent). So that the final concentrations used are 10 µM of SMART-C-Biotin and 1mM of sodium cyanoborohydride.

5.3.10.2. Base-filling reaction on DestiNA-spin tube: SMART-C-Biotin dynamic incorporation reaction on membranes with a colorimetric readout

Samples mixtures for a final volume of 300µL: 45 µL of sPCR product prepared as described above, 35 µL of dynamic chemistry reagents and 220 µL of 0.1M citrate buffer with 0.1% SDS (pH 6).

Protocol: All steps are performed with 300 µL and membranes are centrifuged to remove the solution between each step. Membranes are incubated for 2 minutes at 45ºC with 300 µL of a solution of 0.1M citrate buffer with 0.1% SDS (pH 6). Then, the sample mixture is added and left at 45ºC for 1 hour. After that, three post-hybridization washing steps with reagent A heated at 45ºC are done. This is followed by a blocking step in which membranes are incubated with reagent B for 5 minutes at room temperature. Then, the enzymatic reaction is done by incubating the membranes with reagent C at room temperature for 5 minutes. Four post-enzymatic reaction washing steps with reagent D are done. Then, the chromogen solution (reagent E) is added to the membranes and left at 45ºC for 5 minutes. Finally, three post-chromogen washing steps with reagent F are done. Once the reaction has finished, membranes are visually analyzed.

5.3.10.3. RNA extraction

RNA was extracted from parasites in culture. *T. cruzi* were cultivated in MTL-2 medium and L. major in modified RPMI medium with 10% fetal bovine serum (Sigma- Aldrich) at 28°C and 5% CO_2. Parasites were quantified by counting in a Neubauer chamber.

$1x10^6$ parasitic cells were put in a 15 mL centrifuge tubes and centrifuged at 1,450 r.p.m. for 5 minutes at 4ºC. Then, the supernatant was removed and the pellet was re-suspended in 1 mL of sterile PBS and transferred to a new 1.5 mL tube. The solution was centrifuged at 13,000 r.p.m. for 5 minute at 4ºC and the supernatant was removed. Then, 1 mL of Trizol® was added to the pellet, sample is pipetted up and down several times and it is incubated at room temperature for 5 minutes. After that, 200 µL of chloroform are added, the solution is stirred for 15 seconds and incubated at room temperature for 2-3 minutes. The samples are then centrifuged at 14,000 r.p.m. for 15 minutes at 4ºC. The aqueous phase (superior) is transferred to a clean 1.5 mL vial and 500 µL of isopropanol are added. The solution are cautiously stirred and incubated at room temperature for 10 minutes. It is then centrifuged at 14,000 r.p.m. for 10 minutes at 4ºC and the supernatant is removed. The pellet is washed with 1 mL of 75% ethanol (added, vortexed and centrifuged at 14,000 r.p.m. for 5 minutes at 4ºC). The pellet is left to dry for 5-10 minutes and then re-suspended in 20 µL of DEPC-treated water. It is incubated for 10 minutes at 55-60ºC and then frozen at -80ºC and stored until use. The integrity of the extracted RNA is checked by running an Agilent Bioanalyzer 2100 using a RNA nanochip (figure 78 and table 32).

5.3.10.4. RNA fragmentation

NEBNext® Magnesium RNA Fragmentation Module Protocol is used to fragment RNA. The following reagents are mixed in a sterile PCR tube: 1-18 µL of purified RNA containing 2-50 µg of total RNA, 2 µL of RNA fragmentation buffer and complete with nuclease-free water up to 20 µL. The mixture is incubated at 94ºC for 5 minutes (to get fragments of around 200-mer length. Then the tube is transferred to ice and 2 µL of RNA Fragmentation stop solution are added. After that, the fragmented RNA is cleaned up using ethanol precipitation: 22 µL of fragmented RNA, 2 µL of 3M sodium acetate pH 5.2 and 60 µL of 100% ethanol. The mixture is incubated at -80ºC for 30 minutes and then centrifuged at 14,000 r.p.m. for 25 minutes at 4ºC and ethanol is removed carefully. The pellet is washed with 300 µL of 70% ethanol, centrifuged and removed the ethanol. Finally, the pellet is air-dry for up to 10 minutes at room temperature and re-suspended in 13.5 µL of nuclease-free water. To assess the yield and size distribution of the fragmented RNA, 1 µL of a 10-fold dilution is run in an Agilent Bioanalyzer 2100 using a RNA pico chip (Table 33).

Appendices

6. Appendices

6.1. Appendix 1: Publication (permission)

Copyright Clearance Center **RightsLink®** — Home | Create Account | Help | Chat

Title:	Identification of Trypanosomatids by detecting Single Nucleotide Fingerprints using DNA analysis by dynamic chemistry with MALDI-ToF
Author:	María Angélica Luque-González,Mavys Tabraue-Chávez,Bárbara López-Longarela,Rosario María Sánchez-Martín,Matilde Ortiz-González,Miguel Soriano-Rodríguez,José Antonio García-Salcedo,Salvatore Pernagallo,Juan José Díaz-Mochón
Publication:	Talanta
Publisher:	Elsevier
Date:	1 January 2018

© 2017 Elsevier B.V. All rights reserved.

LOGIN

If you're a copyright.com user, you can login to RightsLink using your copyright.com credentials. Already a RightsLink user or want to learn more?

Please note that, as the author of this Elsevier article, you retain the right to include it in a thesis or dissertation, provided it is not published commercially. Permission is not required, but please ensure that you reference the journal as the original source. For more information on this and on your other retained rights, please visit: https://www.elsevier.com/about/our-business/policies/copyright#Author-rights

BACK | CLOSE WINDOW

Title: Novel bead-based platform for direct detection of unlabelled nucleic acids through Single Nucleobase Labelling

Author: Seshasailam Venkateswaran,Maria Angélica Luque-González,Mavys Tabraue-Chávez,Mario Antonio Fara,Barbara López-Longarela,Victoria Cano-Cortes,Francisco Javier López-Delgado,Rosario María Sánchez-Martín,Hugh Ilyine,Mark Bradley,Salvatore Pernagallo et al.

Publication: Talanta

Publisher: Elsevier

Date: 1 December 2016

BACK   CLOSE WINDOW

Title:	DNA Analysis by Dynamic Chemistry
Author:	Frank R. Bowler, Juan J. Diaz-Mochon, Michael D. Swift, Mark Bradley
Publication:	Angewandte Chemie International Edition
Publisher:	John Wiley and Sons
Date:	Feb 12, 2010

Copyright © 2010 WILEY-VCH Verlag GmbH & Co. KGaA, Weinheim

Order Completed

Thank you for your order.

This Agreement between Miss. Mª Angélica Luque-González ("You") and John Wiley and Sons ("John Wiley and Sons") consists of your license details and the terms and conditions provided by John Wiley and Sons and Copyright Clearance Center.

Your confirmation email will contain your order number for future reference.

printable details

License Number	4243550904669
License date	Dec 07, 2017
Licensed Content Publisher	John Wiley and Sons
Licensed Content Publication	Angewandte Chemie International Edition
Licensed Content Title	DNA Analysis by Dynamic Chemistry
Licensed Content Author	Frank R. Bowler, Juan J. Diaz-Mochon, Michael D. Swift, Mark Bradley
Licensed Content Date	Feb 12, 2010
Licensed Content Pages	4
Type of use	Dissertation/Thesis
Requestor type	University/Academic
Format	Print and electronic
Portion	Figure/table
Number of figures/tables	1
Original Wiley figure/table number(s)	Scheme 1: Dynamic chemistry applied to SNP analysis.
Will you be translating?	No
Title of your thesis / dissertation	Chem-NAT: a unique chemical approach for nucleic acid reading
Expected completion date	Mar 2018
Expected size (number of pages)	250
Requestor Location	Miss. Mª Angélica Luque-González GENYO Avda. de la Ilustración 114 Granada, Granada 18016 Spain Attn: Miss. Mª Angélica Luque-González
Publisher Tax ID	EU826007151
Billing Type	Invoice
Billing address	Miss. Mª Angélica Luque-González GENYO Avda. de la Ilustración 114 Granada, Spain 18016 Attn: Miss. Mª Angélica Luque-González
Total	0.00 EUR

6.2. Appendix 2: Labeled SMART-NBs

6.2.1. SMART-NBs for miR122 detection on ST-In Check LoC: SMART-C-sulfoCy5

Sulfo-Cy5 dye, currently used for LoC platforms, was coupled to SMART-Cytosine. SMART-C-sulfo-Cy5 it is a SMART-Cytosine modified with commercially available Sulfo-Cy5 dye (ϵ_{260} = 271,000 L mol^{-1} cm^{-1}) (Figure 89). SMART-C-sulfoCy5 sample was run in an UPLC WATERS ACQUITY H CLASS coupled to a Triwave$^{®}$ WATERS SYNAP G2 Mass Spectrometer with a time-of-flight (TOF)-electrospray (ES) detector (Figure 90 and 91).
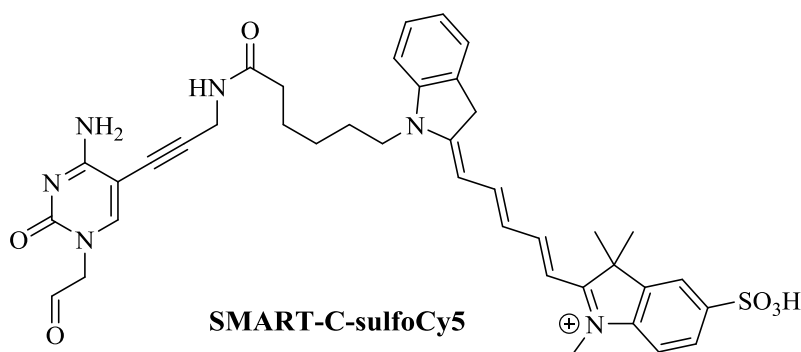
Figure 89: SMART-C-sulfoCy5 chemical structure

UPLC – detection @648nm
>90% purity – hydrated form (0.44min) is detected
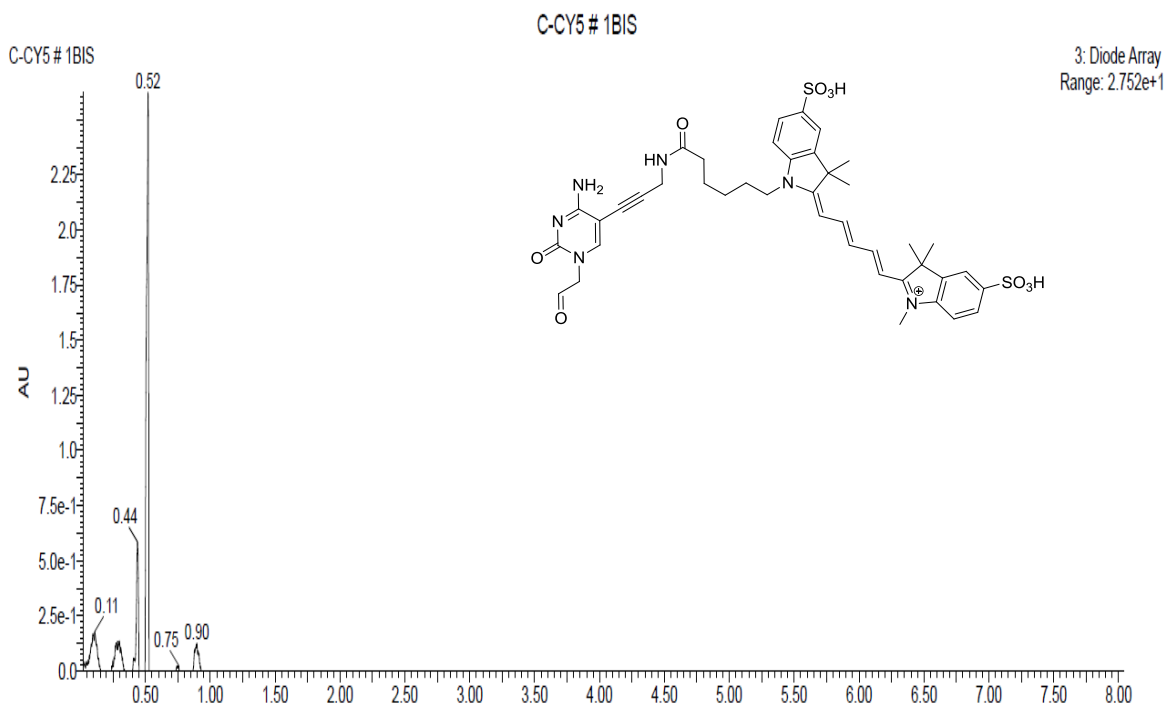
Figure 90: SMART-C-sulfoCy5 Ultra Performance Liquid Chromatography (UPLC) spectrum

HRMS – detection
100% accordance with proposed structure.

HRMS allow identifying peaks corresponding to double charged species as the m/z difference found within their isotopic patterns are less than 1, i.e for double charged species the difference is 0.5 as 425.1491 and 425.6538. That means that this peak correspond to a double charged species. When the specie is mono-charged the difference is 1 as for 831.2729 and 832.2936

Figure 91: SMART-C-sulfoCy5 high resolution mass spectrometry (HRMS) spectrum

6.2.2. SMART-NBs for miR122 detection on MagPlex® microspheres and Trypanosomatids identification on membranes: Biotin-labeled SMART-Cytosines

Two aldehyde-modified cytosines were used. Both of them were tagged with a biotin but they differ in the length of the spacer either a tetraethylenglycol (PEG$_2$) or a dodecylethylenglycol (PEG$_6$): SMART-C-PEG$_2$-Biotin or SMART-C-PEG$_6$-Biotin. They were provided by DestiNA Genomica S. L. and were prepared following the synthetic route described elsewhere [202]. They were characterized by ES+-TOF MS: SMART-C-PEG$_2$-Biotinv(Figure 92) and ES+-TOF MS of SMART-C-PEG$_6$-Biotin (Figure 93).
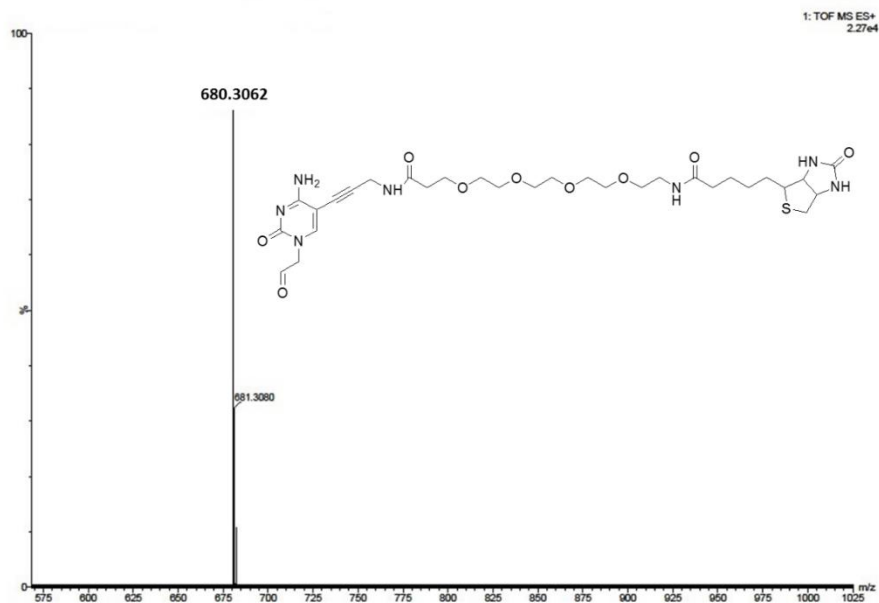
Figure 92: ES+-TOF MS of SMART-C-PEG$_2$-Biotin, m/z 680.3 ([M+H]$^+$). HRMS calcd. for C$_{30}$H$_{46}$N$_7$O$_9$S ([M+H]$^+$) 680.3078, found 680.3102.
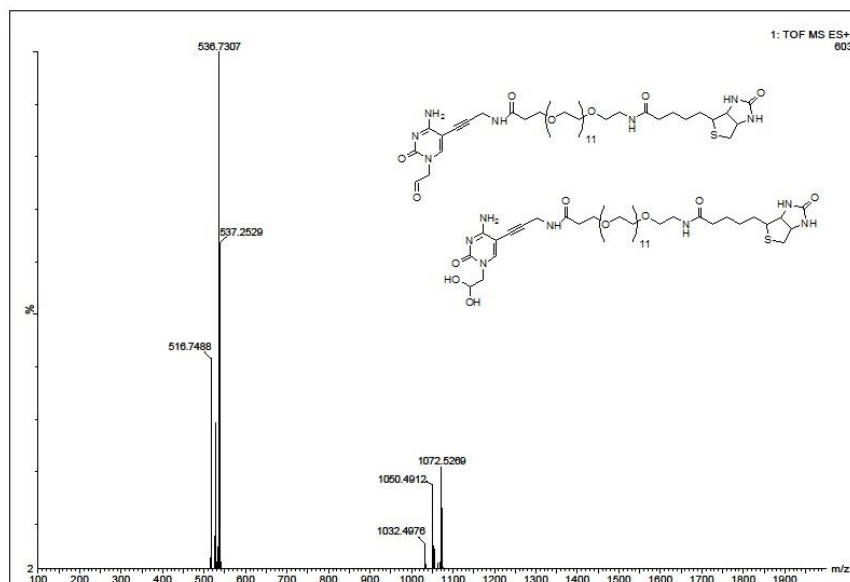
Figure 93: ES+-TOF MS of SMART-C-PEG$_6$-Biotin, m/z 516.7 ([M+2H]$^{2+}$), 536.7 ([M+H$_2$O+H+Na]$^{2+}$), 1032.4 ([M+H]$^+$), 1050.4 ([M+H$_2$O+H]$^+$), 1072.4 ([M+H$_2$O+Na]$^+$). HRMS calcd. for C$_{46}$H$_{78}$N$_7$O$_{17}$S ([M+H]$^+$) 1032.5175, found 1032.5137. The aldehyde and hydrate forms were detected.

6.3. Appendix 3: Excel file formulas to converts MALDI-TOF mass peaks into a trypanosomatid specie

6.4. Appendix 4: Table with the raw mass peak data and its automatic identity assignment

Table 44: Semi-automatic analysis of raw peak data obtained from the MALDI-TOF when using oligo ssDNAs as templating nucleic acid. An event identity, if any, was assigned to each peak ('X' for unknown event, 'DGL#' for the DGL signal, 'SMART-NB' for the signal corresponding to the DGL whose abasic position has been filled by a specific SMART-NB). Then, peaks with a certain threshold (S/N>10 and RI>15%) were selected and taken into account to turn this numerical data into a parasite specie. In these examples, because two of the synthetic ssDNA used mimic the sequence of two parasites (DNA-1TbTc, DNA-2LmTc), the output is both parasites.

	Peak mass	S/N	Relative intensity (%)	LOOKUP	Selection of peaks with S/N>10 and Relative Intensity (%)>15	Assignment of Selected peaks	Condition only if there is DGL#3
DNA-1Lm	5106,02	35	63,7	DGL#1	5106,02	**DGL#1**	**Lm**
	5119,52	56	100	DGL#1	5119,52	**DGL#1**	
	5242,88	4	11,2	SMART-C			
	5258,1	29	54,2	SMART-T	5258,1	**SMART-T**	
	5265,86	13	26,4	SMART-A	5265,86	**SMART-A**	
	5277,76	4	11,3	SMART-G			
DNA-1TbTc	5104,79	15	30,1	DGL#1	5104,79	**DGL#1**	**Tb or Tc**
	5118,87	27	51,1	DGL#1	5118,87	**DGL#1**	
	5242,14	55	100	SMART-C	5242,14	**SMART-C**	
	5255,39	8	19	SMART-T			
	5263,4	8	18,1	SMART-A			

	Peak mass	S/N	Relative intensity (%)	LOOKUP	Selection of peaks with S/N>10 and Relative Intensity (%)>15	Assignment of Selected peaks	condition only if there is DGL#2
DNA-2LmTc	5525,13	6	6,84	X			**Lm or Tc**
	5549,65	12	10,4	X			
	5586,64	6	7,43	X			

	Peak mass	S/N	Relative intensity (%)	LOOKUP	Selection of peaks with S/N> 10 and Relative Intensity (%)>15	Assignment of Selected peaks	Parasite present in a sample regarding mass peak
	5678,05	6	8,74	X			
	5723,62	6	8,79	X			
	5765,61	18	14,1	X			
	5800,6	212	100	DGL#2	5800,6	**DGL#2**	
	5814,59	38	23	DGL#2	5814,59	**DGL#2**	
	5827,59	14	12,3	X			
	5842,55	13	12	X			
	5886,06	6	7,44	X			
	5942,83	10	8,99	SMART-C			
	5978,01	102	49,1	SMART-G	5978,01	**SMART-G**	
	6007,66	8	7,98	X			
	6024,07	9	8,07	X			
DNA-2Tb	5798,82	15	52,3	DGL#2	5798,82	**DGL#2**	**Tb**
	5812,85	32	100	DGL#2	5812,85	**DGL#2**	
	5936,36	11	38,6	SMART-C	5936,36	**SMART-C**	

Table 45: MALDI-TOF raw peak table data obtained o after the dynamic reaction with synthetic aPCR products. The first columns indicates the name of the assay, peaks mass, S/N ratio and relative intensity. Next column calls for the peak identity ('X' for unknown event, 'DGL#' for the DGL signal, 'SMART-NB' for the signal corresponding to the DGL whose abasic position has been filled by a specific SMART-NB). Only peaks with S/N higher than 10 and relative intensity higher than 15% were used for the identification process. Combination of the selected peaks from both DGL probes resulted in trypanosomatid specie.

	Peak mass	S/N	Relative intensity (%)	LOOKUP	Selection of peaks with S/N> 10 and Relative Intensity (%)>15	Assignment of Selected peaks	Parasite present in a sample regarding mass peak
Lm synt DGL#1	5103,99	50	56,5	DGL#1	5103,99	**DGL#1**	**Lm**
	5117,27	3	7,23	DGL#1			
	5220,93	3	7,31	X			
	5242,8	4	8,1	SMART-C			
	5255,99	92	100	SMART-T	5255,99	**SMART-T**	
	5462,72	3	6,09	X			
Lm synt DGL#2	5700,01	3	11,8	X			
	5764,55	5	14,1	X			

	Peak mass	S/N	Relative intensity (%)	LOOKUP	Selection of peaks with S/N> 10 and Relative Intensity (%)>15	Assignment of Selected peaks	Parasite present in a sample regarding mass peak
	5800,53	67	80	DGL#2	5800,53	**DGL#2**	
	5814,25	6	14,8	DGL#2			
	5842,57	4	12,3	X			
	5941,41	6	13,9	SMART-C			
	5977,7	87	100	SMART-G	5977,7	**SMART-G**	
	6020,12	5	12,2	X			
	6186,3	3	8,85	X			

	Peak mass	S/N	Relative intensity (%)	LOOKUP	Selection of peaks with S/N> 10 and Relative Intensity (%)>15	Assignment of Selected peaks	Parasite present in a sample regarding mass peak
	4814,75	6	8,39	X			**Tb**
	4828,99	5	7,75	X			
Tb synt DGL#1	4981,11	3	7,24	X			
	5027,65	4	7,73	X			
	5069,36	10	12,8	X			
	5089,7	8	12,2	X			
	5104,02	140	100	DGL#1	5104,02	**DGL#1**	
	5118,5	13	15,6	DGL#1	5118,5	**DGL#1**	
	5130,17	5	10,1	X			
	5165,95	4	9,66	X			
	5206,08	14	15,9	X	5206,08	**X**	
	5226,93	8	12,1	X			
	5240,99	136	95,7	SMART-C	5240,99	**SMART-C**	
	5254,96	7	11,5	SMART-T			
	5280,15	4	8,7	SMART-G			
	5310,74	6	9,6	X			
	5329,39	6	8,57	X			
	5448,25	8	8,94	X			
	5465,28	7	7,91	X			
Tb synt DGL#2	5700,21	5	7,08	X			
	5722,49	5	7,14	X			
	5764,24	5	7,27	X			

Peak mass	S/N	Relative intensity (%)	LOOKUP	Selection of peaks with S/N> 10 and Relative Intensity (%)>15	Assignment of Selected peaks
5800	105	64,4	DGL#2	5800	**DGL#2**
5813,48	10	10	DGL#2		
5826,71	5	7,23	X		
5860,95	5	7,07	X		
5901,36	9	9,55	X		
5937,25	169	100	SMART-C	5937,25	**SMART-C**
5979,89	7	8,02	SMART-G		
6051,11	3	4,92	X		
6080,66	4	4,73	X		
6144	4	4,46	X		
6161,66	4	4,23	X		

	Peak mass	S/N	Relative intensity (%)	LOOKUP	Selection of peaks with S/N> 10 and Relative Intensity (%)>15	Assignment of Selected peaks	Parasite present in a sample regarding mass peak
	4813,82	24	5,34	X			**Tc**
Tc synt DGL#1	4829,29	28	6,07	X			
	4961,07	13	4,16	X			
	4980,76	13	4,19	X			
	5027,09	14	4,58	X			
	5068,66	57	11,2	X			
	5089,73	42	8,96	X			
	5103,32	626	100	DGL#1	5103,32	**DGL#1**	
	5142,37	16	4,74	X			
	5240,47	98	16,6	SMART-C	5240,47	**SMART-C**	
	5310,2	27	5,46	X			
	5328,29	18	3,71	X			
Tc synt DGL#2	5699,61	5	5,81	X			
	5724,72	4	5,27	X			
	5763,88	11	9,09	X			
	5799,68	191	100	DGL#2	5799,68	**DGL#2**	
	5827,27	7	6,89	X			
	5841,41	6	6,54	X			

	Peak mass	S/N	Relative intensity (%)	LOOKUP	Selection of peaks with S/N> 10 and Relative Intensity (%)>15	Assignment of Selected peaks	Parasite present in a sample regarding mass peak
	5900,72	4	4,96	X			
	5941,15	10	7,92	SMART-C			
	5976,95	152	78,9	SMART-G	5976,95	**SMART-G**	
	6005,84	5	5,29	X			
	6019,21	5	5,53	X			
	6049,11	3	3,82	X			
	6120,08	2	2,91	X			
	6183,61	3	3,34	X			

Table 46: Data extracted from the excel file used to identify the trypanosomatid specie. Raw mass peaks data are translated into an identity ('X' for unknown event, 'DGL#' for the DGL signal, 'SMART-NB' for the signal corresponding to the DGL whose abasic position has been filled by a specific SMART-NB). Then peaks with a certain threshold (S/N higher than 10 and Relative Intensity higher than 15%) are selected. The combination of the information obtained for both probes allow the identification of the parasite present in the sample.

	Peak mass	S/N	Relative intensity (%)	LOOKUP	Selection of peaks with S/N> 10 and Relative Intensity (%)>15	Assignment of Selected peaks	Parasite present in a sample regarding mass peak
Lm gen aPCR DGL#1	4813,82	7	3,51	X			**Lm**
	4830,92	14	5,38	X			
	5068,9	24	9,17	X			
	5089,9	17	7,22	X			
	5103,36	368	100	DGL#1	5103,36	**DGL#1**	
	5220,06	13	6,01	X			
	5241,55	11	5,5	SMART-C			
	5255,03	232	62,4	SMART-T	5255,03	**SMART-T**	
	5309,57	9	4,37	X			
	5325,9	6	3,21	X			
	5461,66	5	2,27	X			
Lm gen aPCR DGL#2	5764,52	3	11,8	X			
	5785,18	3	11,7	X			
	5799,98	38	69,5	DGL#2	5799,98	**DGL#2**	
	5816,35	3	12	DGL#2			

	Peak mass	S/N	Relative intensity (%)	LOOKUP	Selection of peaks with S/N> 10 and Relative Intensity (%)>15	Assignment of Selected peaks	Parasite present in a sample regarding mass peak
	5942,34	4	12,9	SMART-C			
	5977,33	58	100	SMART-G	5977,33	**SMART-G**	

	Peak mass	S/N	Relative intensity (%)	LOOKUP	Selection of peaks with S/N> 10 and Relative Intensity (%)>15	Assignment of Selected peaks	Parasite present in a sample regarding mass peak
Tb gen aPCR DGL#1	4813,73	3	8,03	X			**Tb**
	4829,17	3	7,7	X			
	5070,29	3	8,2	X			
	5103,65	72	73,4	DGL#1	5103,65	**DGL#1**	
	5116,82	4	9,7	DGL#1			
	5205,72	5	9,97	X			
	5240,57	102	100	SMART-C	5240,57	**SMART-C**	
	5256,2	6	11,6	SMART-T			
Tb gen aPCR DGL#2	5699,23	3	9,96	X			
	5724,94	3	9,82	X			
	5764,13	3	10,4	X			
	5799,78	58	71	DGL#2	5799,78	**DGL#2**	
	5813,48	5	12,5	DGL#2			
	5903,08	4	11	X			
	5937,01	84	100	SMART-C	5937,01	**SMART-C**	
	5952,07	4	10,3	SMART-T			
	5979,17	5	11,8	SMART-G			

	Peak mass	S/N	Relative intensity (%)	LOOKUP	Selection of peaks with S/N> 10 and Relative Intensity (%)>15	Assignment of Selected peaks	Parasite present in a sample regarding mass peak
Tc gen aPCR DGL#1	4813,74	10	5,61	X			**Tc**
	4828,34	5	3,66	X			
	5067,64	8	5,77	X			
	5088,19	10	6,29	X			
	5103,08	163	62,1	DGL#1	5103,08	**DGL#1**	

	5117,79	12	7,25	DGL#1		
	5205,49	18	9,29	X		
	5225,86	9	5,89	X		
	5240,02	273	100	SMART-C	5240,02	**SMART-C**
	5445,74	5	2,99	X		
	5464,95	4	2,47	X		
Tc gen aPCR DGL#2	5698,22	4	5,26	X		
	5763,92	8	7,97	X		
	5799,6	115	63,3	DGL#2	5799,6	**DGL#2**
	5812,99	8	7,53	DGL#2		
	5841,45	6	6,5	X		
	5902,99	4	5,8	X		
	5941,2	10	8,68	SMART-C		
	5976,92	189	100	SMART-G	5976,92	**SMART-G**
	6019,18	8	7,13	X		
	6119,72	3	3,87	X		
	6183,42	5	4,55	X		
	6202,04	3	3,63	X		

References

7. References

[1] D.A. Payne, L.E. Sower, Chapter 8: Alternative methods for amplified Nucleic Acid Testing, From Molecular Diagnostics for the Clinical Laboratorian. Second Edition. Section III: Molecular Diagnostics Techonologies, (2006) 75-84.

[2] A. Deshpande, P.S. White, Multiplexed nucleic acid-based assays for molecular diagnostics of human disease, Expert. Rev. Mol. Diagn., 12 (2012) 645-659.

[3] L. O'Connor, B. Glynn, Recent advances in the development of nucleic acid diagnostics, Expert. Rev. Med. Devices, 7 (2010) 529-539.

[4] M.G. Mauk, C. Liu, J. Song, H.H. Bau, Integrated Microfluidic Nucleic Acid Isolation, Isothermal Amplification, and Amplicon Quantification, Microarrays, 4 (2015) 474-489.

[5] S. Conoci, P.D. Pietro, S. Petralia, M.G. Amore, F.S. Biagio, G. Alaimo, G. Iacono, E. Alessi, D. Ricceri, G.D. Trapani, F.D. Francesco, M. Palmieri, Fast and Efficient Nucleic Acid Testing by ST's In-CheckTM Lab-on-Chip Platform, NSTI-Nanotech 2006, 2 (2006) 562-565.

[6] G. Heilek, Nucleic Acids — The Use of Nucleic Acid Testing in Molecular Diagnostics, (2016).

[7] R. Prakash, K. Pabbaraju, S. Wong, R. Tellier, K.V. Kaler, Integrated sample-to-detection chip for nucleic acid test assays, Biomedical microdevices, 18 (2016) 44.

[8] J.D. Watson, F.H.C. Crick, Molecular structure of nucleic acids: a structure for deoxyribose nucleic acid, Nature, 171 (1953) 737-738.

[9] L. H., B. A., Z. S.L., Molecular Cell Biology, in: N.Y.W.H. Freeman (Ed.), 2000, pp. Section 4.1. Structure of Nucleic acids.

[10] A. B, J. A, L. J, Molecular Biology of the Cell. The Structure and Function of DNA, in, New York: Garland Science, 2002, pp. The Structure and Function of DNA.

[11] E.T. Kool, Preorganization of DNA: Design Principles for Improving Nucleic Acid Recognition by Synthetic Oligonucleotides, Chem. Rev., 97 (1997) 1473-1487.

[12] H. Park, A. Germini, S. Sforza, R. Corradini, R. Marchelli, W. Knoll, Effect of ionic strength on PNA-DNA hybridization on surfaces and in solution, Biointerphases, 2 (2007) 80-88.

[13] S. Nakano, M. Fujii, N. Sugimoto, Use of nucleic Acid analogs for the study of nucleic Acid interactions, Journal of nucleic acids, 2011 (2011) 967098.

[14] S. Karkare, D. Bhatnagar, Promising nucleic acid analogs and mimics: characteristic features and applications of PNA, LNA, and morpholino, Applied microbiology and biotechnology, 71 (2006) 575-586.

[15] J. Micklefield, Backbone modification of Nucleic Acids: Synthesis, Structure and Therapeutic Applications, Current Medicinal Chemistry, 8 (2001) 1157-1179.

[16] R. Gambari, Peptide nucleic acids: a review on recent patents and technology transfer, Expert Opin. Ther. Patents, 24 (2014).

[17] J.M. Butler, P. Jiang-Baucom, M. Huang, P. Belgrader, J. Girard, Peptide Nucleic Acid characterization by MALDI-TOF mass spectrometry, Anal. Chem., 68 (1996) 3283-3287.

[18] G. He, S. Rapireddy, R. Bahal, B. Sahu, D.H. Ly, Strand Invasion of Extended, Mixed-Sequence B-DNA by γPNA, J. Am. Chem. Soc., 131 (2009) 12088-12090.

[19] N.T.S.D. Costa, J.M. Heemstra, Evaluating the Effect of Ionic Strength on Duplex Stability for PNA Having Negatively or Positively Charged Side Chains, PLoS ONE, 8 (2013).

[20] I. Sacui, W.C. Hsieh, A. Manna, B. Sahu, D.H. Ly, Gamma Peptide Nucleic Acids: As Orthogonal Nucleic Acid Recognition Codes for Organizing Molecular Self-Assembly, Journal of the American Chemical Society, 137 (2015) 8603-8610.

[21] J.M. Heemstra, D.R. Liu, Templated synthesis of Peptide Nucleic Acids via sequence-selective base-filling reactions, Journal of the American Chemical Society, 131 (2009) 11347-11349.

[22] A. S Khan, Rapid Advances in Nucleic Acid Technologies for Detection and Diagnostics of Pathogens, Journal of Microbiology & Experimentation, 1 (2014).

[23] E.M. Southern, U. Maskos, J.K. Elder, Analyzing and Comparing Nucleic Acid Sequences by hybridization to arrays of oligonucleotides: evaluation using experimental models, Genomics, 13 (1992) 1008-1017.

[24] M.J. Wolcott, Advances in Nucleic Acid-Based Detection Methods, Clinical Microbiology Reviews, 5 (1992) 370-386.

[25] A.C. Yu, G. Vatcher, X. Yue, Y. Dong, M.H. Li, P.H. Tam, P.Y. Tsang, A.K. Wong, M.H. Hui, B. Yang, H. Tang, L.T. Lau, Nucleic acid-based diagnostics for infectious diseases in public health affairs, Frontiers of medicine, 6 (2012) 173-186.

[26] I. Latorre, V. Saludes, J. Díez, A. Meyerhans, Techniques of Nucleic Acids-based diagnosis in the management of Bacterial and Viral Infectious Diseases, in: A.K.a.E. Meese (Ed.) Nucleic Acids as Molecular Diagnostics. First Edition., 2015, pp. 201-216.

[27] R. Higuchi, G. Dollinger, P.S. Walsh, R. Griffith, Simultaneous amplification and detection of specific DNA sequences, Bio/technology, 10 (1992) 413-417.

[28] L.M. Zanoli, G. Spoto, Isothermal amplification methods for the detection of nucleic acids in microfluidic devices, Biosensors, 3 (2013) 18-43.

[29] O. Piepenburg, C.H. Williams, D.L. Stemple, N.A. Armes, DNA detection using recombination proteins, PLoS biology, 4 (2006) e204.

[30] L.J. Kricka, Nucleic Acid Detection Technologies- Labels, strategies, and formats, Clinical Chemistry, 45 (1999) 453-458.

[31] M. Vaneechoutte, J.V. Eldere, The possibilities and limitations of nucleic acid amplification technology in diagnostic microbiology, J. Med. Microbiol., 46 (1997) 188-194.

[32] F.R. Bowler, J.J. Diaz-Mochon, M.D. Swift, M. Bradley, DNA analysis by dynamic chemistry, Angewandte Chemie, 49 (2010) 1809-1812.

[33] F.R. Bowler, P.A. Reid, A.C. Boyd, J.J. Diaz-Mochon, M. Bradley, Dynamic chemistry for enzyme-free allele discrimination in genotyping by MALDI-TOF mass spectrometry, Analytical Methods, 3 (2011) 1656.

[34] S. Pernagallo, G. Ventimiglia, C. Cavalluzzo, E. Alessi, H. Ilyine, M. Bradley, J.J. Diaz-Mochon, Novel biochip platform for nucleic acid analysis, Sensors, 12 (2012) 8100-8111.

[35] M. Bradley, J.J. Diaz-Mochón, Nucleobase characterisation, in: PCT/GB2008/003185, 2009.

[36] B. Boontha, J. Nakkuntod, N. Hirankarn, P. Chaumpluk, T. Vilaivan, Multiplex Mass Spectrometric Genotyping of Single Nucleotide Polimorphisms Employing Pyrrolidinyl Peptide Nucleic Acid in Combination with Ion-Exchange Capture, Anal. Chem., 80 (2008) 8178-8186.

[37] C. Vicentini, M. Fassan, E. D'Angelo, V. Corbo, N. Silvestris, G.J. Nuovo, A. Scarpa, Clinical application of microRNA testing in neuroendocrine tumors of the gastrointestinal tract, Molecules, 19 (2014) 2458-2468.

[38] Y. Shen, F. Tian, Z. Chen, R. Li, Q. Ge, Z. Lu, Amplification-based method for microRNA detection, Biosensors & bioelectronics, 71 (2015) 322-331.

[39] K. Jones, J.P. Nourse, C. Keane, A. Bhatnagar, M.K. Gandhi, Plasma microRNA are disease response biomarkers in classical Hodgkin lymphoma, Clinical cancer research : an official journal of the American Association for Cancer Research, 20 (2014) 253-264.

[40] C.E.S.E.a.F.J. Slack, The role of microRNAs in cancer, Yale Journal of Biology and Medecine, 79 (2006) 10.

[41] K.A. Cissell, S.K. Deo, Trends in microRNA detection, Analytical and bioanalytical chemistry, 394 (2009) 1109-1116.

[42] M. de Planell-Saguer, M.C. Rodicio, Analytical aspects of microRNA in diagnostics: a review, Analytica chimica acta, 699 (2011) 134-152.

[43] Y. Li, K.V. Kowdley, MicroRNAs in common human diseases, Genomics, proteomics & bioinformatics, 10 (2012) 246-253.

[44] A.M. Ardekani, M.M. Naeini, The role of microRNAs in Human Diseases, Avicenna J. Med. Biotech., 2 (2010) 161-179.

[45] R.E. Lanford, E.S. Hildebrandt-Eriksen, A. Petri, R. Persson, M. Lindow, M.E. Munk, S. Kauppinen, H. Ørum, Therapeutic Silencing of MicroRNA-122 in primates with Chronic Hepatitis C Virus Infection, Science, 327 (2010) 198-201.

[46] A.W. Wark, H.J. Lee, R.M. Corn, Multiplexed detection methods for profiling microRNA expression in biological samples, Angewandte Chemie, 47 (2008) 644-652.

[47] K.A. Cissell, S. Shrestha, S.K. Deo, microRNA detectection: challenges for the analytical chemist, Analytical chemistry, (2007) 4755-4761.

[48] W. Li, K. Ruan, MicroRNA detection by microarray, Analytical and bioanalytical chemistry, 394 (2009) 1117-1124.

[49] LorenzoFSempere, S. Freemantle, I. Pitha-Rowe, E. Moss, E. Dmitrovsky, V. Ambros, Expression profiling of mammalian microRNAs uncovers a subset of brain-expressed microRNAs with possible roles in murine and human neuronal differentiation, Genome Biology, 5 (2004).

[50] T. Babak, W. Zhang, Q. Morris, B.J. Blencowe, T.R. Hughes, Probing microRNAs with microarrays: tissue specificity and functional inference, Rna, 10 (2004) 1813-1819.

[51] J.M. Thomson, J. Parker, C.M. Perou, S.M. Hammond, A custom microarray platform for analysis of microRNA gene expression, Nature methods, 1 (2004) 47-53.

[52] J. Shingara, K. Keiger, J. Shelton, W. Laosinchai-Wolf, P. Powers, R. Conrad, D. Brown, E. Labourier, An optimized isolation and labeling platform for accurate microRNA expression profiling, Rna, 11 (2005) 1461-1470.

[53] R.Q. Liang, W. Li, Y. Li, C.Y. Tan, J.X. Li, Y.X. Jin, K.C. Ruan, An oligonucleotide microarray for microRNA expression analysis based on labeling RNA with quantum dot and nanogold probe, Nucleic acids research, 33 (2005) e17.

[54] P.T. Nelson, D.A. Baldwin, L.M. Scearce, J.C. Oberholtzer, J.W. Tobias, Z. Mourelatos, Microarray-based, high-throughput gene expression profiling of microRNAs, Nature methods, 1 (2004) 155-161.

[55] G.A. Calin, C.G. Liu, C. Sevignani, M. Ferracin, N. Felli, C.D. Dumitru, M. Shimizu, A. Cimmino, S. Zupo, M. Dono, M.L. Dell'Aquila, H. Alder, L. Rassenti, T.J. Kipps, F. Bullrich, M. Negrini, C.M. Croce, MicroRNA profiling reveals distinct signatures in B cell chronic lymphocytic leukemias, Proceedings of the National Academy of Sciences of the United States of America, 101 (2004) 11755-11760.

[56] C.G. Liu, G.A. Calin, B. Meloon, N. Gamliel, C. Sevignani, M. Ferracin, C.D. Dumitru, M. Shimizu, S. Zupo, M. Dono, H. Alder, F. Bullrich, M. Negrini, C.M. Croce, An oligonucleotide microchip for genome-wide microRNA profiling in human and mouse tissues, Proceedings of the National Academy of Sciences of the United States of America, 101 (2004) 9740-9744.

[57] Y. Sun, S. Koo, N. White, E. Peralta, C. Esau, N.M. Dean, R.J. Perera, Development of a micro-array to detect human and mouse microRNAs and characterization of expression in human organs, Nucleic acids research, 32 (2004) e188.

[58] S. Baskerville, D.P. Bartel, Microarray profiling of microRNAs reveals frequent coexpression with neighboring miRNAs and host genes, Rna, 11 (2005) 241-247.

[59] B. O, M. E, A. A, A. R, B. A, B. I, E. U, G. S, H. P, K. Y, L. EK, S. E, S. YM, S. M, B. Z, E. P., MicroRNA expression detected by oligonucleotide microarrays: System establishment and expression profiling in human tissues, Genome research, 14 2486-2494.

[60] G.J. Zhang, J.H. Chua, R.E. Chee, A. Agarwal, S.M. Wong, Label-free direct detection of MiRNAs with silicon nanowire biosensors, Biosensors & bioelectronics, 24 (2009) 2504-2508.

[61] Z. Gao, Y.H. Yu, Direct labeling microRNA with an electrocatalytic moiety and its application in ultrasensitive microRNA assays, Biosensors & bioelectronics, 22 (2007) 933-940.

[62] Z. Gao, Z. Yang, Detection of MicroRNAs Using Electrocatalytic Nanoparticle Tags, Analytical chemistry, 78 (2006) 1470-1477.

[63] K.A. Cissell, Y. Rahimi, S. Shrestha, E.A. Hunt, S.K. Deo, Bioluminescence-based detection of microRNA, miR21 in breast cancer cells, Analytical chemistry, 80 (2008) 2319-2325.

[64] J.D. Driskell, A.G. Seto, L.P. Jones, S. Jokela, R.A. Dluhy, Y.P. Zhao, R.A. Tripp, Rapid microRNA (miRNA) detection and classification via surface-enhanced Raman spectroscopy (SERS), Biosensors & bioelectronics, 24 (2008) 923-928.

[65] S. Fang, H.J. Lee, A.W. Wark, R.M. Corn, Attomole microarray detection of microRNAs by nanoparticle-amplified SPR imaging measurements of surface polyadenylation reactions, Journal of the American Chemical Society, 128 (2006) 14044-14046.

[66] L.A. Neely, S. Patel, J. Garver, M. Gallo, M. Hackett, S. McLaughlin, M. Nadel, J. Harris, S. Gullans, J. Rooke, A single-molecule method for the quantitation of microRNA gene expression, Nature methods, 3 (2006) 41-46.

[67] K.A. Cissell, S. Campbell, S.K. Deo, Rapid, single-step nucleic acid detection, Analytical and bioanalytical chemistry, 391 (2008) 2577-2581.

[68] K.A. Cissell, Y. Rahimi, S. Shrestha, S.K. Deo, Reassembly of a bioluminescent protein Renilla luciferase directed through DNA hybridization, Bioconjugate Chem., 20 (2009) 15-19.

[69] A. Etheridge, I. Lee, L. Hood, D. Galas, K. Wang, Extracellular microRNA: A new source of biomarkers, Mutation Research/Fundamental and Molecular Mechanisms of Mutagenesis, 717 (2011) 85-90.

[70] V.K. Velu, R. Ramesh, A.R. Srinivasan, Circulating MicroRNAs as Biomarkers in Health and Disease, Journal of clinical and diagnostic research : JCDR, 6 (2012) 1791-1795.

[71] D. Madhavan, K. Cuk, B. Burwinkel, R. Yang, Cancer diagnosis and prognosis decoded by blood-based circulating microRNA signatures, Frontiers in genetics, 4 (2013) 116.

[72] A.L. Oom, B.A. Humphries, C. Yang, MicroRNAs: novel players in cancer diagnosis and therapies, BioMed research international, 2014 (2014) 959461.

[73] G. Bertoli, C. Cava, I. Castiglioni, MicroRNAs: New Biomarkers for Diagnosis, Prognosis, Therapy Prediction and Therapeutic Tools for Breast Cancer, Theranostics, 5 (2015) 1122-1143.

[74] C. Blenkiron, E.A. Miska, miRNAs in cancer: approaches, aetiology, diagnostics and therapy, Human molecular genetics, 16 (2007) R106-113.

[75] C. Price, J. Chen, MicroRNAs in Cancer Biology and Therapy: Current Status and Perspectives, Genes & diseases, 1 (2014) 53-63.

[76] T.G. Angelini, C. Emanueli, MicroRNAs as clinical biomarkers?, Frontiers in genetics, 6 (2015) 4.

[77] Z. Guo, C. Zhao, Z. Wang, MicroRNAs as ideal biomarkers for the diagnosis of lung cancer, Tumour biology : the journal of the International Society for Oncodevelopmental Biology and Medicine, 35 (2014) 10395-10407.

[78] G. Cheng, Circulating miRNAs: roles in cancer diagnosis, prognosis and therapy, Advanced drug delivery reviews, 81 (2015) 75-93.

[79] C.L. Jopling, Liver-specific microRNA-122: Biogenesis and function, RNA Biology, 9 (2012) 1-6.

[80] U.o.M. Griffiths-Jones lab at the Faculty of Life Sciences, http://www.mirbase.org/cgi-bin/mirna_entry.pl?acc=MI0000442; miRBase: the microRNA data base, in.

[81] D.J. Antoine, J.W. Dear, P.S. Lewis, V. Platt, J. Coyle, M. Masson, R.H. Thanacoody, A.J. Gray, D.J. Webb, J.G. Moggs, D.N. Bateman, C.E. Goldring, B.K. Park, Mechanistic biomarkers provide early and sensitive detection of acetaminophen-induced acute liver injury at first presentation to hospital, Hepatology, 58 (2013) 777-787.

[82] P.J. Starkey Lewis, J. Dear, V. Platt, K.J. Simpson, D.G. Craig, D.J. Antoine, N.S. French, N. Dhaun, D.J. Webb, E.M. Costello, J.P. Neoptolemos, J. Moggs, C.E. Goldring, B.K. Park, Circulating microRNAs as potential markers of human drug-induced liver injury, Hepatology, 54 (2011) 1767-1776.

[83] X. Ding, J. Ding, J. Ning, F. Yi, J. Chen, D. Zhao, J. Zheng, Z. Liang, Z. Hu, Q. Du, Circulating microRNA-122 as a potential biomarker for liver injury, Molecular medicine reports, 5 (2012) 1428-1432.

[84] A.D. Vliegenthart, J.M. Shaffer, J.I. Clarke, L.E. Peeters, A. Caporali, D.N. Bateman, D.M. Wood, P.I. Dargan, D.G. Craig, J.K. Moore, A.I. Thompson, N.C. Henderson, D.J. Webb, J. Sharkey, D.J. Antoine, B.K. Park, M.A. Bailey, E. Lader, K.J. Simpson, J.W. Dear, Comprehensive microRNA profiling in acetaminophen toxicity identifies novel circulating biomarkers for human liver and kidney injury, Scientific reports, 5 (2015) 15501.

[85] R. Kia, L. Kelly, R.L. Sison-Young, F. Zhang, C.S. Pridgeon, J.A. Heslop, P. Metcalfe, N.R. Kitteringham, M. Baxter, S. Harrison, N.A. Hanley, Z.D. Burke, M.P. Storm, M.J. Welham, D.

Tosh, B. Kuppers-Munther, J. Edsbagge, P.J. Starkey Lewis, F. Bonner, E. Harpur, J. Sidaway, J. Bowes, S.W. Fenwick, H. Malik, C.E. Goldring, B.K. Park, MicroRNA-122: a novel hepatocyte-enriched in vitro marker of drug-induced cellular toxicity, Toxicological sciences : an official journal of the Society of Toxicology, 144 (2015) 173-185.

[86] J.W. Dear, J.I. Clarke, B. Francis, L. Allen, J. Wraight, J. Shen, P.I. Dargan, D. Wood, J. Cooper, S.H.L. Thomas, A.L. Jorgensen, M. Pirmohamed, B.K. Park, D.J. Antoine, Risk stratification after paracetamol overdose using mechanistic biomarkers: results from two prospective cohort studies, The Lancet Gastroenterology & Hepatology, (2017).

[87] J.W. Dear, D.J. Antoine, P. Starkey-Lewis, C.E. Goldring, B.K. Park, Early detection of paracetamol toxicity using circulating liver microRNA and markers of cell necrosis, British journal of clinical pharmacology, 77 (2014) 904-905.

[88] K. Kang;, X. Peng;, J. Luo;, D. Gou, Identification of circulating miRNA biomarkers based on global quantitative real-time PCR profiling, Journal of Animal Science and Biotechnology, 3 (2012) 9.

[89] J.V. Tricoli, J.W. Jacobson, MicroRNA: Potential for Cancer Detection, Diagnosis, and Prognosis, Cancer research, 67 (2007) 4553-4555.

[90] H. Arata;, H. Komatsu;, K. Hosokawa;, M. Maeda, Rapid and Sensitive MicroRNA Detection with Laminar Flow-Assisted Dendritic Amplification on Power-Free Microfluidic Chip, PLOS ONE, 7 (2013) 6.

[91] G.K. Geiss, R.E. Bumgarner, B. Birditt, T. Dahl, N. Dowidar, D.L. Dunaway, H.P. Fell, S. Ferree, R.D. George, T. Grogan, J.J. James, M. Maysuria, J.D. Mitton, P. Oliveri, J.L. Osborn, T. Peng, A.L. Ratcliffe, P.J. Webster, E.H. Davidson, L. Hood, K. Dimitrov, Direct multiplexed measurement of gene expression with color-coded probe pairs, Nature biotechnology, 26 (2008) 317-325.

[92] T. Ueno;, T. Funatsu, Label-Free Quantification of MicroRNAs Using Ligase-Assisted Sandwich Hybridization on a DNA Microarray, PLoS ONE, 9 (2014) 7.

[93] T. Wang, E. Viennois, D. Merlin, G. Wang, Microelectrode miRNA sensors enabled by enzymeless electrochemical signal amplification, Analytical chemistry, 87 (2015) 8173-8180.

[94] P.S. Laopa, T. Vilaivan, V.P. Hoven, Positively charged polymer brush-functionalized filter paper for DNA sequence determination following Dot blot hybridization employing a pyrrolidinyl peptide nucleic acid probe, The Analyst, 138 (2013) 269-277.

[95] J. Jin, M. Cid, C.B. Poole, L.A. McReynolds, Protein mediated miRNA detection and siRNA enrichment using p19, BioTechniques, 48 (2010) xvii-xxiii.

[96] H. Yang, A. Hui, G. Pampalakis, L. Soleymani, F.F. Liu, E.H. Sargent, S.O. Kelley, Direct, electronic microRNA detection for the rapid determination of differential expression profiles, Angewandte Chemie, 48 (2009) 8461-8464.

[97] S. Campuzano;, R.M. Torrente-Rodríguez;, E. López-Hernádez;, Felipe Conzuelo, R. Granados;, J.M. Sánchez-Puelles;, J.M. Pingarrón, Magnetobiosensors based on viral protein p19 for microRNA determination in cancer cells and tissues, Angewandte Chemie International Edition, 53 (2014) 6168-6171.

[98] J. He, J. Zhu, C. Gong, J. Qi, H. Xiao, B. Jiang, Y. Zhao, Label-Free Direct Detection of miRNAs with Poly-Silicon Nanowire Biosensors, PLoS One, 10 (2015) e0145160.

[99] T. Kilic, M. Kaplan, S. Demiroglu, A. Erdem, M. Ozsoz, Label-Free Electrochemical Detection of MicroRNA-122 in Real Samples by Graphene Modified Disposable Electrodes, Journal of The Electrochemical Society, 163 (2016) B227-B233.

[100] P.D. Stephen Angeloni, B.A. Robert Cordes, P.D. Sherry Dunbar, B.A. Carlos Garcia, P.D. Grant Gibson, P.D. Charles Martin, M.S. Valerie Stone, C.T. (A.S.C.P.), xMAP Cookbook: A collection of methods and protocols for developing multiplex assays with xMAP Technology, (2014).

[101] J.J.L. Tan, M. Capozzoli, M. Sato, W. Watthanaworawit, C.L. Ling, M. Mauduit, B. Malleret, A.-C. Grüner, R.T.F.H. Nosten, G. Snounou, L. Rénia, L.F.P. Ng, An Integrated Lab-on-Chip for Rapid Identification and Simultaneous Differentiation of Tropical Pathogens, PloS Neglected Tropical Diseases, 8.

[102] S. Petralia, R. Verardo, E. Klaric, S. Cavallaro, E. Alessi, C. Schneider, In-Check system: A highly integrated silicon Lab-on-Chip for sample preparation, PCR amplification and microarray detection of nucleic acids directly from biological samples, Sensors and Actuators B: Chemical, 187 (2013) 99-105.

[103] Y. Xue, M.L. O'Mara, P.P. Surawski, M. Trau, A.E. Mark, Effect of poly(ethylene glycol) (PEG) spacers on the conformational properties of small peptides: a molecular dynamics study, Langmuir : the ACS journal of surfaces and colloids, 27 (2011) 296-303.

[104] G. He;, S. Rapireddy;, R. Bahal;, B. Sahu;, D.H. Ly, Strand Invasion of Extended, Mixed-Sequence B-DNA by γPNAs, Journal of American Chemical Society, 131 (2009) 12088-12090.

[105] H.H. Pham, C.T. Murphy, G. Sureshkumar, D.H. Ly, P.L. Opresko, B.A. Armitage, Cooperative hybridization of gammaPNA miniprobes to a repeating sequence motif and application to telomere analysis, Organic & biomolecular chemistry, 12 (2014) 7345-7354.

[106] A. Panomics, http://cdn.panomics.com/products/luninex-assays/technical-overview/how-it-works; Luminex assays: how it works?, in, pp. Luminex assays and technology description.

[107] E. Socher, L. Bethge, A. Knoll, N. Jungnick, A. Herrmann, O. Seitz, Low-noise stemless PNA beacons for sensitive DNA and RNA detection, Angewandte Chemie, 47 (2008) 9555-9559.

[108] H. Kuhn;, V.V. Demidov;, J.M. Coull;, M.J. Fiandaca;, B.D. Gildea;, M.D. Frank-Kamenetskii, Hybridization of DNA and PNA Molecular Beacons to single-stranded and double-stranded DNA targets, Journal of the American Chemical Society, 124 (2002) 1097-1103.

[109] R. Bahal;, E. Quijano;, N.A. McNeer;, Y. Liu;, D.C. Bhunia;, F. López-Giráldez;, R.J. Fields;, W.M. Saltzman;, D.H. Ly;, P.M. Glazer, Single-stranded yPNAs for In Vivo Site-Specific genome editing Watson Crick recognition, Curr Gene Ther., 14 (2014) 331-342.

[110] J.C. McCrae, N. Sharkey, D.J. Webb, A.D. Vliegenthart, J.W. Dear, Ethanol consumption produces a small increase in circulating miR-122 in healthy individuals, Clinical toxicology, 54 (2016) 53-55.

[111] S. Venkateswaran, M.A. Luque-Gonzalez, M. Tabraue-Chavez, M.A. Fara, B. Lopez-Longarela, V. Cano-Cortes, F.J. Lopez-Delgado, R.M. Sanchez-Martin, H. Ilyine, M. Bradley, S. Pernagallo, J.J. Diaz-Mochon, Novel bead-based platform for direct detection of unlabelled nucleic acids through Single Nucleobase Labelling, Talanta, 161 (2016) 489-496.

[112] M.E. Bienenmann-Ploum, U. Vincent, K. Campbell, A.C. Huet, W. Haasnoot, P. Delahaut, L.A. Stolker, C.T. Elliott, M.W. Nielen, Single-laboratory validation of a multiplex flow cytometric immunoassay for the simultaneous detection of coccidiostats in eggs and feed, Analytical and bioanalytical chemistry, 405 (2013) 9571-9577.

[113] S.K. Fischer, A. Joyce, M. Spengler, T.Y. Yang, Y. Zhuang, M.S. Fjording, A. Mikulskis, Emerging technologies to increase ligand binding assay sensitivity, The AAPS journal, 17 (2015) 93-101.

[114] C.W. Kan, A.J. Rivnak, T.G. Campbell, T. Piech, D.M. Rissin, M. Mosl, A. Peterca, H.P. Niederberger, K.A. Minnehan, P.P. Patel, E.P. Ferrell, R.E. Meyer, L. Chang, D.H. Wilson, D.R. Fournier, D.C. Duffy, Isolation and detection of single molecules on paramagnetic beads using

sequential fluid flows in microfabricated polymer array assemblies, Lab on a chip, 12 (2012) 977-985.

[115] D.M. Rissin, D.R. Fournier, T. Piech, C.W. Kan, T.G. Campbell, L. Song, L. Chang, A.J. Rivnak, P.P. Patel, G.K. Provuncher, E.P. Ferrell, S.C. Howes, B.A. Pink, K.A. Minnehan, D.H. Wilson, D.C. Duffy, Simultaneous detection of single molecules and singulated ensembles of molecules enables immunoassays with broad dynamic range, Analytical chemistry, 83 (2011) 2279-2285.

[116] D.R. Walt, Optical methods for single molecule detection and analysis, Analytical chemistry, 85 (2013) 1258-1263.

[117] D.M. Rissin, C.W. Kan, L. Song, A.J. Rivnak, M.W. Fishburn, Q. Shao, T. Piech, E.P. Ferrell, R.E. Meyer, T.G. Campbell, D.R. Fournier, D.C. Duffy, Multiplexed single molecule immunoassays, Lab on a chip, 13 (2013) 2902-2911.

[118] D.H. Wilson, D.M. Rissin, C.W. Kan, D.R. Fournier, T. Piech, T.G. Campbell, R.E. Meyer, M.W. Fishburn, C. Cabrera, P.P. Patel, E. Frew, Y. Chen, L. Chang, E.P. Ferrell, V. von Einem, W. McGuigan, M. Reinhardt, H. Sayer, C. Vielsack, D.C. Duffy, The Simoa HD-1 Analyzer: A Novel Fully Automated Digital Immunoassay Analyzer with Single-Molecule Sensitivity and Multiplexing, Journal of laboratory automation, 21 (2016) 533-547.

[119] D.M. Rissin, C.W. Kan, T.G. Campbell, S.C. Howes, D.R. Fournier, L. Song, T. Piech, P.P. Patel, L. Chang, A.J. Rivnak, E.P. Ferrell, J.D. Randall, G.K. Provuncher, D.R. Walt, D.C. Duffy, Single-molecule enzyme-linked immunosorbent assay detects serum proteins at subfemtomolar concentrations, Nature biotechnology, 28 (2010) 595-599.

[120] D.M. Rissin, B. Lopez-Longarela, S. Pernagallo, H. Ilyine, A.D.B. Vliegenthart, J.W. Dear, J.J. Diaz-Mochon, D.C. Duffy, Polymerase-free measurement of microRNA-122 with single base specificity using single molecule arrays: Detection of drug-induced liver injury, PLoS One, 12 (2017) e0179669.

[121] L. Song, D. Shan, M. Zhao, B.A. Pink, K.A. Minnehan, L. York, M. Gardel, S. Sullivan, A.F. Phillips, R.B. Hayman, D.R. Walt, D.C. Duffy, Direct detection of bacterial genomic DNA at sub-femtomolar concentrations using single molecule arrays, Analytical chemistry, 85 (2013) 1932-1939.

[122] A. Ricciardi, M. Ndao, Diagnosis of parasitic infections: what's going on?, Journal of biomolecular screening, 20 (2015) 6-21.

[123] R. Duncan, Advancing molecular diagnostics for trypanosomatid parasites, The Journal of molecular diagnostics : JMD, 16 (2014) 379-381.

[124] C. Hernández, J.D. Ramírez, <Molecular Diagnosis of Vector-Borne Parasitic Diseases.pdf>, Air and Water Borne Diseases, 2 (2013).

[125] A.H. Lopes, T. Souto-Padrón, F.A. Dias, M.T. Gomes, G.C. Rodrigues, L.T. Zimmermann, T.L. Alves e Silva, A.B. Vermelho, Trypanosomatids Odd Organisms Devastating Diseases, The Open Parasitology Journal, 4 (2010) 30-59.

[126] C. Sanchez-Ovejero, F. Benito-Lopez, P. Diez, A. Casulli, M. Siles-Lucas, M. Fuentes, R. Manzano-Roman, Sensing parasites: Proteomic and advanced bio-detection alternatives, Journal of proteomics, 136 (2016) 145-156.

[127] M.A. Saeed, A. Jabbar, 'Smart Diagnosis' of Parasites using Smartphones, Journal of clinical microbiology, (2017).

[128] J.E. Rosenblatt, Laboratory diagnosis of infections due to blood and tissue parasites, Clinical infectious diseases : an official publication of the Infectious Diseases Society of America, 49 (2009) 1103-1108.

[129] V.S. Garcia, V.D.G. Gonzalez, L. Gugliotta, A. Burna, A. Demonte, D.G. Arias, M.S. Cabeza, S.A. Guerrero, Development of a simple and economical diagnostic test for canine leishmaniasis, Experimental parasitology, 182 (2017) 9-15.

[130] M.Z. Troncarelli, J.B. Camargo, J.G. Machado, S.B. Lucheis, H. Langoni, Leishmania spp. and/or Trypanosoma cruzi diagnosis in dogs from endemic and nonendemic areas for canine visceral leishmaniasis, Veterinary parasitology, 164 (2009) 118-123.

[131] A. Selvapandiyan, K. Stabler, N.A. Ansari, S. Kerby, J. Riemenschneider, P. Salotra, R. Duncan, H.L. Nakhasi, A Novel Semiquantitative Fluorescence-Based Multiplex Polymerase Chain Reaction Assay for Rapid Simultaneous Detection of Bacterial and Parasitic Pathogens from Blood, The Journal of Molecular Diagnostics, 7 (2005) 268-275.

[132] E. Torres-Guerrero, M.R. Quintanilla-Cedillo, J. Ruiz-Esmenjaud, R. Arenas, Leishmaniasis: a review, F1000Research, 6 (2017) 750.

[133] B. Alemayehu, M. Alemayehu, Leishmaniasis: A Review on Parasite, Vector and Reservoir Host, Health Science Journal, 11 (2017).

[134] J. Bonnet, C. Boudot, B. Courtioux, Overview of the Diagnostic Methods Used in the Field for Human African Trypanosomiasis: What Could Change in the Next Years?, BioMed research international, 2015 (2015).

[135] P. Büscher, G. Cecchi, V. Jamonneau, G. Priotto, Human African trypanosomiasis, The Lancet, (2017).

[136] M.E.M. Contreras, Chagas Disease: A Parasitic Infection with More than 100 Years of Discovery, Advanced Techniques in Clinical Microbiolog, 1 (2017).

[137] E.C. Mattos, C.D.S. Meira-Strejevitch, M.A.M. Marciano, C.C. Faccini, A.M. Lourenco, V.L. Pereira-Chioccola, Molecular detection of Trypanosoma cruzi in acai pulp and sugarcane juice, Acta tropica, 176 (2017) 311-315.

[138] J.A. Pérez-Molina, I. Molina, Chagas disease, The Lancet, (2017).

[139] A. Abras, C. Munoz, C. Ballart, P. Berenguer, T. Llovet, M. Herrero, S. Tebar, M.J. Pinazo, E. Posada, C. Marti, V. Fumado, J. Bosch, O. Coll, T. Juncosa, G. Ginovart, J. Armengol, J. Gascon, M. Portus, M. Gallego, Towards a New Strategy for Diagnosis of Congenital Trypanosoma cruzi Infection, Journal of clinical microbiology, 55 (2017) 1396-1407.

[140] R.T. Barnard, R.A. Hall, E.A. Gould, Expecting the unexpected: nucleic acid-based diagnosis and discovery of emerging viruses Expert. Rev. Mol. Diagn., 11 (2011) 409-423.

[141] A.M. Caliendo, D.N. Gilbert, C.C. Ginocchio, K.E. Hanson, L. May, T.C. Quinn, F.C. Tenover, D. Alland, A.J. Blaschke, R.A. Bonomo, K.C. Carroll, M.J. Ferraro, L.R. Hirschhorn, W.P. Joseph, T. Karchmer, A.T. MacIntyre, L.B. Reller, A.F. Jackson, A. Infectious Diseases Society of, Better tests, better care: improved diagnostics for infectious diseases, Clinical infectious diseases : an official publication of the Infectious Diseases Society of America, 57 Suppl 3 (2013) S139-170.

[142] M. Ndao, Diagnosis of parasitic diseases: old and new approaches, Interdisciplinary perspectives on infectious diseases, 2009 (2009) 278246.

[143] K. Ranjan, P. Minakshi, G. Prasad, Application of Molecular and Serological Diagnostics in Veterinary Parasitology, The Journal of Advances in Parasitology, 2 (2016) 80-99.

[144] C. Cantacessi, F. Dantas-Torres, M.J. Nolan, D. Otranto, The past, present, and future of Leishmania genomics and transcriptomics, Trends in parasitology, 31 (2015) 100-108.

[145] D.D. Giusto, G.C. King, Single base extension (SBE) proofreading polymerases and phosphorothioate primers: improved fidelity in single-substrate assays, Nucleic Acid Research, 31 (2003) 12.

[146] J.B. Weiss, DNA probes and PCR for diagnosis of parasitic infections, Clinical Microbiology Reviews, 8 (1995) 113-130.

[147] P. Srivastava, S. Mehrotra, P. Tiwary, J. Chakravarty, S. Sundar, Diagnosis of Indian Visceral Leishmaniasis by Nucleic Acid Detection Using PCR, PLoS ONE, 6 (2011).

[148] A.L. Torres-Machorro, R. Hernandez, A.M. Cevallos, I. Lopez-Villasenor, Ribosomal RNA genes in eukaryotic microorganisms: witnesses of phylogeny?, FEMS microbiology reviews, 34 (2010) 59-86.

[149] N.M. El-Sayed, P.J. Myler, D.C. Bartholomeu, D. Nilsson, G. Aggarwal, A.-N. Tran, E. Ghedin, E.A. Worthey, A.L. Delcher, G. Blandin, S.J. Westenberger, E. Caler, G.C. Cerqueira, C. Branche, B. Hass, A. Anupama, E. Arner, L. Aslund, P. Attipoe, E. Bontempi, F. Bringaud, P. Burton, E. Cadag, D.A. Campbell, M. Carrington, J. Crabtree, H. Darban, J.F.d. Silveira, P.d. Jong, K. Edwards, P.T. Englund, G. Fazelina, T. Feldblyum, M. Ferella, A.C. Frasch, K. Gull, D. Horn, L. Hou, Y. Huang, E. Kindlund, M. Klingbeil, S. Kluge, H. Koo, D. Lacerda, M.J. Levin, H. Lorenzi, T. Louie, C.R. Machado, R. McCulloch, A. McKenna, Y. Mizuno, J.C. Mottram, S. Nelson, S. Ochaya, K. Osoegawa, G. Pai, M. Parsons, M. Pentony, U. Pettersson, M. Pop, J.L. Ramirez, J. Rinta, L. Robertson, S.L. Salzberg, D.O. Sanchez, A. Seyler, R. Sharma, J. Shetty, A.J. Simpson, E. Sisk, M.T. Tammi, R. Tarleton, S. Teixeira, S.V. Aken, C. Vogt, P.N. Ward, B. Wickstead, J. Wortman, O. White, C.M. Fraser, K.D. Stuart, B. Andersson, The Genome Sequence of Trypanosoma cruzi, Etiologic Agent of Chagas Disease, Science, 309 (2005) 409-415.

[150] J.A. Lake, V.F. De La Cruz, P.C.G. Ferreira, C. Morel, L. Simpson, Evolution of parasitism: kinetoplastid protozoan history reconstructed from mitochondrial rRNA gene sequences, Proc. Natl. Acad. Sci. USA, 85 (1988) 4779-4783.

[151] A.P. Fernandes, K. Nelson, S.M. Beverley, Evolution of nuclear ribosomal RNAs in kinetoplastid protozoa: Perspectives on the age and origins of parasitism, Proc. Natl. Acad. Sci. USA, 90 (1993) 11608-11612.

[152] W. Deng, D. Xi, H. Mao, M. Wanapat, The use of molecular techniques based on ribosomal RNA and DNA for rumen microbial ecosystem studies: a review, Molecular biology reports, 35 (2008) 265-274.

[153] S.M. Thumbi, F.A. McOdimba, R.O. Mosi, J.O. Jung'a, Comparative evaluation of three PCR base diagnostic assays for the detection of pathogenic trypanosomes in cattle blood, Parasites & vectors, 1 (2008) 46.

[154] M. van Puijenbroek, J.W.F. Dierssen, P. Stanssens, R. van Eijk, A.M. Cleton-Jansen, T. van Wezel, H. Morreau, Mass Spectrometry-Based Loss of Heterozygosity Analysis of Single-Nucleotide Polymorphism Loci in Paraffin Embedded Tumors Using the MassEXTEND Assay, The Journal of Molecular Diagnostics, 7 (2005) 623-630.

[155] E.N. Ilina, A.D. Borovskaya, M.M. Malakhova, V.A. Vereshchagin, A.A. Kubanova, A.N. Kruglov, T.S. Svistunova, A.O. Gazarian, T. Maier, M. Kostrzewa, V.M. Govorun, Direct bacterial profiling by matrix-assisted laser desorption-ionization time-of-flight mass spectrometry for identification of pathogenic Neisseria, The Journal of molecular diagnostics : JMD, 11 (2009) 75-86.

[156] W. Thongnoppakhun, S. Jiemsup, S. Yongkiettrakul, C. Kanjanakorn, C. Limwongse, P. Wilairat, A. Vanasant, N. Rungroj, P.T. Yenchitsomanus, Simple, efficient, and cost-effective multiplex genotyping with matrix assisted laser desorption/ionization time-of-flight mass spectrometry of hemoglobin beta gene mutations, The Journal of molecular diagnostics : JMD, 11 (2009) 334-346.

[157] D.H. Farkas, N.E. Miltgen, J. Stoerker, D. van den Boom, W.E. Highsmith, L. Cagasan, R. McCullough, R. Mueller, L. Tang, J. Tynan, C. Tate, A. Bombard, The suitability of matrix assisted laser desorption/ionization time of flight mass spectrometry in a laboratory developed test using cystic fibrosis carrier screening as a model, The Journal of molecular diagnostics : JMD, 12 (2010) 611-619.

[158] S. Yang, L. Xu, H.M. Wu, Rapid genotyping of single nucleotide polymorphisms influencing warfarin drug response by surface-enhanced laser desorption and ionization time-of-flight (SELDI-TOF) mass spectrometry, The Journal of molecular diagnostics : JMD, 12 (2010) 162-168.

[159] S. Schubert, K. Weinert, C. Wagner, B. Gunzl, A. Wieser, T. Maier, M. Kostrzewa, Novel, improved sample preparation for rapid, direct identification from positive blood cultures using matrix-assisted laser desorption/ionization time-of-flight (MALDI-TOF) mass spectrometry, The Journal of molecular diagnostics : JMD, 13 (2011) 701-706.

[160] P.R. Murray, What is new in clinical microbiology-microbial identification by MALDI-TOF mass spectrometry: a paper from the 2011 William Beaumont Hospital Symposium on molecular pathology, The Journal of molecular diagnostics : JMD, 14 (2012) 419-423.

[161] M. Angélica Luque-González, M. Tabraue-Chávez, B. López-Longarela, R. María Sánchez-Martín, M. Ortiz-González, M. Soriano-Rodríguez, J. Antonio García-Salcedo, S. Pernagallo, J. José Díaz-Mochón, Identification of Trypanosomatids by detecting Single Nucleotide Fingerprints using DNA analysis by dynamic chemistry with MALDI-ToF, Talanta, 176 (2018) 299-307.

[162] N. Singhal, M. Kumar, P.K. Kanaujia, J.S. Virdi, MALDI-TOF mass spectrometry: an emerging technology for microbial identification and diagnosis, Frontiers in microbiology, 6 (2015) 15.

[163] J. Kathleen Lewis, Jing Wei, G. Siuzdak, Matrix-assisted Laser Desorption/Ionization Mass Spectrometry in Peptide and Protein Analysis, Encyclopedia of Analytical Chemistry, (2000) 5880-5894.

[164] P. Ross, L. Hall, I. Smirnov, L. Haff, High level of genotyping by MALDI-TOF mass spectrometry, Nature biotechnology, 16 (1998) 1347-1351.

[165] P. Jiang-Baucom, J.E. Girard, DNA Typing of Human Leukocyte Antigen Sequence Polymorphisms by Peptide Nucleic Acid Probes and MALDI-TOF Mass Spectrometry, Anal. Chem., 69 (1997) 4894-4898.

[166] T.J. Griffin, W. Tang, L.M. Smith, Genetic analysis by peptide nucleic acid affinity MALDI-TOF mass spectrometry, Nature biotechnology, 15 (1997) 1368-1372.

[167] O. Bauer, A. Guerasimova, S. Sauer, S. Thamm, M. Steinfath, R. Herwig, M. Janitz, H. Lehrach, U. Radelof, Multiplexed hybridizations of positively charge-tagged peptide nucleic acids detected by matrix-assisted laser desorption/ionization time-of-flight mass spectrometry, Rapid communications in mass spectrometry : RCM, 18 (2004) 1821-1829.

[168] P. Schatz, J. Distler, K. Berlin, M. Schuster, Novel method for high throughput DNA methylation marker evaluation using PNA-probe library hybridization and MALDI-TOF detection, Nucleic acids research, 34 (2006) e59.

[169] S. Ficht, A. Mattes, O. Seitz, Single-Nucleotide-Specific PNA−Peptide Ligation on Synthetic and PCR DNA Templates, Journal of the American Chemical Society, 126 (2004).

[170] A. Mattes, O. Seitz, Mass-Spectrometric Monitoring of a PNA-based ligation reaction for the multiplex detection of DNA Single-Nucleotide polymorphism, Angew Chem Int Ed, 40 (2001) 3178-3181.

[171] I. Boll, R. Krämer, J. Brunner, A. Mokhir, Templated Metal Catalysis for Single Nucleotide Specific DNA Sequence Detection, Journal of the American Chemical Society, 127 (2005) 7849-7856.

[172] B. Boontha, J. Nakkuntod, N. Hirankarn, P. Chaumpluk, T. Vilaivan, Multiplex Mass Spectrometric Genotyping of Single Nucleotide Polymorphisms Employing

Pyrrolidinyl Peptide Nucleic Acid in Combination with Ion-Exchange Capture, Anal. Chem., 80 (2008) 8178-8186.

[173] E.M.B.L. EMBL-EBI, http://www.ebi.ac.uk/Tools/msa/clustalo/; Clustal Omega, multiple sequence alignment program, in, pp. Online tool for multiple sequence alignment, generate alignments between three or more sequences.

[174] T.F. Scientific, https://www.thermofisher.com/us/en/home/products-and-services/product-types/primers-oligos-nucleotides/invitrogen-custom-dna-oligos/primer-design-tools.html; Primer design tips and tools, in, pp. Online tool and tips for primer design.

[175] I.I.D. technologies, https://eu.idtdna.com/calc/analyzer; OligoAnalyzer 3.1, in, pp. Online tool for analyzing sequences and studying self-dimer, hetero-dimer and hairpin formation.

[176] T.F. Scientific, https://www.thermofisher.com/order/catalog/product/K0171; Thermo Scientific PCR Master Mix, in, pp. Thermo Scientific PCR Master Mix Catalog.

[177] T.F. Scientific, https://www.thermofisher.com/us/en/home/brands/thermo-scientific/molecular-biology/molecular-biology-learning-center/molecular-biology-resource-library/thermo-scientific-web-tools/dna-copy-number-calculator.html; DNA copy number and dilution calculator, in, pp. Online tool for calculating the concentration of a stock DNA solution and dilute it to a desired concentration (copies/μL).

[178] A.C. Ivens, C.S. Peacock, E.A. Worthey, L. Murphy, Gautam Aggarwal, Matthew Berriman, Ellen Sisk, Marie-Adele Rajandream, Ellen Adlem, Rita Aert, Atashi Anupama, Zina Apostolou, Philip Attipoe, Nathalie Bason, Christopher Bauser, Alfred Beck, Stephen M. Beverley, Gabriella Bianchettin, Katja Borzym, Gordana Bothe, Carlo V. Bruschi, Matt Collins, Eithon Cadag, Laura Ciarloni, Christine Clayton, Richard M. R. Coulson, Ann Cronin, Angela K. Cruz, Robert M. Davies, Javier De Gaudenzi, Deborah E. Dobson, Andreas Duesterhoeft, Gholam Fazelina, Nigel Fosker, Alberto Carlos Frasch, Audrey Fraser, Monika Fuchs, Claudia Gabel, Arlette Goble, André Goffeau, David Harris, Christiane Hertz-Fowler, Helmut Hilbert, David Horn, Yiting Huang, Sven Klages, Andrew Knights, Michael Kube, Natasha Larke, Lyudmila Litvin, Angela Lord, Tin Louie, Marco Marra, David Masuy, Keith Matthews, Shulamit Michaeli, Jeremy C. Mottram, Silke Müler-

Auer, Heather Munden, Siri Nelson, Halina Norbertczak, Karen Oliver, Susan O'Neil, Martin Pentony, Thomas M. Pohl, Claire Price, Bénédicte Purnelle, Michael A. Quail, Ester Rabbinowitsch, Richard Reinhardt, Michael Rieger, Joel Rinta, Johan Robben, Laura Robertson, Jeronimo C. Ruiz, Simon Rutter, David Saunders, Melanie Schäfer, Jacquie Schein, David C. Schwartz, Kathy Seeger, Amber Seyler, Sarah Sharp, Heesun Shin, Dhileep Sivam, Rob Squares, Steve Squares, Valentina Tosato, Christy Vogt, Guido Volckaert, Rolf Wambutt, Tim Warren, Holger Wedler, John Woodward, Shiguo Zhou, Wolfgang Zimmermann, Deborah F. Smith, Jenefer M. Blackwell, Kenneth D. Stuart, Bart Barrell, P.J. Myler, The Genome of the Kinetoplastid Parasite, Leishmania major, Science, 309 (2005) 436-442.

[179] Matthew Berriman, Elodie Ghedin, Christiane Hertz-Fowler, Gaëlle Blandin, Hubert Renauld, Daniella C. Bartholomeu, Nicola J. Lennard, Elisabet Caler, Nancy E. Hamlin, Brian Haas, Ulrike Böhme, Linda Hannick, Martin A. Aslett, Joshua Shallom, Lucio Marcello, Lihua Hou, Bill Wickstead, U. Cecilia M. Alsmark, Claire Arrowsmith, Rebecca J. Atkin, Andrew J. Barron, Frederic Bringaud, Karen Brooks, Mark Carrington, Inna Cherevach, Tracey-Jane Chillingworth, Carol Churcher, Louise N. Clark, Craig H. Corton, Ann Cronin, Rob M. Davies, Jonathon Doggett, Appolinaire Djikeng, Tamara Feldblyum, Mark C. Field, Audrey Fraser, Ian Goodhead, Zahra Hance, David Harper, Barbara R. Harris, Heidi Hauser, Jessica Hostetler, Al Ivens, Kay Jagels, David Johnson, Justin Johnson, Kristine Jones, Arnaud X. Kerhornou, Hean Koo, Natasha Larke, Scott Landfear, Christopher Larkin, Vanessa Leech, Alexandra Line, Angela Lord, Annette MacLeod, Paul J. Mooney, Sharon Moule, David M. A. Martin, Gareth W. Morgan, Karen Mungall, Halina Norbertczak, Doug Ormond, Grace Pai, Chris S. Peacock, Jeremy Peterson, Michael A. Quail, Ester Rabbinowitsch, Marie-Adele Rajandream, Chris Reitter, Steven L. Salzberg, Mandy Sanders, Seth Schobel, Sarah Sharp, Mark Simmonds, Anjana J. Simpson, Luke Tallon, C. Michael R. Turner, Andrew Tait, Adrian R. Tivey, Susan Van Aken, Danielle Walker, David Wanless, Shiliang Wang, Brian White, Owen White, Sally Whitehead, John Woodward, Jennifer Wortman, Mark D. Adams, T. Martin Embley, Keith Gull, Elisabetta Ullu, J. David Barry, Alan H. Fairlamb, Fred Opperdoes, Barclay G. Barrell, John E. Donelson, Neil Hall, Claire M. Fraser, Sara E. Melville, N.M. El-Sayed, The Genome of the African Trypanosome

Trypanosoma brucei, Science, 309 (2005) 416-422.

[180] D. Pakalapati, S. Garg, S. Middha, J. Acharya, A.K. Subudhi, A.P. Boopathi, V. Saxena, S.K. Kochar, D.K. Kochar, A. Das, Development and evaluation of a 28S rRNA gene-based nested PCR assay for P. falciparum and P. vivax, Pathogens and global health, 107 (2013) 180-188.

[181] C.D. Mamotte, Genotyping of Single Nucleotide Substitutions, Clin Biochem Rev, 27 (2006) 63-75.

[182] S. Tabor;, C.C. Richardson, A single residue in DNA polymerases of the Escherichia coli DNA polymerase I family is critical for distinguishing between deoxy- and dideoxyribonucleotides, Proc. Natl. Acad. Sci. USA, 92 (1995) 6339-6343.

[183] S. Kim;, J.R. Edwards;, L. Deng;, W. Chung;, J. Ju, Solid phase capturable dideoxynucleotides for multiplex genotyping using mass spectrometry, Nucleic Acid Research, 30 (2002).

[184] J.G. Hall, P.S. Eis, S.M. Law, L.P. Reynaldo, J.R. Prudent, D.J. Marshall, H.T. Allawi, A.L. Mast, J.E. Dahlberg, R.W. Kwiatkowski, M.d. Arruda, B.P. Neri, V.I. Lyamichev, Sensitive detection of DNA polymorphisms by the serial invasive signal amplification reaction, PNAS, 97 (2000) 8272-8277.

[185] J.A. Sanchez, K.E. Pierce, J.E. Rice, L.J. Wangh, Linear-After-The-Exponential (LATE)–PCR: An advanced method of asymmetric PCR and its uses in quantitative real-time analysis, PNAS, 101 (2004) 1933-1938.

[186] H. Peery-O'Keefe, X.-W. Yao, J.M. Coull, M. Fuchs, M. Egholm, Peptide nucleic acid pre-gel hybridization: An alternative to southern hybridization, Proc. Natl. Acad. Sci. USA, 93 (1996) 14670-14675.

[187] J.M. Lee, H. Cho, Y. Jung, Fabrication of a structure-specific RNA binder for array detection of label-free microRNA, Angewandte Chemie, 49 (2010) 8662-8665.

[188] R.K. Saiki, P.S. Walsh, C.H. Levenson, H.A. Erlich, Genetic analysis of amplified DNA with immobilized sequence-specific oligonucleotide probes, Proc. Natl. Acad. Sci. USA, 86 (1989) 6230-6234.

[189] Y. Zhang, M.Y. Coyne, S.G. Will, C.H. Levenson, E.S. Kawasaki, Single base mut analysis of cancer and genetic diseases using membrane bound modified oligos, Nucleic Acid Research, 19 (1991) 3929-3933.

[190] K.F.J. Chow, A Membrane-Based Flow-through Hybridization Technology: A Rapid and Versatile tool for Molecular Diagnostics, The Open Biotechnology Journal, 2 (2008) 22-28.

[191] PALL, https://shop.pall.com/us/en/medical/oem-manufacturing/diagnostics/nylon-membrane-zidgri78lty; Nylon membranes types and description, in.

[192] PALL, http://www.pall.com/main/laboratory/product.page?id=35881; Immunodyne ABC® membranes, in, pp. Immunodyne ABC® membranes description and features.

[193] M.D.d.V. group, http://www.masterdiagnostica.com/es-es/productos/kitsdediagn%C3%B3sticomolecular/tecnolog%C3%ADadnaflow/hpvdirectflowchip.aspx; HPV Direct Flow CHIP, in.

[194] M.D.d.V. group, http://www.masterdiagnostica.com/es-es/productos/kitsdediagn%C3%B3sticomolecular/tecnolog%C3%ADadnaflow/sepsisflowchip.aspx; Sepsis Flow CHIP, in, pp. A kit which it allows detection of bacterias responsible of sepsis and antibiotic-resistance forms.

[195] M.D.d.V. group, http://www.masterdiagnostica.com/es-es/productos/kitsdediagn%C3%B3sticomolecular/tecnolog%C3%ADadnaflow/viralcnsflowchip.aspx; Viral CNS Flow CHIP, in, pp. A kit for detecting virus which cause neurological infections

[196] M.D.d.V. group, http://www.masterdiagnostica.com/es-es/productos/kitsdediagn%C3%B3sticomolecular/tecnolog%C3%ADadnaflow/bacterialcnsflowchip.aspx; Bacterial CNS Flow CHIP, in, pp. A kit which detects bacterias that cause meningitis.

[197] M.D.d.V. group, http://www.masterdiagnostica.com/es-es/productos/kitsdediagn%C3%B3sticomolecular/tecnolog%C3%ADadnaflow/tick-bornebacteriaflowchip.aspx; Tick-borne bacteria Flow CHIP, in, pp. A kit which detects pathogen bacteria transmitted by arthropods

[198] V. group, http://www.masterdiagnostica.com/documents/HSP/HSP-HS12V1_MII.pdf; HibriSpot12 user manual, in, pp. Description of the HibriSpot12 system.

[199] M. Dattner, D. Bohn, Chapter 20: Characterization of print quality in terms of colorimetric aspects, in: Printing on polymers. Fundamentals and applications, Matthew Dean, 2016, pp. 329-346.

[200] A. Jones, Appendix 1: Notes on printing glass DNA microarray slides, in: F. Falciani (Ed.) Microarray technology through applications, Taylor & Francis group, 2007, pp. 261-268.

[201] M. Palmieri, E. Alessi, S. Conoci, M. Marchi, G. Panvini, Developments of the "In-Check" Platform for Diagnostic Applications, Proceedings of the SPIE: Microfluidics, BioMEMS, and Medical Microsystems VI, 6886 (2008) 688602-688601–688602-688614. .

[202] O. Seitz, Solid-Phase Synthesis of Doubly Labeled Peptide Nucleic Acids as Probes for the Real-Time Detection of Hybridization, Angew. Chem. Int. Ed., 39 (2000) 3249-3252.